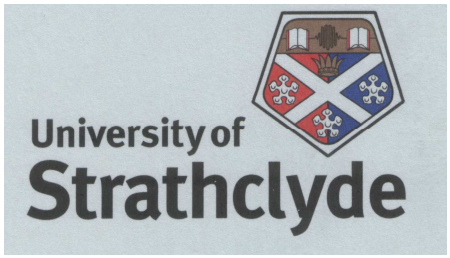

Process Monitoring of Blanking Coarse Grained and Ultra-fine Grained Aluminium Sheets Using Force-Displacement Characteristics and Acoustic Emission Technique

by

Hisham Hamid

This thesis is submitted to the University of Strathclyde in fulfilment of the requirements for the Degree of

Doctor of Philosophy

2010

DMEM Design, Manufacture and Engineering Management

DMEM
James Weir Building
75 Montrose Street
Glasgow G1 1XJ, UK

t: +44 (0)141 548 2091
f: +44 (0)141 552 7986
e: enquiries@dmem.strath.ac.uk
www.dmem.strath.ac.uk

Declaration of Authenticity and Author's Rights

Signed:

Date:

ABSTRACT

The aim of this study is to investigate the feasibility of developing a process monitoring system for blanking operations to monitor the quality of the blank edge for different aluminium materials. In this study, circular blanks of 5 mm diameter and 1 mm thickness of aluminium sheets were produced using different combination of punch-die clearances and the geometry of tool cutting edges. Different forms of aluminium sheets were used: as supplied, annealed, cold worked and ultra-fine grained (UFG). The punch force-displacement signatures were captured and acoustic emission (AE) technique was applied to monitor the real-time blanking processes. Results showed that by varying the blanking parameters, the characteristics of force-displacement signals can be related to the blanking phases of as supplied, annealed and cold worked materials, hence corresponded to the edge profile of the produced blanks. However, UFG aluminium sheets were found to be insensitive to the changing clearance and the state of the tool cutting edges. Clearance was identified to be a dominant factor, followed by the punch and the die sharpness to influence the characteristics of the blank edge profile. The two parameters of AE signals chosen in this study were the maximum amplitude and the maximum peak frequency. The magnitude of these parameters measured varied with the tool clearance, tools' state and the type of material. However, these AE parameters were found not to be the best indicators of quality of the blank edge profile.

Acknowledgements

Praise be upon Almighty God, with His blessings, I managed to complete this thesis. I would like to express my thanks to my Primary Supervisor, Dr. Andrzej Rosochowski for his guidance throughout the duration of this project. His willingness to share his knowledge and expertise helped me to gain deeper understanding of the subject. I would also like to thank my Second Supervisor, Professor Emeritus Raj Balendra for his supports. Last but not least, I would like to extend my heartiest appreciation and many thanks to my beloved families, my loving wife Rodiah, and my sons Akmal and Ahmad for their continuous pray for this success, patience and great support throughout the duration of this work.

Contents

Declaration of authenticity and author's rights *ii*

Abstract *iii*

Acknowledgements *iv*

Contents *v*

List of Figures *xi*

List of Tables *xix*

Nomenclature *xxi*

Glossary of Terms *xxii*

CHAPTER 1 INTRODUCTION

1.1 Introduction to metal forming 1

1.2 Sheet metal forming 4

1.3 Blanking operation 5

1.4 Measurement of blanking quality 7

1.5 Process monitoring in metal blanking/forming and quality control 7

1.6 Aluminium materials 9

1.7 The importance of the study 10

1.8 The aim of the project 12

1.9 Research objectives 12

1.10 Project tasks 14

1.11 Conclusion 14

1.12 The structure of the thesis 15

1.13 References 17

CHAPTER 2 LITERATURE REVIEW

Part I **Blanking operation**

2.1	Definition of blanking operation	25
2.2	Analysis of stages/phases of blanking process	26
2.3	Force-displacement characteristics of blanking operation	27
2.4	The blanking process parameters	28
2.5	Formation of the blank edge profile	37
2.6	Process monitoring and control in metal blanking/forming	38

Part II **Acoustic emission technique**

2.7	Definition of acoustic emission	42
2.8	Sources of acoustic emission	43
2.9	Types of a acoustic emission	45
2.10	Advantage of acoustic emission	45
2.11	Acoustic emission parameters	46
2.12	Acoustic emission instrumentation	46
2.13	Acoustic emission sensor	46
2.14	Preamplifier	48
2.15	Signal conditioning module	49
2.16	Data acquisition hardware	50
2.17	Computer and AE software	50
2.18	Acoustic emission monitoring in metal blanking/forming	51

Part III **Developing ultra-fine grained aluminium**

2.19 Introduction 55

2.20 Grain refinement 56

2.21 Severe plastic deformation 59

2.22 Equal channel angular pressing 61

2.23 Other SPD methods 64

2.23.1 Accumulative roll-bonding 64

2.23.2 High pressure torsion 65

2.23.3 Cyclic extrusion compression 67

2.23.4 The repetitive corrugation and straightening 68

2.24 References 69

CHAPTER 3 EQUIPMENT, MATERIALS AND EXPERIMENTAL PROCEDURES FOR BLANKING PROCESS MONITORING

3.1 Equipment 90

3.1.1 Introduction 90

3.1.2 Blanking tool set 91

3.1.3 Data acquisition system 94

3.1.4 Acoustic emission sensor 94

3.1.5 Preamplifier 95

3.1.6 PCI-2 AE board 96

3.1.7 AE software 96

3.1.8 Desktop computer 97

3.1.9 Force transducer 97

3.1.10 Charge amplifier 97

3.1.11 Inductive displacement transducer 98

3.1.12 MGA amplifier system 99

3.1.13 Laboratory hydraulic servo press 99

3.2 Materials 100
3.2.1 Material preparations 100
3.2.2 Annealing procedures *(A2)* 101
3.2.3 Preparing coarse grained aluminium sheets AA1070 *(A3)* 102
3.2.4 Hardness testing 102
3.2.5 Uniaxial tensile test 103

3.3 Laboratory work for producing UFG aluminium sheets *(A4)* 103
3.3.1 Producing UFG aluminium sheet AA 1070 using ECAP process 103
3.3.2 Upsetting process 104
3.3.3 Rolling process 105
3.3.4 Results of UFG sheets 105

3.4 Experimental program and procedures 106
3.4.1 Tooling sets preparations 106
3.4.2 DAQ preparations 108
3.4.3 Laboratory hydraulic servo press preparations 109
3.5 Discussion 109
3.6 Conclusions 111
3.7 References 113

CHAPTER 4 RESULTS AND DISCUSSION OF BLANKING OPERATIONS: FORCE-DISPLACEMENT AND ACOUSTIC EMISSION SIGNATURES
4.1 Introduction 133
4.2 Force-displacement signatures 136
4.2.1 Influence of clearance 136

4.2.2 Influence of tool wear 140
4.2.3 Influence of material 145
4.2.4 Statistical design of experiment – maximum blanking force as a quality characteristic 146
4.3 Acoustic emission signatures 147
4.3.1 Influence of clearance 149
4.3.2 Influence of tool wear 150
4.3.3 Influence of material 153
4.3.4 Statistical design of experiment – maximum amplitude and maximum peak frequency as a quality characteristic 154
4.4 Discussion 155
4.4.1 Experimental procedures 155
4.4.2 Influence of clearance to affect the characteristics of force-displacement graphs 156
4.4.3 Influence of tool wear to affect the characteristics of force-displacement graphs 159
4.4.4 AE maximum amplitude and maximum peak frequency 161

CHAPTER 5 CONCLUSIONS AND SUGGESTIONS FOR FUTURE WORK

5.1 Summary of the work 206
5.2 Research outcomes and contributions 209
5.3 Suggestions for future work 212

APPENDICES

Appendix 1	AE signal features terminology	215
Appendix 2	Assembly drawing of blanking tool set	217
Appendix 3	Acoustic emission sensor specifications	218
Appendix 4	Preamplifier specifications	220
Appendix 5	Block diagram description for PCI-2 AE board	222
Appendix 6	Mounting of force transducer	225
Appendix 7	Data for aluminium 1050-H14	227
Appendix 8	Chemical composition of aluminium 1070	228
Appendix 9	Half normal plot calculations for maximum blanking force as a quality characteristic	229
Appendix 10	Half normal plot calculations for maximum amplitude and maximum peak frequency of AE signals as a quality characteristic	235

List of Figures

CHAPTER 1 INTRODUCTION

Fig. 1.1 Classification of metal forming into groups and subgroups 21

Fig. 1.2 Schematic illustration of blanking tools 23

Fig. 1.3 The sheared edge profile of the blanked part 23

Fig. 1.4 Elements/factors that influence the product quality 24

CHAPTER 2 LITERATURE REVIEW

Fig. 2.1 Phases of the blanking process 81

Fig. 2.2 Typical force-displacement curve of blanking process 82

Fig. 2.3 Blanking clearance 83

Fig. 2.4 Wear profile of the blanking punch 84

Fig. 2.5 Types of AE signal 85

Fig. 2.6 AE hit feature extraction diagram 85

Fig. 2.7 Block diagram of blanking monitoring system 86

Fig. 2.8 Schematic representation of ECAP process 87

Fig. 2.9 Schematic representation of four processing routes in ECAP 87

Fig. 2.10 Schematic representation of ARB process 88

Fig. 2.11 Schematic representation of HPT process 88

Fig. 2.12 Schematic representation of CEC process 89

Fig. 2.13 Schematic representation of RCS 89

CHAPTER 3 EQUIPMENT, MATERIALS AND EXPERIMENTAL PROCEDURES FOR BLANKING PROCESS MONITORING

Fig. 3.1	Experimental set-up for blanking monitoring system	114
Fig. 3.2	Prototype of blanking tool	114
Fig. 3.3	The blanking tool set	115
Fig. 3.4	Punches and dies	116
Fig. 3.5	Photograph of sharp and rounded punch and die	116
Fig. 3.6	AE sensor and preamplifier	117
Fig. 3.7	Force transducer and charge amplifier	117
Fig. 3.8	LVDT displacement transducer and charge amplifier	117
Fig. 3.9	AE sensor location	118
Fig. 3.10	PCI-2 AE board	118
Fig. 3.11	The block and plates used for LVDT displacement transducer calibration	118
Fig. 3.12	Relationship between corresponding voltage and displacement of LVDT displacement transducer	119
Fig. 3.13	Laboratory hydraulic servo press	119
Fig. 3.14	Micrographs show the grain structure of: as supplied AA 1050 (*A1*), (b) annealed AA (*A2*)1050	120
Fig. 3.15	Annealing process of aluminium sheet AA 1050	120
Fig. 3.16	Plate of aluminium AA 1070 after side upsetting	121
Fig. 3.17	Aluminium sheets AA 1050 after side upsetting and rolling	121
Fig. 3.18	Hardness testing	122
Fig. 3.19	Conducting uniaxial tensile test	122
Fig. 3.20	Relationship of true stress-true strain for material *A1*	123

Fig. 3.21	Relationship of true stress-true strain for material *A2*	123
Fig. 3.22	Schematic representation of the two-turn S channel ECAP	124
Fig. 3.23	Supplied aluminium 1070, 38 mm diameter	125
Fig. 3.24	Larger size of UFG billet of 26x26 mm produced using scaled-up two turn S channel ECAP	125
Fig. 3.25	Upset sample of UFG, 3.8 – 4.0 mm thickness	125
Fig. 3.26	UFG sheets produced after 6 passes of cold-rolled	126
Fig. 3.27	Grain microstructure of AA 1070 for comparison between CG and UFG: (a) Initial CG, (b) UFG after four passes of two-turn S channel ECAP and (c) UFG sheets after ECAP, side upsetting and rolling	127
Fig. 3.28	Visual inspection to check tool alignment using borescope	131
Fig. 3.29	Process flow of blanking monitoring	131
Fig. 3.30	The blanks produced during blanking trials	132

CHAPTER 4 RESULTS AND DISCUSSION OF BLANKING OPERATIONS: FORCE-DISPLACEMENT AND ACOUSTIC EMISSION SIGNATURES

Fig. 4.1(a)	Output signal of voltage-time of force transducer	164
Fig. 4.1(b)	Output signal of voltage-time of LVDT displacement transducer	164
Fig. 4.1(c)	Force-displacement graph of blanking operation	165
Fig. 4.1(d)	Noise signal captured before start blanking operation	166
Fig. 4.1(e)	Noise signal captured after halt blanking operation	166
Fig. 4.1(f)	AE signal captured during blanking operation	166
Fig. 4.1(g)	Hardware setting for blanking *A1, A2, A3* materials	167
Fig. 4.1(h)	Hardware setting for blanking *UFG (A4)* materials	167

Fig. 4.2	Force-displacement graphs for blanking *A1* using a sharp die and sharp punch for 3 – 9% clearance and SEM images of the produced blanks	170
Fig. 4.3	Force-displacement graphs for blanking *A2* using a sharp die and sharp punch for 3 – 9% clearance and SEM images of the produced blanks	171
Fig. 4.4	Force-displacement graphs for blanking *A3* using a sharp die and sharp punch for 3 – 9% clearance and SEM images of the produced blanks	172
Fig. 4.5	Force-displacement graphs for blanking *A4* using a sharp die and sharp punch for 3 – 9% clearance and SEM images of the produced blanks	173
Fig. 4.6(a)	Force-displacement graphs for blanking *A1* using a sharp die and worn punch for 3 – 9% clearance and SEM images of the produced blanks	174
Fig. 4.6(b)	Force-displacement graphs for blanking *A1* using a worn die and sharp punch for 3 – 9% clearance and SEM images of the produced blanks	175
Fig. 4.6(c)	Force-displacement graphs for blanking *A1* using a worn die and worn punch for 3 – 9% clearance and SEM images of the produced blanks	176
Fig. 4.7(a)	Force-displacement graphs for blanking *A2* using a sharp die and worn punch for 3 – 9% clearance and SEM images of the produced blanks	177
Fig. 4.7(b)	Force-displacement graphs for blanking *A2* using a worn die and sharp punch for 3 – 9% clearance and SEM images of the produced blanks	178

Fig. 4.7(c)	Force-displacement graphs for blanking *A2* using a worn die and worn punch for 3 – 9% clearance and SEM images of the produced blanks	179
Fig. 4.8(a)	Force-displacement graphs for blanking *A3* using a sharp die and worn punch for 3 – 9% clearance and SEM images of the produced blanks	180
Fig. 4.8(b)	Force-displacement graphs for blanking *A3* using a worn die and sharp punch for 3 – 9% clearance and SEM images of the produced blanks	181
Fig. 4.8(c)	Force-displacement graphs for blanking *A3* using a worn die and worn punch for 3 – 9% clearance and SEM images of the produced blanks	182
Fig. 4.9(a)	Force-displacement graphs for blanking *A4* using a sharp die and worn punch for 3 – 9% clearance and SEM images of the produced blanks	183
Fig. 4.9(b)	Force-displacement graphs for blanking *A4* using a worn die and sharp punch for 3 – 9% clearance and SEM images of the produced blanks	184
Fig. 4.9(c)	Force-displacement graphs for blanking *A4* using a worn die and worn punch for 3 – 9% clearance and SEM images of the produced blanks	185
Fig. 4.10	Force-displacement graphs for blanking *A1, A2, A4* and *A4* at 3% clearance	186
Fig. 4.11	Force-displacement graphs for blanking *A1, A2, A4* and *A4* at 9% clearance	186
Fig. 4.12(a)	The graphs showing maximum blanking force decreases with increasing clearance for blanking *A1* using a sharp die – sharp punch and a sharp die – worn punch	187

Fig. 4.12(b)	The graphs showing maximum blanking force decreases with increasing clearance for blanking *A1* using a worn die – sharp punch and a worn die – worn punch	187
Fig. 4.13(a)	The graphs showing maximum blanking force decreases with increasing clearance for blanking *A2* using a sharp die – sharp punch and a sharp die – worn punch	188
Fig. 4.13(b)	The graphs showing maximum blanking force decreases with increasing clearance for blanking *A2* using a worn die – sharp punch and a worn die – worn punch	188
Fig. 4.14(a)	The graphs showing maximum blanking force decreases with increasing clearance for blanking *A3* using a sharp die – sharp punch and a sharp die – worn punch	189
Fig. 4.14(b)	The graphs showing maximum blanking force decreases with increasing clearance for blanking *A3* using a worn die – sharp punch and a worn die – worn punch	189
Fig. 4.15(a)	The graphs showing the changing in maximum blanking force is negligible in blanking *A4* using a sharp die – sharp punch and a sharp die – worn punch	190
Fig. 4.15(b)	The graphs showing the changing in maximum blanking force is negligible in blanking *A4* using a worn die – sharp punch and a worn die – worn punch	190
Fig. 4.16	A line listing file	191
Fig. 4.17(a)	Graphs of maximum amplitude and maximum peak frequency of AE signals captured during blanking *A1* using a sharp die and sharp punch for 3 – 9% clearance	194
Fig. 4.17(b)	Graphs of maximum amplitude and maximum peak frequency of AE signals captured during blanking *A2* using a sharp die and sharp punch for 3 – 9% clearance	194

Fig. 4.17(c)	Graphs of maximum amplitude and maximum peak frequency of AE signals captured during blanking *A3* using a sharp die and sharp punch for 3 – 9% clearance	195
Fig. 4.17(d)	Graphs of maximum amplitude and maximum peak frequency of AE signals captured during blanking *A4* using a sharp die and sharp punch for 3 – 9% clearance	195
Fig. 4.18	The graphs of (a) The maximum amplitude and (b) The maximum peak frequency of AE signals captured during blanking *A1* using different tool states for 3 – 9% clearance	196
Fig. 4.19	The graphs of (a) The maximum amplitude and (b) The maximum peak frequency of AE signals captured during blanking *A2* using different tool states for 3 – 9% clearance	197
Fig. 4.20	The graphs of (a) The maximum amplitude and (b) The maximum peak frequency of AE signals captured during blanking *A3* using different tool states for 3 – 9% clearance	198
Fig. 4.21	The graphs of (a) The maximum amplitude and (b) The maximum peak frequency of AE signals captured during blanking *A4* using different tool states for 3 – 9% clearance	199
Fig. 4.22(a)	Graphs of maximum amplitude for blanking *A1 – A4* using a sharp die and sharp punch for 3 – 9% clearance	200
Fig. 4.22(b))	Graphs of maximum peak frequency for blanking *A1 – A4* using a sharp die and sharp punch for 3 – 9% clearance	200
Fig. 4.23(a)	A half normal plot for factors to affect the maximum amplitude of AE signals	201

Fig. 4.23(b)	A half normal plot for factors to affect the maximum peak frequency of AE signals	201
Fig. 4.24	Graphs of maximum blanking force obtained for *A1 – A4* at 3 – 9% clearance	202
Fig. 4.25	(a)The force-displacement graphs of blanking *A1 – A4* using a sharp die – sharp punch at 3% clearance and (b) their equivalent force-displacement characteristics	203
Fig. 4.26	(a)The force-displacement graphs of blanking *A1 – A4* using a worn die – worn punch at 9% clearance and (b) their equivalent force-displacement characteristics	205

List of Tables

CHAPTER 1 INTRODUCTION

Table 1.1 Classification of manufacturing processes 20

Table 1.2 Classification of metal forming processes 22

CHAPTER 2 LITERATURE REVIEW

Table 2.1 Benefits of proper die clearance and drawbacks of insufficient and excessive die clearance 83

Table 2.2 Factors influence the formation of blank edge profile 84

CHAPTER 3 EQUIPMENT, MATERIALS AND EXPERIMENTAL PROCEDURES FOR BLANKING PROCESS MONITORING

Table 3.1 Detail of the rolling process for aluminium sheets AA 1070 121

Table 3.2 Hardness measurements 122

Table 3.3 Yield strength and ultimate tensile strength (UTS) of the materials 124

Table 3.4 Detail of rolling process of UFG sheets 126

Table 3.5 Coding system 128

Table 3.6 Matrix of the blanking experiments 129

CHAPTER 4 RESULTS AND DISCUSSION OF BLANKING OPERATIONS: FORCE-DISPLACEMENT AND ACOUSTIC EMISSION SIGNATURES

Table 4.1 List of figures of force-displacement signatures and the SEM images of blanking material *A1 – A4* with 3 – 9% clearances using different tool states 168

Table 4.2 The maximum blanking force of blanking material *A1 – A2* with 3 – 9% clearances using different tool states 169

Table 4.3 The maximum amplitude of AE signals for A1 – A4 for all combinations of tool states and blanking clearance 192

Table 4.4 The maximum amplitude of AE signals for A1 – A4 for all combinations of tool states and blanking clearance 193

Table 4.5 The measurements of the smooth sheared edge of blanks *A1 – A4* produced using a sharp die – sharp punch at 3% clearance 204

Table 4.6 The measurements of the smooth sheared edge of blanks *A1 – A4* produced using a worn die – worn punch at 9% clearance 205

Nomenclature

The following symbols have been standardised throughout this thesis. The units quoted are for the purpose of calculations. The SI unit system is used in the formulae or in calculations where appropriate.

C	Clearance per side, express as the % of thickness, *t*.
d	Punch penetration in mm.
D_d	Diameter of the die in mm.
D_p	Diameter of the punch in mm.
ε	The equivalent of strain.
F_p	The force exerted by press slide in Newton, N.
F	Blanking force in Newton, N.
L	The total length of sheared edges.
n	Number of deformation passes through ECAP or rolling processes.
τ_m	Sheared strength of the material, $N/m^{2.}$
r	Reduction in thickness of material.
t_0	The initial thickness of material in mm.
ϕ	Intersection channel angle in ECAP die.
ψ	Outer curvature angle of ECAP die.
γ	Shear angle in HPT die.

Glossary of Terms

AA	Aluminium alloy.
ADC	Analogue to digital converter.
Annealing	A heat treatment that alters the microstructure of a material causing changes in properties such as strength and hardness.
Artificial intelligent, AI	The ability of a computer or machines to perform activities that are normally thought to require intelligence or the branch of computer science concerned with the development of machines having this ability.
Artificial neural network, ANN	An Artificial Neural Network (ANN) is an information processing paradigm that is inspired by the way biological nervous systems, such as the brain, process information.
ASCII	American Standard Code for Information Interchange.
ASTM	The American Society for Testing and Materials
Blanking	One of a metal forming processes, during which a metal workpiece is removed from the primary metal strip or sheet when it is punched
Blank	In forming, a piece of sheets metal stock from which a product is made. Material, produced in cutting dies that is usually subjected to further press operations.

Blank holder	The part of a blanking which holds the workpiece against a mating surface of the die to control metal flow.
Bottom dead centre, BDC	When a ram of the press travels the length of its stroke, in normal operation, it is said to have reached bottom dead centre when it is at the lowest position.
Burnish	Smooth or shiny area above the breakout on a sheared edge.
Burr	A thin ridge, raised sharp edge, or roughness left on sheet metal blanks by cutting or shearing operations.
Clearance	The space, per side, between the punch and die.
DAC	Digital to analogue converter.
DAQ	Data acquisition system.
Decibel	A logarithmic unit of measurement that expresses the magnitude of a physical quantity relative to a specified or implied reference level.
Drawing operations	The metal forming process of flat rolled metals to make drawn parts.
Felicity effect	Acoustic emission is detected at stresses below the previous peak stress.
Finite element method, FEM	The finite element method (FEM) is a numerical technique for finding approximate solutions of partial differential equation as well as of integral equations.
FFT	Fast Fourier Transform.

Forging	The process by which metal is shaped by plastic deformation using suitably applying compressive force.
Kaiser effect	additional AE occurs only when the stress level exceeds previous stress level
LVDT	Linear variables displacement transformer
Microforming	The production of parts or structures with at least two dimensions in the sub-millimetre range.
Microsystem technology, MST	The European term for microelectromechanical systems technology (MEMS technology).
NDT or NDE	Non-destructive testing or non-destructive evaluations
PCI	Peripheral Component Interconnect.
PZT	Lead zirconate titanate, is a piezoelectric ceramic element.
Plastic deformation	Permanent deformation occurring in forming of metal after elastic limits have been exceeded under the action of applied stresses.
Shear operations	Type of cutting operation in which the metal object is cut by means of a moving punch or blade and fixed edge or by a pair of moving blades that may be either flat or curved.
Slug	The metal removed when punching or blanking a hole, and also termed as punch out.
SEM	Scanning electron microscope
SNR	Signal to noise ratio

SPD	Severe plastic deformation
TCM	Tool condition monitoring
Tensile load	A stress that causes two parts of an elastic body, on either side of a typical stress plane, to pull apart.
UFG	Ultra-fine grained materials.
Ultrasonic	Waves or signals whose frequency is above the audible range.
UTS	The maximum stress (tensile, compressive, or shear) a material can sustain without fracture
Work hardening	Increase in tensile strength of material resulting from cold working process.
Yield strength	The level of stress when plastic flow begins during a metal forming.

CHAPTER 1

INTRODUCTION

This chapter presents a brief introduction to metal forming technology and sheet metal blanking operations that involve a new type of aluminium material with ultra-fine grained structure. It also highlights various aspects of process monitoring in blanking, which is one of the main subjects in this research. The author also presents the importance of the study, the aim, the objectives and the main tasks of the project. At the end of this chapter the structure of the thesis, which includes Chapter 1 to Chapter 5 is explained.

1.1 Introduction to metal forming

Metal forming is the oldest technologies of mankind and it has never been faded by new development of modern time. Originally, metal forming was practiced at least 3000 years ago in Egypt, where man used hammer forging to produce gold sheets [1]. Nowadays the products produced by metal forming technology are used almost everywhere ranging from the office furniture to engineering components and automotive body panels. With rapid development and emerging new flexible tooling systems, state-of-the-art machines and latest advanced materials, metal forming is by far one of the fast growing fields in manufacturing sectors. Research involving new developments of metal forming technology [2-8] has been increasing over the years to meet the demand for product quality and complexity.

By simple definition, metal forming means changing the shape of the material without actually removing any part of it. Basically, the given shape of the workpiece is converted to another shape without change in the mass or composition of the material, thus maintaining the cohesion of the workpiece material. The mechanism used to cause permanent shape transformation is known as '*plastic deformation'* [9]. It is the phenomenon of the response of metals to an applied stress which is being widely exploited in various metal forming processes. Plastic deformation or metal flow results from the use of a set of tooling, for instance a punch and a die, which apply stresses that exceed the yield strength of the material. With the application of the external forces to the workpiece, internal stress and displacement are generated inside the material causing permanent shape changes to take a shape determined by the geometry of the die. Metal forming is categorised as belonging to the group II of the manufacturing process classification [10, 11]**,** which is presented in Table 1.1.

Numerous methods have been used to deform the materials into required shape of parts or components. Several reports [12, 13] concluded that there are five groups of specific deformation operations as shown in Fig. 1.1, according to the various ways of using predominant stresses during deformation. Five groups of specific forming operations are compressive forming, combined tensile and compressive forming, tensile forming, forming by bending and forming by shearing. The subdivisions of each forming operation are grouped according to the movement of tools relative to the workpiece material, the workpiece geometry, the tool geometry and the interaction between the tool and the workpiece.

Metal forming processes are also classified according to the shape of metal used in a forming operation as *bulk or massive metal forming processes* [14], and *sheet metal forming processes* [15]. The plane stress situation, which is normally present in sheet metal forming, compared to the three-dimensional stresses in bulk forming has been a classical criterion in defining the processes involved in sheet metal forming. Some other criteria [16] are also used to classify metal forming processes as shown in Table 1.2.

Bulk forming processes are characterised by significant deformation, involving multi-axial and compressive loading, with the forces applied being greater than in sheet metal forming. Therefore, large-size machines and stronger tools are required, which leads to higher operation costs. The processes may also involve very large changes in cross section and wall thickness. However, generally the ratio of the surface area to volume of the workpiece is relatively low. The starting workpiece for bulk forming processes usually include cylindrical billets and rectangular bars.

Increasing demands for faster, better and cheaper production has great influence on metal forming industry and has intensified the research and development of bulk metal forming in recent years. Sheet metal forming also has been affected by these challenging issues. Wagener [17] explained the trends in the development of sheet metal forming to meet the increasing quest for productivity and quality. These include various expects of materials, tools and machinery. He also suggested that sheet metal forming specialists are needed, who are an experts in metallurgy, tribology, plasto-mechanics, tool design, metal forming machine tools, computer

science, metrology and instrumentation, manufacturing and industrial engineering, recycling and environmental technologies, economy, general and personnel management.

1.2 Sheet metal forming

Sheet metal forming is one of the most widely used manufacturing technologies for producing a wide range of products. Generally, the forming and related operations are performed on metal sheets, strips and coils. Sheet metal forming is gaining a lot of attention in modern manufacturing due to the ease with which metal may be formed into useful shapes by plastic deformation processes while the volume and mass of the metal are conserved when displaced from one location to another [18].

Contrary to bulk forming, the ratio of the surface area to the volume of workpiece in sheet metal forming is high. Since the sheet thickness is relatively small, in many cases the material can be deformed only as a result of applying tensile stress. Sheet metal forming operations are usually performed using ductile materials, which allow using cold working processes. However, when materials with greater strength such as metal alloys are involved, the operations are performed at elevated temperature. Compared to bulk metal forming, sheet metal forming involves smaller strains and lower forces, which helps reducing the operation cost through employing small presses and using cheaper tool materials.

Technological advances in the sheet metal industry improve the efficiency and precision with which sheet metal products are produced. However, the quality of parts and production costs are still becoming an issue. In 1992, a dedicated forum, established to become of a major platform for reporting and discussing the trends in sheet metal technologies and new developments for industries, was founded through the International Conference on Sheet Metal (SheMet) [19]. Streppel et al. [20] contributed their optimistic views in a special editorial issue, which had three aims: (a) to provide an overview of the latest developments, (b) to report on specific innovations in sheet metal forming processes, machine tools and materials characterisation, and (c) to report on new developments in terms of real-time process monitoring and control of sheet metal forming.

One of the common techniques to make sheet metal parts is blanking. The technique is simple and suitable for mass production. Despite this, detail understanding of blanking processes is still essential since the processes and the behaviour of the materials involved are non-linear. Therefore continuous research in the area of blanking is vital for the academia and many of industrial sectors.

1.3 Blanking operation

Generally, shaping sheet metal into a finished part can be accomplished by cutting (shearing), bending and drawing operations. Cutting by shear is the simplest operation and usually becomes a basic operation followed by secondary operations. Almost any two-dimensional shape with simple as well as complicated geometry can be cut from stock materials using blanking. Unlike other forming processes, blanking

not only deforms the metal plastically but also ruptures the sheet metal in the desired zones.

Blanking, punching or piercing is a constrained shearing operation that involves elastic deflection, plastic deformation, fracture and rupture of the work material. The material or workpiece is subjected to the action of the tools (punch and die), while constrained on the periphery by a blank holder. In principle, the procedures of blanking and punching have no difference. For blanking, the cut out part (slug) is the product and the remainder is a scrap, while in punching the cut out part is a scrap and the remainder is the product.

In blanking operations, usually a large stock of workpiece is cut into small blanks. Initially, a pre-cut flat sheet material is clamped between the die and the blank holder. The blank holder is loaded with a certain force to grip the material at the outer periphery of the die hole. This is to ensure a sufficient constrained force available for constrained shearing operation, in order to control the material flow during deformation phase and thus control the quality of the blank produced. On the other hand, unconstrained shearing such as cutting the sheet metal with hand held cutter operates without a blank holder; this is acceptable only if the quality of sheared edge is not an issue. Shear cutting action in blanking operation involves a complete or enclosed contour of a workpiece. A simplified blanking tool configuration is shown in Fig. 1.2.

1.4 Measurement of blanking quality

The characteristic of the sheared edge profile of a blank and a scrap is shown in Fig. 1.3. The acceptability and the overall quality of the blank parts are determined by the dimensional accuracy, the condition of a sheared edge surface and its suitability for the application.

Gréban et al. [21] expressed the view that the quality of blanking can be measured by means of the ratio of the different zones of the blanked part edge expressed as a percentage of the total height of the blanked part edge; rollover zone, sheared or burnish zone, fracture zone and burr. A larger smooth sheared zone is the most desirable criteria for blanked part. Rollover, fracture zone and burr are the unwanted features because they may cause problems during the assembly with other parts. However, these features can be controlled within the tolerable limits by improving the blanking process. If the blanking operation results in developing the burr beyond the limit of dimensional accuracy, the secondary process such as de-burring operation is required. It can also contribute to a number of rejected parts and adds the overall production cost.

1.5 Process monitoring in metal blanking/forming and quality control

In general, the quality of the products is influenced by various factors in the metal forming system, which consists of machine, tooling, material, process as well as environmental factors and the knowledge and skills of the operators [17, 22-24]. Fig. 1.4 summarises the elements that influence the characteristics of the product, hence the quality of the product. The setting of the system elements such as machine, tools

and materials can be linked to characteristics of the sheared edge of the produced blank and vice versa. Further, information from the product characteristics can be used to optimise the setting of a metal forming system to improve the quality of the produced product.

The methods used to implement a process monitoring system can be divided into two: *direct and indirect monitoring*. Direct monitoring produces more accurate results because the physical characteristics of the product are directly assessed. However, in blanking operations the deformation and fracture of a metal sheet occur inside a die, which makes direct monitoring of the blanking process rather difficult if not impossible. Thus, the strategy for monitoring quality in blanking operations can be based on monitoring the changing parameters of the elements of a metal forming system that correspond to the quality of the blanked parts. In the present study, changes in the process parameters were detected via monitoring the signals that constitute the process signatures. These signals were acquired and processed by a data acquisition system.

The aim of a metal forming operation is to produce products meeting the design specifications and to ensure that the system functions economically. This means that the products produced have to be checked according to quality standard. However, most of the products that deviate from original specifications are only discovered in the final phase of the process. This leads to the demand for process monitoring that can detect significant faults and enable the corrective actions to be undertaken in any stage of the processes.

The traditional approach to process monitoring in metal forming relies upon experience and skills of operators to detect process abnormalities. This manual inspection is insufficient for high-speed production. More sophisticated process monitoring techniques have been employed using acoustic emission, force, displacement, vibration, temperature, torque and power or motor current measurements [25].

Acoustic emission (AE) technique and force-displacement characteristics had been used in blanking operations [26, 27] because of the simplicity in setting up the monitoring equipment and the substantial response of the acquired signals from the blanking process. In many cases, the difficulty in interpretation of the AE signal limits the scope of applications, particularly in blanking. However, due to the nature of the AE signal, which is generated due to the plastic deformation and fracture in blanking material, there has been always a hope that the technique could be improved to produce a better result. Byrne et al. [28] reviewed the state-of-the-art, technological challenges and future development of AE systems. With the advent of sensor technology and advanced signal processing instrumentation, AE monitoring is being gradually accepted by industry, which draws from laboratory developments of this technique.

1.6 Aluminium materials

Aluminium and its alloys are widely used in various sectors and the demand for this metal across the world is increasing every year [29]. Due to its numerous technical advantages, the application of aluminium and its alloys in high technology sectors

such as automotive and aerospace is growing [30]. The utilisation of aluminium sheet could offer one of the solutions to the world-wide efforts of the car manufacturing industry to reduce the weight of the vehicles and to reduce fuel consumption. Aluminium has low density, typically 2.71 g/cm^3, possesses good inherent corrosion resistance and acceptable workability that enables forming it into useful shapes economically.

Further, there has been growing research activities in the area of producing nanostructured materials by severe plastic deformation (SPD) techniques, which involves converting the initial coarse grained (CG) aluminium into ultra-fine grained (UFG) aluminium. The reason why UFG materials have gained ground recently in laboratory research world wide is that they have improved mechanical properties and technological characteristics, which are especially attractive in the area of micro-system technology (MST) [31, 32].

The UFG materials prepared by various SPD processing methods, in particular equal-channel angular pressing (ECAP) are fully dense. ECAP can be performed using simple tools and an ordinary press. The constraints of the ECAP process limit the shape of the produced UFG billet to that of a rectangular or a cylindrical bar, which needs to be processed further in order to produce UFG aluminium sheet.

1.7 The importance of study

Research on online process monitoring outside the area of sheet metal forming, in particular in machining processes, has been extensively reported [33, 34]. However,

little work has been done on process monitoring, which involves sheet metal forming processes and especially blanking. This is due to the complexity of the blanking process, which is not fully understood or captured by any comprehensive model [35]. In addition, the vast majority of blanking activities have involved CG materials, mostly for producing large parts. However, the understanding related to blanking of very small and miniature parts is lacking [36], and even more so in the case of UFG materials, which are expected to gain wider use for these parts.

Although numerous commercial monitoring systems are available on the market nowadays, those systems usually do not meet shop floor requirements due to many drawbacks [25]. They are not robust as well as expensive costs. More frequent users prefer to develop their own customised system to meet their requirements. In metal blanking operations, a monitoring system usually captures the force-displacement signal, which is a prominent data in the operation. Despite this, the variability of the signal due to the response of the data acquisition system and the blanking tool could influence the characteristic of the process signatures. This can cause error and leads to misleading the interpretation of the signals, hence resulting inaccurate result. Therefore, it is a hope that combining another approach, which is in this case, based on AE technique can improve the result. With proper implementation, AE technique could become a complement to the force-displacement method for process monitoring in blanking.

1.8 The aim of the project

The aim of this project is to investigate the feasibility of developing a process monitoring system for blanking operations to monitor the quality of the blank edges for different aluminium materials.

The blanking parameters such as punch-die clearance and punch and die radius (simulating worn tools) have been selected as likely factors affecting the formation of the blank sheared edge profile. Blanking of aluminium sheets, with different grain structure will be compared. The force-displacement signals and AE signals captured during the blanking process will be used as the process signatures, which contain real-time information about the characteristics of the sheared edge, hence the quality of the produced blanks. This should lead to better understanding of requirements and limitations of process monitoring in blanking operations.

1.9 Research objectives

In order to achieve the above aim, the following research objectives have been identified:

1. To design and build a suitable tooling system for a laboratory blanking operation. The blanking tooling system will consist of four main components: blanking tool frame, punches, dies and tool support components. It will provide the means of connecting the AE sensor and force and displacement transducer.

2. To prepare different types of aluminium sheets.

Aluminum AA1050 and AA1070 will be used as the blanking materials. The samples from aluminum AA1050 will be prepared in the two forms of as supplied and annealed. The other types of samples, which are cold worked (referred to CG throughout this thesis) and UFG materials, will be prepared from aluminium AA1070.

3. To develop a process monitoring system for blanking.

Properly configured tooling and data acquisition (DAQ) instrumentation, for AE, force and displacement measurements as well as AEwin software will have to be integrated to form a process monitoring system. The instrumentation will be calibrated and tested prior to the experiment.

4. To acquire the blanking process signatures.

Proper experimental procedures will be established for blanking experiments. There will be included the determination of the programme of tests, using design of experiments (DOE) approach and carrying out these experiments using DAQ hardware and software.

5. To correlate the process signatures with different settings of blanking parameters and product quality.

The characteristics of force-displacement graphs will be correlated with the quality of the blank. The maximum amplitude and maximum peak frequency of AE signals will also be considered as quality dependant.

1.10 Project tasks

The following tasks will have to be accomplished to achieve the research objectives:

1. Design and manufacture a tool system for blanking.

2. Set-up the laboratory hydraulic servo press and configure data acquisition system for blanking operation.

3. Prepare as supplied materials and perform annealing for aluminium AA1050.

4. Prepare CG and UFG materials from aluminium AA1070.

5. Perform blanking trials for different aluminium materials.

6. Capture force-displacement signatures in blanking experiments.

7. Acquire AE signals in blanking experiments.

8. Process AE signals using appropriate software.

9. Apply design of experiments (DOE) approach to capture the effects of clearance and tool states on product quality.

10. Correlate AE results with blanking clearance, tool states and product quality.

1.11 Conclusion

In this study, the circular blanks of 5 mm diameter and 1 mm thickness are to be produced from aluminium sheets using different combinations of punch-die clearance and the state of blanking tools. Punch and die radii are created to study the influence of tool wear on blanking signatures and quality of blanked parts. Different conditions of materials in the form of 'as supplied', annealed, CG and UFG materials are used for comparison. During blanking, punch force-displacement signatures are captured and AE technique is applied to monitor real-time blanking processes.

Various parameters such as the punch-die clearance, punch and die radii and material conditions are considered to influence product quality. The experimental equipment is set-up, which consists of blanking operation tools and data acquisition instrumentation system. Experiments are performed to obtain reliable process signatures, represented by force-displacement curves and the selected AE parameters, to facilitate the monitoring of blanking processes. The trends are observed for the blanking process signatures, which vary steadily according to changing blanking parameters and also correspond to the different quality of the blanks. The results obtained lead to the development of feasible process monitoring of blanking operations using combinations of force-displacement signatures and AE technique.

1.12 The structure of the thesis

The thesis is divided into five chapters related to the project as follows:

Chapter 1: the present chapter contains an introduction to the thesis.

Chapter 2: includes the literature review of blanking, monitoring and control techniques in blanking, description of AE instrumentation, review of process monitoring using AE technique and the theoretical and practical aspects for producing UFG aluminium.

Chapter 3: describes setting-up the equipment, obtaining the materials, which includes the development of UFG aluminium sheets and establishing experimental procedures for blanking experiments.

Chapter 4: presents the results of blanking experiments and the discussion of the findings of the study.

Chapter 5: presents the conclusions and summarises the recommendations for future research.

1.13 References

[1] http://www.makinamuhendisi.com/mechanical/mechanical--engineering-archive/45-Metal-forming.html., 2006.

[2] W. Voelkner, "Present and future developments of metal forming: selected examples," *Journal of Materials Processing Technology*, vol. 106, pp. 236-242, 2000.

[3] K. Lange, "Modern metal forming technology for industrial production," *Journal of Materials Processing Technology*, vol. 71, pp. 2-13, 1997.

[4] R. Balendra and Y. Qin, "Research dedicated to the development of advanced metal-forming technologies," *Journal of Materials Processing Technology*, vol. 145, pp. 144-152, 2004.

[5] R. Kopp, "Some current development trends in metal-forming technology," *Journal of Materials Processing Technology*, vol. 60, pp. 1-4, 1996.

[6] D. Hitz and R. Duggirala, "Future trends in metal forming-equipment, materials and processes in automotive applications," *Journal of Materials Engineering and Performance*, vol. 4, pp. 587-592, 1995.

[7] S. H. Zhang, Z. R. Wang, Z. T. Wang, Y. Xu, and K. B. Chen, "Some new features in the development of metal forming technology," *Journal of Materials Processing Technology*, vol. 151, pp. 39-47, 2004.

[8] A. H. Streppel, W. Klingenberg, and U. P. Singh, "Advances in sheet metal forming applications," *International Journal of Machine Tools and Manufacture*, vol. 48, pp. 483-484, 2008.

[9] S. H. Talbert and B. Avitzur, *Elementary Mechanics of Plastic Flow in Metal Forming*. England: John Wiley & Sons, 1996.

[10] K. Lange, "Handbook of metal forming," K. Pohlandt, P. S. Raghupathi, J. D. Saniter, W. Sauer, J. A. Schey, K. J. Weinmann, and G. E. O. Widera, Eds. USA: McGraw-Hill, 1985.

[11] W. Beitz and K. H. Kuttner, *Handbook of Mechanical Engineering*: Springer Verlag, 1994.

[12] ASM Handbook, *Forming and Forging*, vol. 14: ASM International, American Society for Metals, 1992.

[13] H. Kudo, "An attempt for classification of metal forming operations," *Annals of CIRP*, vol. 29, pp. 469-474, 1980.

[14] ASM Handbook, "Metalworking: Bulk Forming," vol. 14A. Ohio USA: ASM International, 2005.

[15] W. F. Hosford and J. L. Duncan, "Sheet Metal Forming: A Review," *Journal of the Minerals, Metals and Material Society*, vol. 51, pp. 39-44, 1999.

[16] E. M. Mielnik, *Metalworking Science and Engineering*: McGraw-Hill, 1991.

[17] H.-W. Wagener, "New developments in sheet metal forming: sheet materials, tools and machinery," *Journal of Materials Processing Technology*, vol. 72, pp. 342-357, 1997.

[18] R. Pierce, *Sheet metal forming*: Bristol; Philadelphia: Hilger, 1991.

[19] http://www.lft.uni-erlangen.de/SEITEN/SHEMET/.

[20] A. H. Streppel, W. Klingenberg, and U. P. Singh, "Advances in sheet metal forming applications," *International Journal of Machine Tools and Manufacture*, vol. 48, pp. 483-484, 2008.

[21] F. Greban, G. Monteil, and X. Roizard, "Influence of the structure of blanked materials upon the blanking quality of copper alloys," *Journal of Materials Processing Technology*, vol. 186, pp. 27-32, 2007.

[22] H. Kudo, "Towards net-shape forming," *Material processing technology*, vol. 22, pp. 307-342, 1990.

[23] W. Klingenberg and U. P. Singh, "Finite element simulation of the punching/blanking process using in-process characterisation of mild steel," *Journal of Materials Processing Technology*, vol. 134, pp. 296-302, 2003.

[24] K. Kuzman, "Comments on the cold metal forming processes stability control," *Journal of Materials Processing Technology*, vol. 185, pp. 132-138, 2007.

[25] K. Jemielniak and J. Kosmol, "Tool and process monitoring - state of art and future prospects," *Scientific Papers of the Inst. of Mechanical Engineers and Automation of the Technical University of Wroclaw*, Vol. 61, pp. 90-112 1995.

[26] I. Wadi, "The assessment of blanking process characteristics using acoustic emission, sensory fusion and neural networks," in *DMEM*, vol. Phd. Glasgow: University of Strathclyde, 1998.

[27] I. Wadi and R. Balendra, "Using neural network to model the blanking process," *Journal of Materials Processing Technology*, vol. 91, pp. 52-65, 1999.

[28] G. Byrne, D. Dornfeld, I. Inasaki, G. Ketteler, W. Konig, and R. Teti, "Tool Condition Monitoring (TCM) -- The Status of Research and Industrial Application," *CIRP Annals - Manufacturing Technology*, vol. 44, pp. 541-567, 1995.

[29] International Aluminium Institute (IAI): http://www.world-aluminium.org/?pg=statistics, "Aluminium Statistics," 2009.

[30] M. Kleiner, M. Geiger, and A. Klaus, "Manufacturing of lightweight components by metal forming," presented at Annals of the CIRP "Manufacturing Technology" 53rd General Assembly of CIRP, Montreal, Canada, 2003.

[31] A. Rosochowski, W. Presz, L. Olejnik, and M. Richert, "Micro-extrusion of ultra-fine grained aluminium," *The International Journal of Advanced Manufacturing Technology*, vol. 33, pp. 137-146, 2007.

[32] S. Geißdörfer, A. Rosochowski, L. Olejnik, U. Engel, and M. Richert, "Micro-extrusion of ultrafine grained copper," *International Journal of Material Forming*, vol. 1, pp. 455-458, 2008.

[33] G. O'Donnell, P. Young, K. Kelly, and G. Byrne, "Towards the improvement of tool condition monitoring systems in the manufacturing environment," *Journal of Materials Processing Technology*, vol. 119, pp. 133-139, 2001.

[34] A. G. Rehorn, J. Jiang, and P. E. Orban, "State-of-the-art methods and results in tool condition monitoring: a review," *The International Journal of Advanced Manufacturing Technology*, vol. 26, pp. 693-710, 2005.

[35] W. Klingenberg and T. W. de Boer, "Condition-based maintenance in punching/blanking of sheet metal," *International Journal of Machine Tools and Manufacture*, vol. 48, pp. 589-598, 2008.

[36] J. Jeswiet, M. Geiger, U. Engel, M. Kleiner, M. Schikorra, J. Duflou, R. Neugebauer, P. Bariani, and S. Bruschi, "Metal forming progress since 2000," *CIRP Journal of Manufacturing Science and Technology*, vol. 1, pp. 2-17, 2008.

Table 1: Classification of manufacturing processes [10, 11]

Manufacturing Process Classification			
Group	**Types of processes**	**Description of the processes**	**State of material cohesion**
Group I	Primary shaping	Original creation of a shape from molten or gaseous state or from solid particles of undefined shape.	Creation of cohesion
Group II	Metal forming	Converting a given shape of a solid body to another shape without change in mass or material composition.	Maintaining of cohesion
Group III	Separating	Machining or removal of material.	Destruction of cohesion
Group IV	Joining	Uniting of individual workpieces to form subassemblies, filling and impregnating workpieces.	Destruction of cohesion
Group V	Coating	Application of thin layers to a workpiece, example: painting, galvanizing, plastic foil and coating.	Increase of cohesion
Group VI	Changing the material properties	Changing the properties of the workpiece to achieve optimum characteristics, example: diffusion	Increase of cohesion

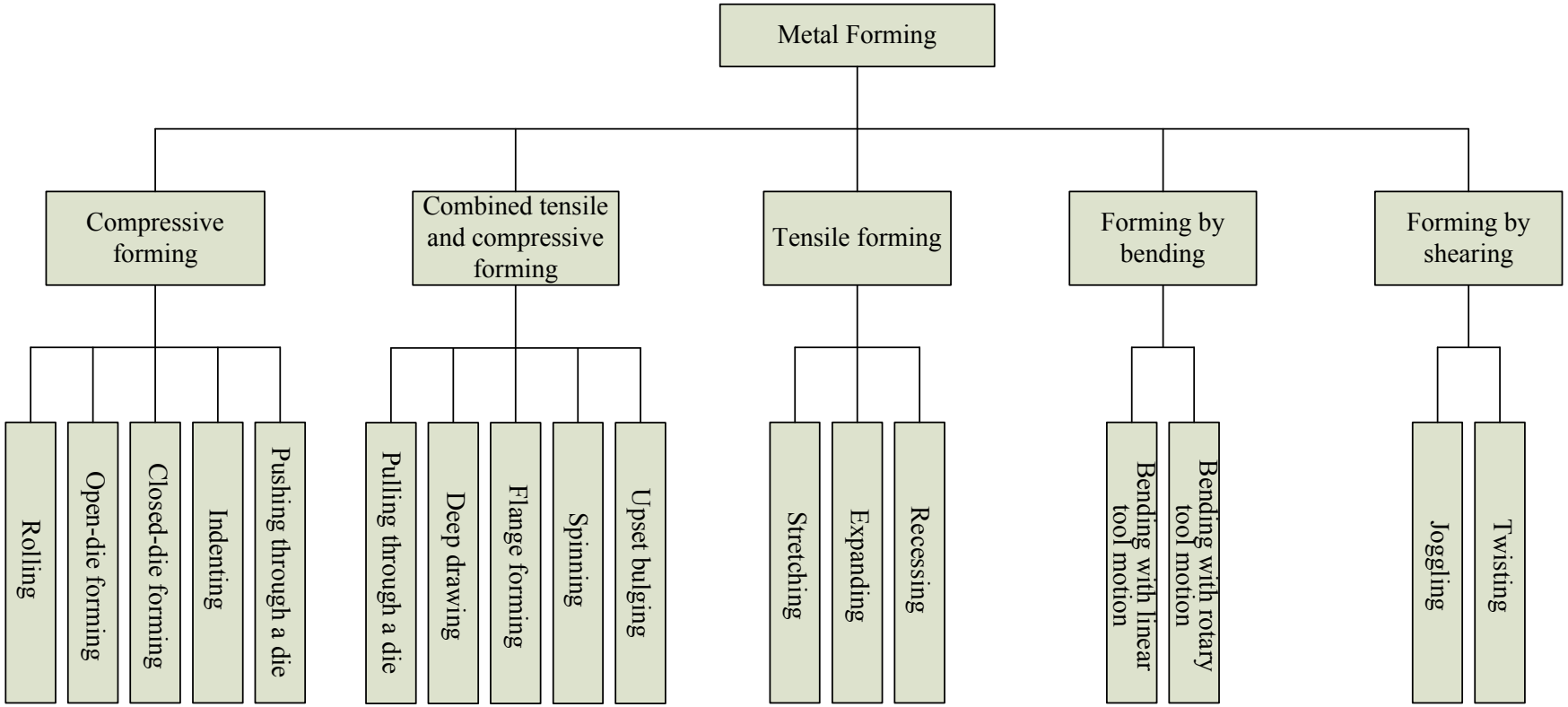

Fig. 1.1: Classification of metal forming into groups and their subgroups according to predominant stresses during deformation [10-14]

Table 1.2: Classification of metal forming processes [16]

Classification of metal forming	
Criteria	**Process description**
According to the type of workpiece	Bulk forming processes – starting material is semifinished shapes, bar; workpiece has small surface to volume ratio; forming causes large changes in shape and cross-section area; elastic recovery is negligible
	Sheet metal forming processes – starting material is rolled sheet; workpiece has large surface to volume ratio; forming causes large changes in surface but small changes in thickness; elastic recovery is significant.
According to the effect of deformation and temperature on mechanical properties	Hot working – dynamic recovery occurs, no strain hardening, deformation temperature range is $>0.5\ T_M$, where T_M = incipient melting temperature
	Warm working – some strain hardening and/or precipitation hardening may occur, deformation temperature range is $0.3< T/T_M<0.5$
	Cold working – e.g. strain hardening occurs, deformation temperature range is $<0.3\ T_M$
According to the mode of deformation	Steady state – e.g. continuous wire drawing
	Non-steady state – e.g. die forging
	Mixed or transitory – e.g. extrusion
According to the system of stresses imposed on the workpiece	Tension
	Shear
	Compression

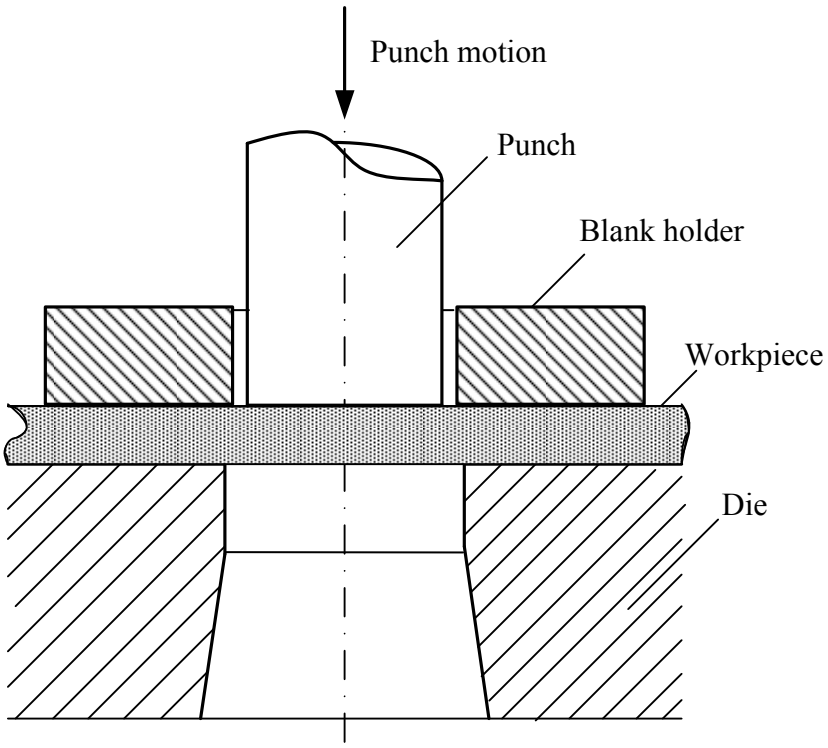

Fig. 1.2: Schematic illustration of blanking tools

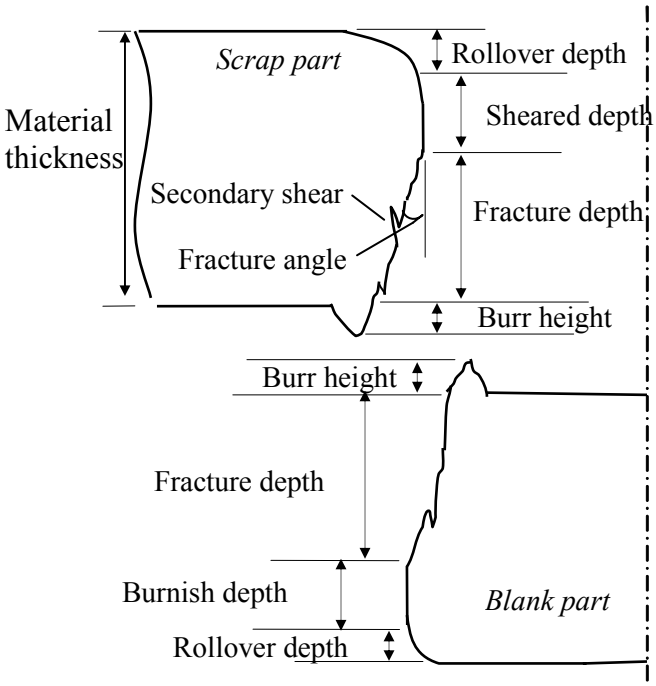

Fig. 1.3: The sheared edge profile of the blanked part

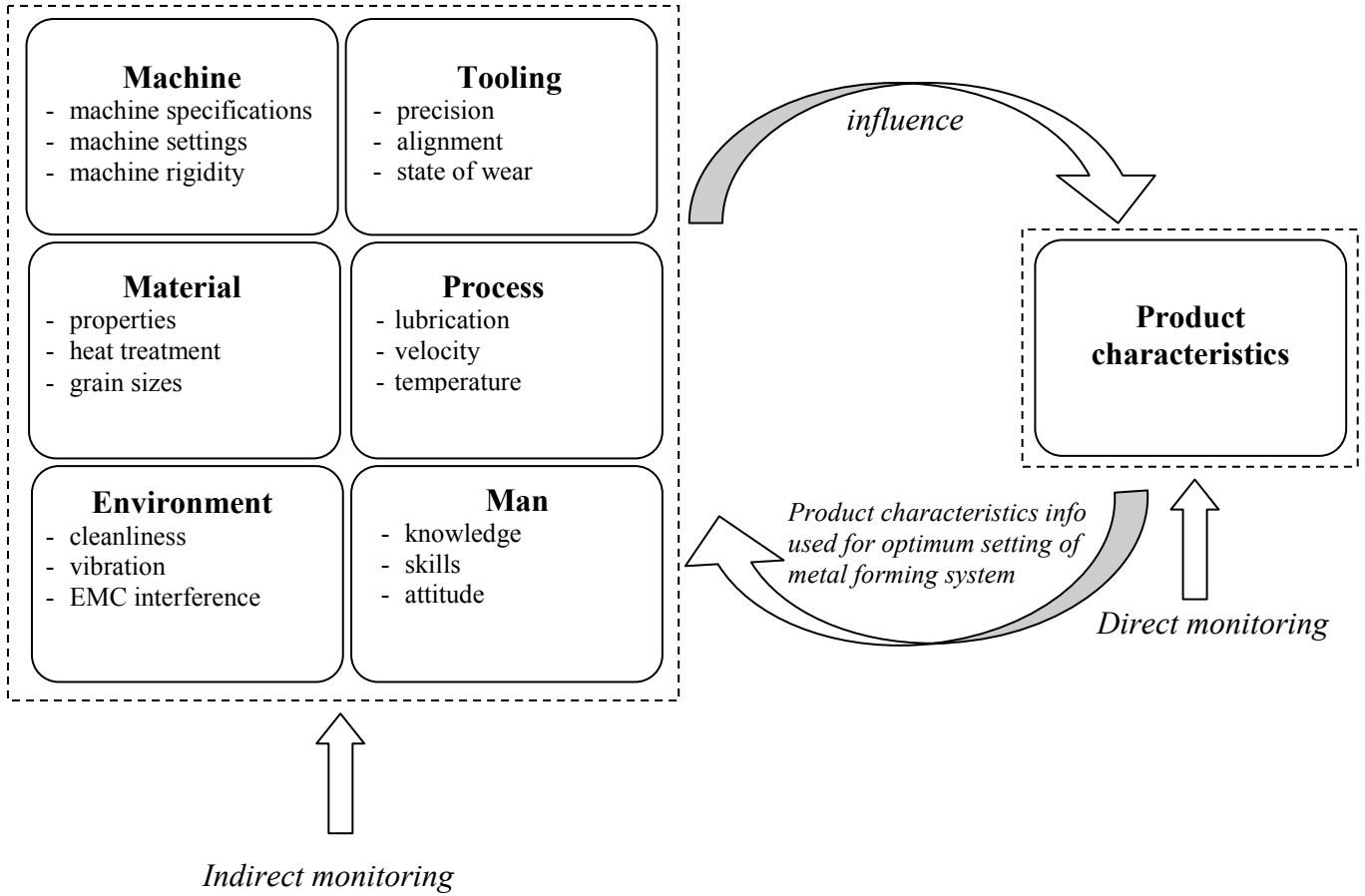

Fig. 1.4: Elements/factors that influence the product quality

CHAPTER 2

LITERATURE REVIEW

This chapter presents the literature review related to the study. It consists of three parts. *Part I* explains the fundamental aspects of blanking operations, blanking process parameters that influence the quality of blanked parts and methods used for process monitoring in metal forming. *Part II* gives the introduction to acoustic emission technique and the use of this technique in monitoring metal forming operations, and *Part III* describes the applications of aluminium materials, the benefits of grain refinement and the theoretical aspects and methods for producing ultra-fined grained metals.

Part I

Blanking operation

2.1 Definition of blanking operation

Sheet metal blanking is fundamentally a constrained shearing operation, whereby the sheet metal is cut to a predetermined contour by subjecting it to shear stresses typically between a punch and a die [1]. The contour is defined by the geometry of the punch and the die. The constrained shearing operations are different from other metal working

processes as the boundary of the deformed material is constrained to a narrow volume of the deformation zone. A gap between the punch and the die (*punch-die clearance*), must be created in order for the shear to occur. This gap or clearance is measured in term of percentage of the material thickness. As a result of shearing, the material experiences transformation that involves elastic deflection, plastic deformation, fracture and total rupture [2]. Atkins [3] demonstrated how the blanking process could be analysed by viewing the deformation of the blank material as essentially a shearing operation.

2.2 Analysis of stages/phases of the blanking process

Blanking involves large deformation followed by fracture in the deformation zone. Consequently, blanking force varies with the punch displacement. To understand details of the process better, it is convenient to divide the blanking process into phases (Fig. 2.1) as explained below:

1. The punch moves toward the workpiece until it comes in contact with the surface of the workpiece. Further movement of the punch will push the material down into the die-opening and cause the process force to rise.

2. As the punch and the die come closer together, the applied force bends the workpiece elastically. The bending moment and the amount of bending of the workpiece depend on the punch-die clearance.

3. The punch indents the material. Stresses in the material become highest at the edges of the punch and the die. As the stress level in these zones reaches the yield point of the

material, the material starts flowing plastically. This can be accomplished by plastic bending.

4. Further movement of the punch causes plastic deformation zones to grow, which eventually leads to linking of these zones into one deformation zone between the cutting edges. The material is strain hardening until the maximum equivalent stress is achieved, indicating shear type of strain localisation.

5. The material starts to fracture by crack initiation propagation. The cracks develop in the vicinity of the cutting edges of the punch and the die. This happens when the fracture criterion is met.

6. When the incipient cracks meet, the material ruptures and the blank part is totally separated from the workpiece. If they do not meet, the material is still not completely separated. In this case, the complete material separation occurs after the punch moves further into the die-opening.

7. The part and the scrap are now separated and the shape of the blank edge is fully developed. The punch moves further to the bottom dead centre *(BDC)* and ejects the blanked part.

8. At *BDC*, the direction of motion is reversed. A stripper or a blank holder has to strip the scrap from the punch. The blanking phases are now fully completed.

2.3 Force-displacement characteristics of blanking operation

The stages of the blanking process can also be characterised using the force-displacement curve of the punch. The typical force-displacement curve for the blanking

process for typical ductile material is shown in Fig. 2.2 [4]. The curve indicates several regions that characterise the blanking phases as explained in section 2.2.

The section (OA) in Fig. 2.2 shows a corresponding straight line in the region where the material experiences elastic bending. However, some materials, depending on their properties, may experience the composition of elastic-plastic bending. The curve (AB) gradually inclines towards the maximum point of blanking force. In this region, stress concentration in the material increases. The material starts to deform once the yield strength of the material is reached. At B, the process attains its maximum force and plastic flow localisation causes the material to deform further without increasing the force (BC). During this stage or as early as plastic deformation occurs, damage initiation or fracture followed by the nucleation and the growth of cracks takes place. The cracks initiated from top and bottom inside the material propagates (CD) until the material ruptures (DEF) leading to the separation of blank from the workpiece material.

2.4 The blanking process parameters

The shearing process in blanking operation is influenced by the following parameters:

1. Punch – die clearance.
2. Punch velocity.
3. Stock material – thickness, mechanical properties, chemical composition, microstructure/grain size.
4. Lubrication.

5. Cutting tools – material, cutting edge geometry.

6. Alignment of the tools, and

7. Strain rate – the strain rate sensitivity of the material influences the punch speed.

Browne and Battikha [5] stated that in addition to the above parameters, other factors that affect the quality of the blanks include the punch and die radii, heat treatment of the tooling and the blank holding force. However, the clearance has a major influence upon the shape and quality of sheared edge. Various experimental studies [6-8] identified that the dimension and geometrical aspects of the blanked edge are affected primarily by the blanking clearance, wear state of the tools, and the thickness of the sheet.

Die clearance is the difference in size between the punch dimension and the die dimension (Fig. 2.3). Usually, it is quoted as clearance per side and expressed as percentage of the sheet thickness:

$$C = 100 \frac{(D_d - D_p)}{2t} (\%)$$

where D_d, D_p and t are the die diameter, the punch diameter and the sheet thickness respectively.

Many experimental researches had concluded that thicker material requires larger clearance, but the smaller the clearance the better the quality of the sheared edge. Large clearance makes the sheet to be pulled into the gap and causes the blank edge becoming rougher and the burnish zone becomes larger. In addition, the burnish zone on the

blanked edge increases with increasing ductility of the material. The burr height increases with increasing clearance and material ductility. The wear of the tools, due to one of the effects of insufficient clearance, contribute significantly to burr formation of the blank. As a rule of thumb, the clearance changes according to the thickness and tensile strength of the material sheet. The benefits of proper die clearance and the drawbacks of insufficient and excessive die clearance are summarised in Table 2.1 [9-12].

Early research work involving blanking operations concentrated on experimental research to understand the influence of the clearance on the quality of the blanks and the study of the maximum blanking force and the energy required. Since the early 1950s, research activity in this area increased significantly and in addition to research on the blanking clearance, the profile of tools had also been studied. Large number of experiments on fine blanking and high speed blanking had been conducted. Since the advent of computers and engineering software in the mid 1970s, research activities on blanking have experienced transformation from mainly experimental into numerical. The new modelling and simulation techniques tremendously contributed to further understanding of blanking [13, 14].

Fang et al. [15] stated that the punch and die clearance is the most important of blanking parameters that influence the quality of the finished parts. The proper selection of the clearance will influence the tool life, the blanking force, the stripper force and the

dimensional precision. He also proved that, an increase in the clearance causes some decrease in the blanking force. The blanking force decreases for only about 6% when the clearances are increased from 0% to 20%.

The first reports concerned with the shearing of metals were published in the early 1900s [16]. The main issue at this time was to predict the maximum force and energy needed to accomplish the shearing operation, which led to enhancement in tooling design. The blanking force for the parallel cutting edges can be estimated from the following equation [1, 17]:

$$F = Lt\,\tau_m = 0.7Lt\ (UTS)$$

where, L = the total length sheared (perimeter of hole),

t = thickness of material,

τ_m= shear strength of material, and

UTS = the ultimate tensile strength of the material

The estimated minimum force F_p, required for the press to perform blanking is given by $F_p = 1.3\ F$.

Tekiner et al. [18] carried out experiments on aluminium sheet to examine the interaction between material thickness, clearance, burr height, diameter of punch and the punch force. He concluded that, for the increasing clearance, the rollover depth is increased and the smooth sheared zone is decreased. On the other hand, decreasing the

clearance causes the smooth sheared edge zone increase with the punch force is increased. Blanking with smaller clearance and higher force may also reduce tool life.

During the blanking process, the punch and die wear out, which leads to a progressive modification of their geometry. This wear process is initiated by interfacial adhesive junctions that form in the contact zone and causes the cutting edges to become rounded [1, 19, 20]. Fig. 2.4 shows the wear profile of the punch. The small radius on the punch or the die, resulting from wear would enable deeper punch penetration, promote material flow in the constrained shearing zone, delay fracture initiation and hence produce greater desirable smooth surface on the blank edge [21]. However, tool radii increase the burr height [22] and cause an increase in maximum blanking force [23]. Hernández et al. [24] analysed the effects of tool wear and proposed to use a new parameter, known as 'effective clearance' to study form errors in the blanking products. Effective clearance is the sum of setting clearance and additional clearance due to the increase in the distance between punch and die cutting edges caused by tool wear during the process.

Hambli [25] used design of experiment based analysis to study the effects of the interaction between the tool wear, the punch-die clearance and the sheet thickness on the variation of the blanking force and the geometry of the blanked edge. The optimum clearance of 10% had been identified as the one minimising the blanking force. The process was less sensitive to changes in tool wear and sheet thickness. However, setting the clearance at 5% minimised the fracture angle and the fracture depth.

The influence of blanking speed on produced blanks had been investigated empirically. It showed that, with a higher blanking speed, the deformation became more concentrated, which was claimed to result in better quality of the blanked product [26]. On the other hand, higher blanking velocities caused the process force and the energy consumed to be increased [27]. Further, Goijaerts et al. [28] established that the blanking velocity of up to 10 mm/s, which is considered within the range of nearly every industrial blanking application has no influence on the punch displacement at ductile fracture initiation and thus, has no effect on the quality of the blanks. Sasada et al. [29] investigated the coefficient of friction between tool and material in the blanking processes. The results confirmed that the punch speed and clearance had little influence on the coefficient of friction.

Gréban et al. [30] investigated the influence of the composition and work hardening upon the blanking quality of copper alloys used as lead frame ('skeleton' of the IC package of electronic component, providing mechanical support to the die during its assembly into a finished part). Five copper alloys of different compositions had been blanked and the results showed that the material composition has a little influence on length of sheared and fracture zone. They also found that increasing work hardening results in larger fracture zone.

With the increase of computational capabilities and software advancement, simulations and modelling have been used extensively for analysis and design of forming processes

to avoid the long and expensive experimental tryout procedures and also to help manufacturing designers to better understand metal forming processes. Due to the presence of large deformation, ductile fracture and crack propagation, research using the finite element (FEM) simulation of blanking is a difficult task. Despite this, it has been carried extensively and numerous pertinent references are available in the literature. FEM simulations allow many aspects of blanking processes to be analysed in detail under various parameters [31-33].

Hambli [34] presented a method of burr height prediction in sheet metal blanking processes using the numerical analysis and artificial neural network modelling. The models had provided fast and accurate prediction and contributed towards the future development of an online monitoring system of burr height evolution during the blanking processes. Brokken et al. [35] performed numerical modelling of the blanking process to predict geometrical properties such as burr, sheared and fractured zone, and the roll-over shape. The model appeared to be capable of handling a large and localised deformations occurring during blanking operations. Hatanaka [22] performed simulation of the blank edge formation process in blanking of sheet metals. He found that the burr height increase linearly with respect to the radius of the tool edge.

Maiti et al. [36] analysed the influence of process parameters such as tool clearance, coefficient of friction, material thickness and diameter of punch and die on blanking of thin sheet of mild steel using FEM analysis. The results indicated that blanking

characteristics for small components had a very similar trend to that of blanking of large size components. The blanking load decreased with increasing the clearance. The blanking load increased as the friction coefficient was increased at the tool-workpiece interfaces. To evaluate the variations of blanking load for different size of blanks, the sheet thickness was kept constant while the punch diameter was changed. The results indicated that the blanking load decreases as the blank diameter decreases.

The quality of the blanking products is also affected by ductile fracture in shear band between the punch and the die. The size of the fracture zone and burr are the most important quality parameters. Yu et al. [37] performed the FEM simulation with ductile fracture criterion for blank geometry such as burr size, sheared surface and fractured surface to investigate the influence of punch-die clearance and die radius for blanking processes. The results of simulation show that if the die radius becomes bigger, the fracture near die edge appears later and the burr height on scrap is also increased. Shim et al. [38] had investigated the blanking operation of thin sheet aluminium and copper foil. The increase in punch-die corner radius caused an increase in the burr height and the punch penetration before crack initiation. The decrease in punch-die radius produced a narrow effective sheared surface and caused early crack initiation.

Faura et al. [39] developed a decision support system, which could help in proper selection of the main blanking process parameters, based on a technical-economic model. The well-established optimisation criteria provided by industry were gathered

into a database and computed to estimate the necessary parameters needed. It permits the selection of individual parameters and the use of previously established optimisation criteria.

Hambli [40] developed a software code called 'BLANKSOFT' for sheet metal forming processes, used to predict the geometry of the blanked profile, hardening state of the blanked edge, the burr height, the force-penetration curve, and the characteristics of punch wear versus the number of blanking cycles. The results indicated a good correlation between the simulation and the experimental work. The program was useful with the proposed of decision support system, capable of shortening the process design cycles and optimising the process conditions.

Hambli and Guerin [41] presented a method for optimum clearance prediction in a sheet metal blanking process using an artificial neural network (ANN) and finite element modelling including damage and fracture simulation. The results obtained permitted the graph of optimum clearance to be plotted versus material elongation. It can be observed also that the optimum clearance decreases with increasing material ductility. The proposed method that combined ANN and finite element can contribute towards the development of optimisation of sheet metal forming blanking process.

Wadi [42] applied ANN to model the blanking process for predicting the blanking parameters such as material hardness, clearance and punch-die radii. Sensory fusion

which involved force/displacement sensor, AE sensor and vibration sensor were used to acquire the respective signals and the features from these signals were fed as inputs to neural network models. Results also showed that the signals from the vibration sensor were less sensitive to the variations of blanking parameters. The sensor configuration would facilitate the on-line monitoring and control system for blanking operation.

2.5 Formation of the blank edge profile

One of the most important factors that determine the quality of the blank is the geometrical forms produced at blank edges which; these are rollover, sheared zone, fractured zone and burr (Fig. 1.2). The rough fracture surfaces on the edges are related to fracture propagation path, and the smooth or burnished surfaces are due to the contact and rubbing of the sheared edges against the wall surfaces of the punch and die.

Typically, rollover develops by plastic deformation of the workpiece as the punch touches the surface of the material, and then pushes the material downward to draw into the die. As the punch moves to penetrate the material, it shears the upper part of the edge and the material becomes locked as compression of the material against the wall of the die opening, creating a burnish zone of a portion of the blank edge. As the punch continues its stroke, fracture occurs at an angle resulting from the punch-die clearance. Since the fracture cracks initiate from the sides of the punch and the die, a burr is created in the blank and scrap. The burnish dimension of the hole of the scrap corresponds approximately to the punch dimension, and the burnish dimension of the blank

corresponds closely to the die dimension. Therefore, the punch diameter determines the size of the hole of the scrap, and the die diameter determines the size of the blank.

An ideal blank is created when the parallel cracks generated from the top and bottom of the workpiece are in alignment with each other [43]. This results in a minimum blanking force and forms a good quality edge. In this condition, optimum clearance has been obtained and has led to an extended tool life. The formation of the blank edge profile, which is influenced by various factors is summarised in Table 2.2.

2.6 Process monitoring and control in metal blanking/forming

Previous work shows that it is possible to detect tool wear and other important aspects of the blanking process from monitoring force-displacement signature. However, interpreting these signals is not an easy task due to a large number of uncontrolled variables in blanking. Wadi and Balendra [44] outlined the current difficulties in achieving the effective monitoring and control in blanking. Among the factors causing these difficulties are the complexity of the signals led to difficulty of interpretation, limitations of the use of the force-displacement signatures and influence of tools set-up and blanking press characteristics on process parameters.

Kligenberg and Boar [45] reviewed the techniques for condition-based maintenance in punching and blanking of sheet metal. The strategy for monitoring and control of metal forming processes has to be integrated and implemented throughout the whole system in

order to obtain comprehensive and optimum results. The requirements are placed not only on tooling system but also on press machine itself. It is essential to monitor the dynamic behaviour of the press because the complex interaction of dynamic effects of the press and the tooling system may dramatically influence the quality of the produced parts [46]. For the past decades, methods for monitoring the forming presses had been performed using maximum force monitoring. If the change in maximum force is detected, it means that the conditions of process variables have changed, and the part quality may also be affected [47].

When monitoring the tooling, force signature analysis is a method widely used to characterise the metal forming processes. The technique not only can provide overload protection to the system but it can also produce real-time feedback for continuous process control, preserve tooling as well as improve the product quality. In blanking, the force or load signature contains useful information about the process condition. The load monitor over a cycle of punch stroke showing the different phases and conditions of the blanking process can be a signature of the process [48]. Each blanking with selected combinations of controlled parameters, results in unique features of a force-displacement curve. A typical force-displacement curve for blanking operation is as shown in Fig. 2.2. The process signature that corresponds to a good quality part is taken as a reference signal. Using the load monitoring system, the force signal is continuously monitored throughout the forming operation and compared to the reference signal to detect a possible change in the force signature. Such change means that the quality of the parts is

affected and thus requires intervention to the system to limit the number of reject parts. Despite the capability to determine the normal and abnormal process conditions, this type of process monitoring approach cannot identify the root causes of the problems when an abnormal condition is detected.

A number of researches have been reported, which used force signals to monitor the forming operation. Breitling et al. [48] studied the use of in-die sensors in process control in punching and blanking. Mahayotsanun et al. [49] had integrated a draw-in sensor and an array of force sensor under sheet metal tooling surface for the online monitoring of stamping operation. Other types of monitoring signals include proximity signal, optical signal, and acceleration signal. However, the challenging issues are encountered at the stage of processing these signals. Some of them limit the capability for further interpretation the information extracted from the signal to identify different conditions of the process due to the low signal-to-noise ratio (SNR) of the signal captured during the process. In many cases the signals tend to be polluted by surrounding random electrical noises and they are also very sensitive to various operating factors such as sensor mounting location, die geometry, workpiece material properties and dimensions, punch speed, adhesive chemical and static electricity. Thus, it is essential to use signal processing techniques to analyse these signals, which also known as feature extraction techniques such as principle component analysis [47] bispectral analysis [50] and other methods that comprehensively discussed in literature.

The fundamental concept for controlling the product quality focuses on the ability to control the material flow into die cavity during a sheet forming process in order to produce parts of good quality. Research in the area of control of sheet metal forming has been largely focused on varying blankholder force [51] and drawbead restraining force [52]. These types of process variables can be actively controlled during the forming process and can be incorporated within a real-time control system. However, the disadvantage of drawbeads is that they severely deform the passing sheet metal, which may result in surface damage or tearing of the sheet.

Siegert et al. [53] developed a closed loop control system, which uses the friction force as control parameter and the blank holder force as feedback for controlling a deep drawing process. Nonetheless, such a system has limited capability to produce parts of complex shape and geometry. Pahl [54] tried to overcome this problem by introducing a multi-point-control system consisting of a hydraulic press, a multiple cylinder unit for the blankholding function and flexible forming elements such as punch drive used to produce difficult parts in deep drawing operation.

Garcia [55] developed a successful system applying artificial intelligence (AI) for automatic supervision, diagnosis and control in sheet metal forming processes. Recently Argandoña et al. [56, 57] also have exploited AI techniques to develop an advanced monitoring and control system in metal forming. The system combines fuzzy logic and expert system techniques, which are linked to two monitoring systems installed in a

mechanical press dedicated to the manufacturing of small retaining rings. The monitoring systems include a force and AE sensor based system and an artificial vision system. This type of monitoring and control system is able to provide feedback to the operator of the machine about the possible errors occurring during the process, and is capable of giving advice on how to correct and prevent the faults [57].

Part II

Acoustic emission technique

2.7 Definition of acoustic emission

It has been recognised over many years that when a solid material is subjected to stress at certain levels, discrete transient acoustic waves are generated in it. The phenomenon of sound generation in materials under stress is termed as acoustic emission (AE); other terms found in literature are stress wave emission [58], micro-seismic activity or microseismic emission.

According to the American Society for Testing and Materials (ASTM) Standard, *"Acoustic emission is the class of phenomena whereby transient elastic waves are generated by the rapid release of energy from a localised source or sources within a*

material, or the transient elastic wave(s) so generated" [59]. In simple terms to describe the mechanical events, it can be said that an AE is a sound wave or a stress wave that travels through a material as the result of some sudden release of strain energy.

2.8 Sources of acoustic emission

AE is produced by material during the changes of its condition [60]. Examples of the change of condition in materials are fractures, crack formation, crack growth, metallurgical changes such as plastic deformation, phase transformation, friction and in various processes of deformation and transformation of materials. The changes of condition in materials are usually due to thermal and mechanical effects. These effects will induce stress, which should be at a sufficiently high level in the material in order for AE to be generated as a series of pulses [61].

Early studies of AE performed by Kaiser demonstrate that the AE is an irreversible phenomenon. He showed that the materials under load in the elastic regime emit acoustic waves only after a primary load level is exceeded. This particular behaviour is known as *"Kaiser Effect"* [62] and it is defined as the absence of detectable AE at a fixed sensitivity level, until previously applied stress levels are exceeded. On the other hand, the presence of detectable AE at a fixed sensitivity level with stress levels below those previously applied is defined as *"Felicity Effect"* [63]. If the Kaiser Effect is permanent for a tested material then it is very little or unlikely that AE will be recorded before the previous maximum stress level is reached. However, beyond the previous

maximum value, the existing damage may continuously propagate or a new damage may initiate, both of which can potentially produce AE.

When a material or a structure is subjected to a load, a part of the deformation energy can be released in the form of sudden elastic waves (AE) that propagate on the surface of the materials. Various sources of AE during forming are due to plastic deformation that results in grain boundary sliding, crack initiation and crack growth, and from external factors such as mechanical impacts, friction and machinery vibration. However, due to the fact that the source of AE is an event inside the body, in many cases it is difficult to relate the actual source of such event or identify the responsible mechanism. Assumptions in such cases have to be proven by detail observation and signal analysis.

AE waves do not travel through air but only through a solid material [64]. They can be detected at the surface of the material. Most materials such as steels, cast iron, aluminium, glasses, fibre as well as concrete and ceramic materials exhibit acoustic energy when stressed. The amount of AE energy released depends primarily on the size and speed of the local deformation process in metal. The formation and movement of a single dislocation does produce an AE stress wave but it is very weak signal. However, when large number of dislocations are forming and moving at the same time, the individual stress waves overlap and superimpose leading to a detectable signal. Korchevskii [65] found that intensity of AE depends on the properties of the metal being investigated, the form and stiffness of the testing machine, the rate of displacement of

loading, and the geometrical dimensions and shape of the samples being tested. Also the amount of AE wave attenuation depends on the properties of material. Attenuation is greater in porous material such as wood and visco-elastic materials than in metallic materials [66].

2.9 Types of acoustic emission

The AE signal frequency can be categorised and usually includes all internal sources of sound that are localised spatially, and lie within the normal bandwidth for AE detection, which is above 20 kHz [67]. Two types of AE signal exist, and these are described as transient or *'burst'* that is giving sudden rise of ultrasonic energy, and *'continuous'* signal, which mostly result from the superposition of large numbers of overlapping discrete transient events. Burst signals are usually generated from crack initiation and those appearing as continuous signals are due to plastic deformation occurring in ductile materials. Fig. 2.5 shows the burst and continuous AE signal.

2.10 Advantage of acoustic emission

AE is a passive testing method, which requires no external excitation of the object under investigation, thus causing little disturbance to the object. It is a dynamic method capable of continuously and in-situ monitoring without the need of intervention to the process or shutting down the operation. Another advantage of using AE is that the frequency range of AE is much higher than that of machine vibration and environmental noise.

2.11 Acoustic emission parameters

A typical an AE hit event is as shown in Fig. 2.6. The fundamental parameters of AE are the peak amplitude, event duration, rise time, energy and count. Detailed definitions of these AE parameters are enclosed in Appendix 1. The threshold voltage, also shown in Fig. 2.6, is selected to differentiate between the unwanted signals (noise) and the actual detectable AE signals.

2.12 Acoustic emission instrumentation

The basic acoustic emission instrumentation consists of a transducer or sensor, a signal conditioning unit (e.g. amplifier), data acquisition (DAQ) hardware and a PC with AE software. DAQ hardware is often represented by a DAQ board, plugged into a PC. It incorporates filters, amplifiers, analogue to digital converters (ADC), digital to analogue converters (DAC), threshold detectors, counters and other signal processing elements. Fig. 2.7 shows the block diagram of the blanking monitoring system used in this work, which consists of the blanking equipment and DAQ instrumentation.

2.13 Acoustic emission sensor

The AE wave travels from the source through the material, and can be detected by piezoelectric transducer (e.g. PZT-5). The sensor is excited by the AE waves impinging on its face and it sends electrical signal to a nearby preamplifier and then to the signal processing equipment. The sensor should be placed or mounted on or at the surface of the material to ensure proper signal coupling. The frequency range of the sensor should

be as high as 1 MHz. The high frequency is used to achieve an effective discrimination against background noise. Other types of transducer also used to capture AE wave are capacitive (e.g. microphone) and optical (e.g. interferometer) transducers, but they are not widely used because of relatively insensitive when compared to piezoelectric types in nature.

Typically, AE wave is in the frequency range of ultrasound, usually between 20 kHz to 1 MHz. These high frequencies do not propagate well over a long distance. In real environment, the AE signal is usually contaminated by unwanted signals, which adversely affect the process of extraction the information from the signal. The lower frequency limit is usually imposed by noises such as from friction or process generated signal itself that superimpose and mask the original AE signal. The upper frequency limit is usually imposed by attenuation, hence limiting the range for AE detection. Due to these reasons, it is usual to choose the wide band or resonant types of AE transducers. Resonant type transducers are only sensitive to a certain frequency range. Therefore, selecting the suitable frequency range for AE detection and signal processing is a critical part in the AE application process. Transducers for process monitoring must meet the following requirements [64]:

(a) Measurement point as close to the event point as possible.

(b) No reduction in the static and dynamic stiffness of the machine tool caused by transducer.

(c) No restriction of working space and cutting parameters.

(d) Wear free and maintenance free, easy to change and low cost.

(e) Resistant to lubricant, dirt, mechanical, electromagnetic and thermal influence.

(f) Function independent of tool or workpiece.

(g) Reliable signal transmission.

In order to achieve the ultimate sensitivity of the sensor, it must be attached to the material under test in such a manner that the acoustic energy passes into the sensor with minimum loss at the sensor-material interface. The required intimate mechanical contact is achieved on flat surfaces using recommended AE couplants such as thin films of grease, oil or epoxy adhesive between the sensor and the material surfaces. Li and Nordlund [68] investigated that liquid-based couplants are better than metal foils as acoustic couplants and they found that the coupling condition is one of the most important factors influencing the transmissibility of the signals.

2.14 Preamplifier

In many cases, the acoustic signals from the transducer can be very weak. A preamplifier with a selectable gain of usually 20/40/60 dB is required to capture the signal and amplify for the next filtering and processing stages. It must be capable to provide effective impedance matching and sufficient gain to drive the signal down a cable and to allow the subsequent signal processing equipment to detect the level of acoustic background noise in the system. The preamplifier is connected closely after the

transducer to minimise the noise interference and prevent signal losses. Sometimes, the preamplifier is produced as a built in unit integrated with the transducer.

2.15 Signal conditioning module

The function of signal conditioning module is to improve the quality of the acquired signal. The process at this stage includes the secondary amplification, filtering and isolation. The amplification boosts the level of the signal so that it is more detectable and better matches the range of measurement of other devices. Filtering is essential to reject a certain unwanted noise within a certain frequency range. A filter may be incorporated in both the preamplifier and AE board. It is essential to eliminate low frequency mechanical and electromagnetic noise at this stage. This can be achieved using a high pass or a band pass filter in the range of 100 kHz to 1 MHz. Isolation can prevent some of measurement problems related to improper grounding of the system.

Noise problems are of great importance and precautions against interfering noise are an integral part of AE technology. The primary measure against noise is the selection of an appropriate frequency range for AE monitoring. Other noise reduction measures include to stopping noise at the source, eliminating noise by applying impedance mismatch barriers and imposing proper techniques of grounding and shielding.

2.16 Data acquisition hardware

The function of DAQ board is to measure, process, store, and generate the desired signals as required and compatible with the software program to be used. In order for a computer to read and measure certain signals, the real world analogue signals have to be converted to digital signals. Therefore, a typical DAQ board contains an analogue-digital converter (ADC), digital input/output channels, parametric channels and also includes counter and timer.

2.17 Computer and AE software

A PC and software are used to display and analyse the collected data. As today's computer technology continuously improves, the DAQ system can fully utilise the PC's enhanced capabilities. The data transfer capabilities of a PC can affect the maximum speed at which the data is acquired continuously. Therefore, it is recommended to use a high-end type of PC with a high speed processor. With the emerging new features, the high speed PC is capable of programmed I/O and includes the ability of interrupt data transfer. In addition, Direct Memory Access (DMA) transfers increase the system throughput by using dedicated hardware facilities to transfer data directly into system memory. This can avoid the processor to be slow down by reducing its loading, and thus providing the ability to transfer data as fast as possible.

2.18 Acoustic emission monitoring in metal blanking/forming

AE differs from most other non-destructing test (NDT) methods in two main aspects. The first one is that the measured signal has its origin in the material itself, which means that the signal is not affected by external sources. This is also known as a passive test. Secondly, AE can detect the dynamic movement inside a material's structure, while other NDT methods detect existing geometric discontinuities or cracks in the normal material structure. Dornfield [69] produced a comprehensive review of applications of the AE sensing techniques in manufacturing process. He analysed the potential of AE application in manufacturing by referring to existing applications since the application of first process monitoring in the 1970s.

Research in the area of AE monitoring in metal forming processes has largely focused on tool condition monitoring (TCM) [70-74] because tools are always subjected to wear problems, which consequently affect the quality of the parts produced by metal forming operations. Short tool life increases the frequency of tool changing, which causes material and energy waste and ultimately economical inefficiency.

Little work has been done to apply AE techniques in monitoring blanking operation. Despite the method had gained various degree of success in various applications in machining processes, only a few attempts had been reported to use AE technique for monitoring blanking. Lee et al. [75] discussed the difficulties that make AE technique for monitoring the blanking operations becoming more complex than those used for

machining processes. In addition to those difficulties, less attention was given to developing the monitoring system for blanking, as a primary process due to the fact that the stringent quality control is usually implemented in secondary processes. However, in the production of precision and small parts by blanking operations, the blanks are becoming final products. Therefore, process monitoring in blanking is vital to meet the demand for high miniature quality products such as those used in microsystems.

AE monitoring is one of the most effective methods for process monitoring [76]. The advantage of using AE monitoring lies in two aspects: its frequency range is much higher than that of machine vibrations and environmental noise, so that the refined signals with relatively low interference can easily be obtained by applying an appropriate high-pass filter to original AE signals, and the sampling process does not interfere with blanking operations and hence makes condition monitoring possible. Wadley and Mehrabian [77] reviewed the potential of AE used in material processing. They highlighted the contribution the AE methods might make toward in-process monitoring and microstructure control during metals processing.

Jayakumar et al. [78] reviewed the application of AE techniques for monitoring of forming and grinding processes. The characteristics of the AE signals generated during forming processes depend on the following factors:

1. Properties of the material – hardness, strength and toughness.
2. The experimental conditions – strain rate, temperature and lubrication.

3. The nature of the AE source mechanism – plastic deformation, fracture and friction.

Skåre et al. [79] conducted experiments using both manufacturing machines and friction tests in laboratory. These showed that the behaviour of two materials in contact and in relative motion can be supervised with acoustic emission. Highest AE signals result from galling, stick-slip and also from cracking. Increased contact between two friction surfaces and increased relative speed of the surfaces result in increased AE signals.

Recent application of AE in sheet metal forming was reported by Kim [80] in his work on the sheet metal punch pressing monitoring. The AE signals emanating from the processes were used to characterise three stages of material deformation: the initial contact of the tool and the surface of the workpiece, shear fracture and sudden rupture of the blank. The process signatures, in terms of a specific AE parameter known as AE counts, were obtained to correlate with the process variables such as material hardness, material thickness and tool wear.

Mardapittas et al. [81] measured an AE wave generated during blanking of steel for a different sheet thickness and different punch speed. The AE waves were classified into impact, shear and fracture waves. It was also found that the maximum AE energy was associated with the fracture wave. The peak amplitude of the AE wave and its energy were dependant on strain-rate. Further, this peak amplitude was also influenced by the

sheet thickness, press velocity and material hardness. Papirov et al. [82] had found that AE is extremely weak at the outset of deformation of superplastic material Zn-0.4% Al alloy and that the signal was virtually absent during superplastic flow. However, a significant increase in AE occurred with increasing grain size or strain rate, when the alloy is non-superplastic.

Liang and Donfield [83] had applied AE technique in their study to monitor the punch stretching to deform sheet. The AE signals were used to characterise the forming process consisting of three stages: punch-workpiece contact and initial yielding, plastic deformation and fracture and post fracture punch-workpiece interaction. Hao et al. [84] reported that AE can be used to monitor an initial stage of deformation in cup drawing. However, the results of monitoring the final stage were doubtful because the AE signal was very weak. Kong and Nahavandi [85] used force and AE signals to monitor the tool condition in forging processes. Wadi and Balendra [86] had attempted to use neural networks to model the blanking processes by extracting the AE signal features and force-displacement characteristics and linking these with the blanking parameters.

Part III

Developing ultra-fine grained aluminium

2.19 Introduction

Aluminium is the world's second most used metal after steel and it was first used commercially for cookware. It is said to be the metal of choice for leading architects and engineers, who are looking for a material, which combines functionality and cost effectiveness with futuristic potential. Nowadays, aluminium has been used in various applications such as packaging, conductors in electrical power transmission, car bodies and modern aircraft constructions. With the remarkable properties such as low density, lack of toxicity, corrosion resistance and good electrical conductivity, aluminium is in great demand in the world market [87]. In the field of micromanufacturing [88], aluminium and its alloys are used to manufacture microparts taking advantages of their features of the material such as lightweight and the ability to be easily formed into shapes. Thus, the use of aluminium in such applications has contributed to the economical wealth and environmental harmony.

Aluminium and its alloys are commonly produced in the form of coarse grained materials in which the grain sizes are in sub-milimeter range. However, there is a growing interest in recent years to use aluminium and its alloy with grain size in the tens to several hundreds of nanometer range. This is due to the knowledge that the refinement

of the traditional polycrystalline metals, generally below 1 μm can lead to a significant improvement of their mechanical, electrical, thermal and other properties. Research [89, 90] had found that refining the coarse grained structure of the material has resulted in increasing its strength. This is why these materials, known as nanostructured materials [91] or nanometals, are nowadays attracting much attention for researchers as promising materials for various applications. Currently, these types of material are used in sputtering targets for physical vapour deposition, artificial organs for medical implant and in aerospace industry. There were also attempts [92, 93] to use this material as one of the solutions for size effects in micro parts production.

With reference to the achievable grain size, there are three categories of metals: coarse grained (CG), ultra-fined grained (UFG) and nanocrystalline (NC) metals. Sometimes a distinction is made when referring UFG and NC metals. Typical polycrystalline metals have CG of tens to several hundreds of microns, UFG metal have 0.1 to 1μm and grain sizes smaller than 0.1 μm can be found in NC metals [94-97].

2.20 Grain refinement

Grain size is one of the important aspects in processing metals and alloys because properties of metallic materials are grain size sensitive. This is explained by the best known effect, represented by Hall-Petch [98, 99] relationship given by the equation below:

$\sigma_o = \sigma_i + \frac{K}{\sqrt{d}}$, where K is a constant, d is the mean grain size, σ_o and σ_i is the yield stress and friction stress opposing dislocation motion of deformed polycrystalline metals, respectively. At room temperature, the yields stress of metallic materials increases with the decreasing grain size.

Traditional mechanisms of plastic deformation determine the deformation of CG polycrystalline metals, which grain sizes greater than 1000 nm. Intensive strain hardening occurs to the metal during this phase. When the grain sizes are refined in the range of 1000 nm down to 30 nm, disordered grain boundaries start to dominate the mechanical behaviour of UFG metal. During this phase, little work hardening occurs. For grain size less than 30 nm at NC regimes, the atomic sliding at grain boundaries increases. This leads to virtually no further work hardening of the deformed metal. From these facts, one can conclude that, employing metal forming can only possible to produce UFG metal, not even approaching NC regimes.

UFG metals exhibit exceptionally high strength and reduced, but reasonably ductility. A higher volume fraction of grain boundaries and the strain hardening resulting from the increased dislocation density make UFG metals much stronger compared to their CG annealed metals. Recently, increasing strength-ductility was obtained in pure metal such as titanium, Ti, when deformed at cryogenic temperature. At lower temperature, UFG metals also exhibit fracture toughness and the grain boundary sliding causes UFG metals

to have excellent superplastic behaviour. Compared to their CG counterparts, other improved properties include higher diffusivity, higher electrical resistance, increased specific heat capacity, lower thermal conductivity and improved magnetic properties.

Various methods have been employed for fabricating UFG and nanomaterials. However, these can be split into two categories of methods. The first category uses a *"bottom-up"* approach, in which bulk nanostructured materials are assembled from individual atoms or from nanoscale building blocks such as nano-particles as precursor to form nanocrystalline materials. The techniques employed in this category are such as inert gas condensation [100], electrodeposition [101], chemical [102] and physical deposition [103]. However, this approach has several disadvantages because the process is fairly complex. It is difficult to remove all residual porosity at grain boundaries, which results in low ductility. The procedure is also limited to the fabrication of relatively small specimens, which restricts their commercial use.

The second method is called a *"top-down"* approach [104], in which existing CG materials are processed to produce substantial microstructured grain refinement and possibly a nanostructure. Two common methods are SPD and classical thermomechanical processes such as mechanical milling [105] and shot-peening [106]. However, SPD technique is most popular as it is characterised by lack of porosity as well as provides an opportunity to produce relatively large samples.

SPD methods take the advantage of the ability of the crystals within metals and alloys to subdivide into very small-scale domains as small as 100 nm when they are subjected to large plastic strain. Before the techniques of SPD have been employed, grain refinement of metals and alloys has been mainly achieved by conventional plastic working technique and subsequent annealing processes, which resulted in recrystallisation by nucleation and growth (discontinuous recrystallisation). The minimum grain size achieved through this procedure has been about 10 μm and the corresponding logarithmic (true) plastic strain (ε) of 1.06 – 1.86. On the other hand, using SPD, the materials are subjected to deformation at a very large plastic strain, usually above 3 in term of true or logarithmic strain. Refining CG metals to smaller grain sizes using thermomechanical process is also difficult and expensive. This process can only be produced in several specific alloys and requires a precisely control processing routes. Thus, the production is very slow and is not suitable to incorporate into mass production. The limitations of thermomechanical processing can be overcome by introducing SPD processes. The processes are potential for formation of sub-micrometer sized grains.

2.21 Severe plastic deformation

Specifically, SPD is the metal forming processes that is used to convert CG into UFG metals and alloys. Various published literature [107-114] explained the techniques used to produce small grains in metals by applying a large level of plastic strain to the former coarse grain metals. In all cases, these were SPD techniques. The typical value of plastic strain in SPD is greater than 3.0, which is more than in conventional metal forming

processes such as rolling and extrusion that have a plastic strain, generally less than 2.0. In addition to large plastic deformation, SPD is characterised by the fact that there is no substantial change in the initial shape and dimensions of the processed samples.

SPD can create grains with submicrometer sizes. The actual mechanism responsible for this effect is still under investigation. So far, it is believed that the grain refinement results from the non-uniform distribution of dislocations, which tend to form cell structures within the original coarse grains. Some other investigation revealed that short and long range intersecting shear bands produced by SPD processes play a major role at grain subdivision and local dynamic recovery and recrystallisation processes contribute to grain refinement [115]. The average grain size that SPD can produce, depend on the material used and SPD parameters such as strain, temperature and pressure.

Two categories of SPD processes have been widely conducted: *batch and continuous SPD processes*. Batch processing represents a more traditional and laboratory based approach, which normally means that small billets are produced on a small scale. This, of course limits their commercialisation prospect. Recently, the trend has been moving toward continuous SPD processes with a view to increasing the productivity. This resulted in large sizes of billets, continuous length stock and was aiming for the ECAP large-scale industrial production. Batch processing includes high pressure torsion (HPT), multi-axial forging (MF) and some other less popular process. While continuous

processes include accumulative roll–bonding (ARB), con-shearing process and ECAP-conform.

2.22 Equal channel angular pressing

The principle of equal channel angular pressing (ECAP), also known as equal channel angular extrusion (ECAE), schematically shown in Fig. 2.8 was invented by Segal et al. in 1977 [116-120].It is a batch SPD process that is based on severely straining a material by simple shear, which is taking place in a die at the intersection of two connected equal channels. As a result, the sample that emerges from one of the channels after ECAP maintains its approximate dimensions and the grain sizes are changed from coarse to very fine. Further developments of producing ultra-fine grained material using this method have been continued by Valiev et al. since 1990s [121]. He had established that the ECAP technique is capable to produce truly bulk, fully dense and contamination free materials with submicron to nanoscale grain sizes.

Three important parameters of ECAP involve: (a) ECAP routes, (b) the angle of the intersecting channels, ϕ and (c) the angle of outer curvature of the channel die, Ψ. The equivalent or effective strain imposed on the sample in every ECAP passage is given by the equation proposed by Iwashi et al. [117] below:

$$\varepsilon = \frac{1}{\sqrt{2}}\left[2\cot\left(\frac{\phi}{2}+\frac{\psi}{2}\right)+\psi\cos ec\left(\frac{\phi}{2}+\frac{\psi}{2}\right)\right]$$

where ϕ and Ψ refer to the respective angles as shown in Fig. 2.8. For a die having an intersecting channel ϕ = 90° and a sharp outer corner of the channel (Ψ = 0°), the imposed strain in each ECAP passage is calculated as 1. The strain can be accumulated to achieve the required value by repeating the process in the same die using different routes between consecutive ECAP passes. Repeating and changing the sample billet orientation after each pass, thereby modifying the shear plane and shear direction, makes it possible to control the microstructure and texture of the material, thus altering the mechanical properties [122]. Furukawa et al. [123] investigated the shearing characteristics for several different pressing and rotation modes. They discovered that certain ECAP processing routes such as route B_C had more influence than other routes on the development of a uniform microstructure of equiaxed grains in UFG materials.

In practice, four different routes have been introduced: (a) Route A, the sample is pressed repetitively without rotation of the sample about the its-axis, (b) Route B_A, the sample is rotated through 90° in alternate direction between each pass, (c) Route B_C, the sample is rotated by 90° in the same direction between each pass, and (d) Route C, the sample is rotated by 180° between each pass. Fig. 2.9 shows schematically the different processing routes in ECAP. Langdon et al. [124] concluded that route B_C is the best processing route for obtaining homogenous microstructure of equiaxed grains separated by high angle grain boundaries which results in better grain refinement.

ECAP has become the most frequently used process compared to other SPD processes due to its low force requirement and the resulting low tool pressure. This, together with the simple tool geometry makes the laboratory set up cheaper and less complicated. In addition, Langdon [125] had outlined other advantages that make the ECAP to be an attractive technique for commercialisation. However, the ECAP technique in its conventional design has several limitations. In particular, the length of the sample is limited; due to the aspect ratio (length/diameter) needing to be smaller than a critical value to prevent the sample from bend during the pressing, and the press ram has a limited travel distance. Thus the ECAP process is a discontinuous process, low production efficiency and increased operation cost.

Further, a significant amount of material near the end of the sample, which contains non-uniform microstructure or macro-cracks, has to be cut off. This leads to a significant portion of material to be wasted, thus increases the cost of the UFG material produced by ECAP. Therefore intensive efforts had been put on ECAP to overcome its limitations. ECAP has experienced further developments particularly modifications and alterations to the die design to improve its processing conditions and performance.

With a view to improving productivity, a two-turn, S-shape [126, 127] channel was developed to reduce the number of passes that are required for a one-turn ECAP channel. The S-shape channel is equivalent to two passes performed in a one-turn ECAP with 180° sample rotation between the passes. A multi-turn ECAP also known as three

dimensional ECAP (3D-ECAP) [128], was also introduced, which enabled 90° rotation to be realised inside the die. The latest development of ECAP was continued by introduction of the new SPD process called Incremental ECAP (I-ECAP) [129]. I-ECAP enables very long billets to be processed by decoupling the feeding stage and the deformation stage of the process. More details conventional and developed ECAP processes had been discussed by Azushima et al. [130, 131].

2.23 Other SPD methods

2.23.1 Accumulative roll-bonding

Accumulative roll-bonding (ARB) process was first proposed by Saito et al. [132] in 1998. Fig. 2.10 shows the schematic illustration of ARB. Basically, ARB process involves the repetition process of cutting, stacking and rolling the sheet metals. First, the sheet is cut into equal dimension and placed stacking on top of another. The interfaces of the two sheets are subjected to surface treatment such as degreasing and wire-brushing to enhance the bonding strength before stacking. The quality of the bonding will determine the final success of the process. This can be achieved by increasing the rolling temperature (at elevated temperature) but below recrystallisation temperature to avoid grain growth, which cancels the accumulated strain. The two layers of material are joined together after passing the rolling process. Then the length of the material is sectioned into two halves.

The sequence of the processes can be repeated to accumulate the strain to a desire level. As a result significant grain structure refinement can be achieved. The strain after n cycles of the ARB process is given by the following equation:

$\varepsilon = n\frac{2}{\sqrt{3}}\ln\left(\frac{T}{t}\right)$, where T is the initial thickness of the stacked material sheets, t is the thickness after roll-bonding and n is the number of deformation passes.

Deformation during rolling is strongly affected by friction between the rolls and the sheet metal that gives rise to shearing at the surfaces of the rolled sheets [133]. The process is also usually performed without lubricant to strengthen bonding, so that large shear strains are distributed into the surface regions at each pass. Nonetheless, ARB is not considered a true continuous process due to several intermediate operations involved and the manageable sheet size. Its performance depends critically on the quality of the bond between multiple layers of the sheets, which may not be easy to achieve.

2.23.2 High pressure torsion

High pressure torsion (HPT) was first investigated by Bridgeman in 1952 [134]. Further development on HPT was continued by Valiev since 1997 [97]. Fig. 2.11 shows the schematic diagram of HPT process. The process involves pressing a thin disk of a material between two punches and simultaneously rotating one of the punches. The friction between the sample and the punches ensures sufficient torque provided for large

deformation of the material to occur, thus providing very high strains. The equivalent strain can be calculated given by the classical expression as:

$\varepsilon = \frac{\tan \gamma}{\sqrt{3}}$, where γ is the shear angle as shown in Fig.2.11.

The punches are required to provide high pressure on the disk to avoid the material slippage and to prevent fracture due to large plastic deformation, which the high pressure is one of the disadvantages from the processing point of view.

It has been reported that processing by HPT produces materials with extraordinary small grain sizes [135] and the possibility to process brittle materials. Previous experiments on processing pure Ti and Ti-based alloys using HPT method produced average grain sizes of ~30 nm [136]. However, little attention has been given to the potential for grain refinement method using HPT as less publication has been reported on this topic compared to ECAP. At present, the work on HPT is suitable for experimental and theoretical studies. The possible reasons for this deficiency are: (i) There are relatively few facilities including machine, tools and dies for HPT available in laboratories world-wide, (ii) The samples produced by HPT are in the small form of a thin circular disks, which are not easy to prepare samples for subsequent tensile testing to verify the mechanical properties, (iii) The imposed strain during deformation varies across the radius of the disk, therefore it is reasonably to anticipate that the microstructure evolution are not evenly distributed causing structural non-homogeneity of the samples

and (iv) The production is rather slow and low volume of the samples, therefore it is difficult to gain interest from industries.

2.23.3 Cyclic extrusion compression

The principle of the cyclic extrusion compression (CEC) process, schematically shown in Fig. 2.12 was developed by Korbel et al. [137] in 1979. In this process, the sample is contained within a chamber and then alternately extruded forwards and backwards. Through the repetitions process of extrusion inside the chamber, a large strain of deformation is induced, which after n passes the accumulated equivalent strain is approximately given by:

$\varepsilon = 4n\ln\left(\frac{D}{d}\right)$, where D is the chamber diameter, d the channel diameter and n is the number of deformation passes.

Due to high hydrostatic pressure generated from the process, which can reach up to 4 GPa, the structure and the materials of the tools to sustain sufficient strength is becoming an issue. Therefore, the CEC is usually used to process soft materials such as aluminium alloys. Further, reducing the size of the samples or decreasing the material yield stress by carrying out the process at an elevated temperature were among the counter measures taken in reducing the maximum tools pressure in CEC process.

2.23.4 The repetitive corrugation and straightening

The repetitive corrugation and straightening (RCS) process was developed by Zhu et al. in 2001 [138, 139]. The schematic diagram of the process is shown in Fig. 2.13. RCS involves the processes of bending a straight billet with corrugated tools and then restoring the straight shape of the billet with flat tools. By repeating the processes, a large strain and structural changes can be induced in the material while maintaining its initial shape. The equivalent strain per one complete operation is given by:

$\varepsilon = 4\ln\frac{[(r+t)/(r+0.5t)]}{\sqrt{3}}$, where t is the thickness of sample and r is the curvature of bent zone.

Previous experiment [138] showed that the maximum strain introduced into the work piece during corrugation was about 20%, which is much lower than the plastic strain per ECAP pass. Further, the formation of fatigue cracks limits the number of RCS cycles that can be applied to a work-piece. With reference to its operations, RCS also does not apply simple shear, which is considered the most appropriate mode of SPD process.

2.24 References

[1] S. Kalpakjian, *Manufacturing engineering and technology*. USA: Addison-Wesley, 1989.

[2] W. Beitz and K.-H. kuttner, *Handbook of Mechanical Engineering*: Springer-verlag, 1994.

[3] A. G. Atkins, "On cropping and related processes," *International Journal of Mechanical Sciences*, vol. 22, pp. 215-231, 1980.

[4] E. M. Mielnik, *Metakworking science and engineering*. New York: McGraw-Hill, c1991.

[5] D. J. Browne and E. Battikha, "Optimisation of aluminium sheet forming using flexible die," *Jounal of Material Processing Technology*, vol. 55, pp. 218-223, 1995.

[6] C. M. Choy, "An investigation of parameters influencing constrained shearing (blanking)," in *DMEM*, vol. PhD. Glasgow: University of Strathclyde, 1997.

[7] W. Klingenberg and U. P. Singh, "Design and optimisation of punching/blanking systems aided by experimental modelling," *International Journal of Vehicle Design*, vol. 39, pp. 125 - 139, 2005.

[8] R. Hambli and A. Potiron, "Finite element modeling of sheet-metal blanking operations with experimental verification," *Journal of Materials Processing Technology*, vol. 102, pp. 257-265, 2000.

[9] S. L. SemiatinChairmanCommittee, "Metal Handbook," in *Forming and Forging*, vol. 14, A. H. Committee, Ed. USA: ASM International, 1988.

[10] SMEAmericanSocietyofToolEngineers, "Die design handbook: a practical reference book on process analysis, product design, metal movements, materials, and proved die designs for every class of sheet-metal pressworking." USA: McGraw-Hill, 1965.

[11] H. W. Pollack, *Tool design*, 2nd ed. Englewood Cliffs, N.J.: Prentice-Hall, 1988.

[12] D. F. R. Eary, *Techniques of pressworking sheet metal: an engineering approach to die design*: Staples Press, 1960.

[13] M. Tisza, "Numerical modelling and simulation in sheet metal forming," *Journal of Materials Processing Technology*, vol. 151, pp. 58-62, 2004.

[14] A. E. Tekkaya, "State-of-the-art of simulation of sheet metal forming," *Journal of Materials Processing Technology*, vol. 103, pp. 14-22, 2000.

[15] G. Fang, P. Zeng, and L. Lou, "Finite element simulation of the effect of clearance on the forming quality in the blanking process," *Journal of Materials Processing Technology*, vol. 122, pp. 249-254, 2002.

[16] S. F. Golovashchenko, "A study on trimming of aluminum autobody sheet and development of a new robust process eliminating burrs and slivers," *International Journal of Mechanical Sciences*, vol. 48, pp. 1384-1400, 2006.

[17] V. Boljanovic, *Sheet metal forming processes and die design*: Industrial Press, 2004.

[18] Z. Tekiner, M. Nalbant, and H. Gurun, "An experimental study for the effect of different clearances on burr, smooth-sheared and blanking force on aluminium sheet metal," *Materials & Design*, vol. 27, pp. 1134-1138, 2006.

[19] K. Lange, "Handbook of metal forming," K. Pohlandt, P. S. Raghupathi, J. D. Saniter, W. Sauer, J. A. Schey, K. J. Weinmann, and G. E. O. Widera, Eds. USA: McGraw-Hill, 1985.

[20] S.Y.Luo, "Effect of the geometry and the surface treatment of punching tools on the tool life and wear conditions in the piercing of thick steel plate," *Jounal of Material Processing Technology*, pp. 122-133, 1999.

[21] C. M. Choy and R. Balendra, "Simulation of the effects of tool geometry changes on blanking operations," presented at Proceeding of the 9th International Cold Forging Congress, Solihull, UK, 1995.

[22] N. Hatanaka, K. Yamaguchi, N. Takakura, and T. Iizuka, "Simulation of sheared edge formation process in blanking of sheet metals," *Journal of Materials Processing Technology*, vol. 140, pp. 628-634, 2003.

[23] J. Slomp and W. Klingenberg, "A proposal to use artificial neural networks for process control of punching/blanking operations," in *Flexible Automation and Intelligent Manufacturing*. Toronto, Canada, 2004.

[24] J. J. Hernandez, P. Franco, M. Estrems, and F. Faura, "Modelling and experimental analysis of the effects of tool wear on form errors in stainless steel blanking," *Journal of Materials Processing Technology*, vol. 180, pp. 143-150, 2006.

[25] R. Hambli, "Design of Experiment Based Analysis for Sheet Metal Blanking Processes Optimisation," *The International Journal of Advanced Manufacturing Technology*, vol. 19, pp. 403-410, 2002.

[26] R. Tilsley and F. Howard, "Recent investigations into the blanking and piercing of sheet materials," *Machinery*, vol. 93, pp. pp. 151-158, 1958.

[27] W. Johnson and R. A. C. Slatter, "A survey of the slow and fast blanking of metals at ambient and high temperatures," presented at Intenational conference of manufacturing technology, Michigan, 1967.

[28] A. M. Goijaerts, L. E. Govaert, and F. P. T. Baaijens, "Experimental and numerical investigation on the influence of process speed on the blanking process," *Manufacturing science and engineering*, vol. 124, pp. 416-419, 2002.

[29] M. Sasada, K. Shimura, and I. Aoki, "Coefficient of friction between tool and material in shearing," *JSME International Journal*, vol. 49, pp. pp. 1171-1178, 2006.

[30] F. Greban, G. Monteil, and X. Roizard, "Influence of the structure of blanked materials upon the blanking quality of copper alloys," *Journal of Materials Processing Technology*, vol. 186, pp. 27-32, 2007.

[31] D. Brokken, W. A. M. Brekelmans, and F. P. T. Baaijens, "Predicting the shape of blanked products: a finite element approach," *Journal of Materials Processing Technology*, vol. 103, pp. 51-56, 2000.

[32] T. Pyttel, R. John, and M. Hoogen, "A finite element based model for the description of aluminium sheet blanking," *International Journal of Machine Tools and Manufacture*, vol. 40, pp. 1993-2002, 2000.

[33] M. Rachik, J. M. Roelandt, and A. Maillard, "Some phenomenological and computational aspects of sheet metal blanking simulation," *Journal of Materials Processing Technology*, vol. 128, pp. 256-265, 2002.

[34] R. Hambli, "Finite element model fracture prediction during sheet-metal blanking processes," *Engineering Fracture Mechanics*, vol. 68, pp. 365-378, 2000.

[35] D. Brokken, W. A. M. Brekelmans, and F. P. T. Baaijens, "Numerical modelling of the metal blanking process," *Journal of Materials Processing Technology*, vol. 83, pp. 192-199, 1998.

[36] S. K. Maiti, A. A. Ambekar, U. P. Singh, P. P. Date, and K. Narasimhan, "Assessment of influence of some process parameters on sheet metal blanking," *Journal of Materials Processing Technology*, vol. 102, pp. 249-256, 2000.

[37] S. Yu, X. Xie, J. Zhang, and Z. Zhao, "Ductile fracture modeling of initiation and propagation in sheet-metal blanking processes," *Journal of Materials Processing Technology*, vol. 187-188, pp. 169-172, 2007.

[38] K. H. Shim, S. K. Lee, B. S. Kang, and S. M. Hwang, "Investigation on blanking of thin sheet metal using the ductile fracture criterion and its experimental verification," *Journal of Materials Processing Technology*, vol. 155-156, pp. 1935, 2004.

[39] F. Faura, M. A. Sebastian, and R. Zamora, "A decision support system for sheet metal blanking process parameters selection," *Journal of Materials Processing Technology*, vol. 118, pp. 371-376, 2001.

[40] R. Hambli, "BLANKSOFT: a code for sheet metal blanking processes optimization," *Journal of Materials Processing Technology*, vol. 141, pp. 234-242, 2003.

[41] R. Hambli and F. Guerin, "Application of a neural network for optimum clearance prediction in sheet metal blanking processes," *Finite Elements in Analysis and Design*, vol. 39, pp. 1039-1052, 2003.

[42] I. Wadi, "The assessment of blanking process characteristics using acoustic emission, sensory fusion and neural networks," in *DMEM*, vol. Phd. Glasgow: University of Strathclyde, 1998.

[43] R. Hambli, S. Richir, P. Crubleau, and B. Taravel, "Prediction of optimum clearance in sheet metal blanking processes," *International Journal of Advanced Manufacturing Technology*, pp. 20-25, 2003.

[44] I. Wadi and R. Balendra, "An intelligent approach to monitor and control the blanking process," *Advances in Engineering Software*, vol. 30, pp. 85-92, 1999.

[45] W. Klingenberg and T. W. de Boer, "Condition-based maintenance in punching/blanking of sheet metal," *International Journal of Machine Tools and Manufacture*, vol. 48, pp. 589-598, 2008.

[46] J. Breitling, D. Wallace, and T. Altan, "Investigations of different loading conditions in a high speed mechanical press," *Journal of Materials Processing Technology*, vol. 59, pp. 18-23, 1996.

[47] J. Jin and J. Shi, "Diagnostic feature extraction from stamping tonnage signals based on design of experiments," *Transactions of the ASME, Journal of Manufacturing Science and Engineering*, vol. 122, pp. 360–369, 2000.

[48] J. Breitling, B. Pfeiffer, T. Altan, and K. Siegert, "Process control in blanking," *Journal of Materials Processing Technology*, vol. 71, pp. 187-192, 1997.

[49] N. Mahayotsanun, J. Cao, M. Peshkin, S. sah, R. Gao, and C. T. Wang, "Integrated sensing system for stamping monitoring control," in *IEEE Sensors*, 2007.

[50] G. C. Zhang, M. Ge, H. Tong, Y. Xu, and R. Du, "Bispectral analysis for on-line monitoring of stamping operation," *Engineering Applications of Artificial Intelligence*, vol. 15, pp. 97-104, 2002.

[51] M. A. Ahmetoglu, T. Altan, and G. L. Kinzel, "Improvement of part quality in stamping by controlling blank-holder force and pressure," *Journal of Materials Processing Technology*, vol. 33, pp. 195-214, 1992.

[52] E. J. Obermeyer and S. A. Majlessi, "A review of recent advances in the application of blank-holder force towards improving the forming limits of sheet metal parts," *Journal of Materials Processing Technology*, vol. 75, pp. 222-234, 1998.

[53] K. Siegert, M. Ziegler, and S. Wagner, "Closed loop control of the friction force. Deep drawing process," *Journal of Materials Processing Technology*, vol. 71, pp. 126-133, 1997.

[54] K.-J. Pahl, "New developments in multi-point die-cushion technology," *Journal of Materials Processing Technology*, vol. 71, pp. 168-173, 1997.

[55] C. Garcia, "Artificial intelligence applied to automatic supervision, diagnosis and control in sheet metal stamping processes," *Journal of Materials Processing Technology*, vol. 164-165, pp. 1351-1357, 2005.

[56] E. Sáenz de Argandoña, A. Aztiria, C. García, N. Arana, A. Izaguirre, and P. Fillatreau, "Forming processes control by means of artificial intelligence techniques," *Robotics and Computer-Integrated Manufacturing*, vol. 24, pp. 773-779, 2008.

[57] P. Fillatreau, F. X. Bernard, A. Aztiria, E. S. de Argandoña, C. García, N. Arana, and A. Izaguirre, "Sheet metal forming global control system based on artificial vision system and force-acoustic sensors," *Robotics and Computer-Integrated Manufacturing*, vol. In Press, Corrected Proof.

[58] R. V. William, *Acoustic Emission*. Bristol UK: Adam Hilger Ltd., 1980.

[59] Annual Book of ASTM Standards, *Nondestructive testing, Section 3: Metals test methods and analytical procedures, E610-89a, Standard Terminology Relating to Acoustic Emission*, 1990.

[60] K. G. Boving, *NDE handbook: Non-destructive Examination Methods for Condition Monitoring*. UK: Butterworths-Heinemann Ltd., 1989.

[61] R. Halmshaw, *Non-destructive Testing (Metallurgy & Materials Science)*, Second ed. London: Edward Arnold, 1991.

[62] P. V. Venkitakrishnan, P. P. Sinha, and R. Krishnamurthy, "Study and analysis of residual stresses due to various secondary processes in AA 2219 annealed sheet using acoustic emission and hole drilling methods," *NDT & E International*, vol. 38, pp. 615-622, 2005.

[63] M. Levy, H. E. Bass, and R. R. Stern, "Modern acoustical techniques for the measurement of mechanical properties," in *Experimental methods in the physical sciences*, vol. 39. San Diego: Academic Press, 2001.

[64] G. Byrne, D. Dornfeld, I. Inasaki, G. Ketteler, W. Konig, and R. Teti, "Tool Condition Monitoring (TCM) -- The Status of Research and Industrial Application," *CIRP Annals - Manufacturing Technology*, vol. 44, pp. 541-567, 1995.

[65] V. V. Korchevskii, "Acoustic Measurements: Measurement of the parameters of the acoustic emission when metals are stretched," *Journal of Measurement Techniques*, vol. 49, pp. 517-523, 2006.

[66] S. Kawamoto and R. S. Williams, "Acoustic emission and acousto-ultrasonic techniques for wood and wood-based composites - A review," United States Department of Agriculture, Madison FPL-GTR-134, 2002.

[67] C. B. Scruby, "An introduction to acoustic emission," *Journal of Physics E: Scientific Instruments*, vol. 20, pp. 946-953, 1987.

[68] C. Li and E. Nordlund, "Effects of couplants on acoustic transmission," *Rock Mechanics and Rock Engineering*, vol. 26, pp. 63-69, 1993.

[69] D. Dornfeld, "Application of acoustic emission techniques in manufacturing," *NDT & E International*, vol. 25, pp. 259-269, 1992.

[70] I. Inasaki, "Application of acoustic emission sensor for monitoring machining processes," *Ultrasonics*, vol. 36, pp. 273-281, 1998.

[71] J. J. Liu and D. A. Donfield, "Modelling and analysis of acoustic emission in diamond turning," presented at ASME Winter Annual Meeting 58, 1992.

[72] K. N. Lou and C. T. Lee, "Intelligent on-line tool monitoring system in milling processes," presented at Proceedings IEEE International Conference, Man Cybern., 1995.

[73] J. M. Lee, D. K. Choi, and C. N. Chu, "Real time tool breakage monitoring for NC turning and drilling," *CIRP Annual*, pp. 81-84, 1994.

[74] H. K. Tonshoff, M. Jung, S. Mannel, and W. Rietz, "Using acoustic emission signals for monitoring of production processes," *Ultrasonics*, vol. 37, pp. 681-686, 2000.

[75] W. B. Lee, C. F. Cheung, W. M. Chiu, and L. K. Chan, "Automatic supervision of blanking tool wear using pattern recognition analysis," *International Journal of Machinery and Tools Manufacture*, vol. 37, pp. 1079-1095, 1997.

[76] W. Sachse, K. Yamaguchi, and J. Roget, "Acoustic emission: Current practice and future direction," ASTM Special Technical Publication, 1991.

[77] H. N. G. Wadley and R. Mehrabian, "Acoustic emission for material processing: a review," *Journal of Materials Science and Engineering*, vol. 65, pp. 245-263, 1983.

[78] T. Jayakumar, C. K. Mukhopadhyay, S. Venugopal, S. L. Mannan, and B. Raj, "A review of the application of acoustic emission techniques for monitoring forming and grinding processes," *Journal of Materials Processing Technology*, vol. 159, pp. 48-61, 2005.

[79] T. Skåre, P. Thilderkvist, and J.-E. Ståhl, "Monitoring of friction processes by the means of acoustic emission measurements--deep drawing of sheet metal," *Journal of Materials Processing Technology*, vol. 80-81, pp. 263-272, 1998.

[80] B. S. Kim, "Punch press monitoring with acoustic emission (AE). Part I. Signal characterization and stock hardness effects," *ASME Engineering material technology*, pp. 295-300, 1983.

[81] A. S. Mardapittas and Y. H. J. Au, "Blanking process characterisation using acoustic emission," presented at COMADEM 89, Kogan Page, 1989.

[82] I. I. Papirov, E. S. Karpov, M. I. Palatnik, and M. B. Mileshkin, "Acoustic emission during plastic and superplastic deformation of a Zn-0.4% Al alloy," *Jounal of Metal Science and Heat Treatment*, vol. 26, pp. 887-891, 1984.

[83] S. Y. Liang and D. A. Donfield, "Punch stretching process monitoring using acoustic emission signal. Analysis - Part I: basic characteristics," *Acoustic emission*, vol. 6, pp. 29-36, 1978.

[84] S. Hao, S. Ramalingam, and B. E. Klamecki, "Acoustic emission monitoring of sheet metal forming: characterization of the transducer, the work material and the process," *Journal of Materials Processing Technology*, vol. 101, pp. 124-136, 2000.

[85] L. X. Kong and S. Nahavandi, "On-line tool condition monitoring and control system in forging processes," *Journal of Materials Processing Technology*, vol. 125-126, pp. 464-470, 2002.

[86] I. Wadi and R. Balendra, "Using neural networks to model the blanking process," *Journal of Materials Processing Technology*, vol. 91, pp. 52-65, 1999.

[87] M. Kleiner, M. Geiger, and A. Klaus, "Manufacturing of Lightweight Components by Metal Forming," *CIRP Annals - Manufacturing Technology*, vol. 52, pp. 521-542, 2003.

[88] A. B. Frazier, R. O. Warrington, and C. Friedrich, "The Miniatirization Technologies; Past, Present, and Future," *IEEE Transaction on Industrial Electronics*, vol. 42, pp. 423-430, 1995.

[89] Y. Prokhazka, "Means of increasing the yield strength of metals and alloys," *Metal Science and Heat Treatment*, vol. 15, pp. 905-911, 1973.

[90] J. W. M. Jr., "The influence of grain size on the mechanical properties of steel," presented at International Symposium on Ultrafine Grained Steels Iron and Steel Institute of Japan, Tokyo, 2001.

[91] C. C. Koh, "Nanostructured materials: processing, properties and applications," in *Material Science and Process Technology Series*, G. M. Guire, Ed., 2 ed. Raleigh, North Carolina: William Andrew, 2006.

[92] A. Rosochowski, W. Presz, L. Olejnik, and M. Richert, "Micro-extrusion of ultra-fine grained aluminium," *The International Journal of Advanced Manufacturing Technology*, vol. 33, pp. 137-146, 2007.

[93] L. Olejnik, W. Presz, and A. Rosochowski, "Backward extrusion using micro-blanked aluminium sheet," *International Journal of Material Forming*, vol. 2, pp. 617-620, 2009.

[94] R. Z. Valiev, Y. Estrin, Z. Horita, T. G. Landon, M. J. Zehetbauer, and Y.T. Zhu, "Producing Bulk Ultrafine-grained materials by Severe Plastic Deformation," *Journal of Minerals, Metals and Materials Society*, vol. 58, pp. 33-39, 2006.

[95] X. Zhang, H. Wang, and C. C. Koch, "Mechanical Behaviour of Bulk Ultra-fine Grained and Nanocrystalline Zn," *Review of Advance Material Science*, vol. 6, pp. 53-93, 2004.

[96] C. C. Koch, "Optimization of strength and ductility in nanocrystalline and ultrafine grained metals," *Scripta Materialia*, vol. 49, pp. 657-662, 2003.

[97] R. Z. Valiev, R. K. Islamgaliev, and I. V. Alexandrov, "Bulk Nanostructured Materials from Severe Plastic Deformation," *Prog. Materials Science*, vol. 45, pp. 103-189, 2000.

[98] E. O. Hall, "The deformation and ageing of mild steel," *Proceedings of the Physical Society*, vol. B, pp. 747-753, 1951.

[99] N. J. Petch, "The cleavage strength of polycrystals," *Journal of Iron Steel Institute*, pp. 25-28, 1953.

[100] G. E. Fougere, J. R. Weertman, and R. W. Siegel, "Processing and mechanical behavior of nanocrystalline Fe," *Nanostructured Materials*, vol. 5, pp. 127-134, 1995.

[101] A. M. El-Sherik and U. Erb, "Synthesis of bulk nanocrystalline nickel by pulsed electrodeposition," *Journal of Materials Science*, vol. 30, pp. 5743-5749, 1995.

[102] C. N. He, N. Q. Zhao, C. S. Shi, and S. Z. Song, "Fabrication of carbon nanomaterials by chemical vapor deposition," *Journal of Alloys and Compounds*, vol. 484, pp. 6-11, 2009.

[103] G. Cao, *Nanostructures & nanomaterials: Synthesis, properties and applications*: Imperial College Press, 2004.

[104] T. Langdon, "The processing of ultrafine-grained materials through the application of severe plastic deformation," *Journal of Materials Science*, vol. 42, pp. 3388-3397, 2007.

[105] C. C. Koh, "Top down synthesis of nanostructured materials: Mechanical and thermal processing methods," *Review of Advance Material Science*, vol. 5, pp. 91-99, 2003.

[106] L.-f. Hou, Y.-h. Wei, B.-s. Liu, and B.-s. Xu, "Microstructure evolution of AZ91D induced by high energy shot peening," *Transactions of Nonferrous Metals Society of China*, vol. 18, pp. 1053-1057, 2008.

[107] L. Kommel, I. Hussainova, and O. Volobueva, "Microstructure and properties development of copper during severe plastic deformation," *Journal of Materials & Design*, vol. 28, pp. 2121-2128, 2007.

[108] V. M. Segal, "Severe plastic deformation: simple shear versus pure shear," *Materials Science and Engineering A*, vol. 338, pp. 331-344, 2002.

[109] S. M. L. Sastry and R. N. Mahapatra, "Grain refinement of intermetallics by severe plastic deformation," *Materials Science and Engineering A*, vol. 329-331, pp. 872-877, 2002.

[110] R. Z. Valiev and I. V. Alexandrov, "Nanostructured materials from severe plastic deformation," *Nanostructured Materials*, vol. 12, pp. 35-40, 1999.

[111] O. N. Senkov, F. H. Froes, V. V. Stolyarov, R. Z. Valiev, and J. Liu, "Microstructure of Aluminum-Iron Alloys Subjected to Severe Plastic Deformation," *Scripta Materialia*, vol. 38, pp. 1511-1516, 1998.

[112] A. Rosochowski, "Processing metals by severe plastic deformation," *Journal of Solid State Phenomena*, vol. 101-02, pp. 13-22, 2005.

[113] A. Rosochowski and L. Olejnik, "Finite element simulation of severe plastic deformation processes," *Journal of Materials: design and Applications*, vol. 221, pp. 187-196, 2007.

[114] M. Furukawa, Z. Horita, and T. G. Langdon, "Developing ultrafine grain sizes using severe plastic deformation," *Journal of Advanced Engineering Materials*, vol. 3, pp. 21-125, 2001.

[115] J. Zrnik, S. V. Dobatkin, and I. Mamuzić, "Processing of metals by severe plastic deformation (SPD) – structure and mechanical properties respond," *Metalurgija*, vol. 47, pp. 211-216, 2008.

[116] V. M. Segal, "Materials processing by simple shear," *Materials Science and Engineering A*, vol. 197, pp. 157-164, 1995.

[117] Y. Iwahashi, J. Wang, Z. Horita, M. Nemoto, and T. G. Langdon, "Principle of equal-channel angular pressing for the processing of ultra-fine grained materials," *Scripta Materialia*, vol. 35, pp. 143-146, 1996.

[118] Y. Iwahashi, Z. Horita, M. Nemoto, and T. G. Langdon, "The process of grain refinement in equal-channel angular pressing," *Acta Materialia*, vol. 46, pp. 3317-3331, 1998.

[119] H. S. Kim, M. H. Seo, and S. I. Hong, "Plastic deformation analysis of metals during equal channel angular pressing," *Journal of Materials Processing Technology*, vol. 113, pp. 622-626, 2001.

[120] M. Furukawa, Z. Horita, M. Nemoto, and T. G. Langdon, "Review: Processing of Metals by Equal-Channel Angular Pressing," *Journal of Material Science*, vol. 36, pp. 2835-2843, 2001.

[121] R. Z. Valiev, N. A. Krasilnikov, and N. K. Tsenev, "Plastic deformation of alloys with submicron-grained structure," *Materials Science and Engineering: A*, vol. 137, pp. 35-40, 1991.

[122] J. M. García-Infanta, S. Swaminathan, F. Carreño, O. A. Ruano, and T. R. McNelley, "Grain shape and microstructural evolution during equal channel angular pressing," *Scripta Materialia*, vol. 58, pp. 17-20, 2008.

[123] M. Furukawa, Y. Iwahashi, Z. Horita, M. Nemoto, and T. G. Langdon, "The shearing characteristics associated with equal-channel angular pressing," *Materials Science and Engineering: A*, vol. 257, pp. 328-332, 1998.

[124] T. Langdon, M. Furukawa, M. Nemoto, and Z. Horita, "Using equal-channel angular pressing for refining grain size," *JOM Journal of the Minerals, Metals and Materials Society*, vol. 52, pp. 30-33, 2000.

[125] T. G. Langdon, "The principles of grain refinement in equal-channel angular pressing," *Materials Science and Engineering: A*, vol. 462, pp. 3-11, 2007.

[126] A. Rosochowski and L. Olejnik, "Numerical and physical modelling of plastic deformation in 2-turn equal channel angular extrusion," *Journal of Materials Processing Technology*, vol. 125-126, pp. 309-316, 2002.

[127] A. Rosochowski and L. Olejnik, "Finite element analysis of two-turn Incremental ECAP," *International Journal of Material Forming*, vol. 1, pp. 483-486, 2008.

[128] A. Rosochowski, L. Olejnik, and M. Richert, "3D-ECAP of Square Aluminium Billets," in *Advanced Methods in Material Forming*, 2007, pp. 215-232.

[129] A. Rosochowski, L. Olejnik, and M. Richert, "Double-billet Incremental ECAP," *Journal of Material Science Forum*, vol. 584-586, pp. 139-144, 2008.

[130] A. Azushima, R. Kopp, A. Korhonen, D. Y. Yang, F. Micari, G. D. Lahoti, P. Groche, J. Yanagimoto, N. Tsuji, A. Rosochowski, and A. Yanagida, "Severe plastic deformation (SPD) processes for metals," *CIRP Annals - Manufacturing Technology*, vol. 57, pp. 716-735, 2008.

[131] L. Olejnik and A. Rosochowski, "Methods of fabricating metals for nano-technology," *Bulletin of the Polish Academy of Sciences Technical Sciences*, vol. 53, pp. 413-423, 2005.

[132] Y. Saito, N. Tsuji, H. Utsunomiya, T. Sakai, and R. G. Hong, "Ultra-fine grained bulk aluminum produced by accumulative roll-bonding (ARB) process," *Scripta Materialia*, vol. 39, pp. 1221-1227, 1998.

[133] L. Jiang, M. T. Pérez-Prado, P. A. Gruber, E. Arzt, O. A. Ruano, and M. E. Kassner, "Texture, microstructure and mechanical properties of equiaxed ultrafine-grained Zr fabricated by accumulative roll bonding," *Acta Materialia*, vol. 56, pp. 1228-1242, 2008.

[134] P. W. Bridgman, *Studies in Large Plastic Flow and Fracture*. New York: McGraw-Hill, 1952.

[135] Z. Horita and T. G. Langdon, "Microstructures and microhardness of an aluminum alloy and pure copper after processing by high-pressure torsion," *Materials Science and Engineering: A*, vol. 410-411, pp. 422-425, 2005.

[136] M. Kai, Z. Horita, and T. G. Langdon, "Developing grain refinement and superplasticity in a magnesium alloy processed by high-pressure torsion," *Materials Science and Engineering: A*, vol. 488, pp. 117-124, 2008.

[137] A. Korbel and M. Richert, "Formation of shear bands during cyclic deformation of aluminium," *Acta Metallurgica*, vol. 33, pp. 1971-1978, 1985.

[138] J. Huang, Y. T. Zhu, D. J. Alexander, X. Liao, T. C. Lowe, and R. J. Asaro, "Development of repetitive corrugation and straightening," *Materials Science and Engineering: A*, vol. 371, pp. 35-39, 2004.

[139] Y. Zhu, H. Jiang, J. Huang, and T. Lowe, "A new route to bulk nanostructured metals," *Metallurgical and Materials Transactions A*, vol. 32, pp. 1559-1562, 2001.

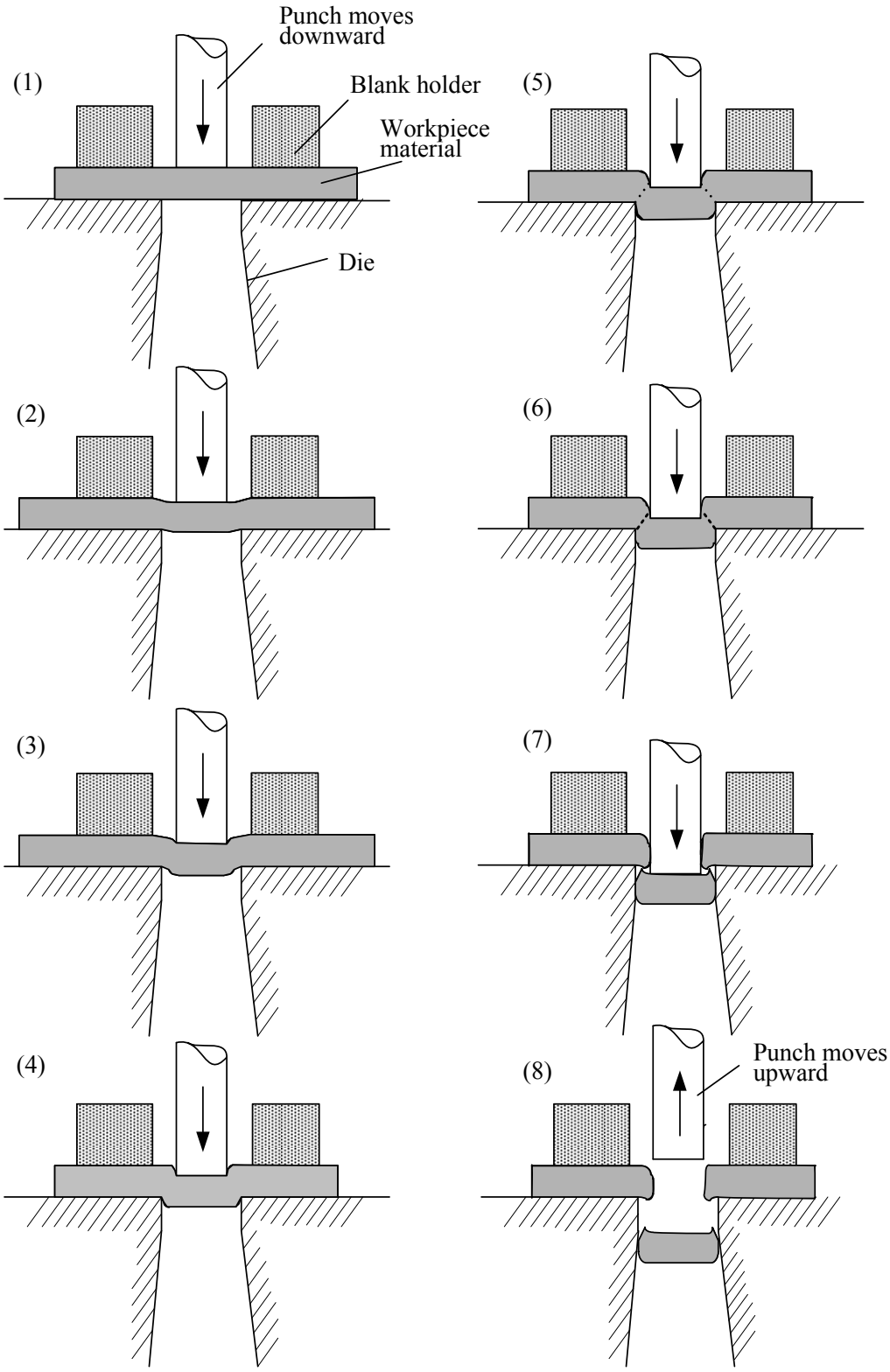

Fig. 2.1: Phases of blanking process

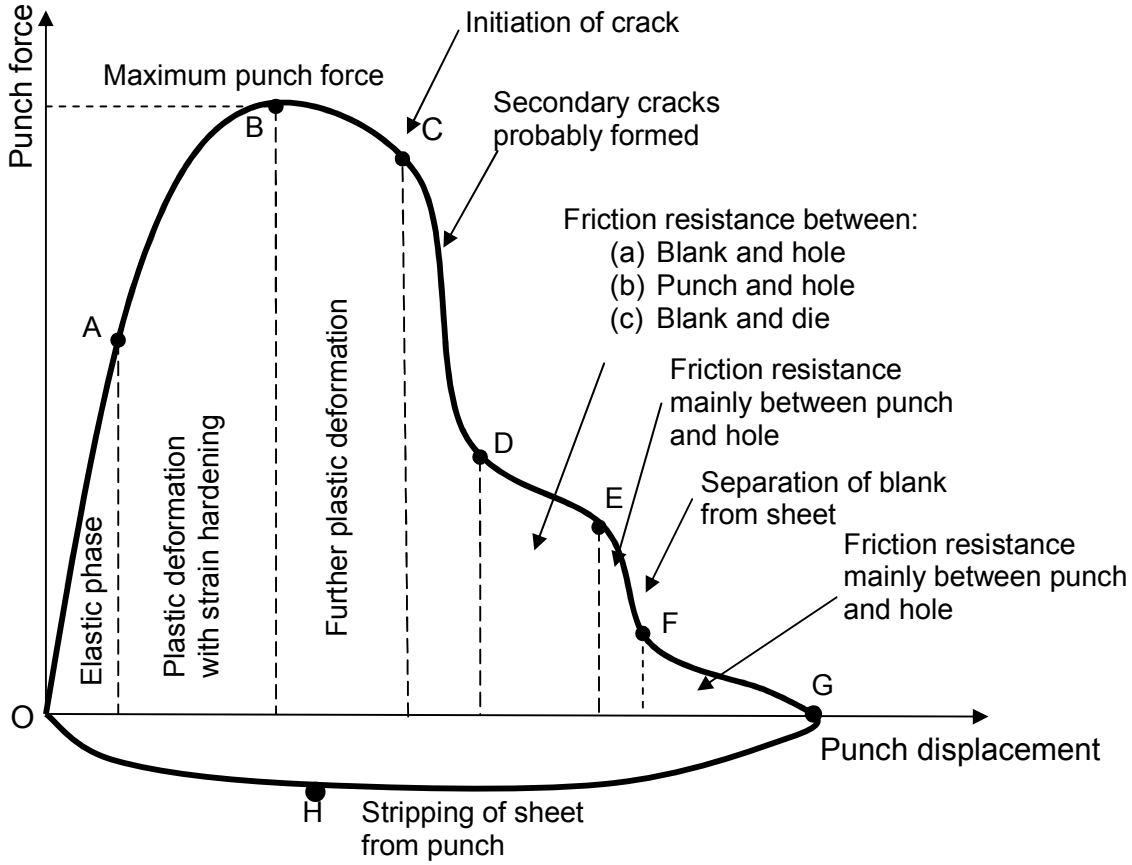

Fig. 2.2: Typical force-displacement curve of blanking process [4]

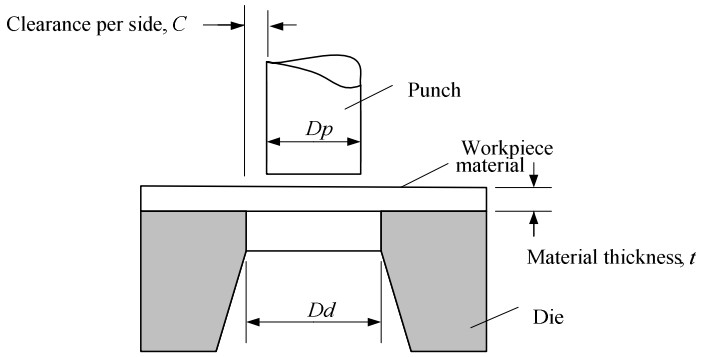

Fig. 2.3: Blanking tool set showing punch-die clearance

Table 2.1: Benefits of proper die clearance and drawbacks of insufficient and excessive die clearance [9 – 12]

Proper die clearance	Insufficient die clearance	Excessive die clearance
▪ Longer tool life. ▪ Better stripping. ▪ Smaller average burr height. ▪ Smaller average burr thickness. ▪ More uniform blank edges. ▪ No shavings required. ▪ Reduced galling. ▪ Flatter workpieces. ▪ Lowest force required.	▪ Galling. ▪ Shortened tool life. ▪ Slow/erratic stripping. ▪ Poor blank quality. ▪ Excessive heat. ▪ Warped sheet materials. ▪ Smaller initial burr. ▪ Larger, thicker running burr. ▪ Reduced rollover. ▪ Reduced slug pulling	▪ Poor blank quality. ▪ Increased workpiece distortion. ▪ Increased burr. ▪ Increased rollover. ▪ Work hardened burrs.

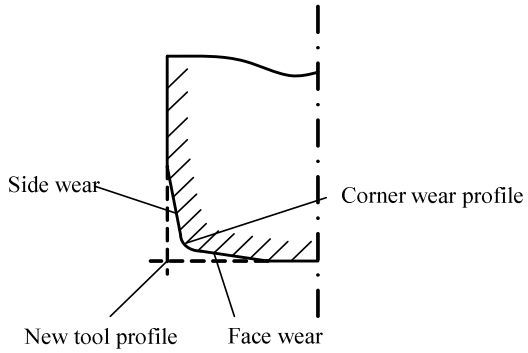

Fig. 2.4: Wear profile of the blanking punch

Table 2.2: Factors which influence the formation of blank edge profile

Zone of blank edge profile	Factors influence
Burr	Ductility of the material, clearance, tool wear, cutting speed
Rollover	Material properties, clearance, tool wear
Punch penetration depth	Tool wear, material properties, clearance
Shear zone (burnish)	Material properties, tool wear, cutting speed, clearance
Secondary shear	Ductility of material, clearance, sheet thickness

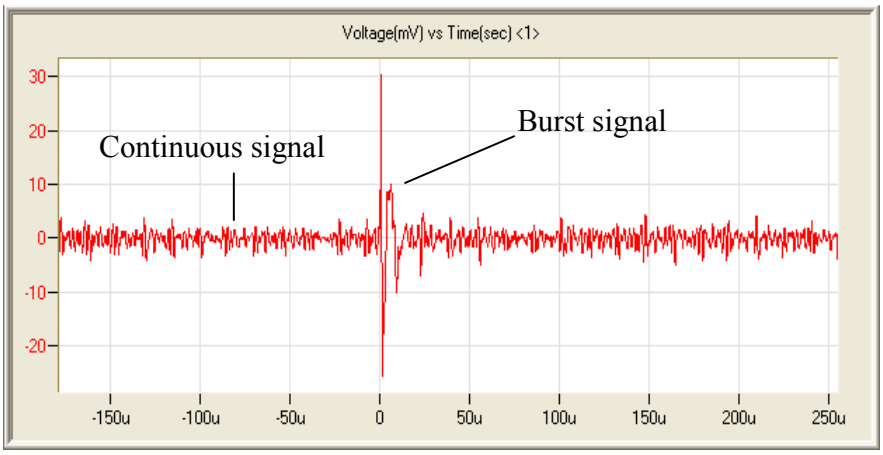

Fig. 2.5: Types of AE signal

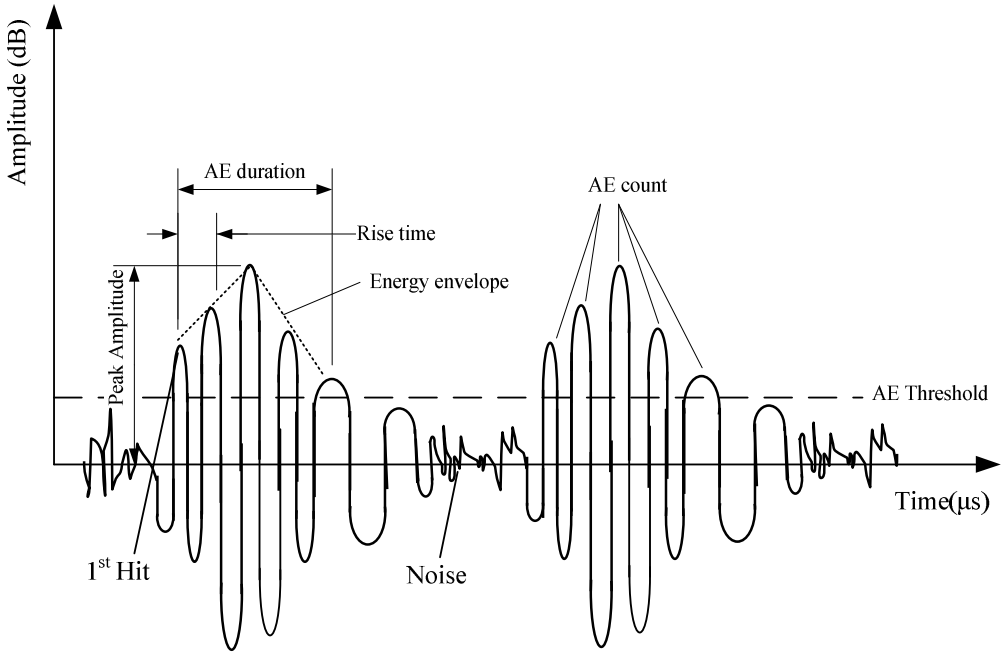

Fig. 2.6: AE hit feature extraction diagram

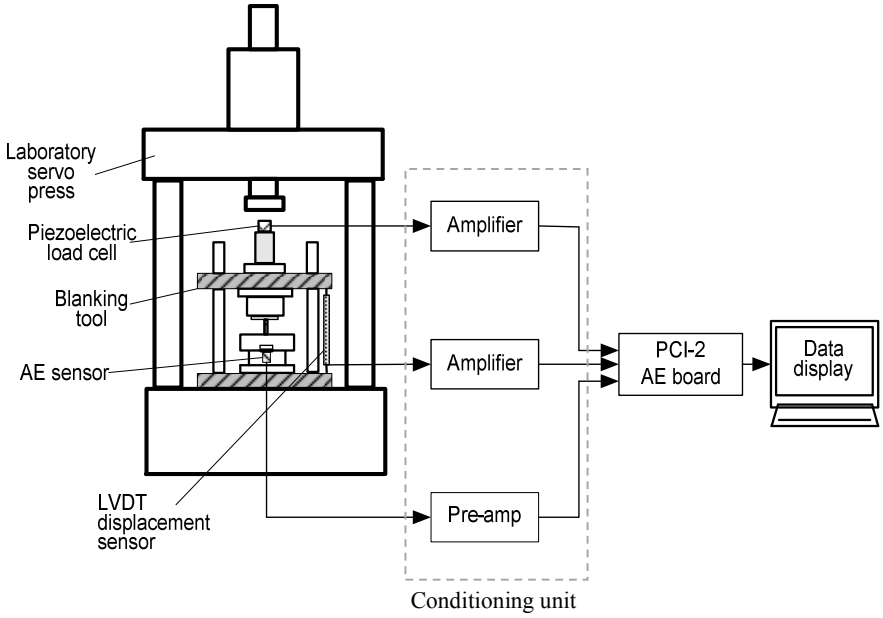

Fig. 2.7: Block diagram of blanking monitoring system

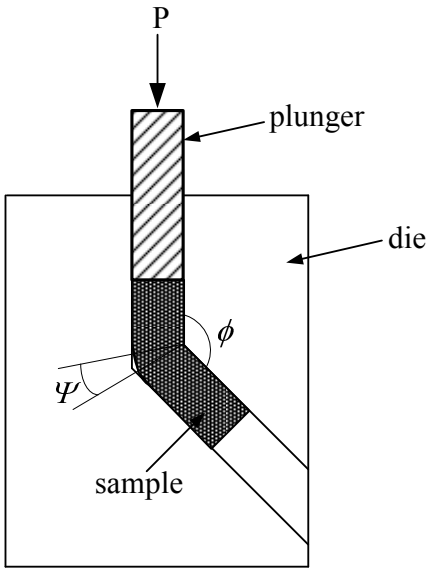

Fig. 2.8: Schematic representation of ECAP process

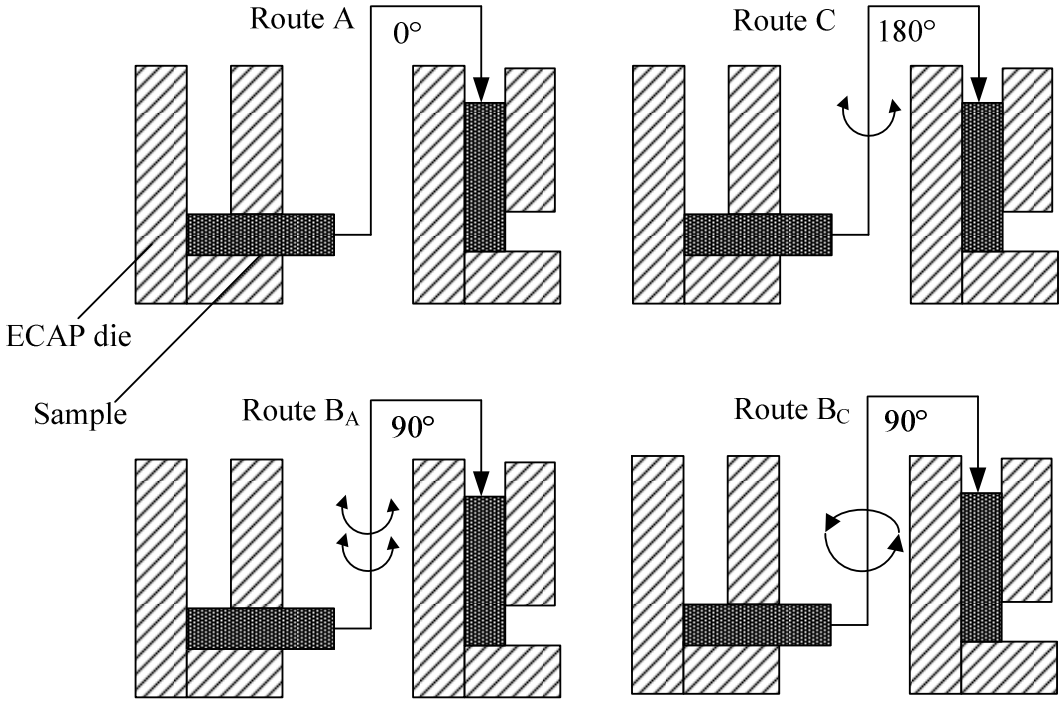

Fig. 2.9: Schematic representation of four processing routes in ECAP

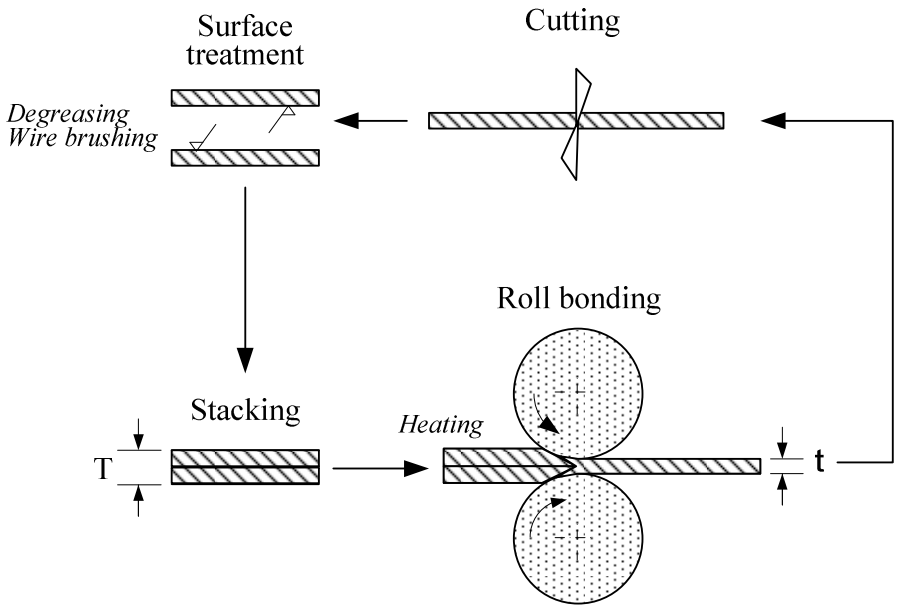

Fig. 2.10: Schematic representation of ARB process

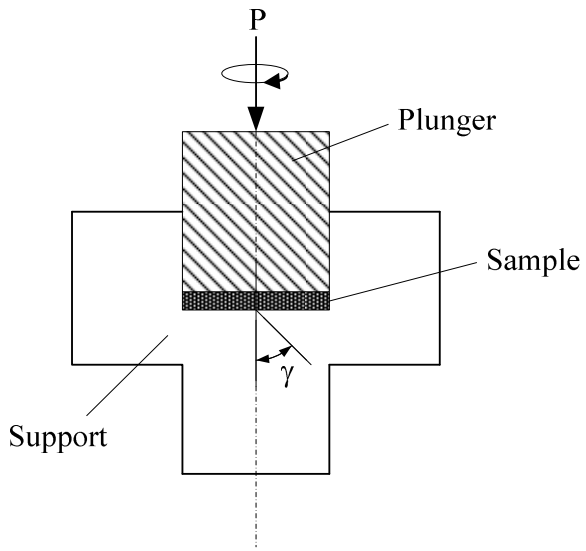

Fig. 2.11: Schematic representation of HPT process

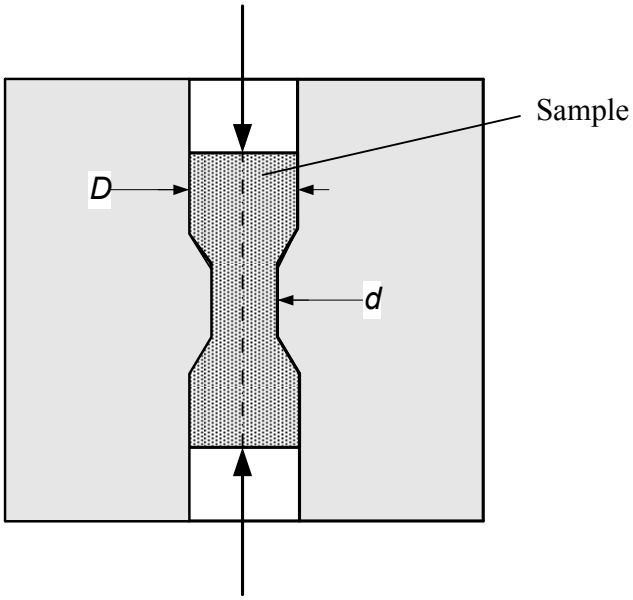

Fig. 2.12: Schematic representation of CEC process

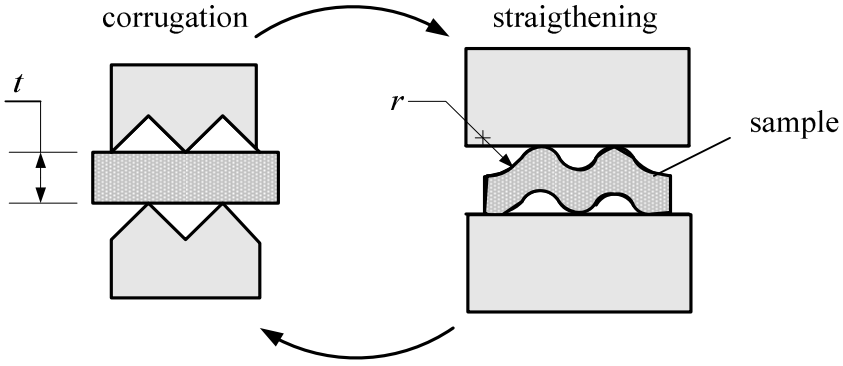

Fig. 2.13: Schematic representation of RCS

CHAPTER 3

EQUIPMENT, MATERIALS AND EXPERIMENTAL PROCEDURES FOR BLANKING PROCESS MONITORING

This chapter consists of three main parts: 1. Equipment, which discusses the preparations of the equipment (tool set, data acquisition instrumentation and blanking press), 2. Material preparation and the results for material testing are presented. The laboratory work and the results of the process transforming classical coarse grained (CG) aluminium into ultra-fine grained (UFG) aluminium sheets using equal channel angular pressing (ECAP) technique, upsetting and rolling process are included, and 3. Experimental procedures, which explains the detail procedures for setting up the experiment for blanking process monitoring. The discussion includes brief explanations of the limitations of the tooling set and precautions to avoid the problems. The limitations of the ECAP, upsetting and rolling processes are also discussed with the conclusion that producing UFG sheets is feasible using the proposed techniques.

3.1 Equipment

3.1.1 Introduction

In order to conduct experiments on a blanking operation, the blanking tools had been developed. The main components of the tools were punches, dies, blank holder, punch holder, die holder and the blanking frame. The development of the tooling

involved several iterative design stages to obtain the optimum design, which conformed to the process specification. Once the design had been completed, it was sent to manufacturer to make the tools. The manufactured blanking tools were assembled and integrated with the data acquisition (DAQ) instrumentation system. The tool set was tested and the DAQ system was calibrated on a laboratory hydraulic servo press to be used for the blanking experiments. Fig. 3.1 shows the experimental set up for process monitoring of blanking operations, which consists of three main parts: blanking tools, DAQ equipment and a laboratory servo press. The materials for blanking trials were prepared and the experiments were conducted according to established procedures. The details of the equipment, materials and experimental procedures are discussed in the following section.

3.1.2 Blanking tool set

The initial concept for the design and construction of the blanking tools was established with the view that it should be suitable to function as a laboratory test apparatus, taking into account the cost saving, simplicity, and its functionality. Design guidelines suggest how to design tools for a particular manufacturing process in terms of their shape, dimensions and the materials used [1, 2]. Designing a precision tool set is not an easy task; accuracy (close tolerances) and tool alignment are among the challenging issues. The idea of developing a prototype prior to manufacture the actual tools was considered. The prototype of the blanking tool had been developed by machining a block of pure aluminium to model the parts and components of the tools as shown in Fig. 3.2. Using the model, several modifications

and alterations were made to improve the tools before the actual tools could be manufactured.

The final blanking tool set is divided into two parts, top and bottom parts (Fig. 3.3). The top part consists of a upper plate, a punch holder supporting disc, a punch holder and the punch. The punch plate is used to locate the punch holder that is used to hold the punch. The bottom part consists of a lower plate, die holder, blank holder and the die. A precise hole was made in the middle of the die holder to locate the die. Another hole was made adjacent to the die's hole to locate the AE sensor.

Using four screws, the blank holder was clamped to the disc to provide the constraining pressure to the blank. The blanked sheet was located inside a shallow groove made on the top surface of the die holder. Each of four screws was tightened to an average torque of 4.5 Nm. The precise cylindrical hole in the centre of the blank holder was designed to have a sliding-fit with the punch, so it could guide the punch toward the die opening. The punch supporting disc and the die holder were attached to the upper and the lower plate respectively. The top and the bottom plate were separated by a couple of load springs to facilitate the opening of the tool set. The four columns located at the corners of the bottom plate provided the vertical alignment during the axial movement of the top plate towards the bottom plate. The assembly drawing of the blanking tools is attached in Appendix 2.

High strength tool steels are used to make a blanking tool set to provide greater wear resistant, rigidity and strength. The top and bottom plates were made from steel

alloy of grade AISI P20. The punch holder supporting disc, punch holder, blank holder and the die holder were made from hardened tool steel standard grade D2 [3]. The punches and dies were made from tungsten carbide (WC), with 6% of cobalt (Co), so the hardness of punches and dies measured using the Vickers scale was 2000 HV.

In order to study the effect of clearance and the tool state on the blanked edge quality, the total of 8 punches and two dies were used as shown in Fig. 3.4. Two sets of punches were produced, whereby one set of four punches has sharp edges and another set of four punches has rounded edges of 150 μm radius. Each set of punches has diameter of 4.94 mm, 4.90 mm, 4.86 mm and 4.82 mm respectively. Two dies, each of 5 mm diameters were produced, which is one that has sharp edge and the other has rounded edge of 150 μm radius. Fig. 3.5 shows the photographs of the punches and dies taken with a digital camera equipped with 15x zoom.

There are four different clearances (clearance per side) of 3%, 5%, 7% and 9% resulted from using the combination of four different sizes of punches and a die. These values were found to be the most used clearances in industry for blanking soft material such as aluminium sheet. The punches and a die with radius of 150 μm were used to indicate as a set of worn tools. This value of radius created on the shearing edge of the tools corresponds to the moderate level of the wear state of tools that usually found in blanking industry.

3.1.3 Data acquisition system

The configuration of DAQ system was based on the three main functions: acquiring blanking load signals, punch displacement signals and AE signals (Fig. 2.7). The devices associated with acquiring these signals are as follows:

(a) Acoustic emission (AE) signal: AE sensor and pre-amplifier (Fig. 3.6).

(b) Load signal: piezoelectric transducer (load cell) and charge amplifier (Fig. 3.7).

(c) Punch displacement signal: linear variable differential transformer (LVDT) displacement transducer and 4.8 kHz carrier frequency measuring amplifier (Fig. 3.8).

All those three signals were channelled to a computer, via PCI-2 AE board and controlled by AE software called AEwin, the product from Physical Acoustic Corporation [4].

3.1.4 Acoustic emission sensor

The AE sensor used was a wide band, type WD, according to the Physical Acoustic Corporation terminology. The technical specification of this AE sensor is given in Appendix 3. There are two requirements regarding the correct mounting of the AE sensor. First, good acoustic coupling interface between the sensor and the surface must be ensured in terms of retaining the frequency and amplitude of the acquired signal. The second one is the proper fixing of sensor to the surface of the tested material [5].

During blanking experiments, the sensor was attached to the bottom side of the blanked sheet. It was positioned as close as possible to the die edge, where the AE source was generated, to achieve a good signal to noise ratio [6]. The sensor was mounted in a hole bored inside the die holder that holds the die as shown in Fig. 3.9. In order to prevent electrical contact between the sensor case and the die holder, the sensor was inserted into a tube, which was made of non-conductive material (plastic). Then it was pushed against a small plug made of rubber. This plug acted like a spring, which pushed the sensor upwards to provide a good contact with the surface of the material under test. Furthermore, the rubber material could absorb vibration transmitted from the die holder and possibly affecting the genuine AE signals.

Petroleum oil based couplant (Vaseline) was applied on the sensor face to ensure sufficient acoustic coupling between the sensor face and the sheet surface. Any gap between two surfaces would affect the signal transmission. Visual and manual inspection was carried out to ensure good contact between the AE sensor and the blanked sheet in each test.

3.1.5 Preamplifier

The 2/4/6 preamplifier family type was used to amplify the generated AE signal before it was transmitted to the measurement circuitry. The technical specification is attached in Appendix 4. This type of preamplifier has selected gain of 20 dB, 40 dB or 60 dB and operates with either a single-ended or differential input. It was connected to the sensor and the PCI-2 AE board input channel via a BNC cable.

In this blanking experiment, the gain of 40 dB was selected and the sensor was connected using a differential input of the preamplifier. Connection to differential input has an advantage in the case of measuring a low level signal where noise can be a problem. Differential input eliminates the possibility of current flowing between the sensor and the preamplifier through the ground, which can generate a noise signal.

3.1.6 PCI-2 AE board

The two-channel acoustic emission system on a single AE board, from the Physical Acoustics Corporation, was used to provide digital signal processing capability. A PCI-2 system was inserted to a standard PC desktop as shown in Fig. 3.10. It was connected to the computer via its PCI bus. The specifications and the layout of the PCI-2 AE board are attached in Appendix 5. The output from the preamplifier that carried AE signals from the AE sensor was connected to channel-1 of the board. The force signal was connected to an analogue input channel-1 and the displacement signal was connected to an analogue channel-2 (parametric channel) of the PCI-2 AE board.

3.1.7 AE software

The software program used to control the data acquisition, visualisation and post-processing was known as AEwin^{TM}: it is a 32 bit WINDOWS based, AE acquisition, analysis and replay program provided with the PCI-2 AE board as standard software.

The step-by-step installations and setting procedures were followed according to the user manual instructions [7].

3.1.8 Desktop computer

A desktop PC was used to integrate the hardware and run the program. The specifications of the computer used to run the system are as follows: Dell Dimension 8300 Pentium 4, with a Pentium® 2.39 GHz processor, 1.50 GB of RAM, and 80 GB hard-drive.

3.1.9 Force transducer

A force transducer, also called load cell was used to convert the measured force into an electrical signal. In this project, a piezoelectric force transducer, type 9001A from Kistler [8] was used. This transducer could measure the force up to the maximum load of 7.5 kN. The transducer mounting set was designed to preload the transducer up to 30% of its maximum load. In this case, the preload force was 2.2 kN. Electrically, the transducer was positioned on top of a cylindrical block resting on the top plate. It was connected to a charge amplifier. The specifications of the schematic design of the mounting are attached in Appendix 6.

3.1.10 Charge amplifier

The function of charge amplifier is to convert the charge output from a force transducer into a proportional voltage signal, which was used as an input to analogue input channel 1 of the AE board. The charge amplifier used was a Kistler 5011.

3.1.11 Inductive displacement transducer

The inductive displacement transducer or inductive linear variable differential transformer (LVDT) is a passive transducer that requires external source of power. The LVDT transducer of type W5K from Hottinger Baldwin Messtechnik (HBM) was used to measure the punch displacement within the range of ± 5 mm. LVDT transducer consists of two parts: the transducer housing and the plunger. The plunger was attached to the top plate while the housing was mounted to the bottom plate of the blanking tool set. The maximal (nominal) output signal for W5K was ±80±1% mV/V, so it required amplification. Thus, the transducer was connected to the HBM MGA amplifier system with a plug-in module ME50.

The setting up procedures for the LVDT transducer and the amplifier system were conducted according to their operating manuals. Displacement calibration was done using a measured distance block of 65.01 mm height and four gauge plates, each 0.92 mm thick as shown in Fig. 3.11. At initial position, the height between the top plate and the bottom plate was 68.90 mm. This is the position, whereby the blanking tool set was completely assembled. At this position, the first voltage reading from LVDT transducer was taken, which corresponded to zero displacement. At second position, the top plate was slightly lowered down and it was rested on the distance block and 4 plates. The second voltage reading was taken, which corresponded to a measured displacement of 0.21.

The measurements at the following positions were made by reducing the number of plates each time the top plate moved downwards until it reached the lowest position

and rested only on the block. The tangent of the line plotted in Fig. 3.12 was given by:

$$= \frac{(4.23 - 1.54)}{(2.95 - 1.08)}$$

$$\approx 1.44 \text{ (V/mm)}$$

The reciprocal of this value equals 0.7 (mm/v), is the scaling factor for connecting the measurement voltage in Volts into displacement in mm.

3.1.12 MGA amplifier system

The MGA amplifier from HBM [9] was used to amplify voltage signal from LVDT transducer. It is an amplifier system device integrated with Eurocard modules of ME 50, which also known as 4.8 kHz carrier frequency measuring amplifier. The output of LVDT transducer was connected to the ME 50, which inserted to one of the amplifier slots. The MGA amplifier was capable to produce an output range of ±10V. This output was connected to an analogue input 2 (parametric channel 2) of PCI-2 AE board.

3.1.13 Laboratory hydraulic servo press

The load necessary to carry out a blanking operations was supplied by a 250 kN laboratory hydraulic servo press which shown in Fig. 3.13. The press was connected to a separate control panel and controlled by EHS Ltd. servo controller.

3.2 Materials

3.2.1 Material preparations

Two types of blanking materials in different states were used in this study. The first was a commercial cold-rolled aluminium AA 1050-H14 produced by cold rolling. The data sheet for this material is attached in Appendix 7. The specimens of dimensions 70 mm x 25 mm x 1 mm were cut using guillotine a press machine and referred to as in *"as supplied"* condition: the length of 70 mm was in the rolling direction. All specimens were visually inspected, cleaned and degreased using white spirit. The specimens were divided into two batches: one batch was retained in as supplied condition (*A1*), and the other batch was annealed (*A2*) to vary the material properties. The effects of annealing were inspected by verifying the microscopic structure of the grain (Fig. 3.14) and conducting the hardness test on the samples.

The other type of materials was aluminium AA 1070. Chemical compositions of aluminium AA 1070 is shown in Appendix 8. These materials were initially available in the form of cylindrical bars with diameter of 38 mm. They were processed in a laboratory to transform these cylindrical bars into several aluminium sheets, which can be divided into two batches: CG aluminium sheets *(A3),* and UFG aluminium sheets *(A4)*. The specimens from these materials were prepared in a similar way with the samples of material *A1* and *A2*.

In this study, commercially available aluminium AA1070, converted into UFG aluminium sheets by employing severe plastic deformation (SPD), was used. The UFG sheets had been produced by a laboratory of Warsaw University of Technology,

using the material provided by the University of Strathclyde. This was within a framework of research collaboration between these two universities.

The procedure for converting CG into UFG aluminium sheets included three stages. The initial coarse grained (CG) aluminium billets had been extruded into a two-turn, S-channel ECAP die to produce UFG billets. Subsequently, these billets were subjected to side upsetting to produce plates. Finally, the UFG plates were subjected to several passes of cold rolling to produce UFG sheets with thickness of 1 mm. Detail explanations of laboratory works for producing UFG aluminium sheets are included in section 3.3.

3.2.2 Annealing procedures (*A2)*

The specimens *A2* were cut from the same stock that used for specimens *A1*. They were visually inspected and cleaned. Meanwhile, the oven was heated with its door closed until a stable pre set temperature was obtained. The type of the oven used was Phyro-Therm furnace. The specimens were arranged in slanting inside the oven chamber with slightly raising their ends from the other ends, so that the heat would be distributed evenly in all direction to the surface of the specimens as shown in Fig. 3.15. The temperature was set at 343°C and the specimens were annealed for 45 minutes [10, 11]. After the time reached 45 minutes, the specimens were taken out of the chamber and cooled at room temperature.

3.2.3 Preparing coarse grained aluminium sheets AA 1070 *(A3)*

The aluminium Al 1070 was supplied in the form of hot extruded bar of 38 mm diameter. The bar was cut to be a 100 mm long billet. Further, it was milled along the lateral dimension (top and bottom sides) to produce flat surface for upsetting process. This resulted to a 26 mm thickness, an approximate rectangular billet being produced with the remaining of the arc portion on both sides. The billet was visually inspected and cleaned for further process.

At the next stage, this billet was subjected to a cold upsetting process of 250 kN using flat and smooth platens. As a result of upsetting, the billet was severely deformed as shown in Fig. 3.16. The final thickness of the sample produced was reduced to 3.8 – 4.0 mm thickness.

The final stage was to perform multi-pass cold rolling to produce the sample in the form of a plate into a sheet of 1 mm thickness. The total of rolling passes required to achieve 1 mm thickness was 7 and can be summarised in Table 3.1. The final product was shown in Fig. 3.17. The blanking specimens *A3* were cut from this stock and they were subjected to further straightening process to ensure that the surface was flat.

3.2.4 Hardness testing

Metallurgical testing for all different states of materials for blanking specimens was performed using hardness test. Hardness testing of vickers scales (HV-5kg) as shown in Fig. 3.18 was used because the specimens were soft material. Five samples of each

material were sent for the test and the average values were taken as final results. The results of the hardness test are shown in Table 3.2.

3.2.5 Uniaxial tensile test

The uniaxial tensile tests [12] were conducted as shown in Fig. 3.19 to define the initial yield strength and ultimate tensile strength of the stock materials. The true stress-true strain relationships of *A1* and *A2* stock materials were established as shown in Fig. 3.20 and Fig. 3.21 respectively. The true stress and true strain analysis is more related as compared to the engineering stress-strain curve in the analysis of forming processes because it is based on current stress value and current (instantaneous value) cross sectional area of the sample during the tensile test [13]. The values of yield strength and ultimate tensile strength of *A1, A2, A3* and *A4* are summarised in Table 3.3.

3.3 Laboratory work for producing UFG aluminium sheets *(A4)*

3.3.1 Producing UFG aluminium sheet AA 1070 using ECAP process

Earlier laboratory trials had successfully used small (8 x 8 x 46 mm) of coarse grained (CG) aluminium billets to convert them to UFG sheets. This amount of material was sufficient only to conduct metallurgical and basic mechanical testing of the UFG material. In order to carry out the blanking experiments, a bigger amount of material was required. This has led to a bigger cross-section of ECAP channel to be used. Based on the knowledge and experience on the previous work, a scaled-up, two-turn, S-channel ECAP, also called 2 x 90º ECAP (Fig. 3.22) was developed by

Olejnik and Rosochowski [14, 15]. From this stock, the specimens *A4* were cut in a similar way as it was done for the other types of specimens.

In this project, aluminium AA 1070, supplied as a hot extruded bar (Fig. 3.23) was milled to produce a squared cross-section of 26 x 26 mm CG billet. The billet was cleaned and visually inspected to check structural discontinuity. Next, it was subjected to four passes of two-turn, S-channel ECAP. This resulted in the total strain of 9.42, which was equivalent to eight passes of single turn ECAP plus a small amount of strain of about 0.22: a strain accumulated due to the upsetting of the billet in the die, which occurred at the point of the channels intersection and extrusion after ECAP, which occurred during the insertion of the billet into the die. The maximum force of up to 318 kN was required to conduct the scaled up ECAP at room temperature, which was 6.3 times higher than required for a small of 8 x 8 mm billet. After each consecutive pass, the billet was rotated about its axis by 90º. This rotation together with 180º in-die rotation had realised a route known as $C+B_C$. Fig. 3.24 shows the UFG billet after four passes of two-turn, S-channel ECAP process.

3.3.2. Upsetting process

The deformed ends of UFG billet were cut-off to obtain the dimensions of 26 x 26 x 100 mm. In order to change the shape of the billet to plate, the billet was subjected to cold upsetting along its lateral dimension using flat and smooth platens. The process was interrupted several times in order to replenish a graphite lubricant. The upsetting was stopped when the thickness of the plate reduced to about 3.8 – 4.0 mm. Fig. 3.25 shows the plate produced after upsetting process. To reduce the thickness further

with good uniformity for the sheet, the material was subjected to cold-rolling process.

3.3.3 Rolling process

The upset sample of UFG AA 1070 was subsequently trimmed to get rid of uneven or fractured edges and cold rolled to the final gauge of 1 mm thickness. The direction of rolling was assured to coincide with the ECAP direction. No lubrication was used during rolling process.

3.3.4. Results of UFG sheets

The total of 6 rolling passes was required to obtain 1 mm thickness UFG sheet. Fig. 3.26 shows the UFG sheets produced after rolling. After each pass, the measurements of thickness of the sheet were made at different locations. The average readings were taken as the final thickness of the sheet. Table 3.4 summarises the detail of the rolling process with the thickness reduction and equivalent strain obtained during each passes. The microstructure of UFG sheet was compared with the initial CG, after four passes of ECAP and after side upsetting and rolling (Fig. 3.27) using transmission electron microscopy (TEM) to show the effect of grain refinery. The new material was created from the initial CG (average grain size was 300 μm), which consisted of grains with sizes in nanometer range and subgrains with low angle boundaries.

3.4 Experimental program and procedures

A coding system was designed to classify the experiments so that they can be referred by a short acronym for simplifying the description of the experiment. Codes were derived from the specifications shown in Table 3.5. *D1* and *P1* represent a sharp die and a sharp punch, while *D2* and *P2* represent a worn die and a worn punch. Number *3, 5, 7* and *9*, used at the end, represent the percentage of clearance. For example: *A1D1P13* represents blanking the as supplied aluminium AA 1050 *(A1)*, using a combination of sharp die *(D1)* and sharp punch *(P1)* at 3% clearance. These codes were used throughout this thesis.

There were a total of 64 experiments, which involved all the combinations of tool states and for all clearances. A total of 16 experiments were carried for each material to complete all the combinations. Table 3.6 is the matrix, which simplifies the description of the experimental program to test the different sets of tool states for 3%, 5%, 7% and 9% clearance in these blanking experiments.

Experimental procedures were divided into three parts: 1. Tooling set preparations, 2. DAQ preparations and 3. Press machine preparations. Stringent check was carried out for the preparations to avoid damage to the blanking tool and to retain the consistency for every experiment as explained below.

3.4.1 Tooling set preparations

1) Secure the punch and the die on the upper and lower plate of the test rig.

2) Verify the alignment of the punch inside the die using a borescope. This was to ensure that the punch has aligned properly inside the die.
3) Once the alignment inspection was done, separate the top plate from the bottom plate to insert the sample.
4) Check the position of the AE sensor and apply couplant on the sensor's surface.
5) Insert and position the sample inside the groove of the die holder.
6) Verify the contact between the surface of the sample and the AE sensor.
7) Position the blank holder inside the die holder.
8) Screw the blank holder to the die holder, and verify the torque.
9) Position the top plate on the test rig.
10) Check the movement of the top plate manually. Verify the alignment of the punch inside the blank holder to prevent friction between the punch and the blank holder.
11) Position the tooling set on the press.
12) Attach force transducer on the top of the top plate.
13) Check the connections of the transducers to the DAQ system.
14) Start the signal acquisition system.
15) Check any detected noise into the system.
16) Start the blanking operation by energising the ram to move downward to the lowest position (BDC).
17) Pause/stop the signal acquisition system when the punch reached the lowest position.
18) Energise the ram to move upward to initial position.
19) Withdraw the tooling set from the press.

20) Inspect the blank and the result of the signals.

21) The blanking test is completed.

3.4.2 DAQ preparations

1) Turn on the DAQ system: turn on the MGA amplifier system, charge amplifier and the computer. Setting the amplifiers according to the predetermined requirements.
2) Run the AEwin software. Check the acquisition set up menu according to the predetermined requirements.
3) Connect the AE sensor to the preamplifier and direct to the channel-1 of the AE PCI-2 AE board.
4) Connect the force transducer to the charge amplifier input and its output connected to the parametric 1 of the PCI-2 AE board.
5) Connect LVDT transducer to the input of the MGA amplifier and direct to the parametric 2 of the PCI-2 AE board.
6) Start the acquisition to test the transducers functionality: use pencil-lead break to calibrate the AE sensor, test the LVDT transducer by moving the ram downward to give sufficient displacement on the force transducer.
7) The LVDT transducer and the force transducer can also be tested using multi-meter voltage readings, which can be connected to their output supply.
8) Once the signal test produces a result, the preparation for DAQ is completed.

3.4.3 Laboratory hydraulic servo press preparations

1) Connect the 250 kN hydraulic servo press cable of control module to the press control panel. Select the press selector switch. Switch on the mains supply to the hydraulic system of the press. Switch on the power for the control panel.
2) Open the water supply valve for the hydraulic motor cooling system.
3) Switch on the hydraulic motor.
4) Check the hydraulic control unit.
5) Check servo controller according to stroke control requirements.
6) Setup the speed of the press slide to be 10 mm/s.
7) Test the slide movement corresponding to the displacement required for the tooling set.
8) Move the slide to the initial position and ready for the blanking operation.

3.5 Discussion

The tool set was designed to meet the precision requirements. The smallest clearance between punch and die is 30 μm. Hence, alignment of punch and die is very crucial to avoid damage of the tools. The movement of the upper plate, which hold the punch, was guided by the diagonal pillars permanently attached to the bottom part of the test rig. The punch was centred using the blank holder to align with the die. However, due to such a simple construction of the blanking tool, each consecutive blanking test required the upper plate to be removed and then reinstalled on the pillars after inserting the workpiece. Such a process would prone to a misalignment of the tools. In order to verify the alignment after reposition the upper plate, the plate was pushed manually to ensure that the punch could move inside the blank holder

hole without friction. Further, the visual inspection using borescope was used as shown in Fig. 3.28 to verify the alignment of the punch and die after changing the tools.

The attempt to develop UFG aluminium sheet AA 1070, from its initial coarse grained state had been successfully realised using a two-turn, S-channel ECAP technique. The initial CG was subjected to the stages of processes: ECAP, upsetting and rolling. Although the process was scaled up and adopted from the previous successful small scale batch production, by using a larger cross section of the ECAP die and a higher capacity press, the processes of producing UFG sheet was slow. The problems related to the process chain, material waste and tooling contributed to the complexity of the process making it suitable for mass production yet.

During upsetting and rolling processes, the heat would be induced due to friction and deformation, thus rising the temperature of the material. This could cause the grain growth inside the material and ruining the effect of the fine grain. One of the solutions was by applying a lubricant during the upsetting and ensuring sufficient time for cooling the sheet between each consecutive rolling passes.

The piece of UFG sheet produced was bent slightly in the middle due to the repeated rolling process. This was overcome by using manual press to gradually straighten the bent surface. The jagged edges of the sheets were cut off and this contributed to a significant amount of material waste. Due to the multiple forming processes, the materials experienced work hardening and slight reduction of ductility.

The experimental procedures for monitoring the blanking operation are summarised in Fig. 3.29. It starts with a proper setting the blanking tool set on the press. The DAQ system is then integrated with the blanking tool and AEwin software starts to acquire signals. If signals were found due to surrounding noise or vibration of the press, the system was adjusted, such as resetting the filters and the threshold voltage. Otherwise, the AEwin software continues to monitor the signals. The press machine starts to run by allowing the ram to move downward and pushing the upper plate to start the blanking operation. The ram stops when it reaches the lowest downward position. The blanking operation is completed. The press stroke is set for ±10 mm displacement. The process is repeated several times in order to obtain reliable process signature.

3.6 Conclusions

Blanking trials were performed to check that all equipment work and function properly. The procedures were verified at every stage. All precautions were observed in setting up the blanking experiment to ensure that the results obtained were valid and reliable. Further, aspects of health and safety were also observed to avoid accident when dealing with mechanical handling and press machine. During the blanking trials, the tool set, together with the monitoring system had been working properly to produce the blanks. The sample of the produce blank is shown in Fig. 3.30. The AE sensor was sensitive to unwanted signals such as vibration signals. Therefore, proper hardware setting and intensive tests were required to verify the blanking process signatures. Tools were inspected and cleaned to prevent debris between consecutive tests. The results of each repeated test for blanking experiments

were compared and closed observations were made to obtained meaningful results from the process signatures.

From the experiment performed to produce UFG sheets, it was learnt that the methods used were feasible to produce UFG sheet metals for laboratory purposes. The results showed that the grain size was reduced, which subdividing the initial large grains into much smaller grains and sub-grains. The two-turn, S-channel ECAP increased the productivity of process by doubling the plastic strain in one pass, thus reducing the number of passes required to achieve a UFG structure. However, a higher tool pressure was required because of longer strain and increased friction. This would reduce tool life and increase the production costs.

3.7 References

[1] K. G. Swift, *Process Selection: From Design to Manufacture*: Butterworth Heinemann, 2003.

[2] B. Fynes and S. De Búrca, "The effects of design quality on quality performance," *International Journal of Production Economics*, vol. 96, pp. 1-14, 2005.

[3] http://www.wisetool.com/designation/toolsteel.htm.

[4] http://www.pacndt.com/.

[5] S. Colombo, A. Giannopoulos, M. C. Forde, R. Hasson, and J. Mulholland, "Frequency response of different couplant materials for mounting transducers," *NDT & E International*, vol. 38, pp. 187-193, 2005.

[6] K. Jemielniak, "Some aspects of AE application in tool condition monitoring," *Ultrasonics*, vol. 38, pp. 604-608, 2000.

[7] Physical Acoustic Corporation, "PCI-2 Based AE System User's Manual Rev 1a," 2003.

[8] http://www.kistler.com/.

[9] http://www.hbm.com/.

[10] Aluminium International, "Standard Practice for Heat Treatment of Wrought aluminium Alloy," 2001.

[11] G. E. Totten and D. S. Mackenzie, "Handbook of Aluminum: Physical Metallurgy and Processes," vol. 1: CRC Press, 2003.

[12] ASM Handbook, *Mechanical Testing*: ASM International, 1992.

[13] Z. Marciniak, J. L. Duncan, and S. J. Hu, *Mechanics of Sheet Metal Forming*: Butterworth-Heinemann, 2002.

[14] L. Olejnik and A. Rosochowski, "Scaled-up ECAP with enhanced productivity," *Journal of Steel Research International*, vol. 2, pp. 439-446, 2008.

[15] L. Olejnik and A. Rosochowski, "Scaled-up ECAP with enhanced productivity," in *Special Edition Metal Forming Conference*, Krakow, Poland, 2008, pp. 439-446.

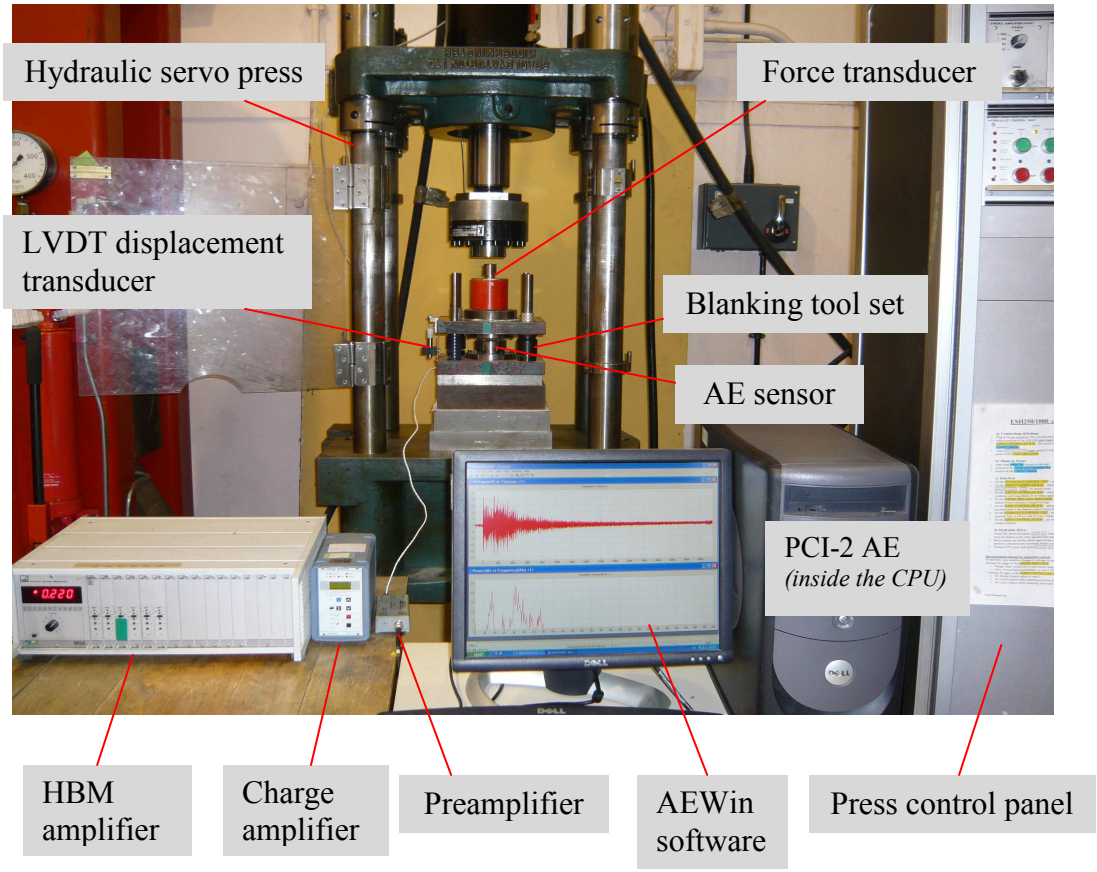

Fig. 3.1: Experimental set-up for the blanking monitoring system

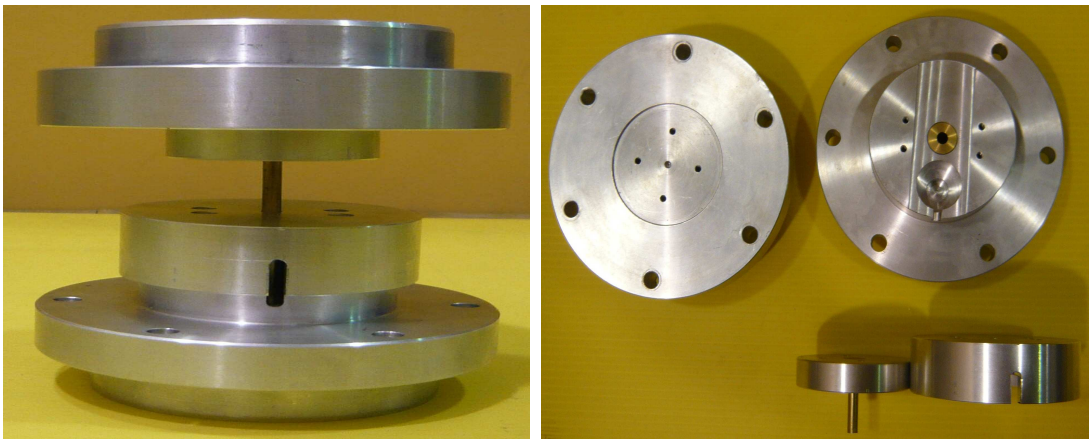

Fig. 3.2: Prototype of blanking tool

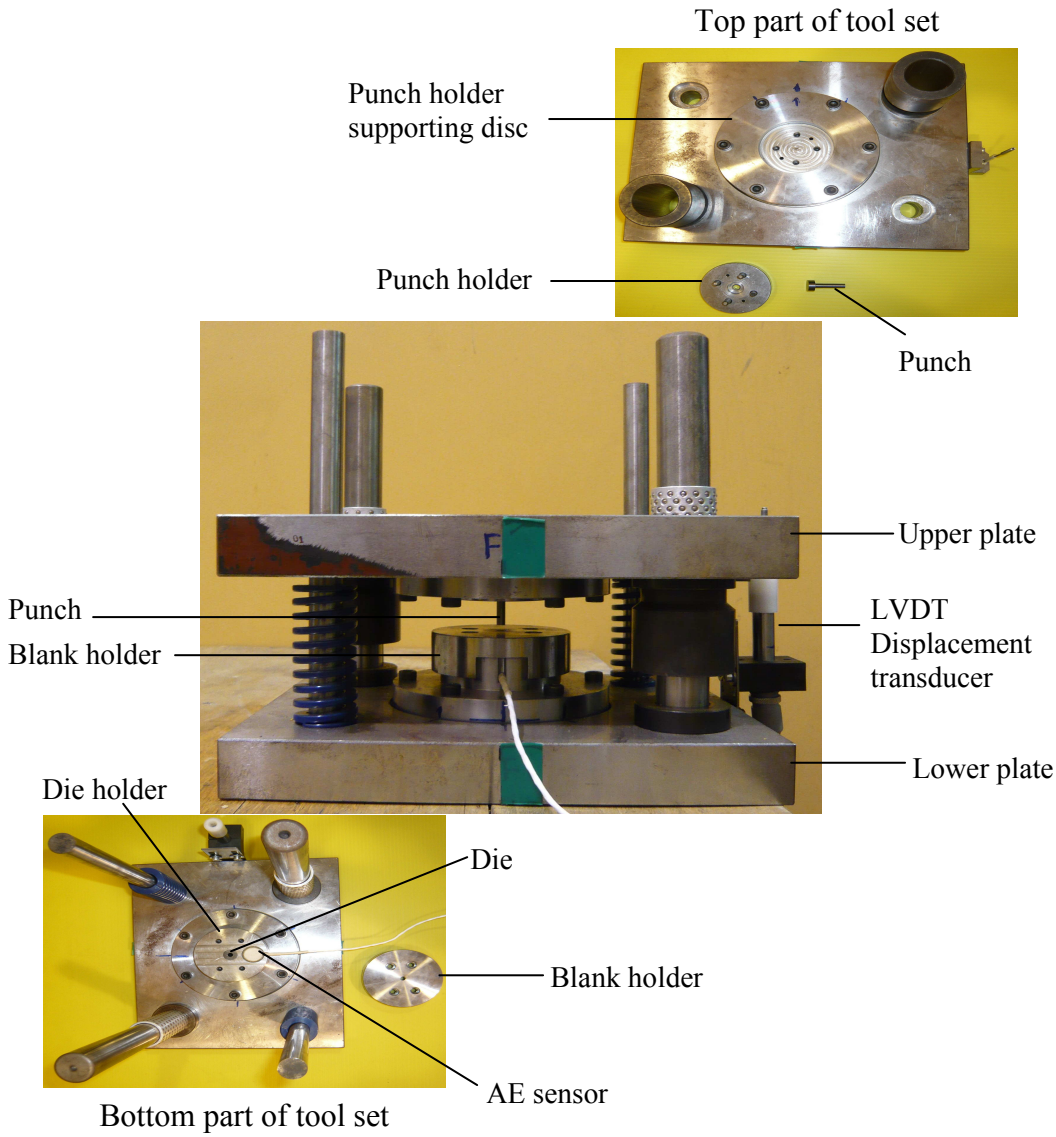

Fig. 3.3: The blanking tool set

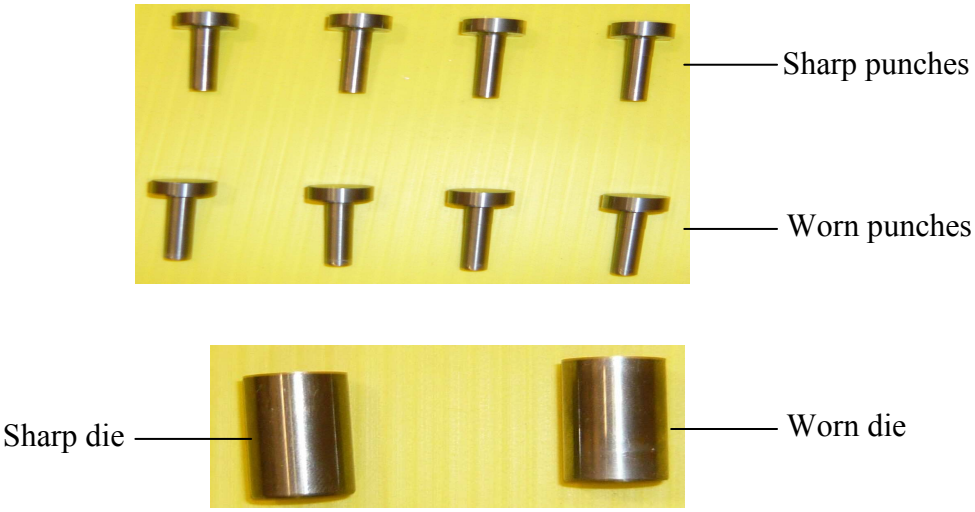

Fig. 3.4: Punches and dies

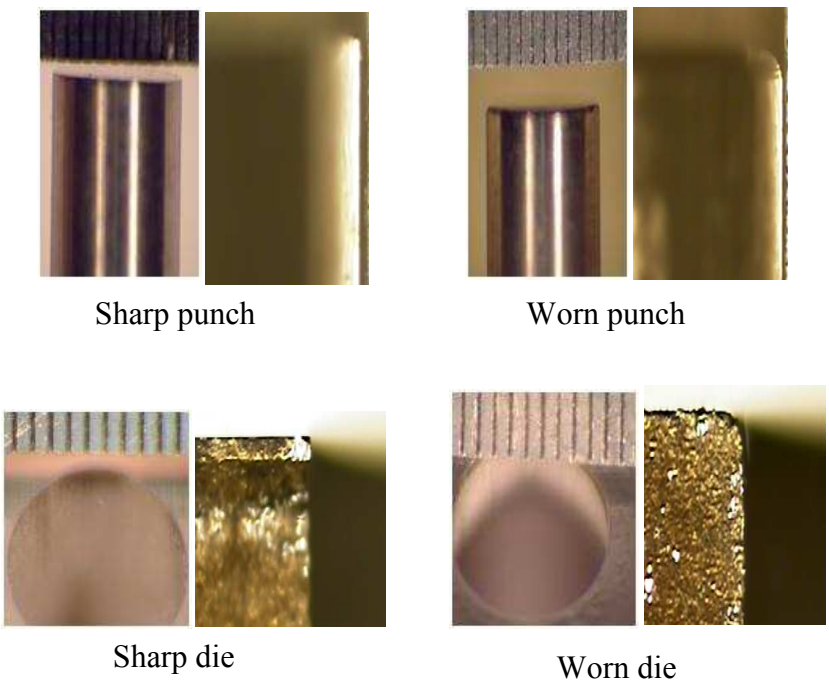

Fig. 3.5: Photograph of sharp and worn punch and die

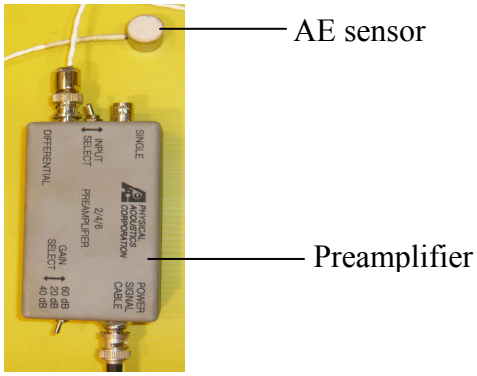

Fig. 3.6: AE sensor and preamplifier

Fig. 3.7: Force transducer and charge amplifier

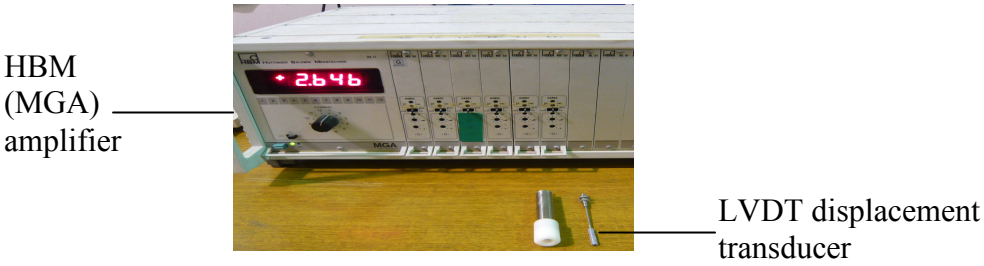

Fig. 3.8: LVDT displacement transducer and HBM amplifier

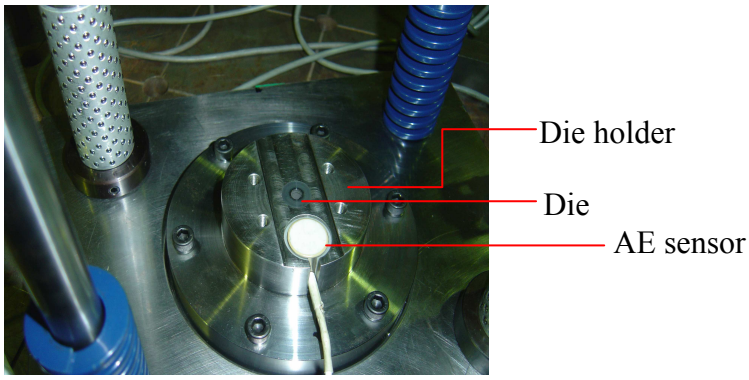

Fig. 3.9: AE sensor location

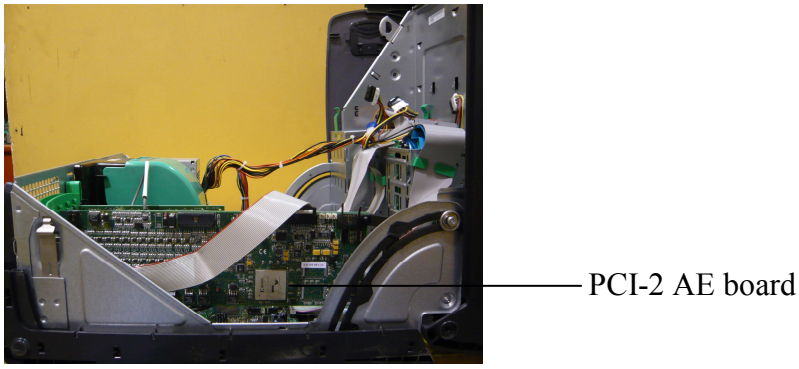

Fig. 3.10: PCI-2 AE board

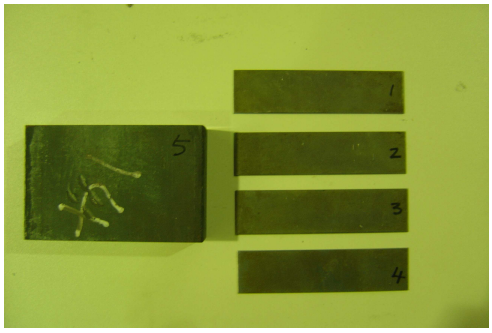

Fig. 3.11: The block and plates used for LVDT displacement transducer calibration

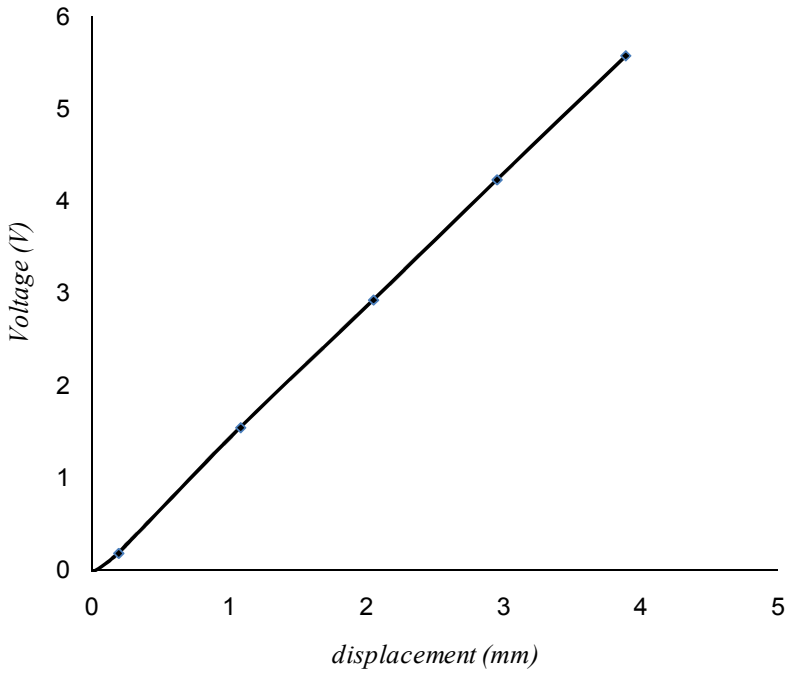

Fig. 3.12: Relationship between corresponding voltage and displacement of the LVDT displacement transducer

Fig. 3.13: Hydraulic servo press

(a)

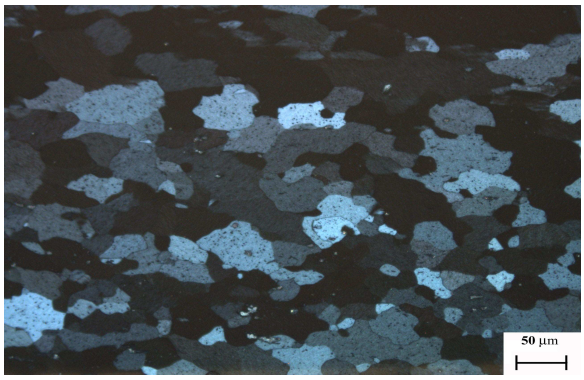

(b)

Fig. 3.14: The micrograph showing the grain structure of (a) as supplied *(A1)*, (b) annealed *(A2)* aluminium sheet AA 1050

Fig. 3.15: Annealing process of aluminium sheet AA 1050

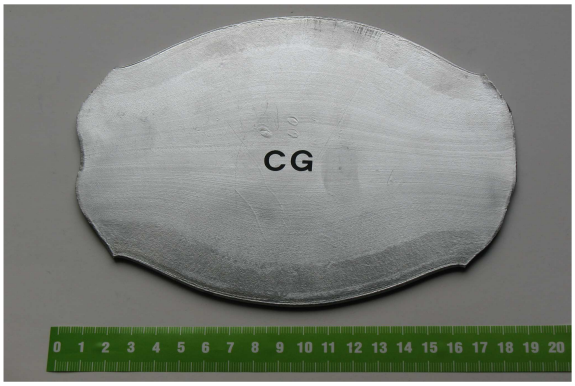

Fig. 3.16: Plate of aluminium AA 1070 after side upsetting

Table 3.1: Detail of the rolling process for aluminium sheets AA 1070

No. of passes	Material thickness (mm)	Thickness reduction, %	Equivalent strain
0	3.7	-	-
1	3.2	13.5	0.17
2	2.8	12.5	0.15
3	2.2	21.4	0.28
4	1.6	27.3	0.37
5	1.2	25.0	0.33
6	1.0	16.0	0.21

Fig. 3.17: Aluminium sheets AA 1070 after side upsetting and rolling

Fig. 3.18: Hardness testing

Table 3.2: Hardness measurements

Sample	Hardness value (HV – 5 kg)
A1	33.4
A2	28.0
A3	46.0
A4	48.1

Fig. 3.19: Uniaxial tensile test

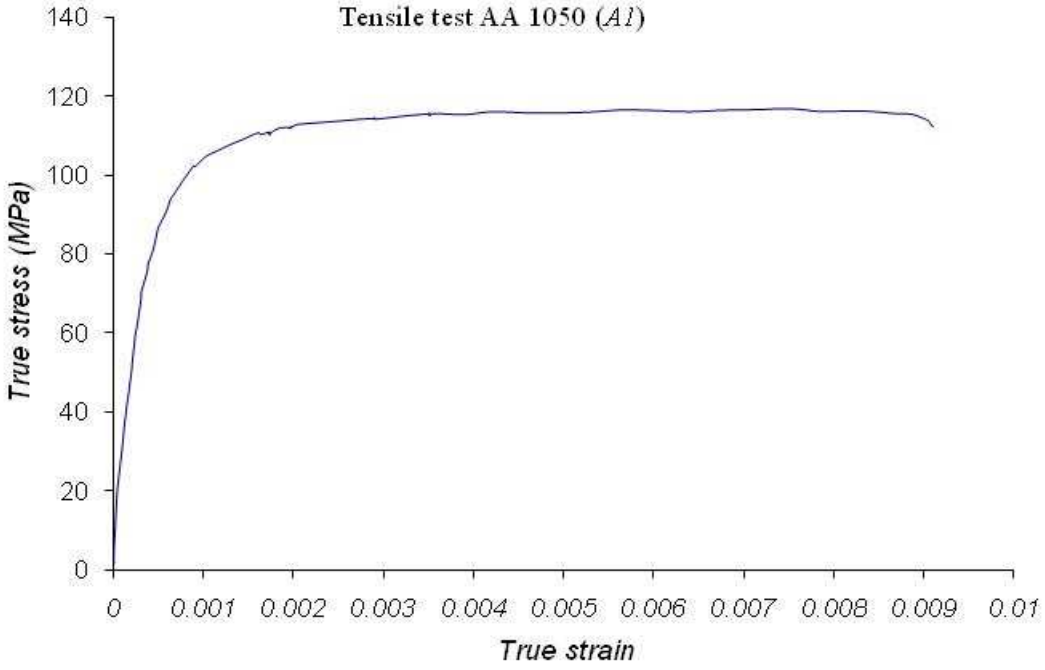

Fig. 3.20: Relationship of true stress-true strain for material *A1*

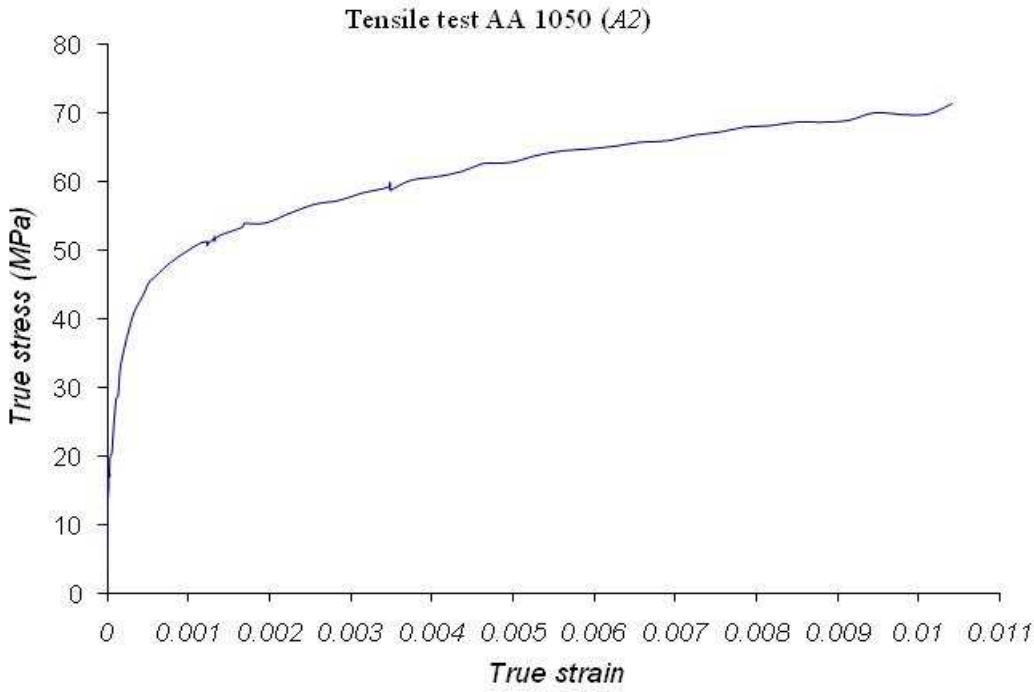

Fig. 3.21: Relationship of true stress-true strain for material *A2*

Table 3.3: Yield strength and ultimate tensile strength (UTS) of the materials

Material	Yield strength (MPa)	Ultimate tensile strength UTS (MPa)
AA 1050 as supplied *A1*	86	117
AA 1050 annealed *A2*	38	71
AA 1070 coarse grained *A3*	117.8	184
AA 1070 UFG *A4*	130.3	199

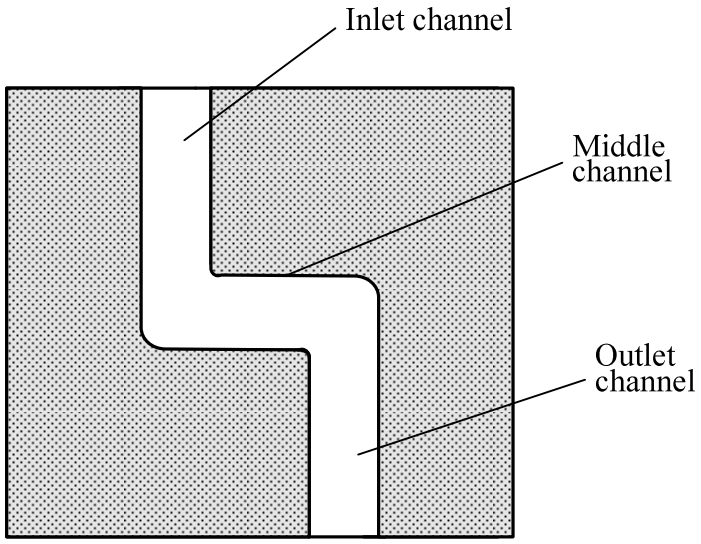

Fig. 3.22: Schematic representation of the two-turn, S-channel ECAP

Fig. 3.23: Supplied aluminium 1070, 38 mm diameter

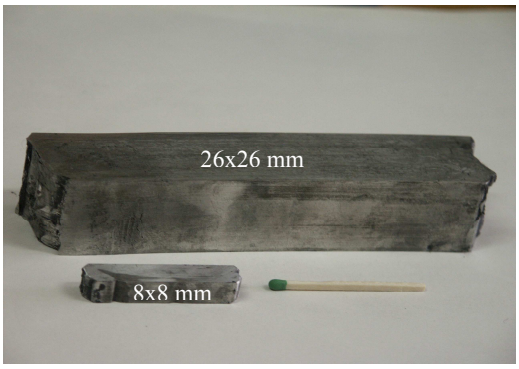

Fig. 3.24: Larger size of UFG billet of 26x26 mm produced using the scaled-up two-turn,S-channel ECAP

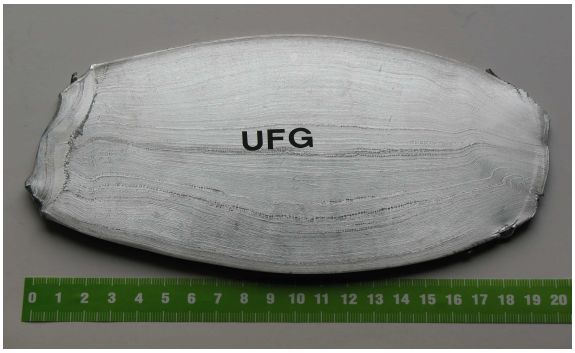

Fig. 3.25: Upset sample of 3.8 – 4.0 mm thickness

Fig. 3.26: UFG sheets produced after 6 passes of cold-rolled

Table 3.4: Detail of the rolling process of UFG sheets

No. of passes	Material thickness (mm)	Thickness reduction, %	Equivalent strain
0	3.80	-	-
1	3.45	9.2	0.22
2	2.80	18.8	0.24
3	2.20	21.4	0.28
4	1.60	27.3	0.36
5	1.25	22.0	0.29
6	1.00	20.0	0.26

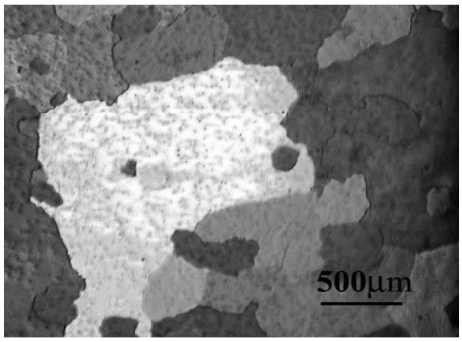

(a)

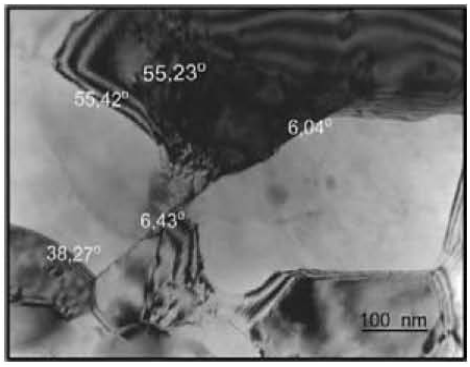

(b)

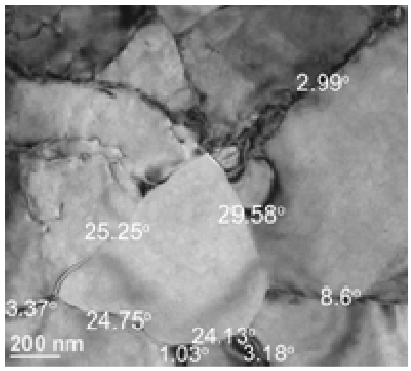

(c)

Fig. 3.27: Grain microstructure of AA 1070 for comparison between CG and UFG: (a) Initial CG , (b) UFG after four passes of two-turn, S-Channel ECAP (c) UFG sheets after ECAP, side upsetting and rolling

Table 3.5: Coding system

Coding	Explanation
A1	Specimen of "as supplied" material AA 1050
A2	Specimen of annealed material AA 1050
A3	Specimen of CG material AA 1070
A4	Specimen of UFG material AA 1070
D1	Die bushing with sharp edge
D2	Die bushing with rounded (worn) edge
P1	Punch of sharp edge
P2	Punch of rounded (worn) edge

Table 3.6: Matrix of the blanking experiments

Experiment	Material				Die state		Punch state		Clearance per side			
	A1	*A2*	*A3*	*A4*	sharp	worn	sharp	worn	3%	5%	7%	9%
A1D1P13	√				√		√		√			
A1D1P15	√				√		√			√		
A1D1P17	√				√		√				√	
A1D1P19	√				√		√					√
A1D1P23	√				√			√	√			
A1D1P25	√				√			√		√		
A1D1P27	√				√			√			√	
A1D1P29	√				√			√				√
A1D2P13	√					√	√		√			
A1D2P15	√					√	√			√		
A1D2P17	√					√	√				√	
A1D2P19	√					√	√					√
A1D2P23	√					√		√	√			
A1D2P25	√					√		√		√		
A1D2P27	√					√		√			√	
A1D2P29	√					√		√				√
A2D1P13		√			√		√		√			
A2D1P15		√			√		√			√		
A2D1P17		√			√		√				√	
A2D1P19		√			√		√					√
A2D1P23		√			√			√	√			
A2D1P25		√			√			√		√		
A2D1P27		√			√			√			√	
A2D1P29		√			√			√				√
A2D2P13		√				√	√		√			
A2D2P15		√				√	√			√		
A2D2P17		√				√	√				√	
A2D2P19		√				√	√					√
A2D2P13		√				√		√	√			
A2D2P25		√				√		√		√		
A2D2P27		√				√		√			√	
A2D2P29		√				√		√				√

… Continued

Experiment	Material				Die state		Punch state		Clearance per side			
	A1	*A2*	*A3*	*A4*	sharp	worn	sharp	worn	3%	5%	7%	9%
A3D1P13			√		√		√		√			
A3D1P15			√		√		√			√		
A3D1P17			√		√		√				√	
A3D1P19			√		√		√					√
A3D1P23			√		√			√	√			
A3D1P25			√		√			√		√		
A3D1P27			√		√			√			√	
A3D1P29			√		√			√				√
A3D2P13			√			√	√		√			
A3D2P15			√			√	√			√		
A3D2P17			√			√	√				√	
A3D2P19			√			√	√					√
A3D2P23			√			√		√	√			
A3D2P25			√			√		√		√		
A3D2P27			√			√		√			√	
A3D2P29			√			√		√				√
A4D1P13				√	√		√		√			
A4D1P15				√	√		√			√		
A4D1P17				√	√		√				√	
A4D1P19				√	√		√					√
A4D1P23				√	√			√	√			
A4D1P25				√	√			√		√		
A4D1P27				√	√			√			√	
A4D1P29				√	√			√				√
A4D2P13				√		√	√		√			
A4D2P15				√		√	√			√		
A4D2P17				√		√	√				√	
A4D2P19				√		√	√					√
A4D2P23				√		√		√	√			
A4D2P25				√		√		√		√		
A4D2P27				√		√		√			√	
A4D2P29				√		√		√				√

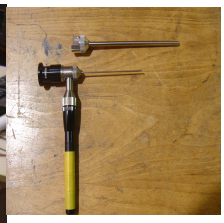

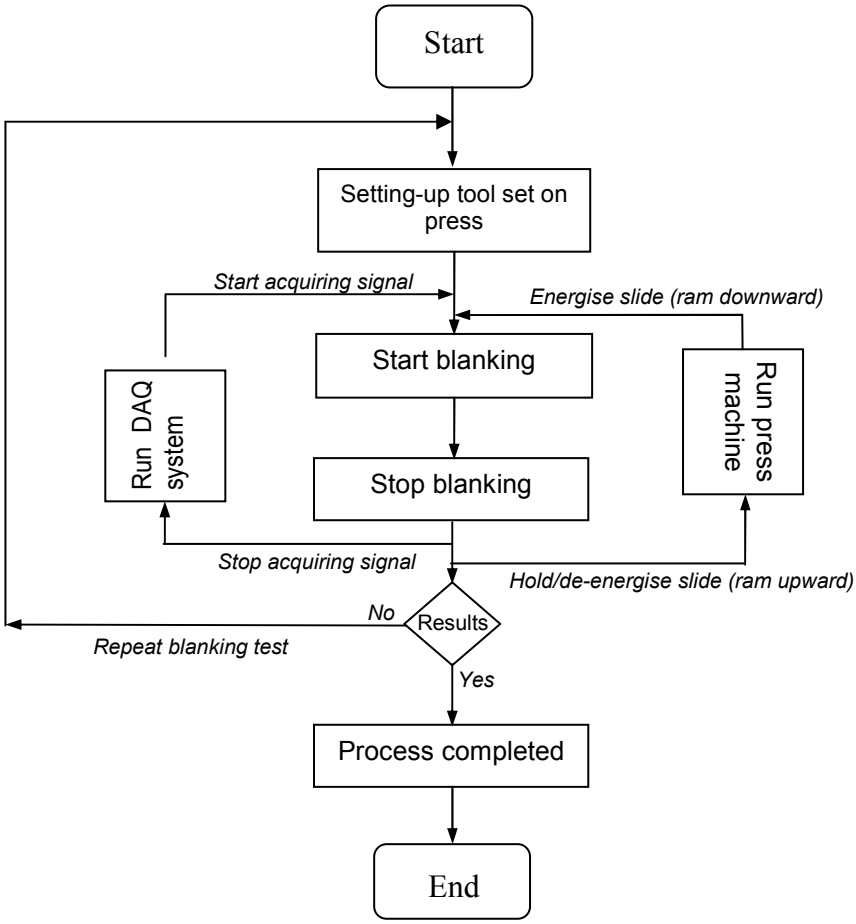

Fig. 3.29: Process flow for blanking monitoring

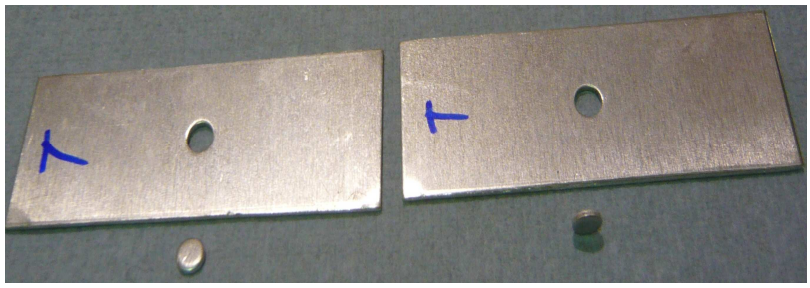

Fig. 3.30: The blanks produced during blanking trials

CHAPTER 4

RESULTS AND DISCUSSION OF BLANKING OPERATIONS: FORCE-DISPLACEMENT AND ACOUSTIC EMISSION SIGNATURES

This chapter presents the results and discussion of the blanking operations. The results can be divided into two sets: 1. the blanking signatures represented by the graphs of force-displacement, and 2. the graphs of selected AE parameters, which are represented by maximum amplitude in decibels (dB) and maximum peak frequency in kilohertz (kHz) of the AE signals. The details of discussion include the main effects and the interactions of blanking parameters, which were derived from different process outputs such as the maximum blanking force, obtained from the force-displacement signatures, the maximum amplitude and the maximum peak frequency captured from AE signatures.

4.1 Introduction

The results of the blanking operation were presented in the form of punch force-displacement curves and AE signatures. The raw data for the punch force and punch displacement was acquired by AEwin software and converted into ASCII outputs. This data was expressed as DC voltage *(V)* against time *(sec)* as illustrated in Fig. 4.1(a) and Fig. 4.1(b). The raw data was converted into the actual punch force-displacement data

using appropriate calibration characteristics. The force in Newton (N) was directly obtained from the voltage reading of the charge amplifier multiplied by a calibration multiplier, appropriate for a measured range of forces. The DC voltage from LVDT was converted into displacement using a corresponding value established by the LVDT transducer calibration results.

Fig. 4.1(c) shows that the initial portion of the force-displacement graph was taken up by the slack in the tooling system and that the final portion represented a stationary force resulting from friction between the progressing punch and the workpiece. Despite the blank thickness of only 1 mm, the total punch displacement from the initial position to the lowest position was 4 mm to give an ample stroke allowance for total separation of the blank from the workpiece material. However, only the initial 1.6 mm of this displacement, from the point of punch touching the surface of the workpiece to an arbitrary point chosen to represent the well advanced stationary stage of the process after blank separation.

Several tests were carried out in order to obtain stable AE signals, leading to reliable information associated to blanking operations. A minimum of at least five tests for each experiment were performed to capture the trends of the acquired AE signals. Factors that affected the quantity of AE signals, such as improper positioning of AE sensor on the surface of the material and incorrect hardware settings were observed. Selecting the proper hardware settings, in particular, the voltage threshold levels and frequency

filtering were based on a trial and error approach in order to monitor the noise levels. Noise was monitored before, during and after blanking by differentiating the noise signals from the AE signals generated from blanking. Fig. 4.1 (d) and Fig. 4.1(e) show the noise signals that can be distinguished from the wanted AE signals as in Fig. 4.1(f) captured during one of the blanking tests.

In order to discriminate the noise from the AE signals, the voltage threshold level was fine tuned. The threshold level, as shown in Fig. 4.1(g) for blanking aluminium *A1, A2* and *A3* sheets, was set at 40 dB, whereas the threshold level for blanking *A4* UFG sheets (Fig. 4(h)) was increased to 55 dB. Initially, threshold level for blanking UFG sheets was set at 40 dB, however, noise was detected even before starting the blanking operation. This led to several repetitions of the tests, with gradually increasing the threshold level to limit the noise. In addition, the lower and upper analogue filters were set at 100 kHz and 1 MHz respectively, with the sampling rate of 5 megasamples per second (MSPS).

The graphs of the AE signatures were presented by plotting the AE parameters: maximum amplitude (dB) and maximum peak frequency against the clearance. Attempts to use other AE parameters such as root-mean-square, signal energy and average signal level were made, but the values obtained were apparently low and unstable to produce a sustainable trending.

4.2 Force-displacement signatures

The force-displacement signatures during blanking operations can be used to monitor the quality of the blanking products. To compare results for different blanking clearances (3%, 5%, 7% and 9%), the force-displacement signatures were always plotted on the same graph. These were accompanied by the scanning electron microscopy (SEM) images, showing the edge profile of the produced blanks. The results of the blanking experiments for different materials (*A1, A2, A3* and *A4*) and different tool states were discussed in terms of three influences: 1. Influence of clearance, 2. Influence of tool wear, and 3. Influence of material.

Table 4.1 summarises the figures, showing the force-displacement signatures and the corresponding blanks for blanking materials *A1 – A4*, using different combination of tool states and different clearances. These results enabled a detail investigation of the influence of different tool states and different clearances on the maximum blanking force and the resulting blank edge quality. The values of the maximum blanking force obtained in these experiments can be referred in Table. 4.2.

4.2.1 Influence of clearance

Both clearance and tool wear have interrelated effects in a blanking process. In a long-running production of blanks, tool wear would alter the punch-die geometry, thus changing the clearance. As a result, the process of blanking and the form of the sheared surface of the blanks are influenced. However, in this particular work, experiments with

only using a sharp die and a sharp punch were considered in order to investigate the influence of clearance. Other combinations of different tool states were discussed in the following section of the influence of tool wear.

To study the influence of clearance on the maximum blanking force, the first combination tests was that of the sharp die and the sharp punch for blanking the "as supplied" material *A1*. Fig. 4.2 illustrates this case for four different clearances of 3%, 5%, 7% and 9%. Blanking with 3 – 5% clearances had indicated no significant different in values between the two ranges (1.2%), resulted in the highest maximum blanking force (1218 N). The shape of force-displacement graph started to be narrower with 7% clearance and greater. This can be noted that the maximum blanking force dropped to 1077 N with 7% clearance and further down to 1005 N to the lowest at the 9% clearance, giving a 17.5% difference in values between the lowest and the highest maximum blanking force.

The blank edge profiles obtained for four different clearances are shown in the same figure (Fig. 4.2). It can be observed that the blanking with smaller clearance (3%) produced a larger smooth sheared edge. With larger clearances (5 – 9%), the workpiece was bent farther before it deformed inside the die. This bending at initial stage of blanking caused a larger roll-over to be created at the bottom side of the blank. Blanking with 9% clearance produced a narrow sheared edge zone as the crack was initiated at lower punch penetration of about 55% of the sheet thickness.

The second series of tests involved blanking of annealed material *A2*. The force-displacement graphs for four blanking clearances are shown in Fig. 4.3. For a 3% blanking clearance, the highest maximum blanking force of 1157 N was obtained. This was followed by 997 N for 5% clearance. In contrary to what was obtained in blanking of *A1*, blanking with 7 and 9% clearances produced only a slight difference in obtaining the maximum force (2%), with the lowest maximum blanking force (886 N) obtained for a 9% clearance. It can also be shown that these forces were lower than those obtained for blanking *A1* because *A2* was softer as a result of annealing.

Comparing SEM images of Fig. 4.3, it can be noted that blanking *A2* with 3% and 5% clearances produced the best quality of sheared edge with a relatively large smooth surface. This resulted from a delay in the crack initiation during punch penetration into the workpiece material. From the force-displacement graphs, the crack initiation for blanking with clearances 7 – 9%, was slightly more delayed, which led to the smooth surface spreading over 70% of the sheet thickness. However, the rollover dominated the sheared edge profile. In this case, together with the burr formed, adversely affected the quality of the blanks.

The third group of tests was that of blanking CG material *A3*; the force-displacement signatures and the SEM images of the blanks are shown in Fig. 4.4. Four different values of maximum blanking forces (1599 N, 1558 N, 1501 N and 1397 N) were obtained for the increasing clearances. These values were greater than those obtained in blanking *A1*

and *A2*, which indicated that *A3* was harder. The force-displacement graphs started to decrease, after the punch progressing into the sheet about 50 – 55% of the sheet thickness. This implied that the fracture could be started at a shallow penetration, which led to a narrow smooth sheared zone and longer fracture zone of the blank edge.

From the SEM images (Fig. 4.4), blanking with 3% clearance produced a smooth edge for about 50% of the sheet thickness and created smaller rollover. By increasing the clearance to 5 – 9%, the rollover became more developed, reducing effectively the length of the smooth sheared surface. The fracture angle of the blank edge produced with 7 and 9% clearance increased. Further, with a larger clearance (9%), the shortest smooth sheared zone and the large of rollover were created.

The final tests to observe the influence of clearance on the maximum blanking force and the sheared edge profile of the blanks were carried out on UFG sheet, *A4*, and the results are shown in Fig. 4.5. Similar to other tests, the maximum blanking force was the highest (1714 N) for 3% clearance. However, there was only a small difference of the maximum blanking force (1630 N, 1602 N and 1589 N) obtained for blanking with 5, 7 and 9% clearances, respectively. Comparing with blanking material *A3,* the maximum blanking forces were higher, in which the relative difference was 7 – 13%, when the clearances vary from 3% to 9%. Further, these forces were obtained when the punch reached the same depth of penetration (about 30% of the sheet thickness) as in blanking *A3,* but crack initiation started at the punch penetration of about 45 – 50% of the

material thickness. From this point, the force-displacement graphs for four clearances decreases and this would characterise a low deformation of the blank, resulting in a narrow smooth edge.

From the SEM images (Fig. 4.5), it can be seen that blanking UFG sheet, *A4* with smaller clearances (3 – 5%) produced a longer smooth sheared zone compared to blanking with a larger clearance (7 – 9%). However, increasing the clearances, the fracture angle increased, creating a slope on the overall geometry of the blank edge. With 9% clearance, a larger rollover was developed to take a portion of deformation zone on a blank edge, thus reducing the smooth part, which was of an undesirable characteristic in terms of producing good quality blank.

4.2.2 Influence of tool wear

Wear of the blanking tool is a slow degradation process in the part of the tool, which is caused by friction between the tool and sheet metal or due to tool misalignment during the process. Initially, the evolution of wear of the punch and die consists of the flank wear, face wear and the rounding of the shearing edge. However, wear on the shearing edge will gradually become more severe.

In this experimental study, the different states of the tool wear were created by rounding the punch face edge and die-shearing edge with 150 μm radius. The influence of using a worn die (a die with corner radius), a worn punch (a punch with corner radius) or both

on the maximum blanking force and the profiles of the blank edge were investigated. Blanking experiments were carried out on different materials (*A1 – A4)*, with four clearances (3 – 9%) using three different combinations of tool states: a sharp die and a sharp punch (sharp die – sharp punch), a worn die and a sharp punch (worn die – sharp punch) and a worn die and a worn punch (worn die – worn punch).

The force-displacement graphs and the corresponding SEM images of the blanks for blanking material *A1*, for 3 – 9% clearances using the tools: a sharp die – worn punch (Fig. 4.6(a)), a worn die – sharp punch (Fig. 4.6(b)) and both, a worn die – worn punch (Fig. 4.6(c)) are shown. From the graphs of blanking, for all three different combinations of tool wear and comparing for all clearances, the highest maximum blanking force was obtained for 3 %, followed by 5% and 7% and 9% clearance. The values had a small difference (6.5%) between the highest and the lowest for all clearances for a combination of sharp die – worn punch, compared with those obtained using a worn die – sharp punch (13%) and both, a worn die – worn punch (15%). It can be observed also that higher forces were required for blanking with 3% (1344N), 5% (1292 N) and 7% (1280 N) clearances using a worn die – worn punch than those for other combination of tool states.

From the SEM images of the *A1* blanks (Fig. 4.6(a – c)), it can be seen that blanking with 3% and 5% clearances produced larger smooth sheared zone. With increasing clearances (7 – 9%), more material initially flowed inside the die and was locked on the

wall of the die, at the very beginning of the deformation, causing an increased in rollover depth. For 3% and 5% clearances and using a worn die, a deeper penetration was achieved before the initiation of fracture. This led to a greater deformation zone. However, the quality of these produced blanks was affected due to the significant size of rollover.

Fig. 4.7(a – c) present the force-displacement graphs and the SEM images of the corresponding blanks for material *A2*, for different tool states and clearances. The highest maximum blanking forces were obtained for 3% (1236 N) clearance and followed by second highest for 5% (1196 N) clearance in blanking with a sharp die – worn punch. However, there were no significant different in these values, obtained for blanking with the other combinations of tool states. For 7% and 9% clearance, the maximum blanking forces were reduced to the third and the lowest values, respectively. Further, the maximum blanking force obtained with these range of clearances using a sharp die – worn punch (916 – 938 N) and a worn die – sharp punch (915 – 938 N) had only a small difference. Unlike in blanking using either a worn die or a worn punch, the different between the highest and the lowest maximum blanking force using both a worn die – worn punch was also small (8%).

The SEM images of the blanks produced by a worn die – sharp punch and a worn die – worn punch showed that a deeper punch penetration was achieved for all clearances, causing a delay in crack initiation. It can be seen from the images in Fig. 4.7(b) and (c)

that the fracture zone was decreased compared with the blank edge produced by a sharp die. For all combinations of tool wear, for smaller clearances (3 – 5%), the rollover depth was relatively reduced than that of obtained with higher clearances (7 – 9%).

The results of blanking CG material *A3* are shown in Fig. 4.8(a – c). The maximum blanking forces of all the different combinations of tool wear were higher (1397 – 1864 N) than those obtained in blanking material *A1* and *A2*. The decreasing of force-displacement graphs for *A3* started early compared for *A1* and A2, when the punch progressed about 40 – 45% into the material. For all different combinations of tool states, blanking with 3% and 7% clearance produced only a small difference (less than 21 N) of maximum blanking force. For the same tool combinations, the difference between the highest and the lowest maximum blanking force for 3% and 9% clearance was only a 15%.

From the SEM images (Fig. 4.8(a – c)), it can be observed that the deformation zone was reduced, compared to the blank edge profiles for *A1* and *A2*. Using a worn die – sharp punch, the smooth sheared zone was larger for 3% and 5% clearance, compared with the other tool combinations. For 7% and 9% clearance, this zone was about the same size for all combinations of tool states. However, a larger rollover was developed in blanking using a worn die – worn punch, with 9% clearance.

The force-displacement graphs and the SEM images for blanking *A4* using different tool states and clearances are shown in Fig. 4.9(a – c). For all combination of tool states and for all clearances, the maximum blanking forces were higher compared with *A1, A2* and *A3*. These conformed that the strength of the material *A4* was higher due to the effect of ECAP. The highest maximum blanking force was obtained, first for 3% clearance, followed by 5%, 7% and 9% clearance. For 5% and 9% clearance, the difference of the maximum blanking force was small when using a sharp die – worn punch and a worn die – sharp punch. In all cases, the graphs decreased after the punch penetrating about 38 – 40% of the sheet thickness. Comparing the three combinations of the tool states, using a worn die – worn punch produced the highest maximum blanking force (2081 N) for 3% clearance, while the lowest maximum blanking force (1797 N) was obtained using a sharp die – worn punch for 9% clearance.

In general, the deformation zone in blanking material *A4* decreased, comparing with *A1*, *A2* and *A3*. However, it can be seen from SEM images (Fig. 4.9(a)) that using a sharp die – worn punch, with 3% and 5% clearance produced a larger smooth sheared zone. For 7% and 9% clearance and for all combinations of tool states, a large rollover was developed. This effect was clearly shown in blanking using a worn die – worn punch with 9% clearance (Fig. 4.9(c)).

4.2.3. Influence of material

In order to investigate the influence of the material in blanking, the results of blanking materials *A1 – A4*, using only a combination of a sharp die and a sharp punch were used. Further, only blanking with 3% and 9%, which represents the smallest and the largest clearance were chosen to enable the monitoring of any significant difference in the maximum blanking force for different types of material. The SEM images of the corresponding blanks were already presented in section 4.2.1.

Fig. 4.10 shows the force-displacement graphs obtained for blanking of material *A1 – A4* using a combination of a sharp die – sharp punch with 3% clearance. The material *A4* and *A3* produced the highest (1714 N) and the second highest (1599 N) maximum blanking force, respectively, compared with blanking *A1* (1218 N) and *A2* (1157 N), which was the lowest. The force for *A3* and *A4* started to decrease after the punch progress into the sheet of about 40 – 45% of sheet thickness. However, it can be seen that, there was a delay in force decrease for *A1* and *A2*, which occurred about 60 – 70% of the punch progress. These indicated that the plastic deformation of materials *A3* and *A4* was lower than that of *A1* and *A2*. This effect can also be observed in the corresponding SEM images of the produced blanks.

The force-displacement graphs for blanking material *A1 – A4* with 9% clearance are shown in Fig. 4.11. The characteristics of blanking with 9% clearance were similar to blanking with 3% clearance. The maximum blanking force was the highest for *A4* (1589

N) then *A3* (1397 N), *A1* (1005N) and the lowest, *A2* (886 N). As explained earlier these values are always lower than those obtained for a smaller, 3% clearance. The depth of the punch penetration at the onset of fracture was almost the same in for blanking *A3* and *A4* with 3% clearance, but this depth increased to more than 70% of the sheet thickness for blanking *A1* and *A2*.

4.2.4 Statistical design of experiment – Maximum blanking force as a quality characteristic

The statistical design of experiment (DOE) was conducted to investigate the variation in the response directly to the changes in the factor level. From DOE, it could determine which one of the chosen factors, in this case were a die, a punch and clearance had an important effect on the response. In this particular work, the maximum blanking force was chosen as the response or a quality characteristic.

Three factors and two levels were identified as follows:

1) A die – sharp die (-), worn die (+)
2) A punch – sharp punch (-), worn punch (+)
3) The clearance – 3% (-), 9% (+)

The 3% and 9% clearance were selected as an extreme case to represent the smallest and the largest clearance, in order to observe a significant result.

A half normal plot was employed to distinguish the real effect. The detailed statistical calculations were enclosed in Appendix 9. From the half normal plot for all materials, it can be seen that the dominant real effect to influence the maximum blanking force was the clearance, followed by the punch and the die. Fig. 4.12(a – b) shows the results of DOE for blanking *A1*. The attainment of the maximum blanking force was shown as a function of clearance with the punch as a parameter and for two different die states in terms of a sharp die (-) and a worn die (+). The graphs show that for any combination of a sharp die – sharp punch and a sharp die – worn punch, or vice versa, the maximum blanking force decreased with the increasing clearance from 3% to 9% clearance. Similar trends were observed for *A2* (Fig. 4.13(a – b)), *A3* (Fig. 4.14(a – b)) and *A4* (Fig. 4.15(a – b)). However, the change of maximum blanking force obtained from smallest to largest clearance for *A4* was small compared to *A1, A2* and *A3.*

4.3 Acoustic emission signatures

The AE signatures associated with blanking materials *A1 – A4* were studied. The effects of blanking using different combination of tool states at different clerance on the maximum amplitude (Amp_{max}) and maximum peak frequency $(fpeak_{max})$ of the AE signals were presented by plotting the graphs of these AE parameters versus clearance. For blanking with a sharp die and a sharp punch, these parameters were plotted on the same graph, while separate graphs were used to present the results of using the combination of different tool states.

In this study, the maximum amplitude of AE was defined as the highest value of AE amplitude obtained in the AE event during blanking process. The amplitude is expressed in decibels (dB) using the relationship as follows:

$$\text{Amplitude in decibel (dB)} = 21 \log \left(\frac{\text{Vmax}}{1\mu\text{-volt}}\right) - (\text{preamplifier Gain in dB})$$

$$= 21 \log \left(\frac{\text{Vmax}}{1\mu\text{-volt}}\right) - (40 \text{ dB})$$

In AE data processing system, a real time Fast-Fourier transforms (FFT) was performed on the AE waveforms associated with the AE hits to produce frequency spectrum. The peak frequency was defined for the point in the power spectrum at which the peak magnitude occurs. Further, the maximum peak frequency was the highest value of peak frequency, expressed in kilohertz (kHz) obtained in the AE event during blanking process. In order to gather, the magnitude of the AE parameters associated with blanking, AE data was extracted directly from the statistics that were established by the AEwin software. These statistics are available in one of the menus known as a 'line listing display". An example of a line listing file is shown in Fig. 4.16.

The AE signals were recorded carefully during blanking operations. Each test was performed repeatedly, minimum five times to get average values of maximum amplitude and maximum peak frequency for a selected clearance. The error for these data was controlled within a two standard deviation (2σ). The magnitude of maximum amplitude and maximum peak frequency for all combinations of different tool states are shown in Table 4.3 and Table 4.4, respectively.

4.3.1 Influence of clearance

In the case of investigating the effects of blanking clearance on maximum amplitude and maximum peak frequency of the AE signals, only a combination of a sharp die and sharp punch was used. Results of AE signatures for materials *A1 – A4* are shown in Fig. 4.17(a – d). It can be observed from the graphs that the maximum amplitude and maximum peak frequency for blanking *A1* were decreasing slightly with increasing clearance from 3 – 7% clearance but then increased for the highest clearance of 9%. In contrast, the highest values of AE parameters for blanking material *A2* and *A3* were obtained for 3% clearance and then decreased as the clearance increased to the lowest values for 9% clearance. However, for material *A4* both AE parameters exhibited only a small change as clearance increased from the smallest (3%) to the largest clearance (9%).

Comparing the AE signatures for the sharp tools AE and for all materials, the maximum amplitude of blanking *A1* was the lowest, followed by *A4* (64 dB), *A2* (68 dB) and *A3* (75 dB) for 3% clearance. With 9% clearance, material *A1* had the highest maximum amplitude (64 dB), followed by *A4* (53 dB), *A3* (46 dB) and *A2* (45 dB). The maximum peak frequency for *A1* decreased from 278 kHz for 3% clearance to 207 kHz for 7% clearance and then increased to 278 kHz at the largest clearance. The decrease in maximum peak frequency after 5% clearance was significant for *A3*. This trend was also observed in *A2* from 3 – 7% clearance, in which *A2* had the lowest maximum peak frequency of 148 kHz for 7% clearance. This AE parameter had then increased to 205

kHz for 9% clearance. The highest maximum peak frequency was captured in *A4,* giving the results of 512 – 468 kHz from 3 – 9% clearance.

4.3.2 Influence of tool wear

The combinations of a sharp die – worn punch, a worn die – sharp punch and a worn die – worn punch were used in order to investigate the influence of tools wear on maximum amplitude and maximum peak frequency of the AE signals captured during blanking material *A1 – A4*. However, the graphs of blanking using a sharp die – sharp punch were also included for comparison with other tool states. Fig. 4.18(a – b) to Fig. 4.21(a – b) present these results.

The maximum amplitude for blanking *A1* using a sharp die – worn punch and a worn die – sharp punch decreased with increasing clearance (Fig. 4.18(a)). The values reduced from 53 to 49 dB for a sharp die – worn punch and 66 to 50dB for a worn die – sharp punch as the clearance increased from 3 – 9%. However, the maximum amplitude for a combination of worn die – worn punch remains constant for about 47 dB from 3 – 5% clearance and then increases significantly to the highest maximum amplitude of 64 dB for 9% clearance. Similar trend was observed for 3 – 7% clearance for the maximum peak frequency when using a sharp die – worn punch and a worn die – sharp punch (Fig. 4.18(b)). The maximum peak frequency for these combinations of tools decreased from 278 kHz to 101 kHz, which was the lowest and from 298 kHz to 210 kHz, respectively.

The highest maximum peak frequency of 478 kHz was obtained for a worn die – worn punch for 9% clearance.

Also for blanking *A2*, the maximum amplitude had decreased from 63 to 46 dB, for the increasing clearance from 3 – 9% when a worn die – sharp punch were used (Fig. 4.19(a)). With a sharp die – worn punch, only a small variation of the maximum amplitude was detected from 54 dB for 3% clearance to 44 dB for 9% clearance. Further, these values remained at the 50 dB level for 5% and 7% clearance. A significant increase in maximum amplitude from 47 dB to 66 dB was obtained using a worn die – worn punch. Unlike blanking *A1*, all combination of tool states in blanking *A2* had produced different values of the maximum peak frequency for 3% clearance (Fig. 4.19(b)). For a sharp die – worn punch and a worn die – sharp punch, the values decreased with increasing the clearance, in which a combination of sharp die – worn punch produced the lowest maximum peak frequency (102 kHz) for 9% clearance. The trend of increasing this AE parameter with clearance for *A2* was similar to *A1* for a worn die – worn punch, which resulted in the highest maximum peak frequency of 586 kHz captured at 9% clearance.

It can be seen from monitoring the blanking of *A3* that only a small change of maximum amplitude from 48 dB to 44 dB, measured for 3 – 9% clearance, was obtained using a combination of sharp die – worn punch (Fig. 4.20(a)). However, for a worn die – sharp punch, these values decreased from 64 dB to 49 dB for 3 – 5% clearance and then

increased from 50 dB to 70 dB for 7 – 9% clearance. With a worn die – sharp punch, the maximum amplitude increased with clearance from 55 dB to 71 dB. Unlike for *A1* and *A2*, the maximum peak frequency for a worn die – sharp punch increased with clearance from 278 kHz to 478 kHz (Fig. 4.20(b)). This trend was also followed by a worn die – worn punch, in which the values increased from 403 kHz to 507 kHz. In contrast, the maximum peak frequency for a sharp die – worn punch decreased with increasing clearance from 278 kHz to 112 kHz.

Comparing with previous results for *A1, A2* and *A3*, the maximum amplitude for *A4* had decreased with increasing clearance from 72 to 52 dB and 73 to 51 dB using a combination of sharp die – worn punch and worn die – sharp punch respectively (Fig. 4.21(a)). The same trend was also observed for a worn die – worn punch, in which the maximum amplitude decreased from 84 to 64 dB. It was also found that for all combinations of tool states, there was only a small variation of maximum peak frequency for *A4* in the range of 375 kHz to 590 kHz, which was measured from 3 – 9% clearance. For a sharp die – worn punch and a worn die – sharp punch, these values decreased from 585 kHz to 448 kHz and 548 kHz to 498 kHz, respectively (Fig. 4.21(b)). Similarly, the maximum peak frequency for a worn die – worn punch decreased from 590 kHz, which was the highest, to 375 kHz as the clearance increased from 3 – 9%.

4.3.3 Influence of material

In order to study the influence of material on the maximum amplitude and maximum peak frequency, the results for blanking *A1 – A4* using only a sharp die and a sharp punch were compared. The maximum amplitude for *A1*, initially 48 dB for 3 % clearance, decreased to 45 dB for 7% clearance and then increased to 64 dB for 9% clearance (Fig. 4.22(a)). For *A2* and *A3*, the maximum amplitude decreased with increasing clearance from 68 to 45 dB and 75 to 46 dB. The decreasing of maximum amplitude from 66 to 53 dB for 5 – 9%% clearance could be observed also in *A4,* which amplitude was initially measured as 64 dB for 3% clearance.

Comparing with other materials, the maximum peak frequency for *A4* reached the highest values for all clearances, however these values decreased with increasing clearance from 512 kHz to 453 kHz, measured for 3 – 7% clearance and then increased slightly to 468 kHz for 9% clearance (Fig. 4.22(b)). This trend was similar for *A1* and *A2*, which produced the maximum peak frequency of 278 kHz and 478 kHz for 3% and decreased to 207 kHz and 148 kHz for 7% clearance respectively. These values were then increased to 258 kHz and 205 kHz for 9% clearance. For *A3*, the maximum peak frequency initially of 478 kHz for 3% clearance decreased significantly after 5% clearance from 483 kHz to 150 kHz at the largest clearance of 9%.

4.3.4 Statistical design of experiment – Maximum amplitude and maximum peak frequency as quality characteristics

The DOE approach was also used to investigate the real effect and the interaction of the die, punch, clearance and material to affect the maximum amplitude and the maximum peak frequency of the AE signals in blanking operations. In this case, the maximum amplitude and the maximum peak frequency were chosen as the quality characteristics.

Four factors, each with two levels were identified as follows:

1) Die – sharp die (-), worn die (+)
2) Punch – sharp punch (-), worn punch (+)
3) Clearance – 3% (-), 9% (+)
4) Material – A2(-), A4(+)

The 3% and 9% clearance were also selected as before to represent the smallest and the largest clearance. Material *A2* and *A4* were chosen to give a significant result between two levels of different ductility. A half normal plot was established from the experimental design for each AE parameter and the statistical calculations for these were attached in Appendix 10.

Fig. 4.23(a) and Fig. 4.23(b) represent a half normal plot for four factors to affect the maximum amplitude and maximum peak frequency of the AE signals. It can be observed from both half normal plots that all factors (die, punch, clearance and material) proved to be the real effects to influence the maximum amplitude and the maximum

peak frequency. Further, there was also the interaction between die and punch in affecting the maximum amplitude and the interaction between all those factors to affect the maximum peak frequency. The observation made from DOE also contradicted with the experimental results obtained for *A4*, in which *A4* was insensitive to the changing of clearance and tool states. From these results, it was not easy to draw the conclusion to identify the chosen factors that were statistically significant to affect the measured AE parameters.

4.4 Discussion

4.4.1 Experimental procedures

Due to the simple construction of the blanking apparatus, several parts of the blanking tools set are required to be removed and reassembled for every consecutive blanking test. To insert the new sample for the following test after the previous blanking experiment completed, the upper plate, which hold the punch was removed from the guide pillars and then repositioned to ready for other blanking tests. Special care and precautions had been taken such as using the borescope to ensure that problems of misalignment of the punch and die was avoided, thus maintaining the same amount of clearance as previous readings. This was essential for good repeatability and reliable results. The minimum of five blanking operations were performed and the average readings were taken as final results.

A total number of 64 experiments were carried out, involving all materials, combinations of tool states and clearance. In order to summarise these influencing factors, a design of experiment was developed with four factorial set of experiments to control the separate influences: two sets of 3% and 9% clearance (taken as two extreme cases of smallest and largest clearance), four sets of material marked as *A1, A2, A3* and *A4* (*A2* and *A4* were taken as two factors to represent different ductile material) and two sets of punch and die states. These enabled to encompass the effects and interaction effects with variation of clearances and tool states in effecting the maximum blanking force and the measured AE parameters (maximum amplitude and maximum peak frequency).

4.4.2. Influence of clearance to affect the characteristics of force-displacement graphs

Previous research had proven that the clearance between the punch and die (blanking clearance) is a major process parameter in blanking process, which has a significant effect on blanking force and sheared edge quality. Many reports that involved blanking operations have showed the final results of interests, less explanations about what are actually happening during the punch movement to deform the workpiece, in particular the characteristics of force-displacement curves. Further, numerous literature can be reported involved blanking classical sheet metal, in which many cases using existing polycrystalline or coarse grained metals. At present, little work that involved blanking UFG material had been reported. In this study, success attempts had been made to

monitor the force-displacement signatures of the blanking process, which influenced by varying the clearances.

The characteristics of force-displacement curves in Fig. 4.2 to Fig. 4.5 have proved that the maximum blanking forces decrease as the clearance increases, as simplified in Fig. 4.24. The forces caused the material flow during plastic deformation were retarded by small clearances, thus increasing additional forces used to exert material to deform inside the die. The phenomenon of: small clearance – higher force and larger clearance – lower force also can be observed in blanking UFG materials, as many previous reports that described the same effects of clearance on blanking forces were only involved blanking classical coarse grained material. Cold-rolled material such as *A1* materials is characterised by slightly lower ductility with higher shear yield strength. Blanking signatures of *A1* materials illustrated that the maximum blanking forces attained were higher as compared to blanking annealed *A2* materials, which were soften due to the annealing effects. Ductility of *A2* materials was also improved as the indication that point of crack initiation was delayed until 30 – 40% of punch penetration when compared to A1 materials of 22 – 28% punch penetration.

Theoretically, the point of the crack initiation, which affecting the blank edge profile, could be determined directly from the force-displacement characteristics. This is the point when the force started to decrease sharply after reaching the point of the maximum blanking force. However, it was not easy to check this point from the force-displacement

graphs obtained in these experiments. Therefore, a new approach was established to characterise the force-displacement graphs linking to the quality of the blank, based on three criteria:

1. The point on the curve representing the maximum blanking force,
2. The slope of the decreasing force to the point of separation and
3. The punch stroke required for blank separation.

Fig. 4.25(a) shows the force-displacement graphs of blanking *A1, A2, A3* and *A4* for 3% clearance using a combination of sharp die and sharp punch. These graphs was converted to equivalent force-displacement graphs (Fig. 4.25(b)), indicating a line connecting the starting point of the punch touches the surface of workpiece material, the point of the maximum blanking force and the point when the force starts to decrease to the point of the blank separation. From Fig. 4.25(b), the stroke of the maximum blanking force, the slope of the decreasing force to the point of separation and the punch stroke required for blank separation were measured. These measurements were correlated with the length of the smooth sheared edge produced in the blank as shown in Table 4.5.

From the characteristics of equivalent force-displacement graphs, it can be observed that a longer stroke of reaching maximum blanking force, lower slope of decreasing force to separation and longer punch stroke to separation produced a greater smooth sheared edge profile, which was produced by *A2* material. On the other hand, *A4*, produced a

shorter smooth sheared edge profile had the characteristics values in contrast with *A2*. Similar method was used to quantify the blank edge quality for other clearance.

The grain refinery process produced stronger material, which could be proved by the results of blanking UFG (*A4*) materials as compared to blanking *A3* materials. As the clearance increases, it could be observed that a reduction in the maximum blanking force, an increase in the punch penetration at fracture and consequently an increase in the burnished depth of the cut of the blank. It can be seen on SEM images that the blanking clearance has also a strong effect on rollover and fracture depth of sheared profile of the blanks. Larger blanking clearance allows the material to flow more easily between the punch and the die. As a result of the bending stage of the material increased, the rollover was also increased.

4.4.3. Influence of tool wear to affect the characteristics of force-displacement graphs

The effect of decreasing blanking force with decreasing clearance could also be observed when blanking using a combination of different states of tool. From the design of experiment, the punch had a greater influence than the die in affecting the attainment of the maximum blanking force. The influence of tool wear on the maximum blanking force at 3% and 9% blanking clearance were compared. These sets of clearances were taken as comparison as they represent the smallest and the largest clearance within this scope of study.

With smaller clearance (3%) and comparing with different state of tool, blanking using a worn punch resulted in the highest maximum blanking force. Considering only using a worn die itself was not necessary to affect the maximum blanking force. This was shown by the results of blanking using a combination of worn die and sharp punch, which led to lower maximum blanking force as compared to either blanking using a combination of sharp die and worn punch or a worn die and a worn punch. With a larger clearance (9%), blanking using a combination of worn die and worn punch resulted to the highest maximum blanking force.

The characteristic of force-displacement graphs (Fig. 4.26(a)) and the equivalent force-displacement graph (Fig. 4.26(b)) of blanking *A1 – A4* using a worn die and a worn punch at 9% clearance were used to correlate with the sheared edge of the produced blanks. The measurements of the smooth sheared edge of the produced blanks *A1 – A4* were verified using SEM images and the results are shown in Table 4.6. A larger smooth sheared edge profile of the blank was produced with a longer stroke for maximum force and stroke for separation and lower slope of decreasing force to blank separation. Blanking using a worn die and a worn punch at a larger clearance resulted in a deeper punch penetration, but the rollover increased, which in turn reduced the smooth sheared edge in the deformation zone.

The introduction of a radius on the tip of the tool causes additional plastic deformation of the blank, since blank material is forced to obey the shape of the tool and flow around

the radius of the punch. The radius at the tip of the punch also caused a delay in the start of shear cutting and additional forces required to accelerate the flow of the materials.

4.4.4 AE maximum amplitude and maximum peak frequency

During blanking operations, hits or events of AE were generated on each stroke by several possible occasions from the following sources:

1. Friction between the punch and the blank holder and friction between the punch and the scrap.
2. The impact of initial contact point of the punch on the surface of workpiece.
3. Plastic deformation of the material workpiece.
4. Crack initiation and fracture propagation, and
5. Vibration of the press and the tools set.

With proper control, the AE signals were measured from the beginning of the punch touches the surface of the workpiece, continues to deform the workpiece and up to the total rupture occurrence. Pre-test was performed to move the punch while capturing the AE signals to ensure that the hits generated from friction between the punch and the blank holder were not added to the sum of AE generated from blanking process. Likewise, the AE generated due to the vibration of the press and the tools set were measured and threshold control was adjusted to eliminate the AE hits from these sources. The assumptions that the results of AE signatures, measured as AE parameters of maximum amplitude in dB and maximum peak frequency in kHz were fully justified to represent the AE signatures for blanking processes.

From the trending of the graphs of AE maximum amplitude and maximum peak amplitude, it is not easy to conclude the influence of the clearances on these AE parameters. In general, the measured AE parameters from blanking *A2, A3* and *A4* were gradually declined to the lower values as the clearances increased except when using a worn die and a punch. However, the maximum amplitude for blanking *A1* was either maintained or slightly reduced until it started to increase when the clearance greater than 7% clearance. In contrast, the values of AE parameters measured for blanking using both worn die and punch had increased significantly as the clearance increased for all types of materials.

In order to observe the influence of tool wear on AE maximum amplitude and maximum peak frequency, the results of blanking operations performed at 3% and 9% clearance were compared. The AE signatures due to using different combination of blanking tools wear were varied for all types of materials. However, it was not easy to find a specific trend to correlate the wear state of the tools with the values of maximum amplitude and the maximum peak frequency of the AE signals.

The maximum amplitudes of AE signals for blanking *A1* and *A2* at 3% clearance using either a worn die or a worn punch, or both a worn die and punch produced about the same magnitudes. However, when using sharp tools, those magnitudes were far different. Comparing *A3* and *A4*, the maximum amplitude for blanking *A4* using any combination of worn tools was higher than blanking *A3.* The maximum peak frequency

obtained for blanking *A1* and *A2* using a worn die and a worn punch produced almost the same magnitude. However, the maximum peak frequency of blanking *A4* with any type of tool states had still attained the highest level. With larger clearance at 9%, blanking using a worn die and a worn punch produced higher maximum amplitude of AE signals as compared to using other types of tools states.

From the experiments, it was difficult to obtain a trend that could correlate the chosen AE parameters with the blanking parameters due to the variations of the AE signals. This led to complexity in monitoring the blanking process using AE technique. Possible causes could be identified to contribute to these problems:

1. The nature of the blanking process, which provides to a short period of time in capturing the AE signals.
2. The inconsistency of contacts between the AE sensor surface and the workpiece material.
3. The location and the distance of the AE sensor from the source of the signals. Improper positioning of the AE sensor could affect the AE signal propagation.

However, it is still a hope that by improving the design of the blanking tools and correcting the ways the AE sensor being used could lead to a better usefulness of AE technique for monitoring the blanking process.

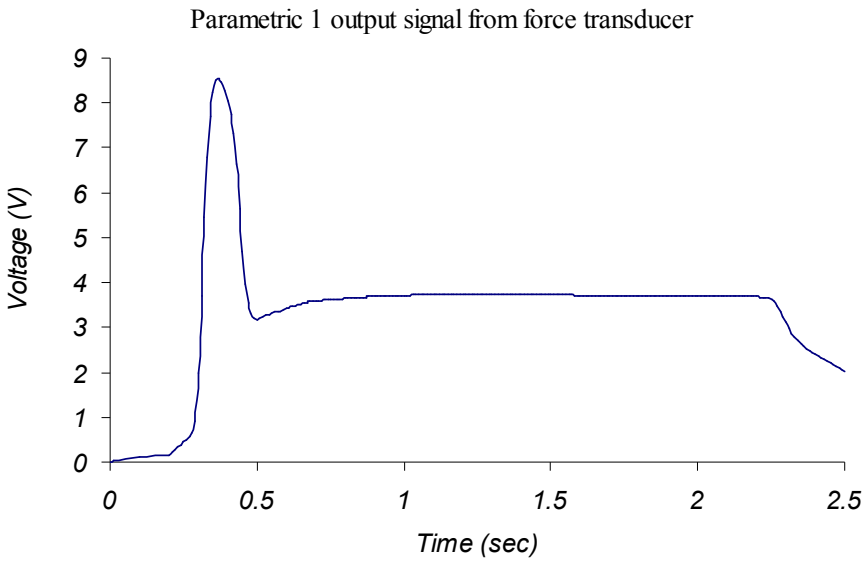

Fig. 4.1(a): Output signal of voltage-time of force transducer

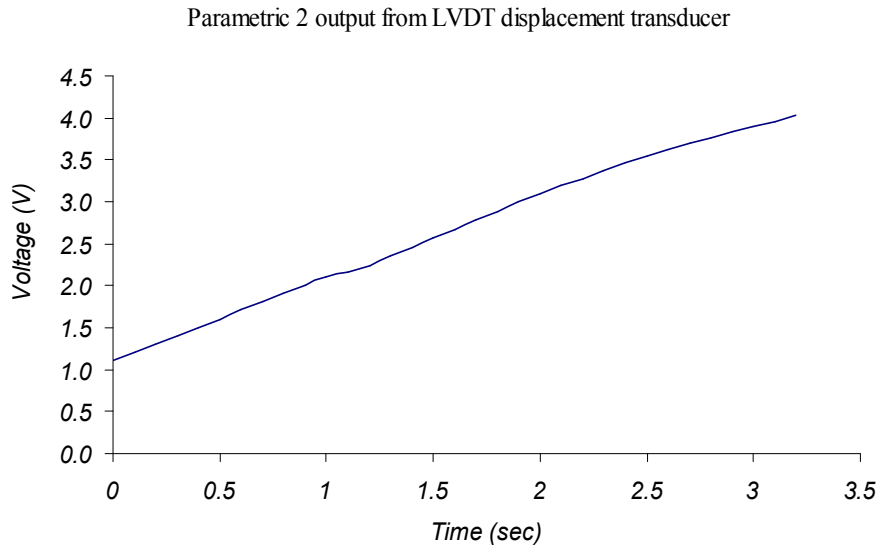

Fig. 4.1(b): Output signal of voltage-time of LVDT displacement transducer

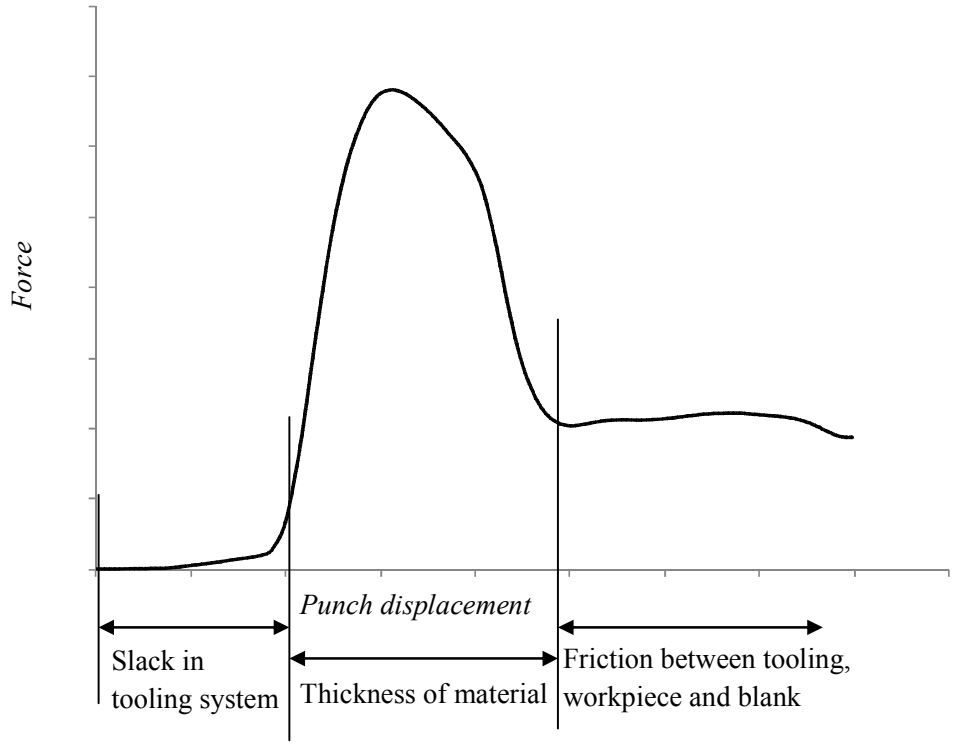

Fig. 4.1(c): Part of slack in tooling system showed in force-displacement graph

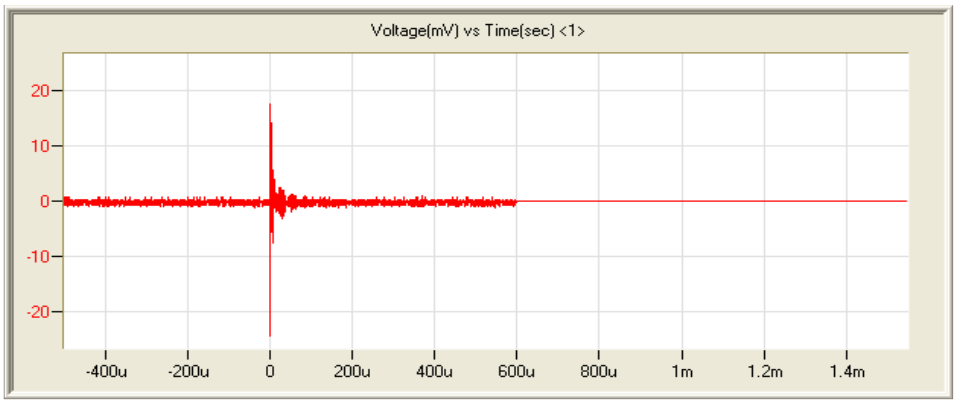

Fig. 4.1(d): Noise signal captured before start of blanking operation

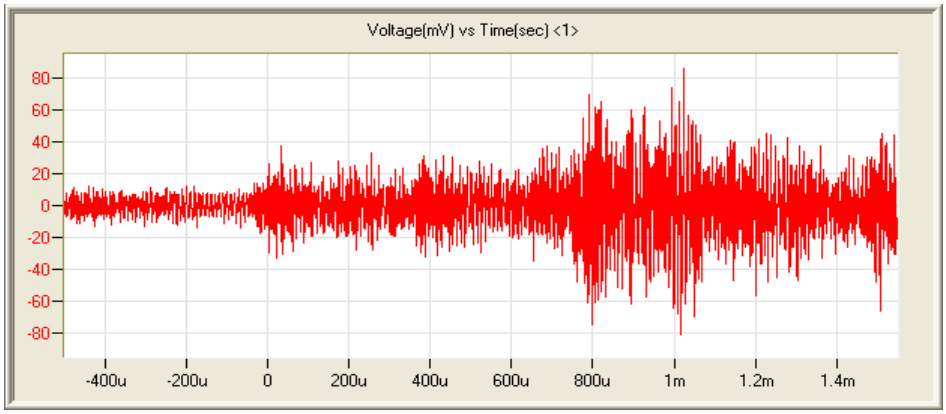

Fig. 4.1(e): Noise signal captured after halt the blanking operation

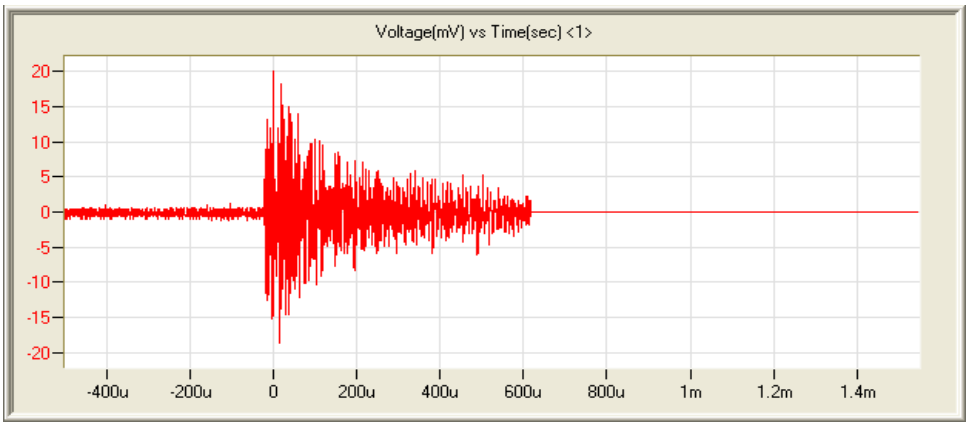

Fig. 4.1(f): AE signal captured during blanking operation

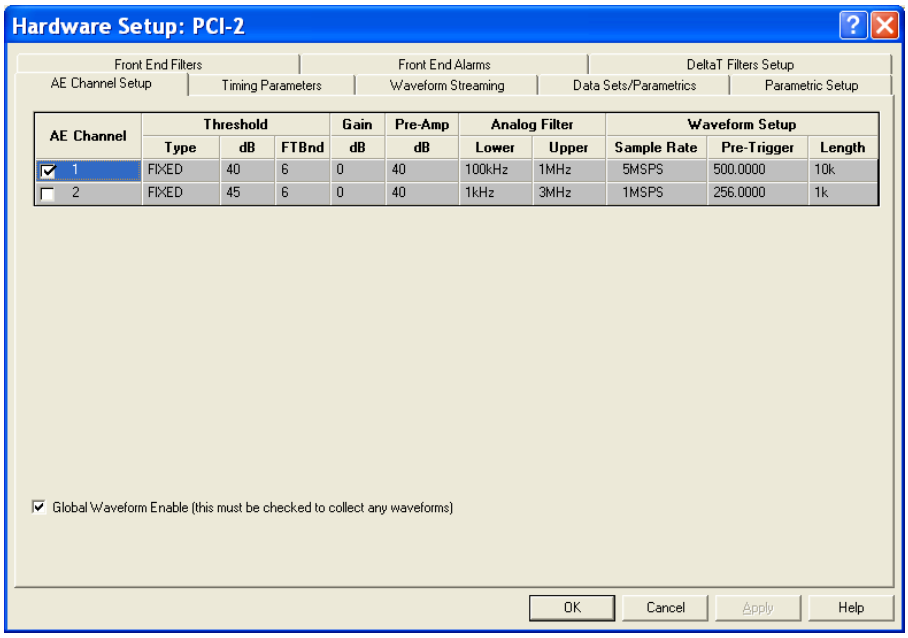

Fig. 4.1(g): Hardware setting for blanking *A1, A2, A3* materials

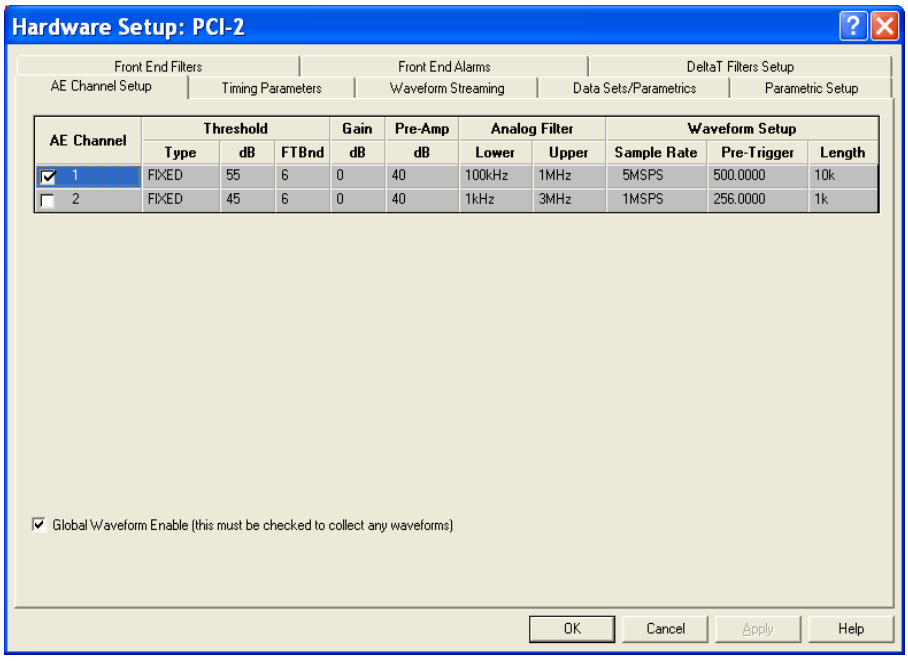

Fig. 4.1(h): Hardware setting for blanking *UFG (A4)* materials

Table 4.1: List of figures of force-displacement signatures and the SEM images of the blanks of blanking material *A1 – A4* with 3 – 9% clearances using different tool states

Material	**Tool states & clearances 3 – 9%**			
	Sharp die – sharp punch *D1P1*	**Sharp die – worn punch** *D1P2*	**Worn die – sharp punch** *D2P1*	**Worn die – worn punch** *D2P2*
A1	Fig. 4.2	Fig. 4.6(a)	Fig. 4.6(b)	Fig. 4.6(c)
A2	Fig. 4.3	Fig. 4.7(a)	Fig. 4.7(b)	Fig. 4.7(c)
A3	Fig. 4.4	Fig. 4.8(a)	Fig. 4.8(b)	Fig. 4.8(c)
A4	Fig. 4.5	Fig. 4.9 (a)	Fig. 4.9 (b)	Fig. 4.9 (c)

Table 4.2: The maximum blanking force of blanking material *A1 – A4* with 3 – 9% clearances using different tool states

	Maximum blanking force (N)																
Tool states	Sharp die – sharp punch *D1P1[3 – 9]*					Sharp die – worn punch *D1P2[3 – 9]*					Worn die – sharp punch *D2P1[3 – 9]*					Worn die – worn punch *D2P2[3 – 9]*			
Clearance	3%	5%	7%	9%		3%	5%	7%	9%		3%	5%	7%	9%		3%	5%	7%	9%
Material																			
A1	1218	1205	1077	1005		1237	1215	1182	1156		1211	1178	1142	1053		1344	1292	1280	1143
A2	1157	997	907	886		1236	1196	938	916		1066	1053	938	915		1114	1110	1056	1025
A3	1599	1558	1501	1397		1826	1804	1666	1590		1675	1660	1627	1606		1864	1861	1831	1728
A4	1714	1630	1602	1589		1912	1848	1812	1797		1875	1834	1810	1788		2081	2043	1986	1800

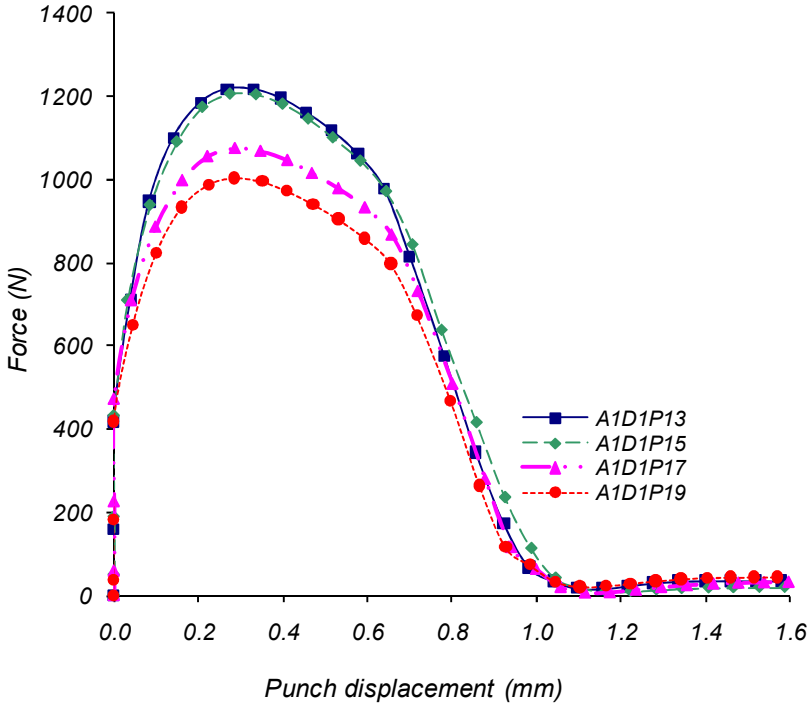

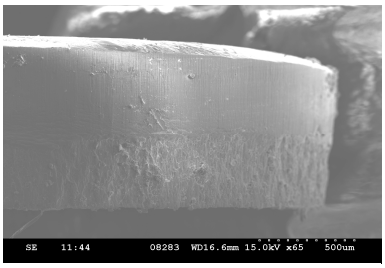

A1D1P13

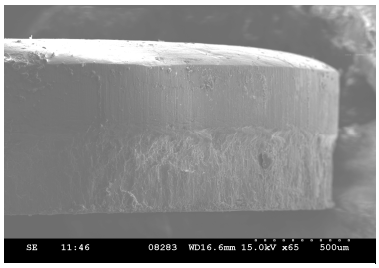

A1D1P15

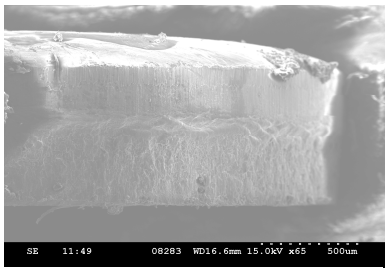

A1D1P17

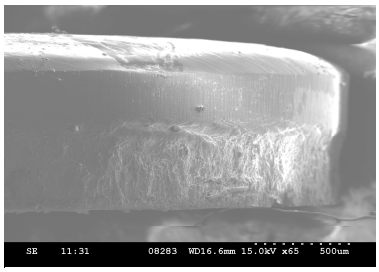

A1D1P19

Fig. 4.2: The force- displacement graphs for blanking aluminium *A1* using a sharp die and sharp punch with 3 – 9% clearances, and the SEM images of the produced blanks

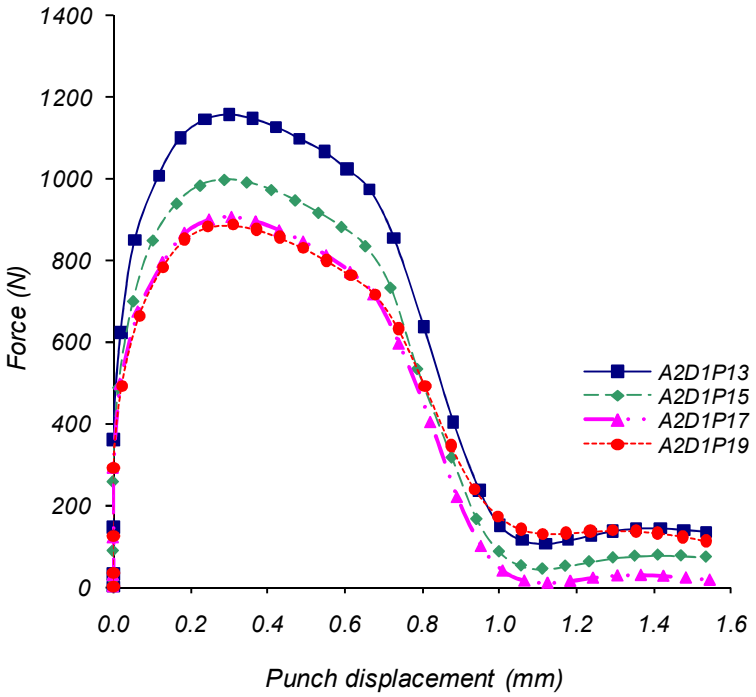

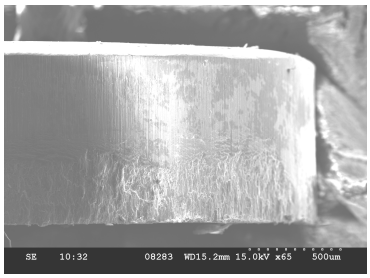

A2D1P13

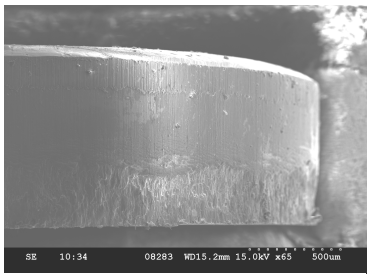

A2D1P15

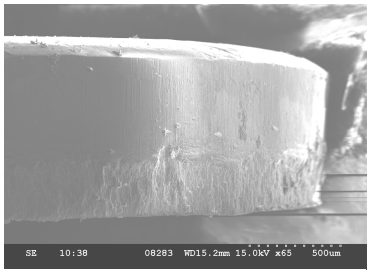

A2D1P17

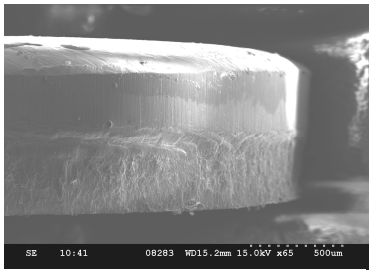

A2D1P19

Fig. 4.3: The force-displacement graphs for blanking aluminium *A2* using a sharp die and sharp punch with 3 – 9% clearances, and the SEM images of the produced blanks

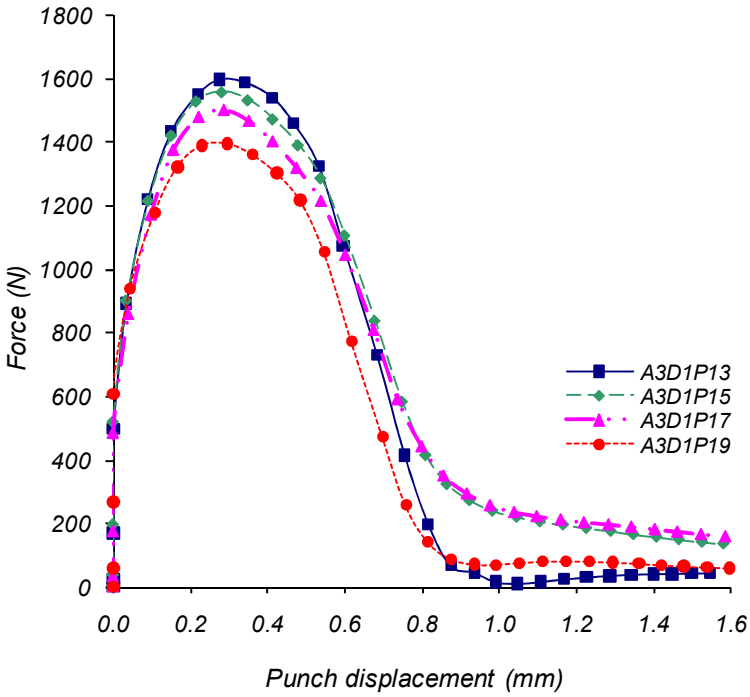

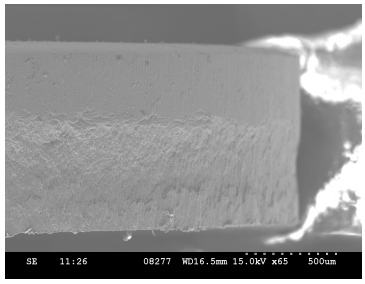

A3D1P13

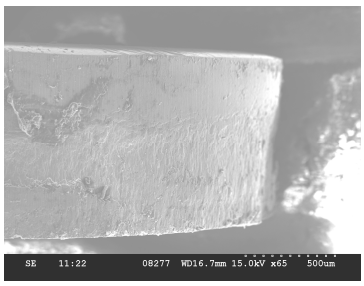

A3D1P15

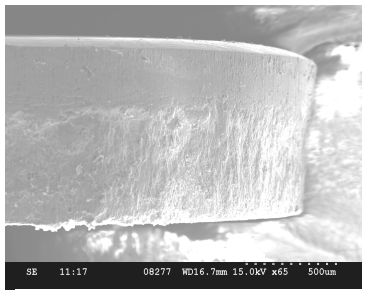

A3D1P17

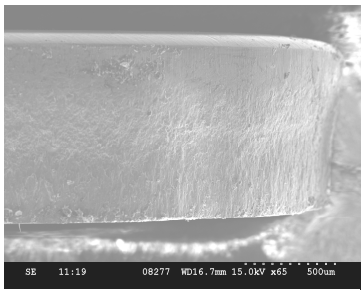

A3D1P19

Fig. 4.4: The force- displacement graphs for blanking aluminium *A3* using a sharp die and sharp punch with 3 – 9% clearances, and the SEM images of the produced blanks

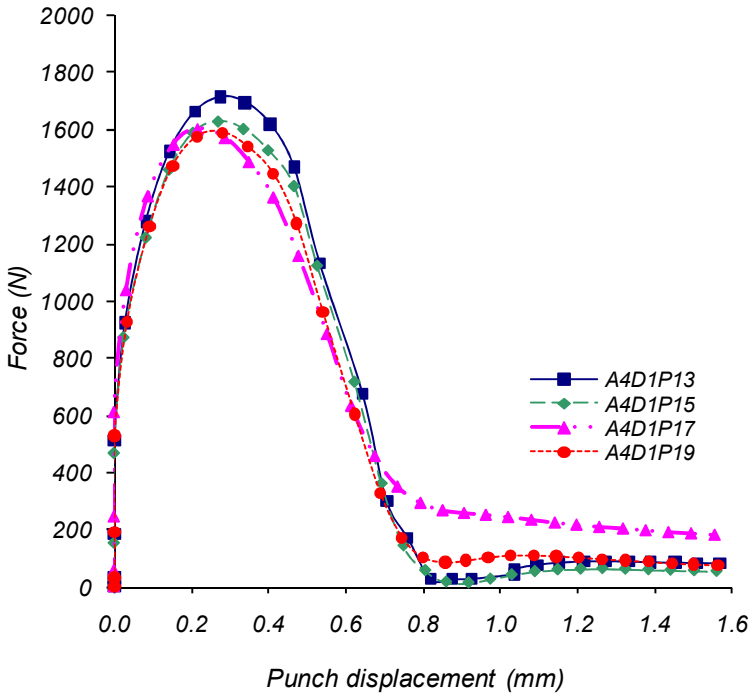

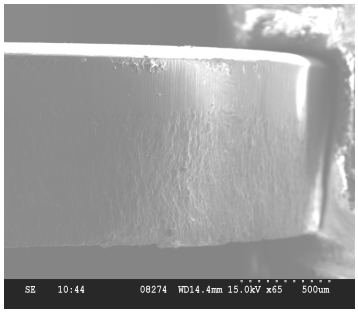

A4D1P13

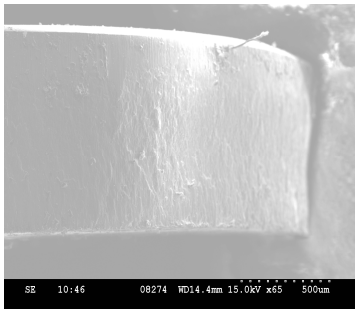

A4D1P15

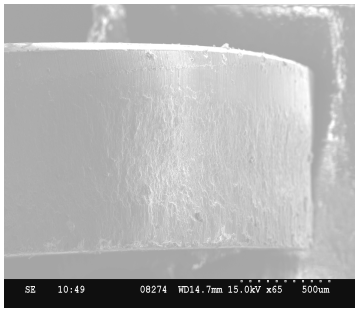

A4D1P17

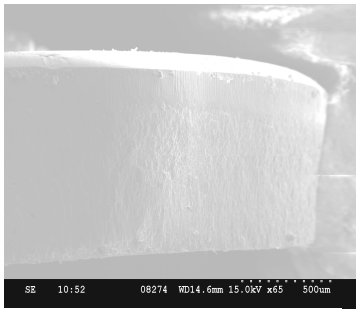

A4D1P17

Fig. 4.5: The force- displacement graphs for blanking UFG aluminium *A4* using a sharp die and sharp punch with 3 – 9% clearances, and the SEM images of the produced blanks

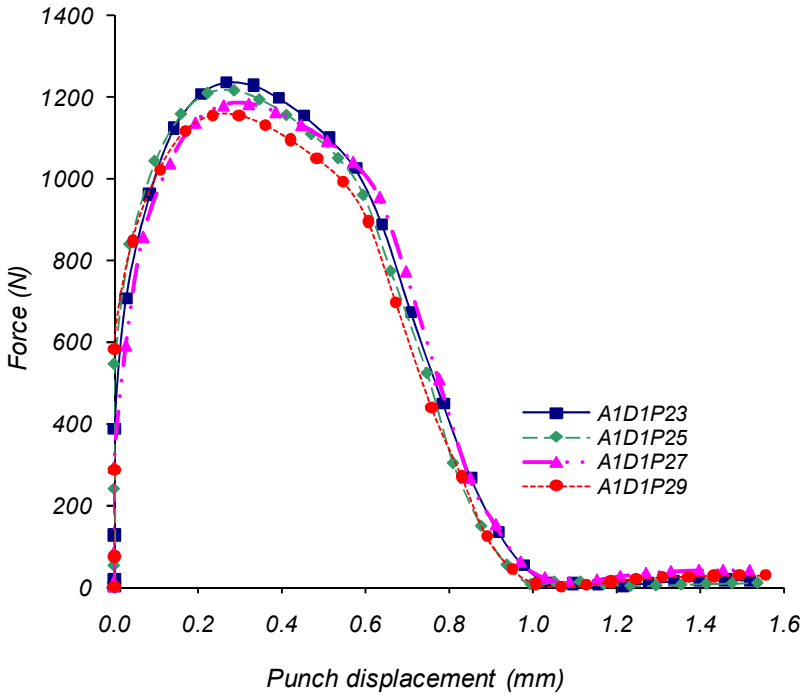

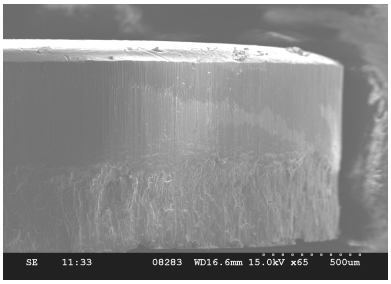

A1D1P23

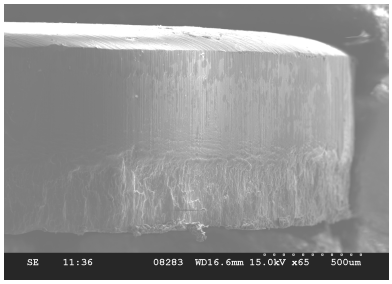

A1D1P25

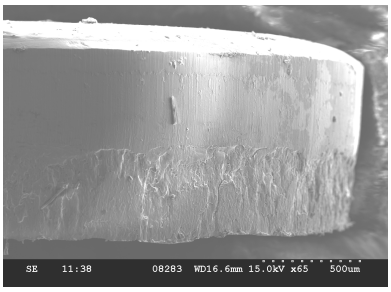

A1D1P27

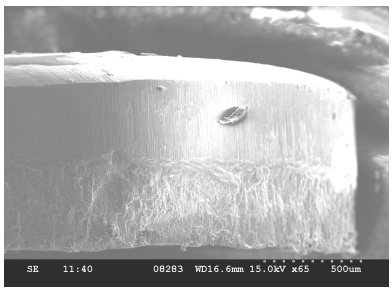

A1D1P29

Fig. 4.6(a): The force- displacement graphs for blanking aluminium *A1* using a sharp die and worn punch with 3 – 9% clearances, and the SEM images of the produced blanks

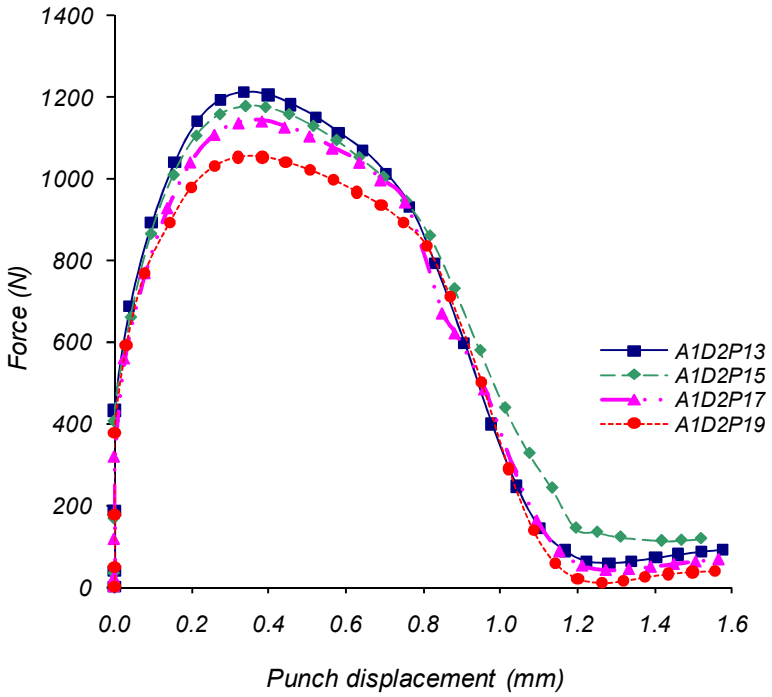

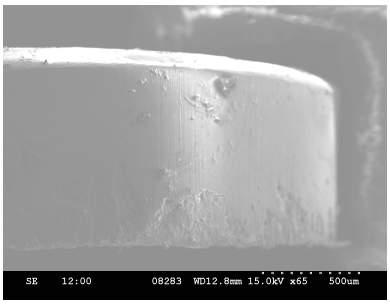

A1D2P13

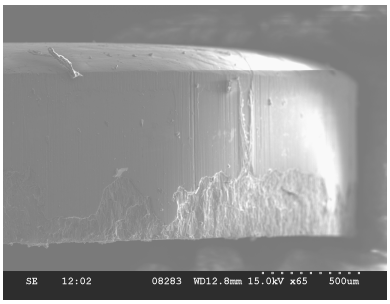

A1D2P15

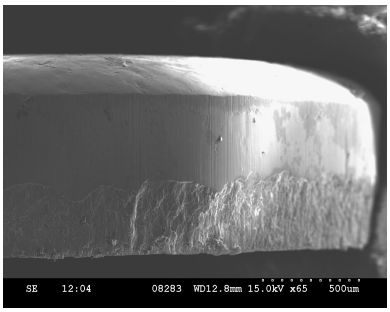

A1D2P17

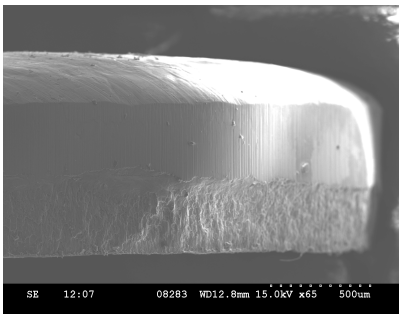

A1D2P19

Fig. 4.6(b): The force- displacement graphs for blanking aluminium *A1* using a worn die and sharp punch with 3 – 9% clearances, and the SEM images of the produced blanks

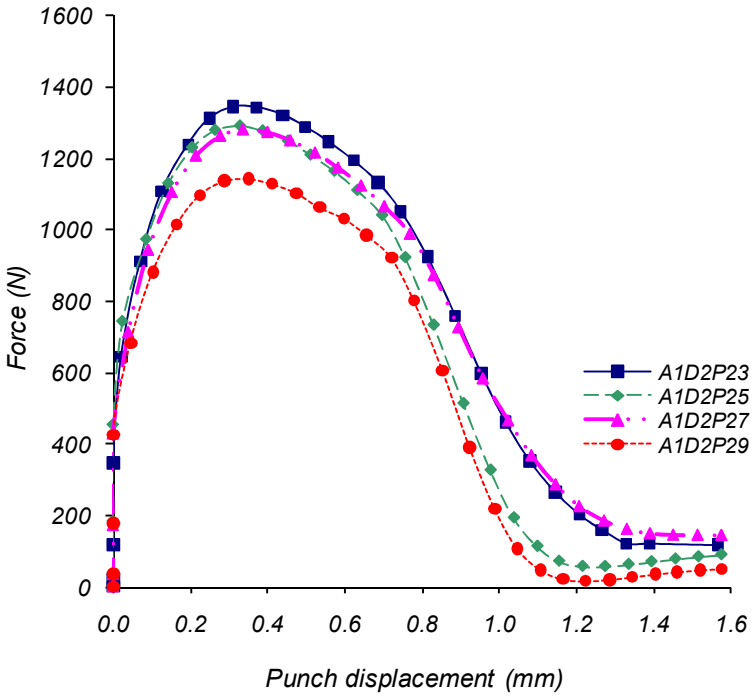

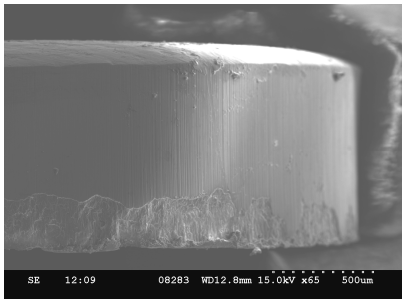

A1D2P23

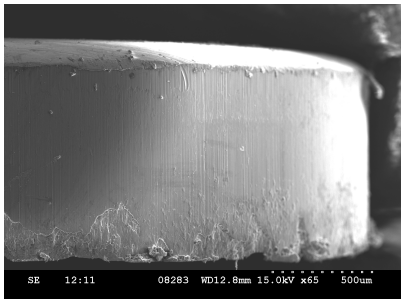

A1D2P25

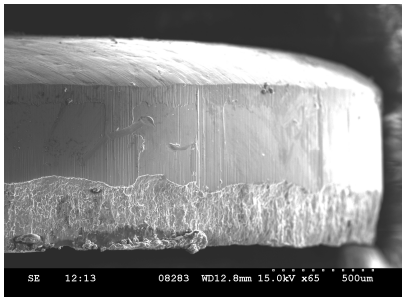

A1D2P27

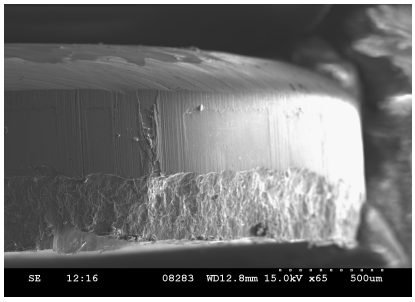

A1D2P29

Fig. 4.6(c): The force- displacement graphs for blanking aluminium *A1* using a worn die and worn punch with 3 – 9% clearances, and the SEM images of the produced blanks

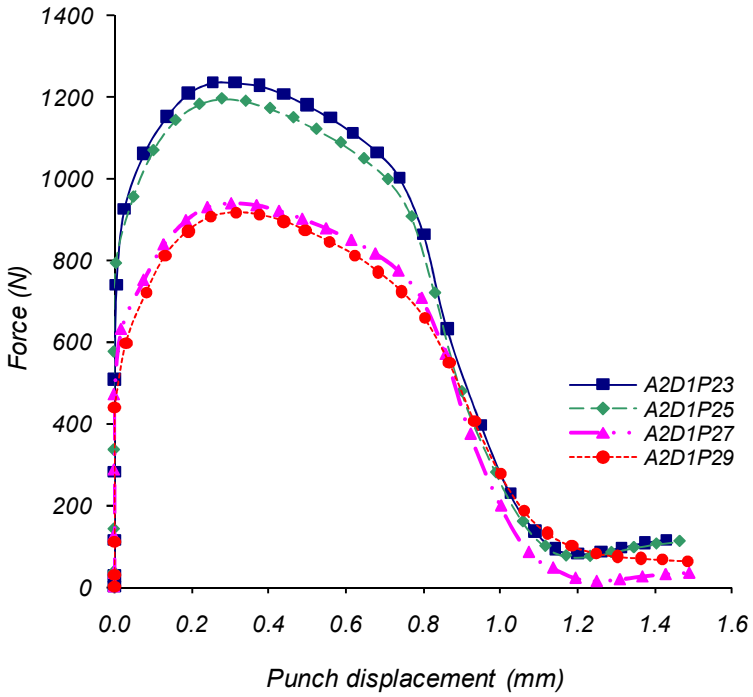

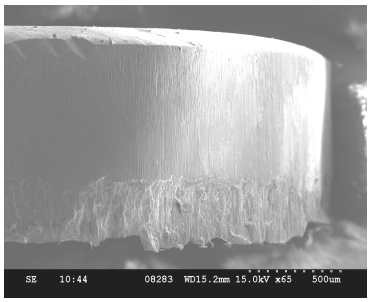

A2D1P23

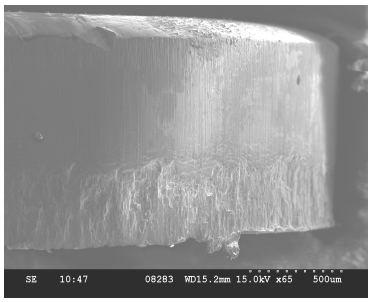

A2D1P25

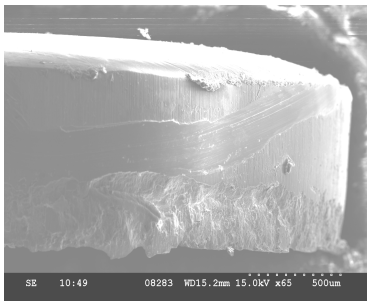

A2D1P27

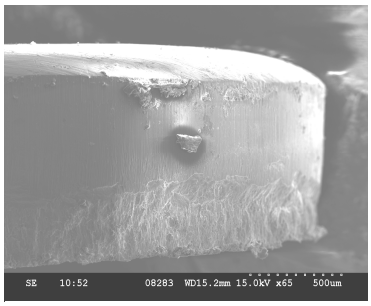

A2D1P29

Fig. 4.7(a): The force- displacement graphs for blanking aluminium *A2* using a sharp die and worn punch with 3 – 9% clearances, and the SEM images of the produced blanks

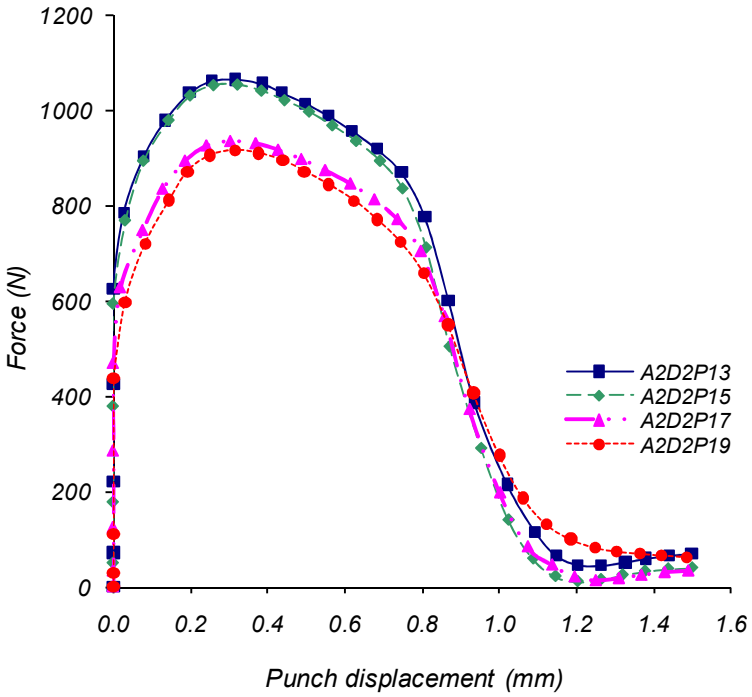

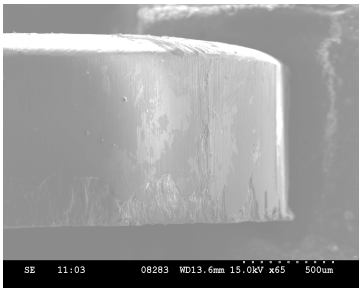

A2D2P13

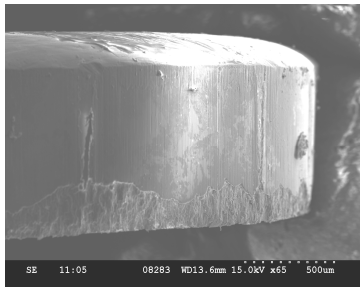

A2D2P15

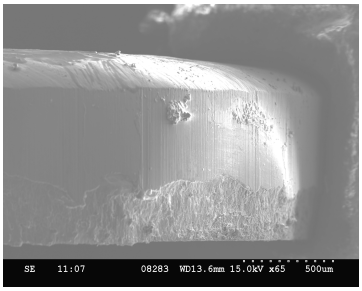

A2D2P17

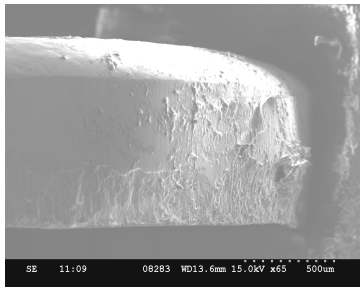

A2D2P19

Fig. 4.7(b): The force- displacement graphs for blanking aluminium *A2* using a worn die and sharp punch with 3 – 9% clearances, and the SEM images of the produced blanks

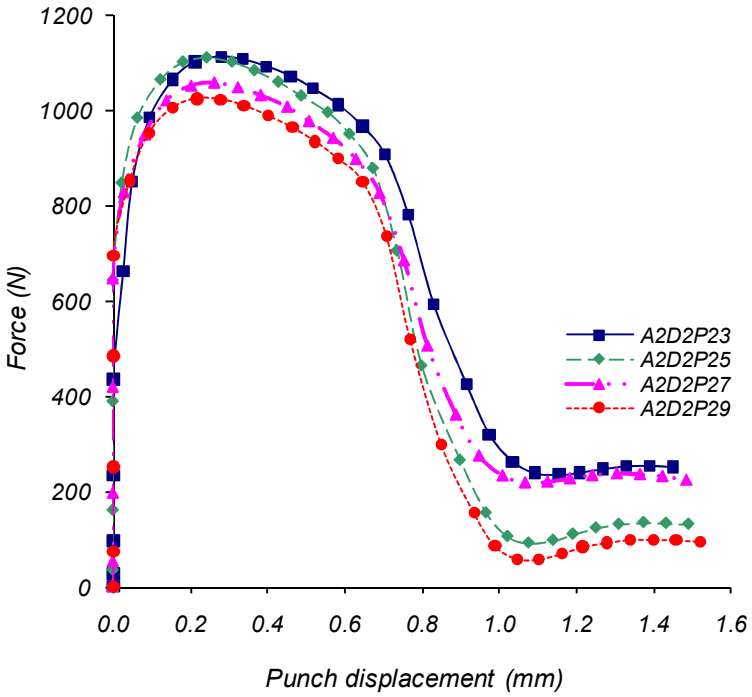

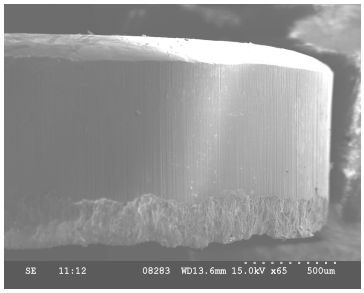

A2D2P23

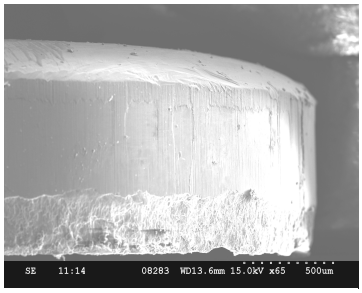

A2D2P25

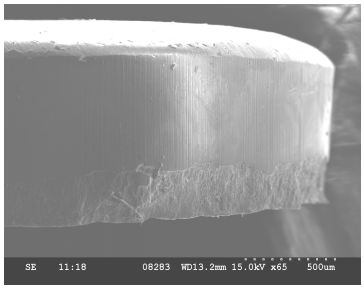

A2D2P27

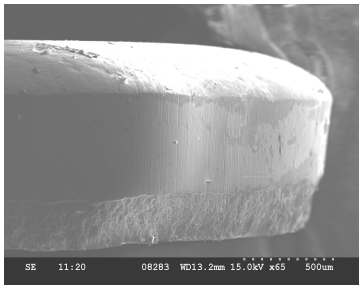

A2D2P29

Fig. 4.7(c): The force- displacement graphs for blanking aluminium *A2* using a worn die and worn punch with 3 – 9% clearances, and the SEM images of the produced blanks

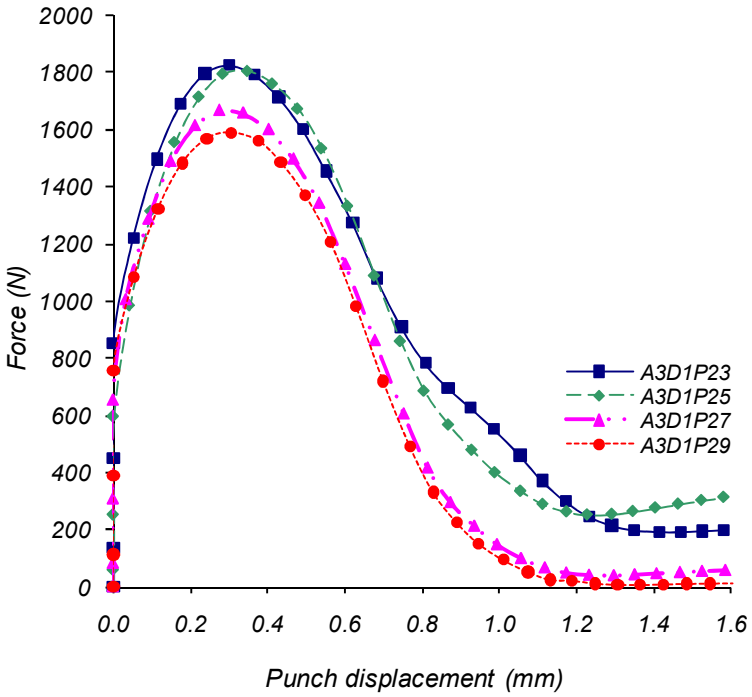

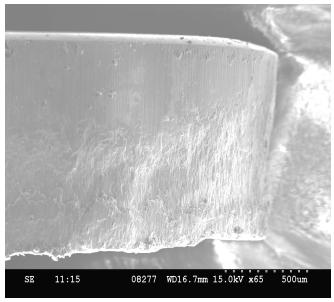

A3D1P23

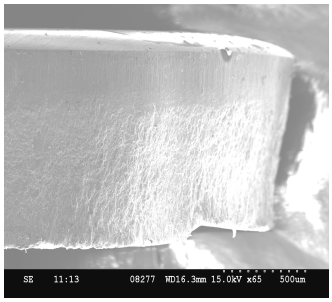

A3D1P25

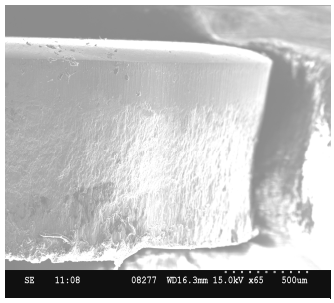

A3D1P27

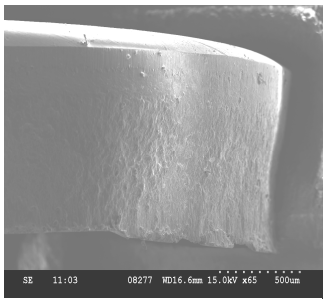

A3D1P29

Fig. 4.8(a): The force- displacement graphs for blanking aluminium *A3* using a sharp die and worn punch with 3 – 9% clearances, and the SEM images of the produced blanks

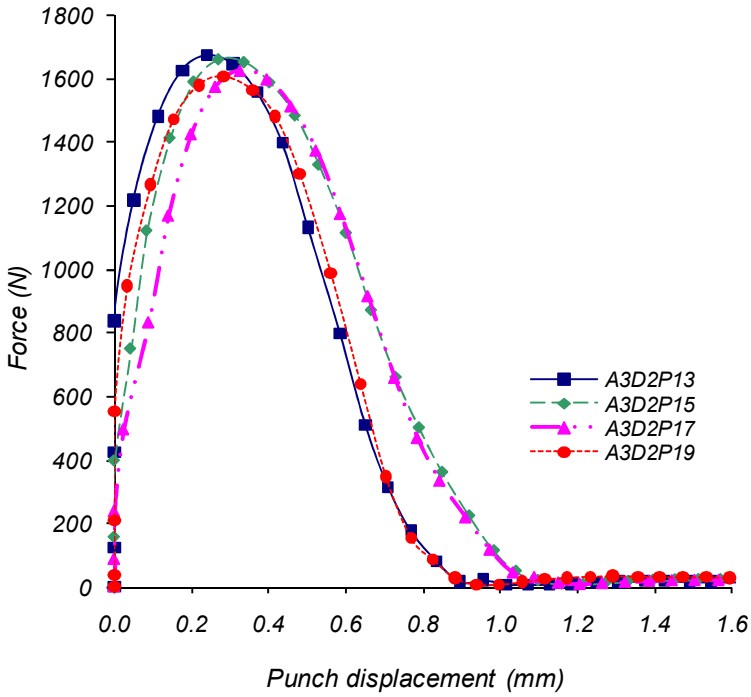

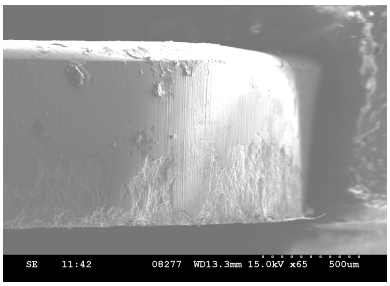

A3D2P13

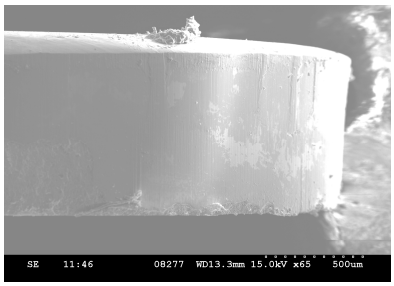

A3D2P15

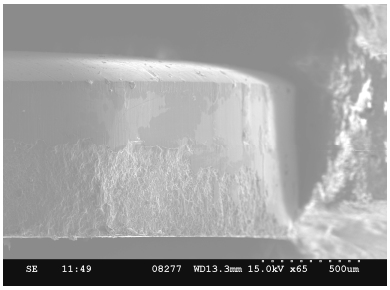

A3D2P17

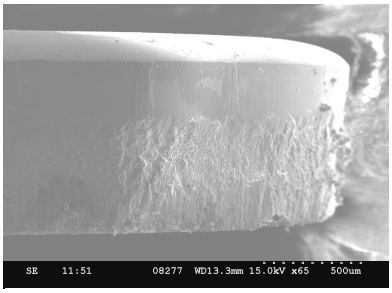

A3D2P19

Fig. 4.8(b): The force- displacement graphs for blanking aluminium *A3* using a worn die and sharp punch with 3 – 9% clearances, and the SEM images of the produced blanks

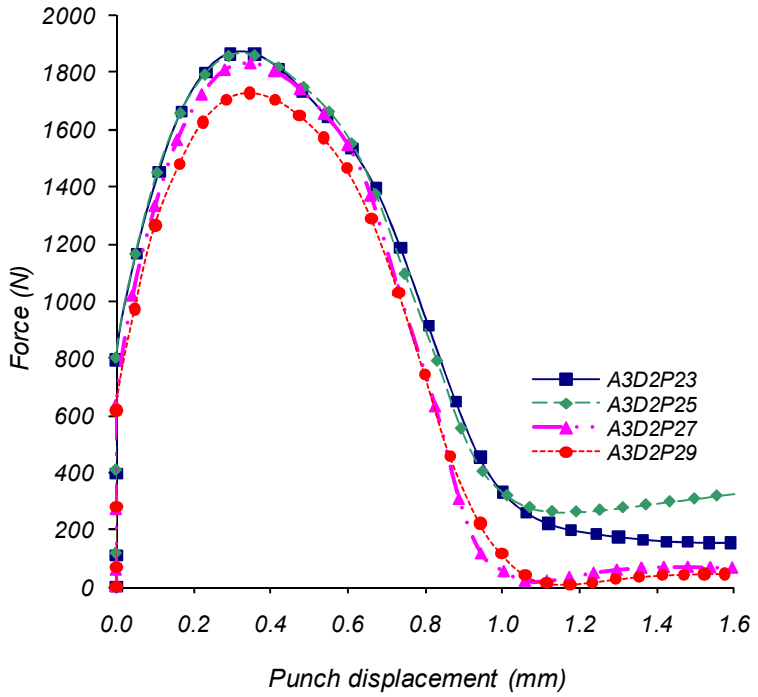

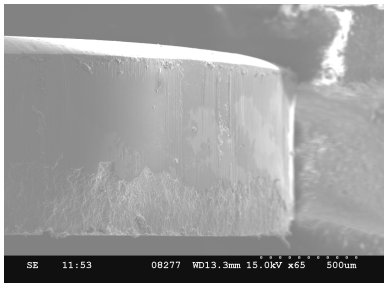

A3D2P23

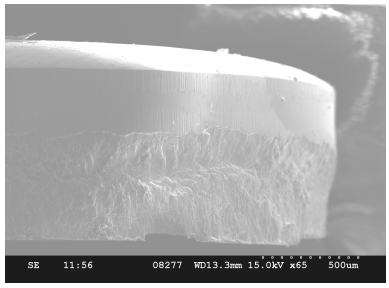

A3D2P25

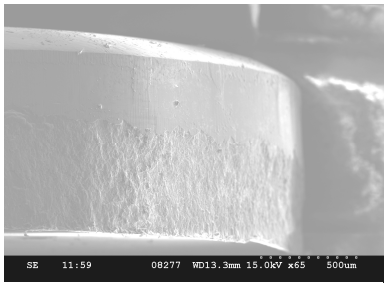

A3D2P27

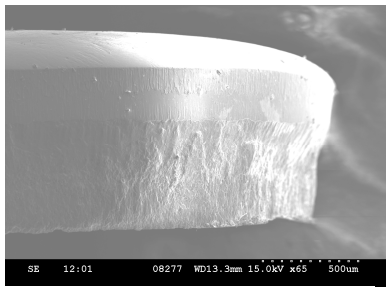

A3D2P29

Fig. 4.8(c): The force- displacement graphs for blanking aluminium *A3* using a worn die and worn punch with 3 – 9% clearances, and the SEM images of the produced blanks

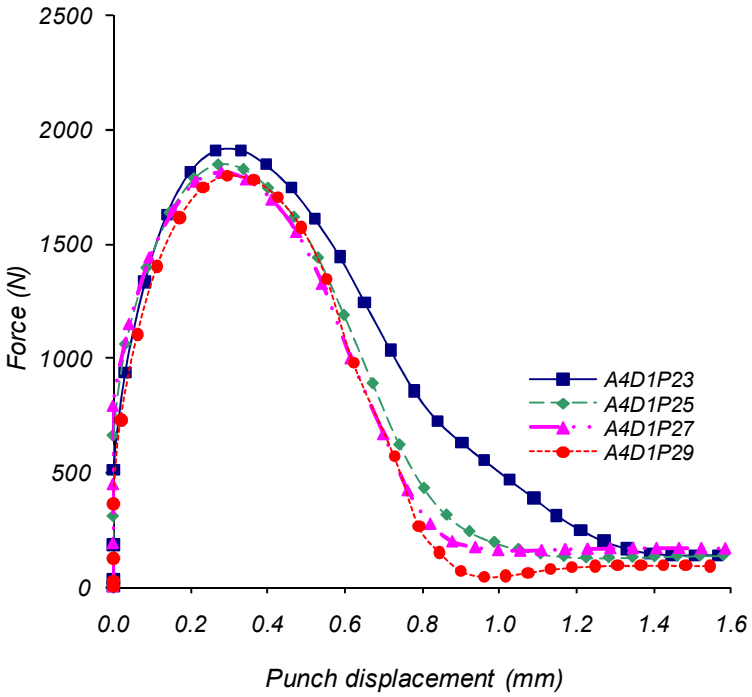

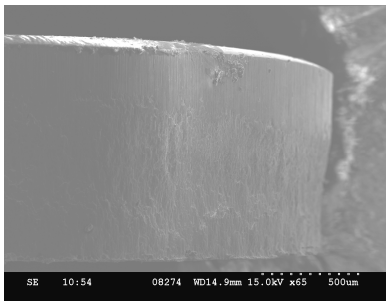

A4D1P23

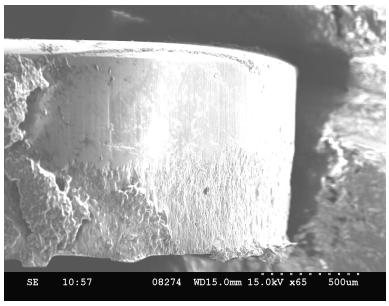

A4D1P25

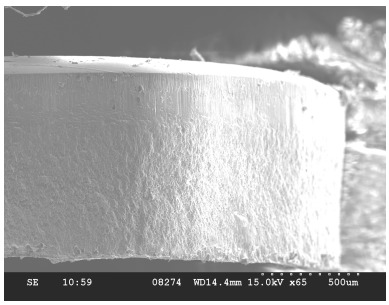

A4D1P27

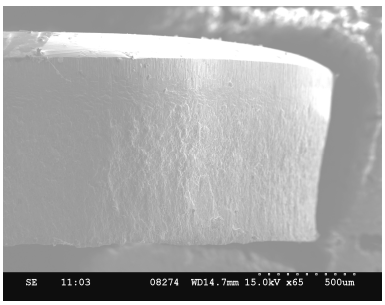

A4D1P29

Fig. 4.9(a): The force- displacement graphs for blanking UFG aluminium *A4* using a sharp die and worn punch with 3 – 9% clearances, and the SEM images of the produced blanks

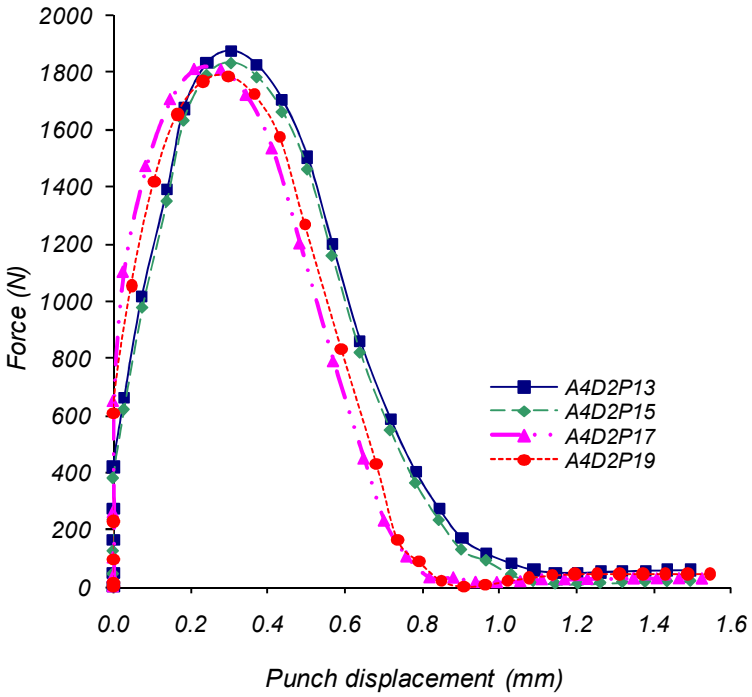

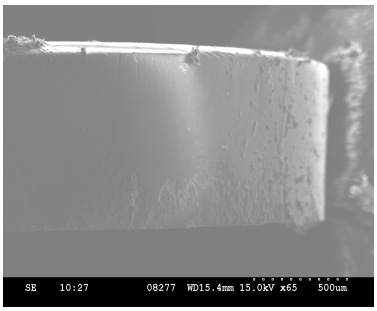

A4D2P13

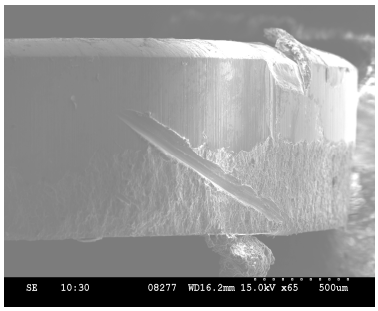

A4D2P15

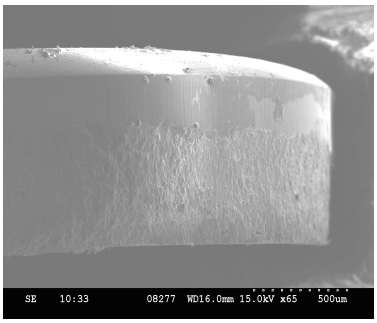

A4D2P17

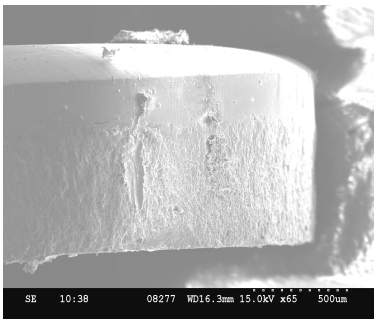

A4D2P19

Fig. 4.9(b): The force- displacement graphs for blanking UFG aluminium *A4* using a worn die and sharp punch with 3 – 9% clearances, and the SEM images of the produced blanks

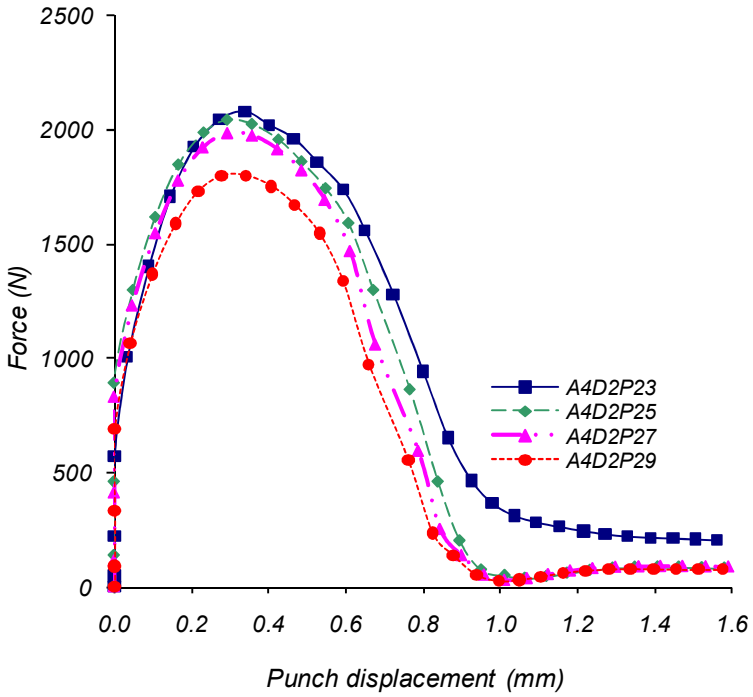

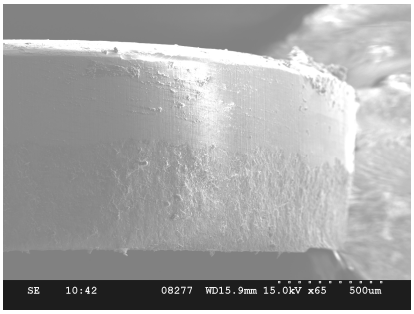

A4D2P23

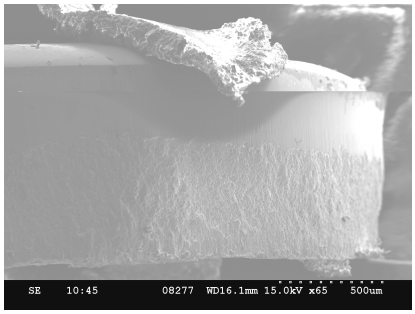

A4D2P25

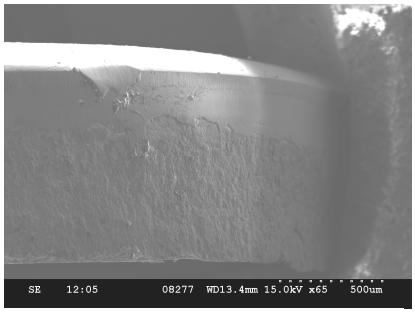

A4D2P27

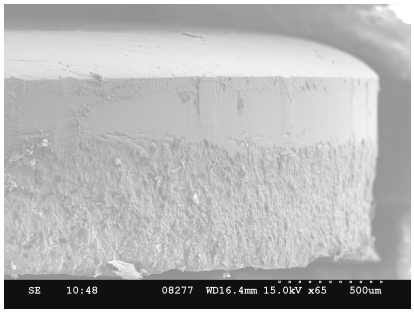

A4D2P29

Fig. 4.9(c): The force- displacement graphs for blanking UFG aluminium *A4* using a worn die and worn punch with 3 – 9% clearances, and the SEM images of the produced blanks

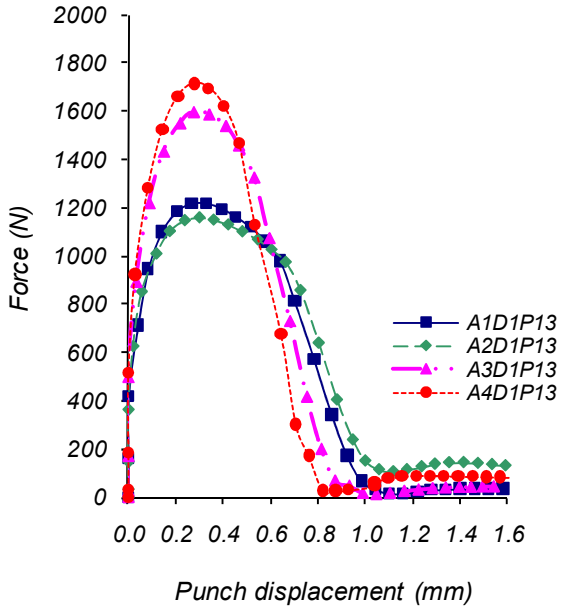

Fig. 4.10: The force-displacement graphs for blanking *A1, A2, A3* and *A4* at 3% clearance

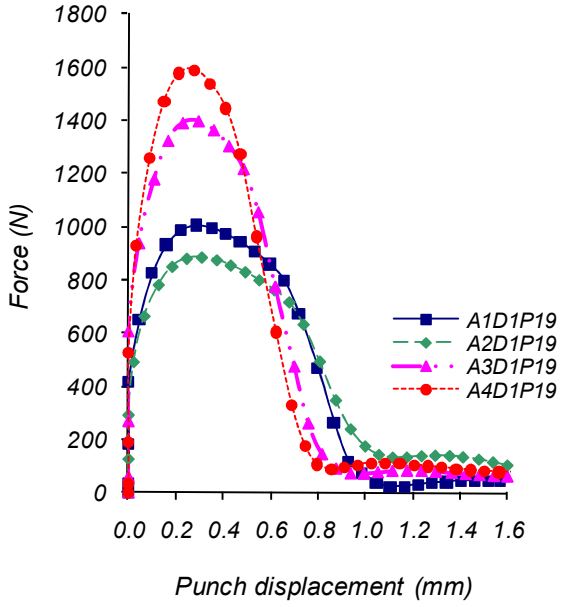

Fig. 4.11: The force-displacement graphs for blanking *A1, A2, A3* and *A4* at 9% clearance

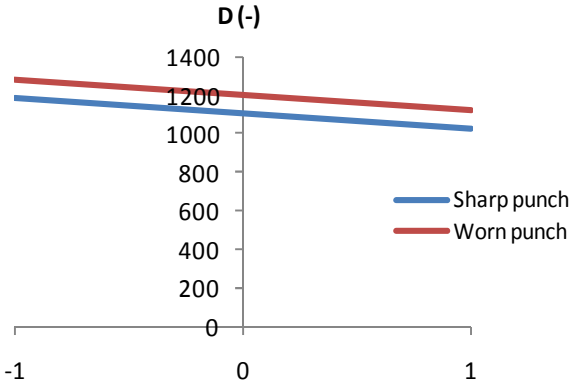

Fig. 4.12(a): The graphs showing the maximum blanking force decreases with increasing clearance for blanking *A1* using a sharp die – sharp punch and a sharp die – worn punch

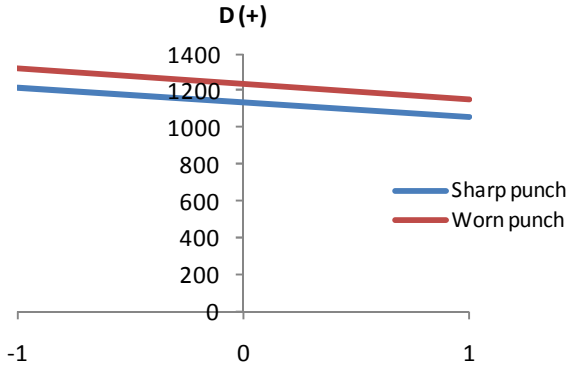

Fig. 4.12(b): The graphs showing the maximum blanking force decreases with increasing clearance for blanking *A1* using a worn die – sharp punch and a worn die – worn punch

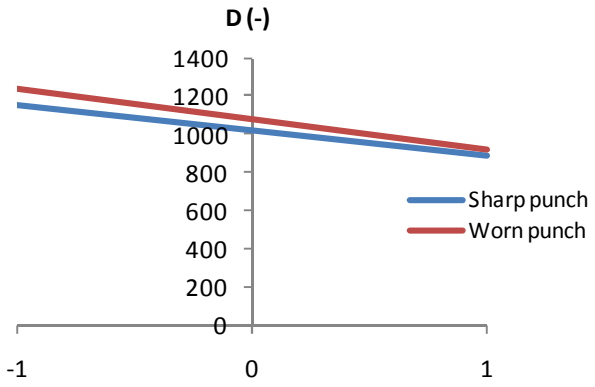

Fig. 4.13(a): The graphs showing the maximum blanking force decreases with increasing clearance for blanking *A2* using a sharp die – sharp punch and a sharp die – worn punch

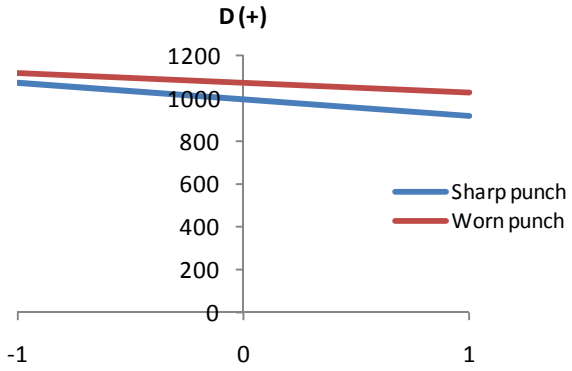

Fig. 4.13(b): The graphs showing the maximum blanking force decreases with increasing clearance for blanking *A2* using a worn die – sharp punch and a worn die – worn punch

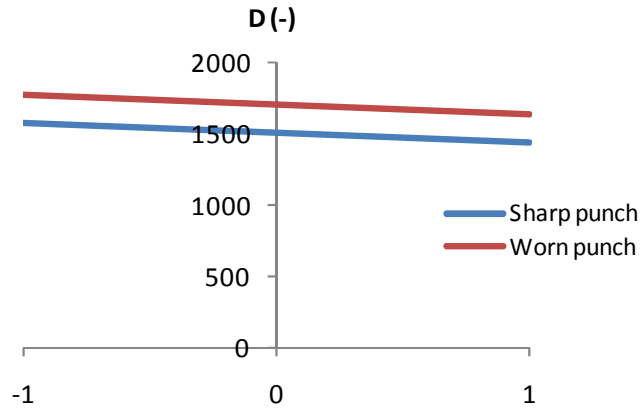

Fig. 4.14(a): The graphs showing the maximum blanking force decreases with increasing clearance for blanking *A3* using a sharp die – sharp punch and a sharp die – worn punch

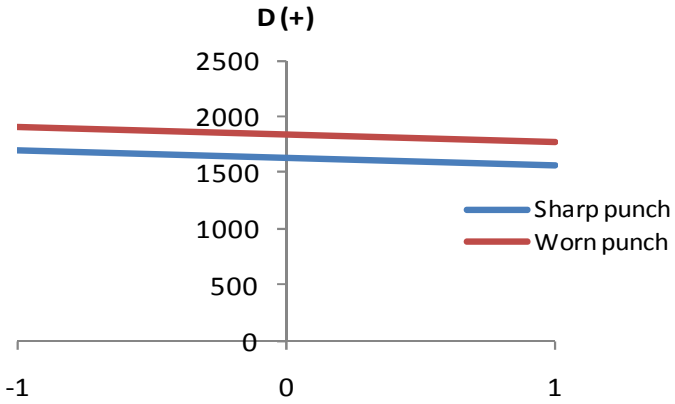

Fig. 4.14(b): The graphs showing the maximum blanking force decreases with increasing clearance for blanking *A3* using a worn die – sharp punch and a worn die – worn punch

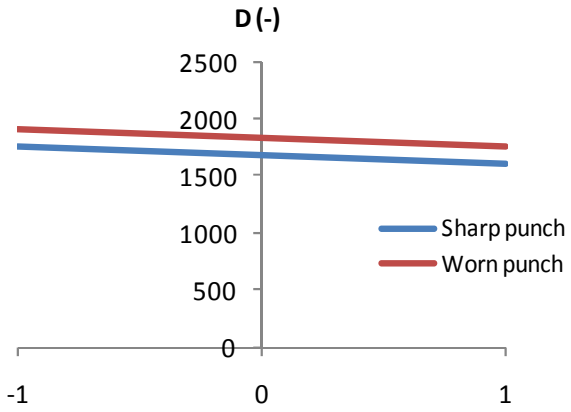

Fig. 4.15(a): The graphs showing the changing in maximum blanking force is negligible for blanking *A4* using a sharp die – sharp punch and a sharp die – worn punch

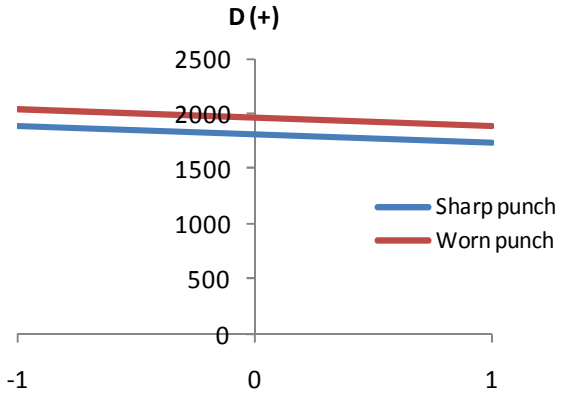

Fig. 4.15(b): The graphs showing the changing in maximum blanking force is negligible for blanking *A4* using a worn die – sharp punch and a worn die – worn punch

C:\Program Files\Physical Acoustics\AEwin for PCI2\AEData\EXPERIMENT \EXP A3 D2 P5-P8\Blanking Trial\TEST001.DTA

Total AEHits : 8
Total TDDs : 1460
Total Waveforms: 8
Total Resumes : 1
Total Pauses : 1
Total TimeMarks: 0

Channel	AEHits
1	8

HIT DRIVEN DATA:

Feature	Chan	Minimum	Maximum	Average	Std Dev
Risetime	1	0.0000	23.0000	7.8750	10.1173
CountsPeak	1	1.0000	3.0000	1.3750	0.6960
Counts	1	1.0000	22.0000	5.8750	7.9912
Energy	1	0.0000	12.0000	2.5000	4.4441
Duration	1	0.0000	290.0000	46.0000	95.1262
Amplitude	1	55.0000	77.0000	58.6250	7.1052
Asl	1	39.0000	43.0000	42.5000	1.3229
Threshold	1	40.0000	40.0000	40.0000	0.0000
AvgFreq	1	0.0000	500.0000	101.5000	169.2092
Rms	1	0.0068	0.0108	0.0103	0.0013
SigStrength	1	0.0000	75457.0000	16736.1133	28534.4813
AbsEnergy	1	886.0867	11586.6797	2774.5613	3514.9341
PeakFreq	1	278.0000	473.0000	436.7500	60.5367

TIME DRIVEN DATA:

Feature	Chan	Minimum	Maximum	Average	Std Dev
Parametric1		-0.0662	5.0826	0.3387	0.6596
Parametric2		-5.7076	-0.8231	-4.1531	2.1933

Fig. 4.16: A line listing file

Table 4.3: The maximum amplitude of AE signals for A1 – A4 for all combinations of tool states and blanking clearances

	Maximum amplitude *(Amp_{max})* in dB																
Tool states	Sharp die – sharp punch					Sharp die – worn punch					Worn die – sharp punch					Worn die – worn punch			
Clearance	3%	5%	7%	9%		3%	5%	7%	9%		3%	5%	7%	9%		3%	5%	7%	9%
Material																			
A1	48	47	45	64		53	50	48	49		66	54	47	50		47	48	57	64
A2	68	51	50	45		54	50	50	45		63	52	47	46		47	57	58	66
A3	75	72	51	46		48	49	46	44		64	49	50	70		55	60	64	71
A4	64	66	59	53		72	65	58	52		73	54	60	51		84	80	79	64

Table 4.4: The maximum peak frequency of AE signals for A1 – A4 for all combinations of tool states and blanking clearances

	Maximum peak frequency *(fpeak$_{max}$)* in kHz																
Tool states	Sharp die – sharp punch					Sharp die – worn punch					Worn die – sharp punch					Worn die – worn punch			
Clearance	3%	5%	7%	9%		3%	5%	7%	9%		3%	5%	7%	9%		3%	5%	7%	9%
Material																			
A1	278	219	207	278		278	107	101	102		298	205	170	210		298	310	402	478
A2	478	210	148	205		178	108	102	102		415	290	278	305		305	410	478	639
A3	498	483	278	150		278	272	109	111		278	419	454	478		473	493	502	507
A4	512	506	453	468		585	460	453	448		548	517	488	498		590	572	568	375

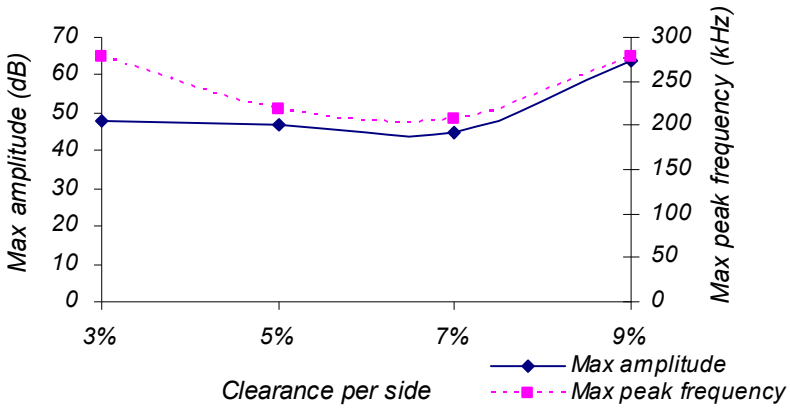

Fig. 4.17(a): Graphs of maximum amplitude and maximum peak frequency of AE signals captured during blanking *A1* using a sharp die and sharp punch for 3 – 9% clearance

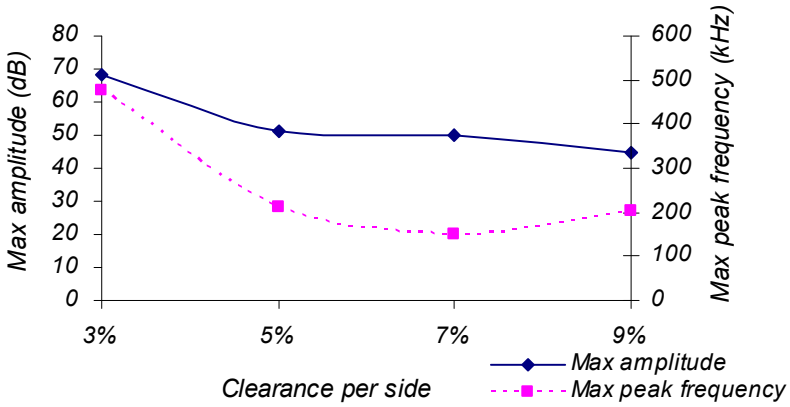

Fig. 4.17(b): Graphs of maximum amplitude and maximum peak frequency of AE signals captured during blanking *A2* using a sharp die and sharp punch for 3 – 9% clearance

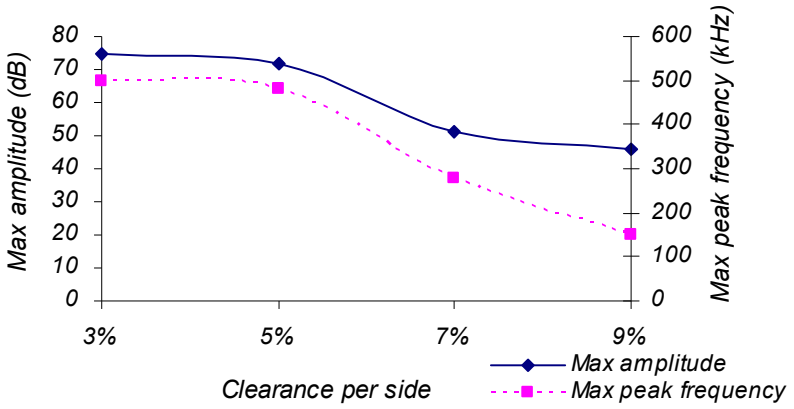

Fig. 4.17(c): Graphs of maximum amplitude and maximum peak frequency of AE signals captured during blanking *A3* using a sharp die and sharp punch for 3 – 9% clearance

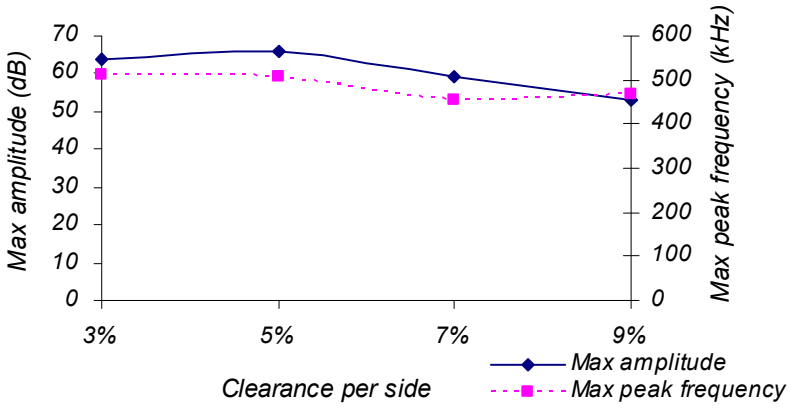

Fig. 4.17(d): Graphs of maximum amplitude and maximum peak frequency of AE signals captured during blanking *A4* using a sharp die and sharp punch for 3 – 9% clearance

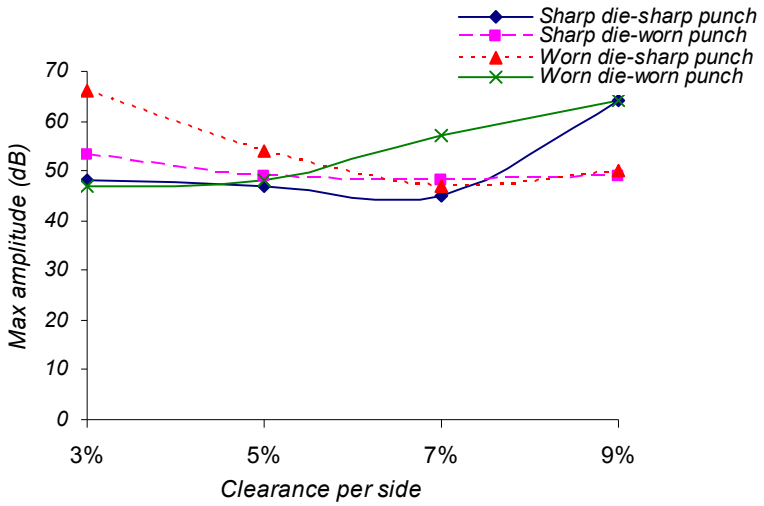

(a)

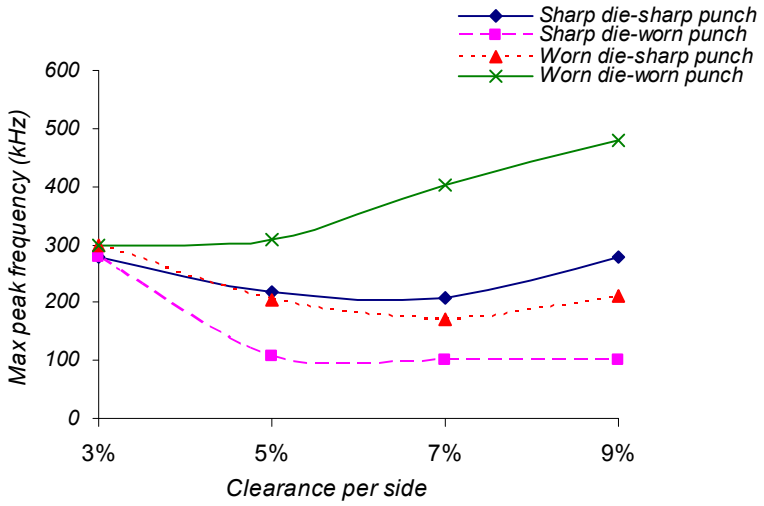

(b)

Fig. 4.18: (a) The maximum amplitude,
(b) The maximum peak frequency of AE signals
captured during blanking *A1* using different tool states for 3 – 9% clearance

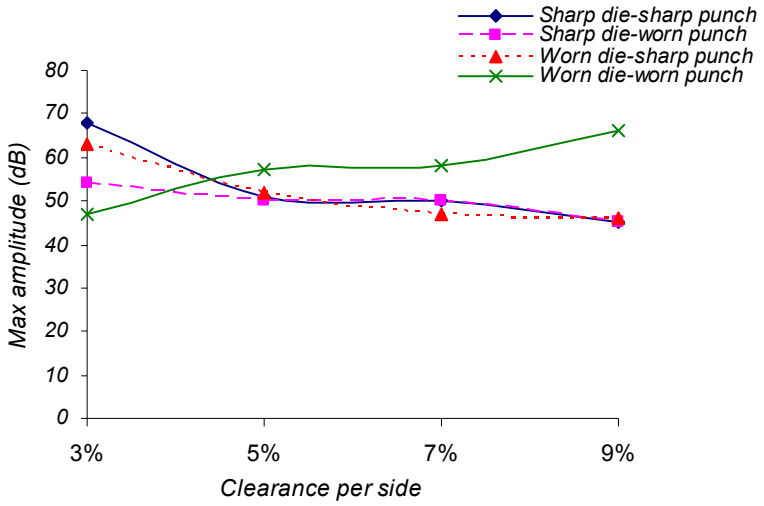

(a)

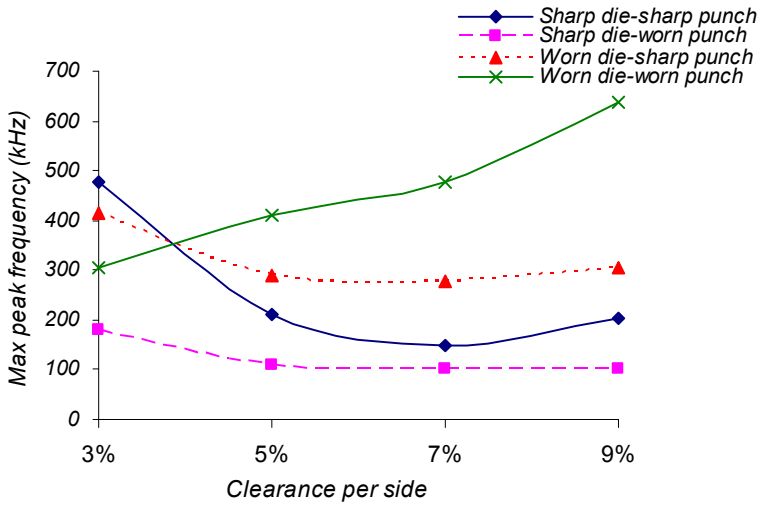

(b)

Fig. 4.19: (a) The maximum amplitude,
(b) The maximum peak frequency of AE signals
captured during blanking *A2* using different tool states for 3 – 9% clearance

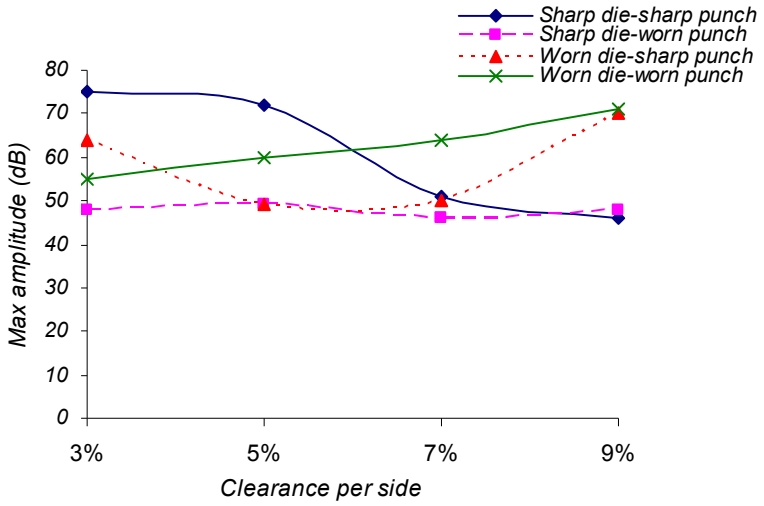

(a)

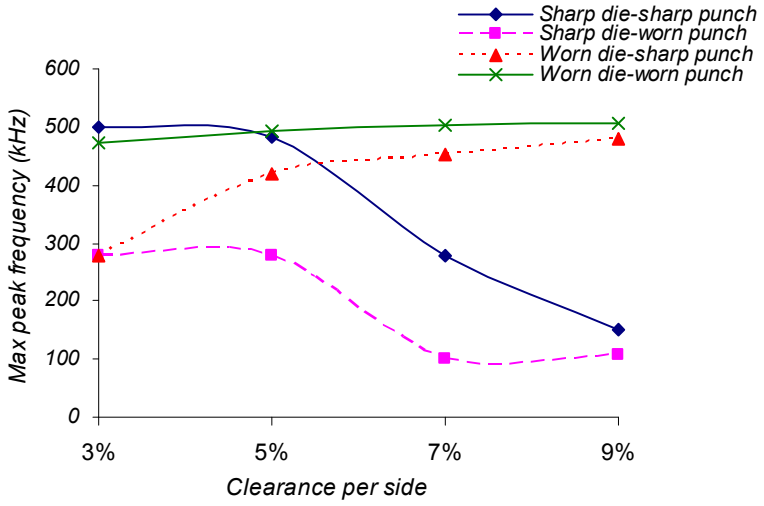

(b)

Fig. 4.20: (a) The maximum amplitude,
(b) The maximum peak frequency of AE signal,
captured during blanking *A3* using different tool states for 3 – 9% clearance

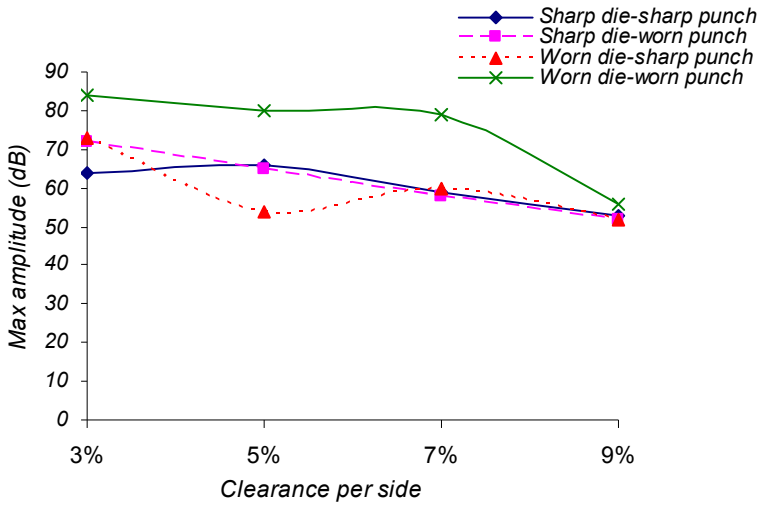

(a)

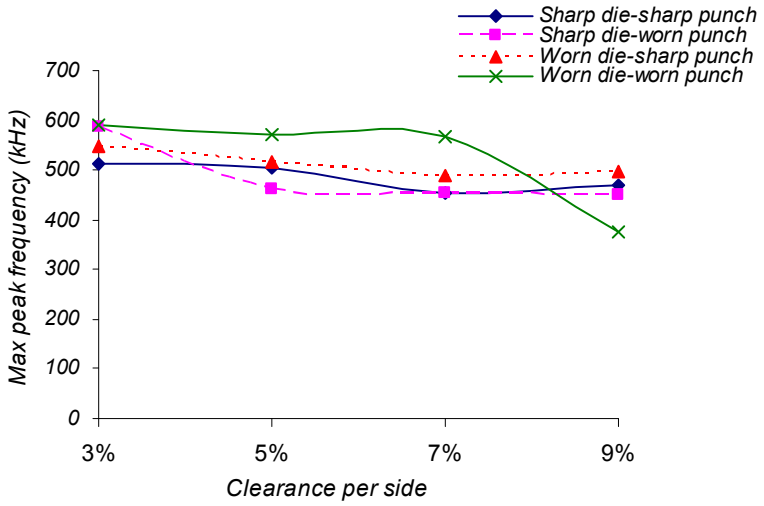

(b)

Fig. 4.21: (a) The maximum amplitude,
(b) The maximum peak frequency of AE signals
captured during blanking *A4* using different tool states for 3 – 9% clearance

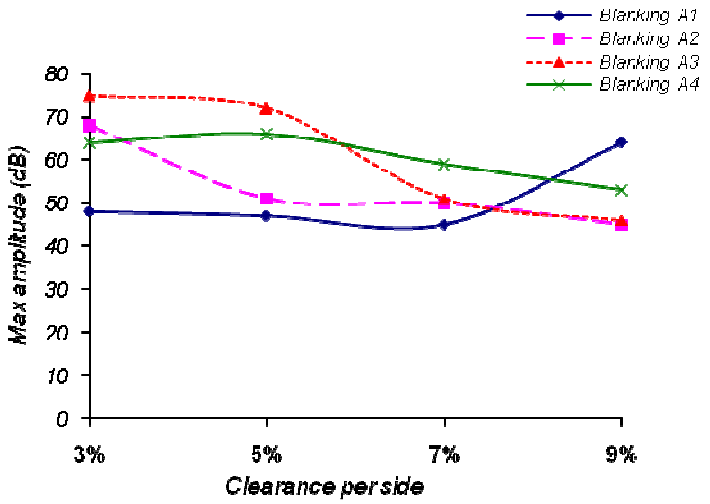

Fig. 4.22(a): Graphs of maximum amplitude for blanking *A1 – A4* using a sharp die and sharp punch for 3 – 9% clearance

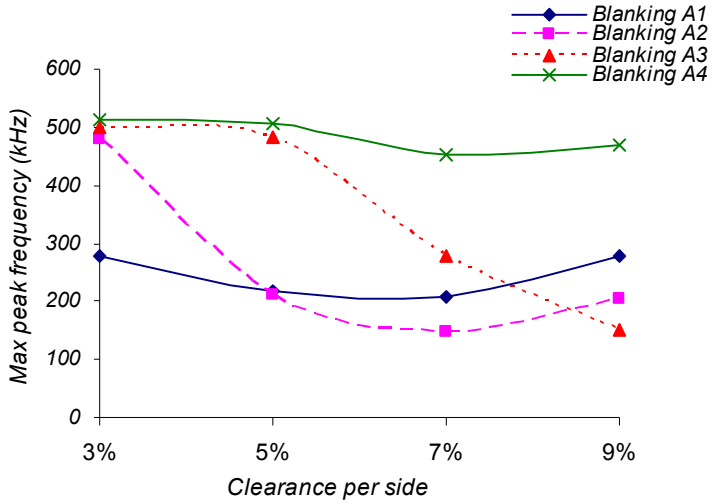

Fig. 4.22(b): Graphs of maximum peak frequency for blanking *A1 – A4* using a sharp die and sharp punch for 3 – 9% clearance

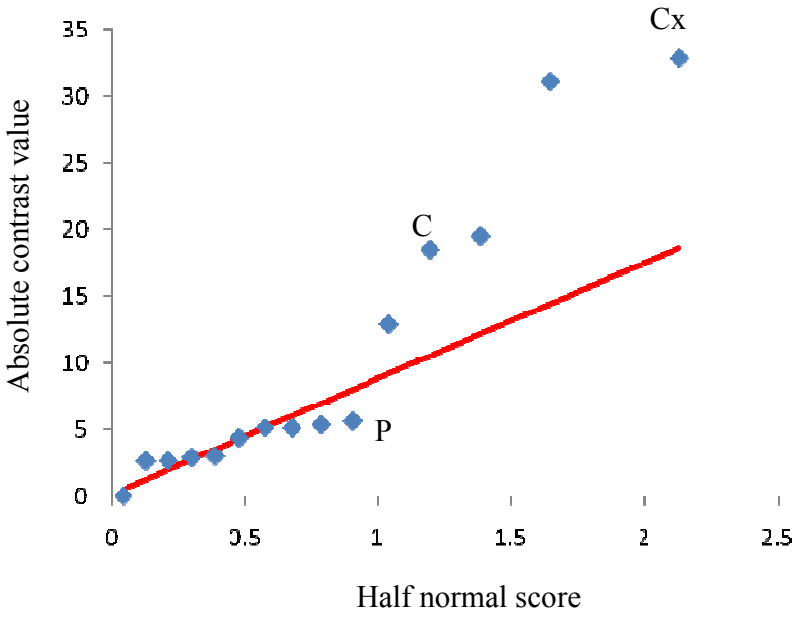

Fig. 4.23(a): A half normal plot for factors to affect the maximum amplitude of AE signals

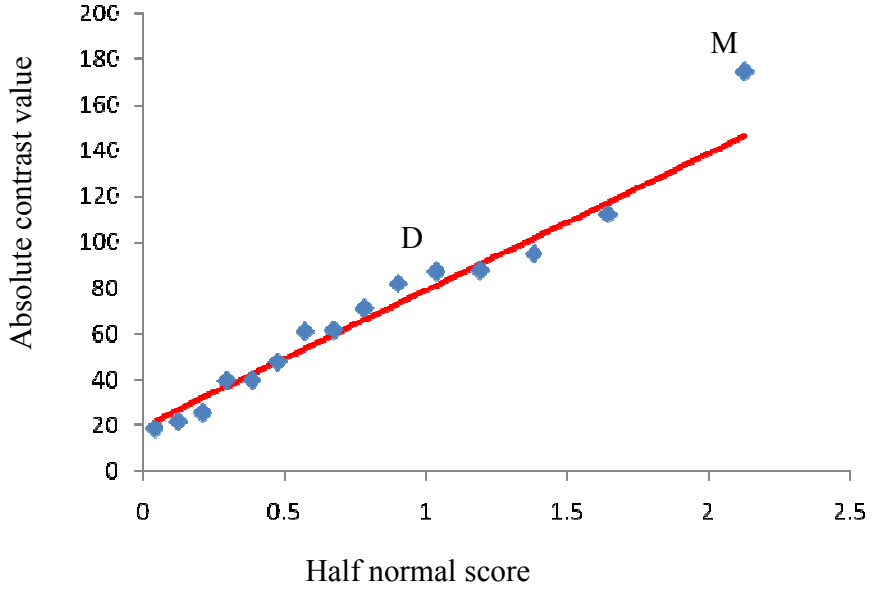

Fig. 4.23(b): A half normal plot for factors to affect the maximum peak frequency of AE signals

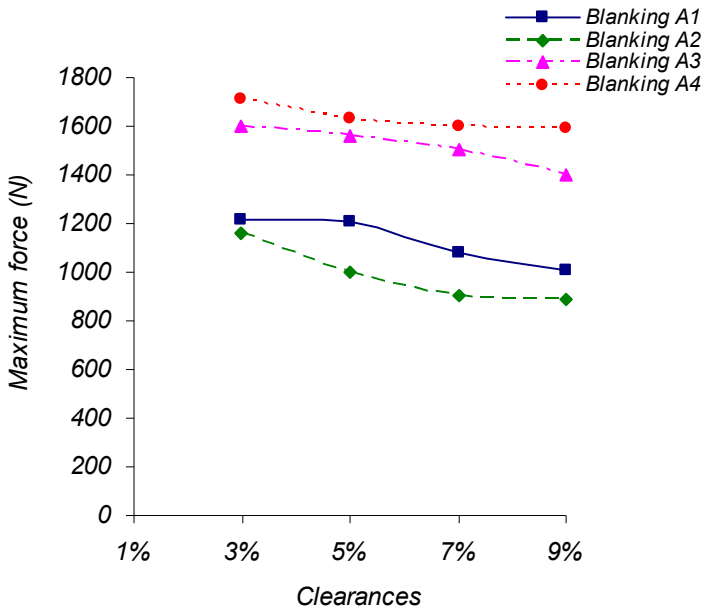

Fig. 4.24: Graphs of maximum blanking force obtained for *A1 – A4* at 3 – 9% clearance

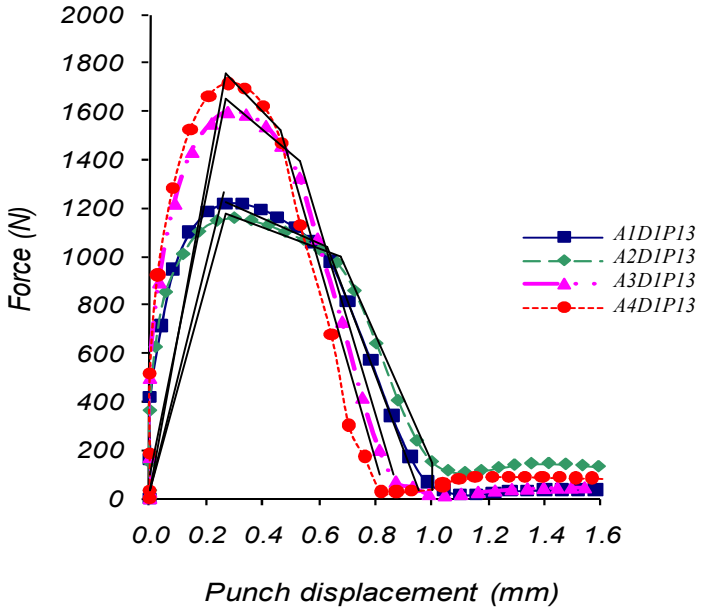

(a)

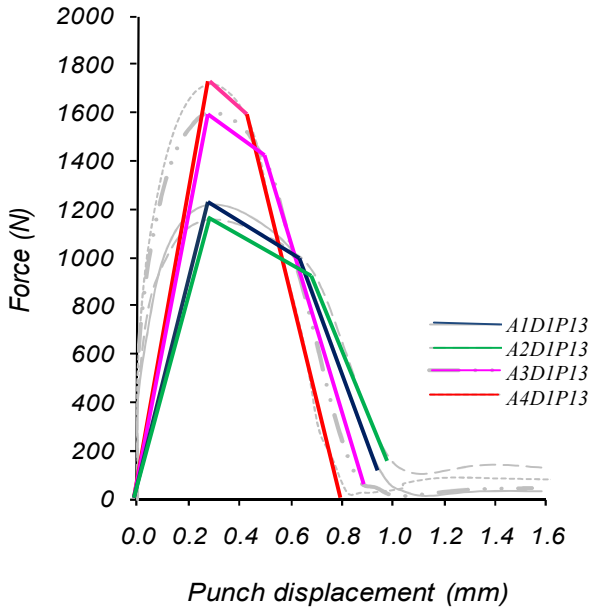

(b)

Fig. 4.25: (a) The force-displacement graphs of blanking *A1 – A4* using a sharp die – sharp punch at 3% clearance and (b) their equivalent force-displacement characteristics

Table 4.5: The measurements of the smooth sheared edge of blanks *A1 – A4* produced using a sharp die – sharp punch at 3% clearance

Material	Stroke for maximum Force (mm)	Slope of decreasing force to separation (degrees from horizontal)	Punch stroke for separation (mm)	Smooth sheared length (mm)
A1	0.33	73	0.90	0.59
A2	0.35	70	0.98	0.61
A3	0.30	79	0.83	0.42
A4	0.28	82	0.79	0.37

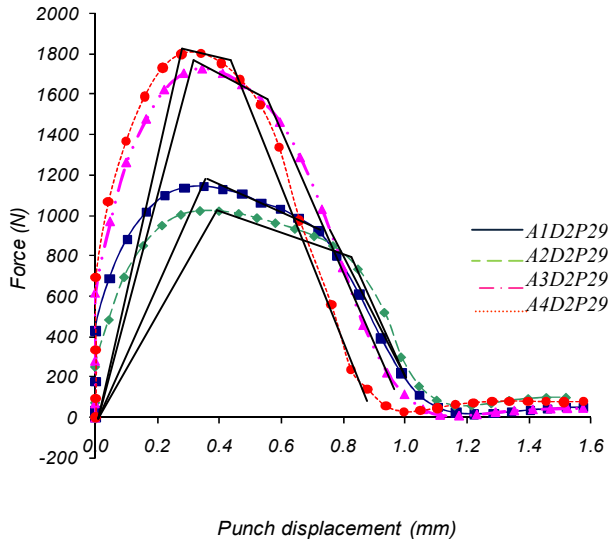

(a)

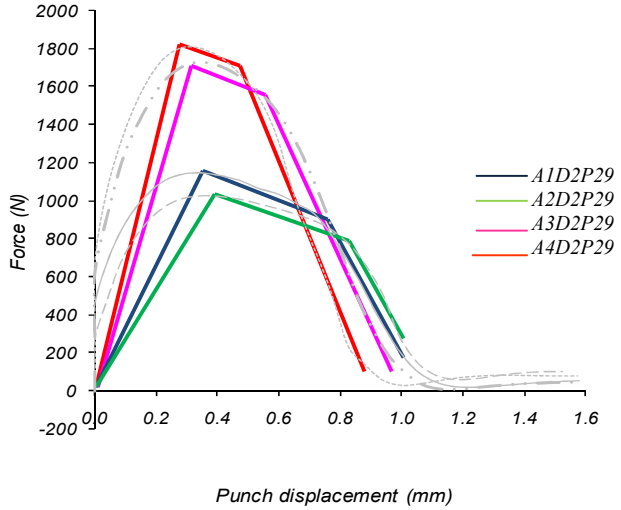

(b)

Fig. 4.26: (a) The force-displacement graphs of blanking *A1 – A4* using a worn die – worn punch at 9% clearance and (b) their equivalent force-displacement characteristics

Table 4.6: The measurements of the smooth sheared edge of blanks *A1 – A4* produced using a worn die – worn punch at 9% clearance

Material	Stroke for maximum Force (mm)	Slope of decreasing force to separation (degrees from horizontal)	Punch stroke for separation (mm)	Smooth sheared length (mm)
A1	0.37	60	1.00	0.51
A2	0.40	59	1.00	0.54
A3	0.34	66	0.88	0.43
A4	0.32	70	0.84	0.39

CHAPTER 5

CONCLUSIONS AND SUGGESTIONS FOR FUTURE WORK

This chapter summarises the work involved in this study. It outlines the research outcomes and the conclusions of the thesis. Suggestions for future work, which considered being essential for further research in this area, are also discussed.

5.1 Summary of the work

The purpose of this study was to develop a process monitoring system for blanking operations. In order to build the system, the work involved four main areas: tooling and machine, material, process and data acquisition system (DAQ). The blanking tools were designed and manufactured, taking into account the requirement of precision movement of a punch with reference to the die and the flexibility to attach the DAQ instruments. The hydraulic servo press of 25 kN was used to provide blanking force of up to 2.1 kN.

The materials used to produce circular blanks of 5 mm diameter and 1 mm thickness were aluminium sheets AA 1050 and AA 1070. The samples from aluminium AA 1050 were prepared in two batches: as supplied *(A1)* and annealed *(A2)*. The other two batches were prepared from aluminium AA 1070: CG sheets, produced after side upsetting and rolling (A3) and UFG sheets (A4), produced after ECAP, side upsetting and rolling.

Shearing of the blanks was performed using a combination of punch and die representing different states of the cutting edge and different clearances. A sharp die and a sharp punch were manufactured with sharp shearing edges while a worn die and a worn punch were manufactured by making the shearing edges rounded with 150 μm radii. The blanking clearances were set at 3%, 5%, 7% and 9% of the material thickness. These enabled the study of blanking to be carried out for various combinations of process parameters such as blanking tool states, clearances and materials with different grain structure and properties.

The DAQ system was integrated with the blanking tools to monitor process signatures during blanking. The system was capable of capturing two types of signals: force-displacement and acoustic emission (AE) signals. A force transducer, displacement transducer and AE sensor were used to capture and direct these signals to the PCI-2 board via conditioning units. The PCI-2 AE board was interfaced with a desktop PC equipped with AEwin software. This software enabled processing the signals as well as presenting the results in the form of graphs and charts.

The force-displacement and AE signals varied with different blanking parameters that were set up for each blanking experiment. The significant characteristics of the force-displacement signature were the maximum blanking force and the displacement of the punch from the moment of touching the workpiece material to the point where the blank was fully separated. From the force-displacement graph, it can be seen that the force

increases with increasing displacement from the point the punch touches the surface of the material to the point of the maximum force, which is the point of reaching a balance between work hardening and geometrical softening of the material. The force starts to decrease, creating a force decreasing slope, when the punch moves further to reach the point where the crack starts to develop inside the material. The force then decreases to a minimum level as the blank is ruptured from the material. At minimum level, the force-displacement is affected by a certain amount of residual force before the ram moves upward to its initial position. This residual force is due to friction between punch and the workpiece material and friction between the die and the blank.

The AE signals were monitored during the whole process of blanking. Noise interference and signal attenuation factors had influenced the quality of the AE signals. With repeated blanking trials and proper filtering, the unwanted signals could be filtered out and the AE signals, representing the blanking process, were retained. In one complete blanking operation, several AE hits were generated. Therefore, several AE waves were composed and convolved together within a measured duration. Appropriate AE parameters were identified, which could correspond with the blanking parameters. In this case, the maximum amplitude and the maximum peak frequency of the AE signals were selected to represent the AE signatures for monitoring the blanking operations.

The quality of the produced blanks was determined by analysing the formation of the blank edge. The profile of the blank edges was assessed under the scanning electron

microscope (SEM). High quality of blanks that achieved with a greater sheared zone (burnished zone) is desirable. On the other hand, higher burr and larger size of rollover reduce the quality of the blank. The characteristics of force-displacement were used to correlate with rollover, smooth sheared edge and fracture angle of the blanks. This implied that the quality of the blank could be indirectly monitored using the process signature in a blanking operation, which was represented by a force-displacement graph. The maximum amplitude and maximum peak frequency of AE signals appeared to be less suitable for this purpose because of a high level of uncertainty (errors) experienced during measurements.

5.2 Research outcomes and conclusions

The research outcomes and conclusions, which can be drawn from this study, are as follows:

1. A blanking tool set, capable to produce circular blanks of 5 mm diameter and 1 mm thickness, at a punch speed of 10 mm/s, for 3%, 5%, 7% and 9% of blanking clearances and different cutting edge states of the punch and the die was developed.

2. The process of annealing was performed on a cold-rolled aluminium AA 1050 by heating it to a temperature of 343°C for a minimum duration of 45 minutes. This affected the micro structure of the material by increasing the grain size to approximately 50 μm. The annealing also reduced the hardness and increased the ductility of the material.

3. It was shown that UFG sheets of aluminium AA 1070 could be produced from the CG billets by combining the ECAP technique, followed by cold side upsetting and rolling. The other type of aluminium AA 1070 sheets, referred to as CG sheets, could also be produced by subjecting the initial CG billets to cold side upsetting and followed by rolling.

4. By monitoring the process signatures of blanking, which were represented by force-displacement graphs, several observations could be made:

(a) Clearance as a dominant factor, followed by the punch and the die state, influence the maximum blanking force. However, in the case of annealed material the interaction between the die state and the clearance has also been identified as a real effect, which influences the quality of the blank.

(b) Evidence from the graphs suggests that smaller clearance leads to a higher maximum blanking force.

(c) Blanking using the combination of worn die and sharp punch, sharp die and worn punch and worn die and worn punch results in increasing the maximum blanking force, when compared to a combination of sharp die and sharp punch. However, a combination of worn die and worn punch produces the highest maximum blanking force.

(d) The force-displacement graphs can be linked to the profile of the blank edge, hence quantifying the product quality. The three characteristics of the force-displacement curve, which enable this, are the point on the curve representing the maximum blanking force, the slope of the decreasing force and the punch stroke required for blank

separation. Longer stroke for the maximum blanking force and lower slope of decreasing force correspond to a large smooth sheared edge. However, these together with lower maximum blanking force, result in a large rollover. This profile of the blank edge can be found on the blanks produced from soft material with good ductility. A shorter stroke for a higher maximum blanking force, a shorter stroke for blank separation and a higher slope of decreasing force correspond to a reduced sheared edge zone, which is produced in a stronger and less ductile material.

5. Changing the clearance and using different tool states has some influence on the maximum amplitude and the maximum peak frequency of the AE signals acquired during blanking. However, the nature of the AE technique suggests that it is not the best method for monitoring the blanking process. This study suggests that the improvements are needed for AE technique to complement the force-displacement signatures in order to provide a reliable method for processes monitoring of blanking operations.

6. Comparing all materials, UFG sheets were stronger and less ductile. Further, changing the clearance and using different tool states had a negligible effect on their maximum blanking force and other force-displacement characteristics. These lead to a conclusion that the quality of UFG blanks does not depend on the blanking parameters. Therefore, it is difficult to use force-displacement signatures for monitoring the blanking process for UFG material.

5.3 Suggestions for future work

This study involved a labour intensive experimental work to monitor the process of blanking operations. The work started from developing the tools and continued with preparing the materials, conducting blanking trials and acquiring the process signatures. A complicated relationship between blanking parameters, product quality and process signatures has been reported in this thesis. However, it should be recognised that many aspects in this study could be improved further, by those who would continue to work in this area. Tooling system was one of the important aspects needed to be improved. A flexible blanking tool set is required for easy tool changing and reduction of mechanical handling when repeating the tests and providing proper access for DAQ instruments. These would help to shorten the time required for the experiment and reduce the errors of the acquired signals.

The materials used could be further extended to other types of materials commonly used in sheet metal work such as cooper alloys and various steels. It is also recommended to include other type of UFG metals for blanking, since the interest in these materials is growing in the academic as well as industrial research. Apart from materials, blanking involves a number of process variables. Variables such as blanking speed, temperature, friction and blank holder force could also influence the quality in blanking. Therefore, it is encouraged to undertake further investigation related to these variables in blanking.

Finite element (FE) modelling is a useful tool and is generally recommended for blanking simulation to predict the stress and strain distribution in the material and obtain the process signature. It is difficult to model blanking that can represent the actual blanking operation due to the complexity of the process, which involves crack and fracture propagation, however, with proper input data, an approximate solution could be found. Modelling results from modelling could be compared with the results obtained from experiment, and once validated can contribute to the improvement of the whole system including tooling, processes and quality control.

Methods for modelling AE should still be considered. Previous research reported an approach based on representing the energy as a series of triangular pulses; the rising part representing the accumulation of energy at the workpiece/tool interface and the falling part representing the release of energy as blank becomes separated. It is important to identify what the sources of AE in blanking processes are, so that the AE results can be correlated to process signatures in a meaningful way. This requires a mathematical AE modelling to be employed to represent the phase of elastic and plastic deformation and fracture initiation.

It might be desirable to have an intelligent process monitoring system. The system that can monitor, diagnose and control, so that less human intervention is required. Research had been conducted to monitor metal forming processes using artificial intelligence based systems, in particular, neural networks. This was implemented using a limited

number of process variables. In practice, complex processes involve many process variables. Therefore, integrated frameworks for process monitoring, diagnosing and controlling are needed, which enable using knowledge-based system and artificial intelligent to handle more data, achieve fast-response and reliable results.

There is also a suggestion with a view to extend the work in process monitoring of blanking operations to other fields of manufacturing process such as microforming. Microforming is one of the emerging new areas in manufacturing process. Therefore, research in microblanking is essential. Apart from main problem of dimensional scaling effects, other aspects of microforming such as designing the forming tools, materials for tooling, handling the tiny objects, quality control and automation are becoming the challenging issues. In relation to these, research into microblanking is still lacking. The classical knowledge of tool design is insufficient to address the issues in designing microtools such as accuracy and repeatability. Therefore, increasing research in this area is needed to contribute to the new knowledge as well as address the industrial needs in the near future.

Appendix 1

AE Signal Features Terminology

Term	Explanation
Time of Hit ("Time of Test" clock)	This is the time at which a hit has been detected by the PCI-2. This is detected the instant that the AE signal exceeds the AE threshold.
Amplitude	The AE amplitude is the maximum (positive or negative) AE signal excursion during an AE hit. The amplitude is expressed in dB using relationship: $dB = 20 \log (V_{max}/1_{\mu\text{-volt}}) - (\text{Preamplifier Gain in dB})$
Energy ("PAC – Energy")	"PAC – Energy" is a 2-byte parameter derived from the "integral of the rectified voltage signal over the duration of the AE hit" (or waveform), hence the voltage – time units. Although PAC – Energy has the same definition as Signal Strength, the only difference is in the sensitivity, size and dynamic range of this parameter. Unit μV-sec for 1 count.
Counts (AE Threshold Crossing Counts)	The counts of the AE signal excursions over the AE Threshold.
Duration	AE Duration is the time from the first threshold crossing to the end of last threshold crossing of the AE signal from the AE threshold
RMS	Root Mean Square is a measure of the continuously varying AE signal "voltage" into the AE system. RMS is defined as rectified, time average AE signal, measured on a linear scale and reported in volts.
ASL	Average Signal Level is a measure of the continuously varying and "averaged" amplitude of the AE signal. This measurement is similar to that of RMS in that it is an average reading. It is following the amplitude variation and is measured in dB.
Threshold	The Threshold feature records the value of the Threshold at the time of an AE hit.
Rise Time	Rise Time is the time between the AE hit start and the peak amplitude of the AE hit.

Continued ...

Counts to Peak	Counts to Peak is a measure of the number of AE counts between the AE hit start and the peak amplitude of the AE hit.
Average Frequency	Average Frequency reported in kHz, determines an average frequency over the entire AE hit. Average Frequency = (AE counts) / (Duration)
Signal Strength	Signal Strength is mathematically defined as the integral of the rectified voltage signal over the duration of the AE waveform packet.
Absolute Energy	This feature is a true energy measure of the AE hit. It is derived from the integral of the squared voltage signal divided by the reference resistance (10 kΩ) over the duration of the AE waveform packet.
Peak Frequency	The peak frequency is a 2-byte value, reported in kHz, defined as the point in the power spectrum at which the peak magnitude occurs. A real time FFT is performed on the waveform associated with the AE hit. The frequency, which contains the largest magnitude is reported.

Appendix 2

Assembly drawing of blanking tool set

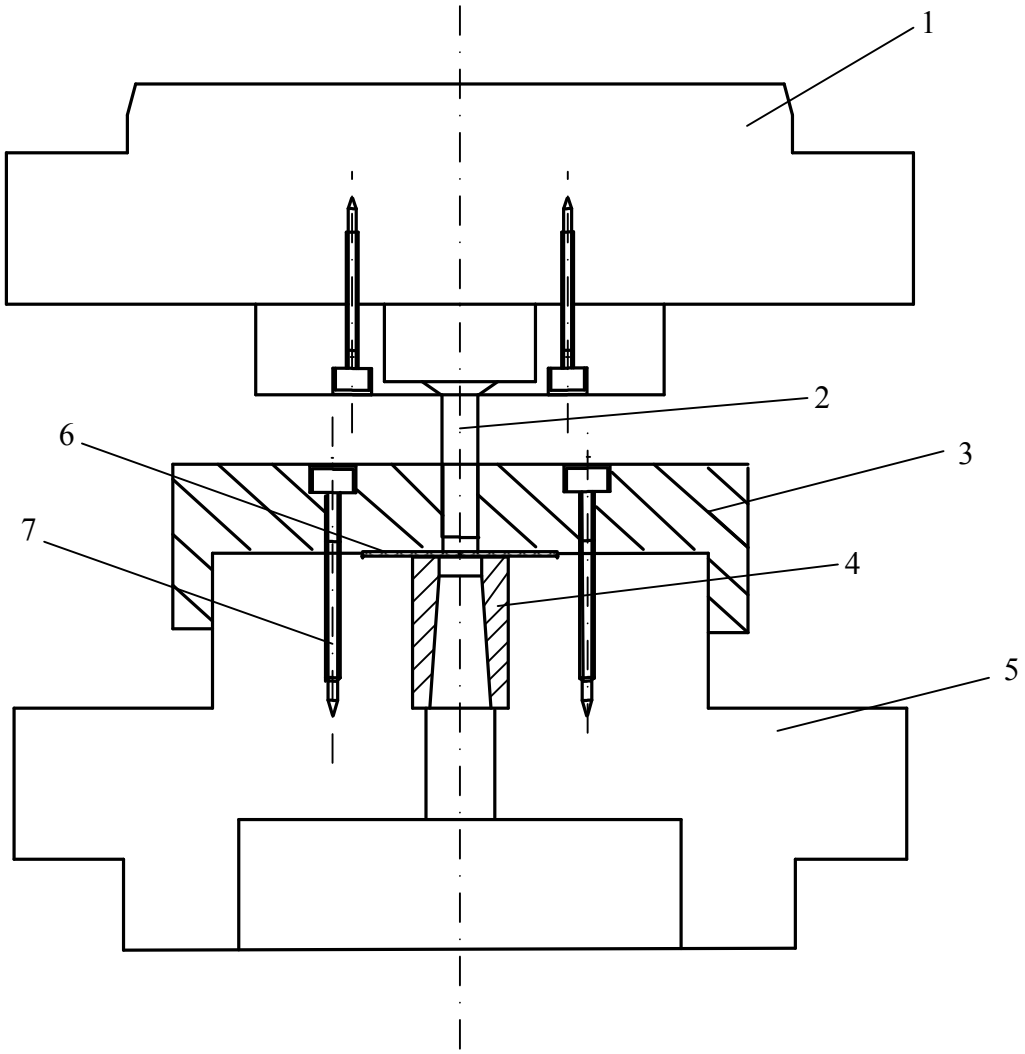

No. 1. Punch holder supporting disc
2. punch
3. Blank holder
4. Die
5. Die holder
6. Workpiece material
7. Screws

Appendix 3

Acoustic emission sensor specifications

The single most important factor in AE testing is the selection of an AE sensor. Physical Acoustic Corporation (PAC) prides itself on its ability to continually design and manufacture quality high sensitivity/low noise AE sensors. At PAC, quality, materials, which are specially designed by its subsidiary company, PiezoKinetics (PKI), and workmanship combine to produce reliable, high performance sensors. The sensor housing and integral electronics are design to eliminate RFI/EMI and microphonic interference.

Calibration, traceable to the U.S. National Institutes of Standards and Technology (NIST) is the important element of the sensor manufacturing process. PAC calibration uses either the NIST Transient Surface Wave Calibration (ASTM E1106 – 86, Standard Method for Primary Calibration of AE sensors) or the White Noise Continuous Sweep (ASTM E976 – 84, Standard Guide for Determining the Reproducibility of AE Sensor Response), otherwise kwon as the Face-to-Face Technique.

... Continued

Group	Model	Dimensions Dia x Ht mm)	Weight (gm)	Operating temperature (°C)	Shock limit (g)	Case material
Wide-Band	WD	18 x 17	8	-65 to +177	10,000	Stainless Steel (304)

Face material	Connector type	Connector location	Peak sensitivity Ref V/(ms/s)/[Ref V/mbar]	Operating freq. range (kHz)	Resonant freq. (kHz)
Ceramic	Dual BNC	Side	55 [-62.5]	100 - 1000	125 [650]

Directionality (dB)	Grounding	Seal type	Comment	Recommended accessories
±1.5	B	Epoxy	True differential design	MHSTD Hold-down

Appendix 4

Preamplifier specifications

The 2/4/6 preamplifier family includes the 0/2/4 (gain selection from 0 dB, 20 dB and 40 dB) and 2/4/6 type (gain selection ranges from 20 dB, 40 dB and 60 dB). These preamplifiers were designed to be used with all available AE systems that have their power supplied via the output signal BNC. Provided with three selectable gain settings (switch selectable), this preamplifier operates with either a single-ended or differential input sensor.

Type	Electrical specifications	Environment specifications	Physical specifications
2/4/6	Gain selectable: 20/40/60 dB ± 0.5% dB Input impedance: 10 kΩ // 15 pF Power required: 18 – 28 Vdc Operating current: 28 mA (without AST installed) Dynamic range: 80 dB (50 Ω Input)	Temperature -40°C to + 65°C	Dimensions: 13.97 cm x 6.03 cm x 3.49 cm Weight: 205 g

2/4/6 Gain related specifications

Gain selection	**20 dB**	**40 dB**	**60 dB**
Bandwidth (-3 dB)	10 kHz – 2.5 MHz	10 kHz – 2.0 MHz	10 kHz – 900 kHz
Output voltage (50 Ω load)	20 V p-p	20 V p-p	6 V p-p
CMRR (500 kHz)	42 dB	42 dB	42 dB

Appendix 5

Block diagram description of PCI-2 AE board

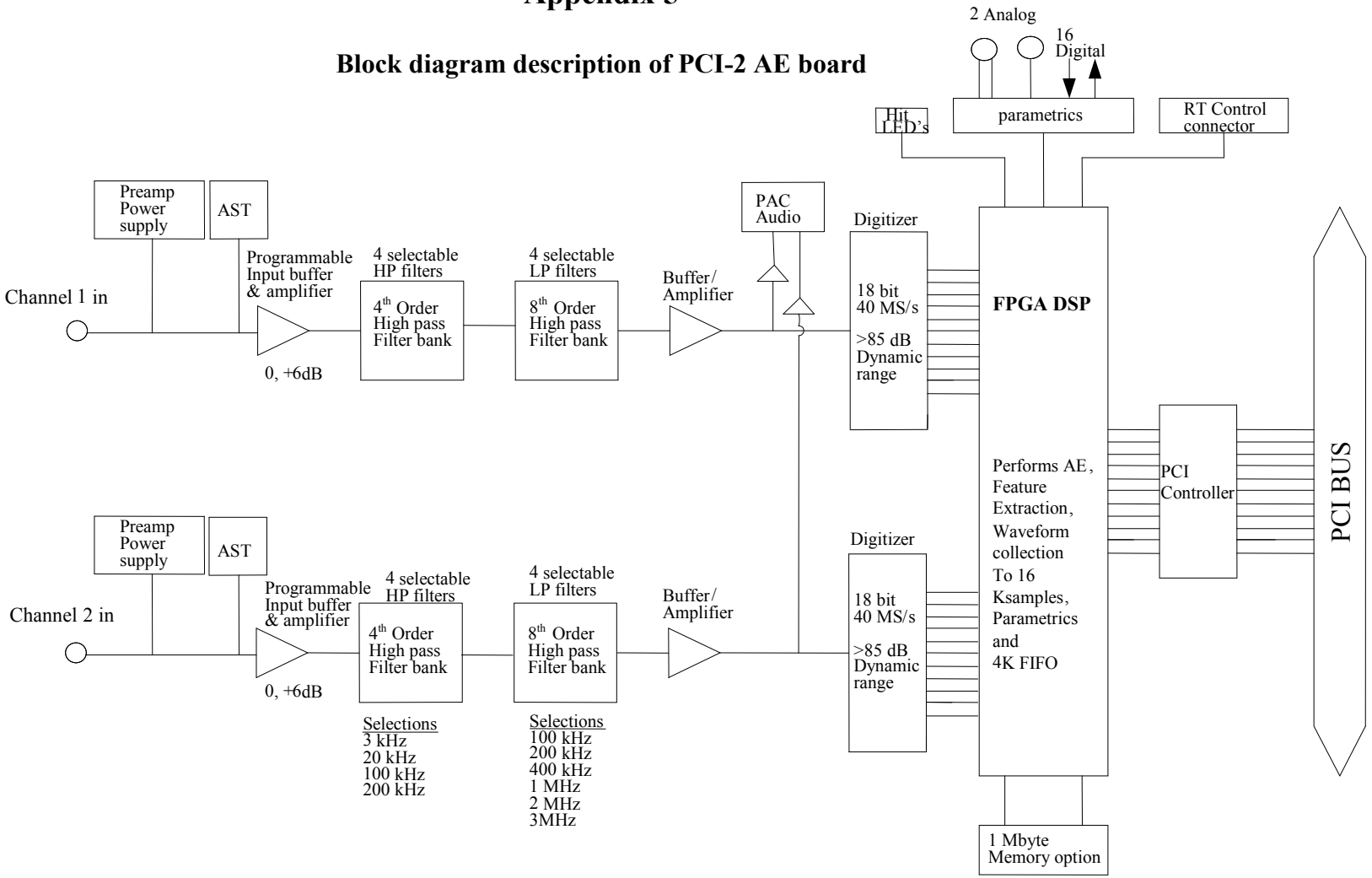

PCI-2 AE board specifications

Physical Specifications	**Electrical Specifications**	Signal Processing	
Size (cm): 34 x 12.2 x 1.78 Weight: 499 g Power consume: 12 Watts DC Power: +12 V, 0.6 A -12 V, 0.05 A +5 V, 0.8 A	Electrical Spec AE input: 2 channels Input impedance: 50 Ω - 1000 Ω Preamp power: 0 – 28 Vdc 100 mA Current limited Sensor testing: AST built-in Frequency Response: 3 kHz – 3 MHz at -3 dB points	AE signal gain: 0, 6 dB (selectable) Filters: 4 HP selectable filters: 3 kHz, 20 kHz, 100 kHz, 200 kHz, 4th order Butterworth 6 LP selectable filters: 100 kHz, 200 kHz, 400 kHz, 1000 kHz, 2000 kHz, 3000 kHz, 6th order Butterworth Noise (wideband): Filters: 3 kHz – 3 MHz ASL(no input): 4 dB Min. Threshold: 17 dB w/o preamp or sensor Max. signal amp: 100 dB AE ASL 99 dB ADC type: 18 bit 40 MSPS per channel maximum Dynamic range: >85 dB	Sample rate (Selectable): 100 kS/s, 200 kS/s, 500 kS/s, 1 MS/s, 2 MSPS, 5 MSPS, 10 MSPS, 20 MSPS, 40 MSPS - (40 MSPS with 2x averaging, for a 20 MSPS effective sampling rate) - (40 MSPS with 4x averaging, for a 10 MSPS effective sampling rate) Extracted AE features: Time of 1st Threshold Crossing. Time to Peak, Peak Amplitude, Envelope Strength, Duration, Rise Time, Counts, true energy, RMS, ASL, Parametric 1 & 2

Analog Parametrics	Digital I/O	Audio Monitor Interfaces	LED Activity Monitor
Number of parametric channel: 2 Parametric A/D resolution: 16 bits Parametric sample rate: 10 kHz Time driven data rate: controlled by software; 10 msec – 60 sec Time parametrics: all parametric available in data set. Parametric 1 functions: input range ±10.0 V, ±1.0 V, ±0.10 V, ±0.01 V Selectable 30 Hz LP or none 5.0 V software programmable offset control with 12 bit DAC 0 – 10 V programmable excitation voltage for strain gauge bridges Parametric 2 functions: input range ±10.0 V, x 1 gain , no filter	8 digital inputs, 8 digital outputs (0 – 3.3 V, 5 V tolerance, TTL level compatible)	Analog switch and buffer to select desired channels to be routed to standard PAC audio monitor board.	On board LED driver to directly drives LED's on front panel, LED minimum on time is 0.05 seconds.

Appendix 6

Mounting of force transducer

The force transducer used was piezoelectric force transducer from Kistler, type 9001A. The transducer must be installed between two plane-parallel, rigid and fine-machined (preferably ground) faces. This is necessary to achieve a good load distribution on one hand and a wide frequency response on the other hand.

The force transducer should always be installed under certain preload. Preload is essential to achieve the ultimate goal of any measurement process – linearity. In this case, the transducer is always fixed under preload force to measure compression or tension. The faces are pressed together, which allows to fully benefiting of the high rigidity of the transducer. A good rule of thumb, the amount of preload force given to transducer is 25 – 30% of the transducer range. For preloading, the force must always be measured with the transducer itself, using the sensitivity indicated in the technical data. The preloading screw always shunts part of the force and therefore the transducer must be calibrated again after installation to determine the final sensitivity of the completed measuring setup. The mounting set shown below allows the transducer to be preloaded up to 30% of its range. The centring clip also serves to centre the transducer with the screw.

Dimensions (mm)									Preload
M	D	L_1	L_2	L_3	H_1	H_2	S_1	S_2	F_p [kN]
M3x0.5	5.5	16	4.2	3	6.5	6	3.5	7	≤2.5

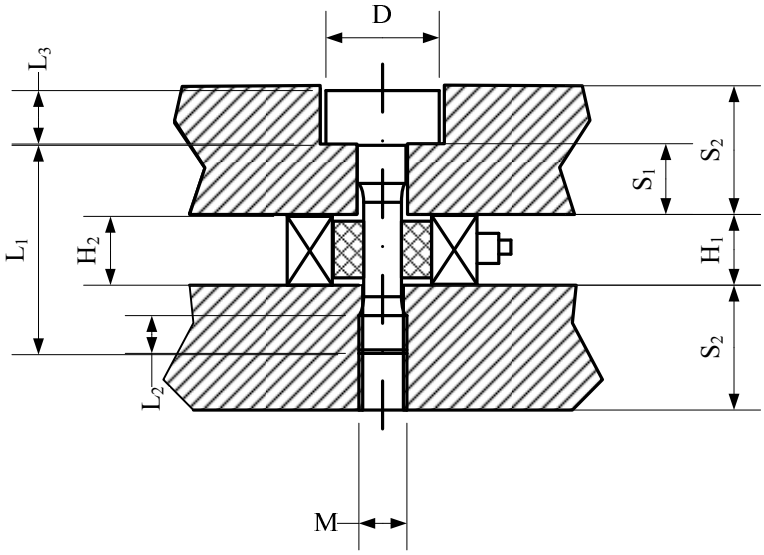

Appendix 7

Aluminium 1050-H14

Component properties	Mechanical properties	Thermal properties	Physical properties	Electrical properties
Aluminium, Al >= 99.5% Copper, Cu <=0.0500% Iron, Fe <=0.400% Magnesium, Mg <=0.0500% Manganese, Mn <=0.0500% Other, each <=0.0300% Silicon, Si <=0.250% Titanium, Ti <=0.0300% Vanadium, V <=0.0500% Zinc, Zn <=0.0500%	Hardness, Brinell = 30 Tensile Strength = 110 MPa Ultimate Tensile Strength = 103 MPa Yield elongation at break = 10.0% Modulus of elasticity = 69.0 GPa Poissons Ratio = 0.0330 Shear Modulus = 26.0 GPa Shear Strength = 69.0 MPa	Heat of Fusion = 390 J/g CTE, linear 20°C = 23.6 µm/m-°C CTE, linear 250°C = 25.5 µm/m-°C Specific Heat Capacity = 0.900 J/g-°C Thermal conductivity = 227 W/m-K Melting point = 646 - 657°C Solidus = 646°C Liquidus = 657°C	Density = 2.705 g/cc	Electrical resistivity = 0.00000290 Ω-cm

Appendix 8

Chemical composition of aluminium AA 1070

Component element properties	Physical properties
Aluminium, Al = 99.7% Copper, Cu <= 0.040% Iron, Fe <= 0.25% Magnesium, Mg < 0.030% Manganese, Mn <= 0.030% Other, each <= 0.030% Silicon, Si <= 0.20% Titanium, Ti <= 0.030% Vanadium, V <= 0.050% Zinc, Zn <= 0.040%	Density = 2.70 g/cc

Appendix 9

Design of experiment

Half normal plot (using the maximum blanking force as a quality characteristic)

Material *A1*

3 factors with 2 levels

Factor: Sharp die (-) Worn die (+)
Sharp punch (-) Worn punch (+)
Small clearance 3% (-) Large clearance 9% (+)

Experimental plan for *A1*

Material *A1*

Run	D	P	C	Max Force
1	-	-	-	1218
2	+	-	-	1211
3	-	+	-	1237
4	+	+	-	1344
5	-	-	+	1005
6	+	-	+	1053
7	-	+	+	1156
8	+	+	+	1143

	D	P	DxP	C	DxC	PxC	DxPxC	Max Force	Predicted Fmax
	-1	-1	+1	-1	+1	+1	-1	1218	1186.5
	+1	-1	-1	-1	-1	+1	+1	1211	1220.25
	-1	+1	-1	-1	+1	-1	+1	1237	1284.75
	+1	+1	+1	-1	-1	-1	-1	1344	1318.5
	-1	-1	+1	+1	-1	-1	+1	1005	1023.25
	+1	-1	-1	+1	+1	-1	-1	1053	1057
	-1	+1	-1	+1	-1	+1	-1	1156	1121.5
	+1	+1	+1	+1	+1	+1	+1	1143	1155.25
								1170.875	
Divisor	4	4	4	4	4	4	4		
Contrast value	33.75	98.25	13.25	-163.3	-16.25	-22.25	-43.75		

		a	b
Half normal plot		34.968	8.2645
0.08964	13.25	0.0896	11.399
0.27188	16.25	0.2719	17.772
0.46371	22.25	0.4637	24.479
0.67449	33.75	0.6745	31.85
0.92082	43.75	0.9208	40.464
1.24187	98.25	1.2419	51.69
1.80274	163.25	1.8027	71.303

A half normal plot for *A1*

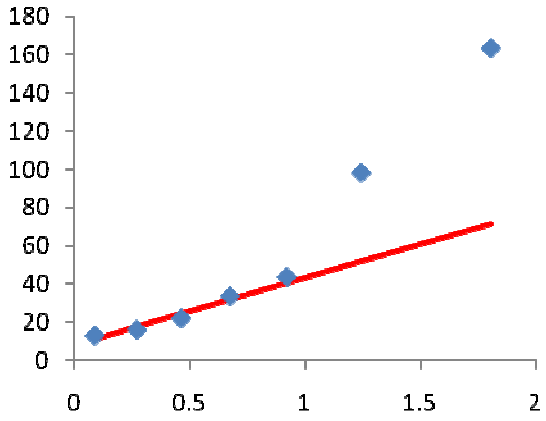

Material *A2*

Material *A2*

Run	D	P	C	Max Force
1	-	-	-	1157
2	+	-	-	1066
3	-	+	-	1236
4	+	+	-	1114
5	-	-	+	886
6	+	-	+	915
7	-	+	+	916
8	+	+	+	1025

	D	P	DxP	C	DxC	PxC	DxPxC	Max Force	Predicted Fmax
	-1	-1	+1	-1	+1	+1	-1	1157	1119.25
	+1	-1	-1	-1	-1	+1	+1	1066	1100.5
	-1	+1	-1	-1	+1	-1	+1	1236	1186
	+1	+1	+1	-1	-1	-1	-1	1114	1167.25
	-1	-1	+1	+1	-1	-1	+1	886	911.5
	+1	-1	-1	+1	+1	-1	-1	915	892.75
	-1	+1	-1	+1	-1	+1	-1	916	978.25
	+1	+1	+1	+1	+1	+1	+1	1025	959.5
								1039.375	
Divisor	4	4	4	4	4	4	4		
Contrast value	-18.75	66.75	12.25	-208	87.75	3.25	27.75		

		a	b
Half normal plot		41.07	0.102
0.08964	3.25	0.09	3.783
0.27188	12.25	0.272	11.27
0.46371	18.75	0.464	19.15
0.67449	27.75	0.674	27.8
0.92082	66.75	0.921	37.92
1.24187	87.75	1.242	51.1
1.80274	207.75	1.803	74.14

A half normal plot for *A2*

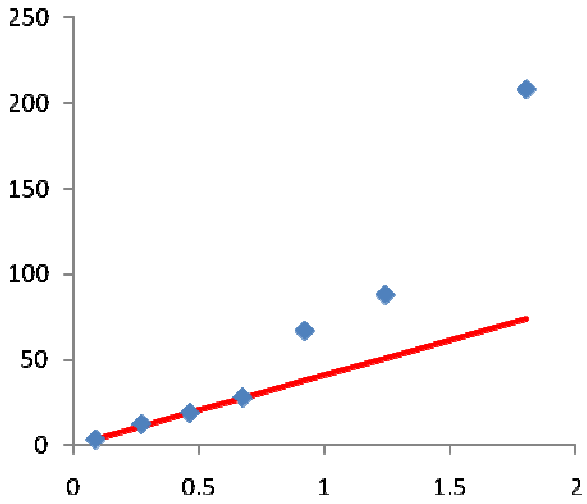

Material *A3*

Material *A3*

Run	D	P	C	Max Force
1	-	-	-	1599
2	+	-	-	1675
3	-	+	-	1826
4	+	+	-	1864
5	-	-	+	1397
6	+	-	+	1606
7	-	+	+	1590
8	+	+	+	1800

	D	P	DxP	C	DxC	PxC	DxPxC	Max Force	Predicted Fmax
	-1	-1	+1	-1	+1	+1	-1	1599	1574
	+1	-1	-1	-1	-1	+1	+1	1675	1707.25
	-1	+1	-1	-1	+1	-1	+1	1826	1774.75
	+1	+1	+1	-1	-1	-1	-1	1864	1908
	-1	-1	+1	+1	-1	-1	+1	1397	1431.25
	+1	-1	-1	+1	+1	-1	-1	1606	1564.5
	-1	+1	-1	+1	-1	+1	-1	1590	1632
	+1	+1	+1	+1	+1	+1	+1	1800	1765.25
								1669.625	
Divisor	4	4	4	4	4	4	4		
Contrast value	133.25	200.75	-9.25	-142.8	76.25	-7.25	9.75		

		a	b
Half normal plot		109.09	-15.27
0.08964	7.25	0.0896	-5.496
0.27188	9.25	0.2719	14.384
0.46371	9.75	0.4637	35.309
0.67449	76.25	0.6745	58.303
0.92082	133.25	0.9208	85.174
1.24187	142.75	1.2419	120.2
1.80274	200.75	1.8027	181.38

A half normal plot for *A3*

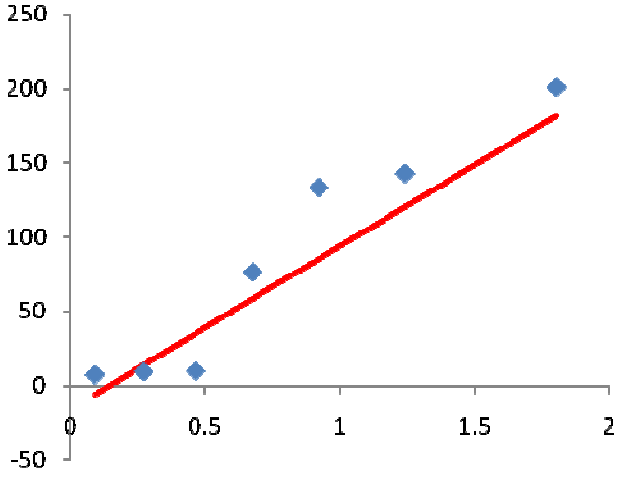

Material *A4*

Material *A4*

Run	D	P	C	Max Force
1	-	-	-	1714
2	+	-	-	1875
3	-	+	-	1912
4	+	+	-	2081
5	-	-	+	1589
6	+	-	+	1788
7	-	+	+	1797
8	+	+	+	1800

	D	P	DxP	C	DxC	PxC	DxPxC	Max Force	Predicted Fmax
	-1	-1	+1	-1	+1	+1	-1	1714	1751
	+1	-1	-1	-1	-1	+1	+1	1875	1884
	-1	+1	-1	-1	+1	-1	+1	1912	1907
	+1	+1	+1	-1	-1	-1	-1	2081	2040
	-1	-1	+1	+1	-1	-1	+1	1589	1599
	+1	-1	-1	+1	+1	-1	-1	1788	1732
	-1	+1	-1	+1	-1	+1	-1	1797	1755
	+1	+1	+1	+1	+1	+1	+1	1800	1888
								1819.5	
Divisor	4	4	4	4	4	4	4		
Contrast value	133	156	-47	-152	-32	-46	-51		

		a	b
Half normal plot		29.43	32.966
0.089642	32	0.0896	35.604
0.27188	46	0.2719	40.967
0.463708	47	0.4637	46.613
0.67449	51	0.6745	52.816
0.920823	133	0.9208	60.065
1.241867	152	1.2419	69.514
1.802743	156	1.8027	86.02

A half normal plot for *A4*

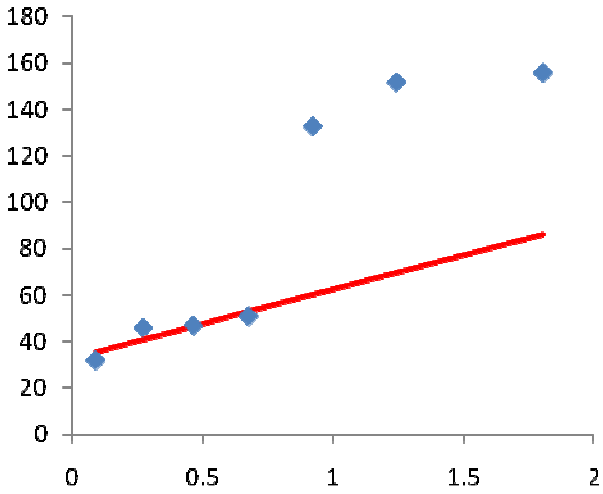

Appendix 10

Design of experiment

Half normal plot (using the maximum amplitude and maximum peak frequency as a quality characteristic)

Material *A1*

D(-)	Sharp die	D(+)	Worn die
P(-)	Sharp punch	P(+)	Worn punch
C(-)	3% clear	C(+)	9% clear
M(-)	*A2*	M(+)	*A4*

Maximum amplitude

Run	D	P	C	M	Max Amplitude, dB
1	-	-	-	-	68
2	+	-	-	-	63
3	-	+	-	-	54
4	+	+	-	-	47
5	-	-	+	-	45
6	+	-	+	-	46
7	-	+	+	-	45
8	+	+	+	-	66
9	-	-	-	+	64
10	+	-	-	+	73
11	-	+	-	+	72
12	+	+	-	+	84
13	-	-	+	+	53
14	+	-	+	+	51
15	-	+	+	+	52
16	+	+	+	+	64

D	P	DxP	C	DxC	PxC	M	DxM	PxM	CxM	DxPxC	DxCxM	PxCxM	DxPxM	DxPxCxM	Max Amp
-1	-1	1	-1	1	1	-1	1	1	1	-1	-1	-1	-1	1	68
1	-1	-1	-1	-1	1	-1	-1	1	1	1	1	-1	1	-1	63
-1	1	-1	-1	1	-1	-1	1	-1	1	1	-1	1	1	-1	54
1	1	1	-1	-1	-1	-1	-1	-1	1	-1	1	1	-1	1	47
-1	-1	1	1	-1	-1	-1	1	1	-1	1	1	1	-1	-1	45
1	-1	-1	1	1	-1	-1	-1	1	-1	-1	-1	1	1	1	46
-1	1	-1	1	-1	1	-1	1	-1	-1	-1	1	-1	1	1	45
1	1	1	1	1	1	-1	-1	-1	-1	1	-1	-1	-1	-1	66
-1	-1	1	-1	1	1	1	-1	-1	-1	-1	1	1	1	-1	64
1	-1	-1	-1	-1	1	1	1	-1	-1	1	-1	1	-1	1	73
-1	1	-1	-1	1	-1	1	-1	1	-1	1	1	-1	-1	1	72
1	1	1	-1	-1	-1	1	1	1	-1	-1	-1	-1	1	-1	84
-1	-1	1	1	-1	-1	1	-1	-1	1	1	-1	-1	1	1	53
1	-1	-1	1	1	-1	1	1	-1	1	-1	1	-1	-1	-1	51
-1	1	-1	1	-1	1	1	-1	1	1	-1	-1	1	-1	-1	52
1	1	1	1	1	1	1	1	1	1	1	1	1	1	1	64

59.1875

Divisor	8	8	8	8	8	8	8	8	8	8	8	8	8	8	8
Contrast value	5.13	2.63	4.375	13	2.875	5.38	9.9	2.625	5.125	5.375	-4.125	-5.625	-7.125	-0.125	-1.375

Half normal plot		a	b
		4.3826	1.27
0.041789	0.13	0.0418	1.45
0.125661	1.38	0.1257	1.82
0.210428	2.63	0.2104	2.19
0.296738	2.63	0.2967	2.57
0.38532	2.88	0.3853	2.95
0.47704	4.13	0.477	3.36
0.572968	4.38	0.573	3.78
0.67449	5.13	0.6745	4.22
0.7835	5.13	0.7835	4.7
0.902735	5.38	0.9027	5.22
1.036433	5.38	1.0364	5.81
1.191816	5.63	1.1918	6.49
1.382994	7.13	1.383	7.33
1.644854	9.88	1.6449	8.47
2.128045	12.9	2.128	10.6

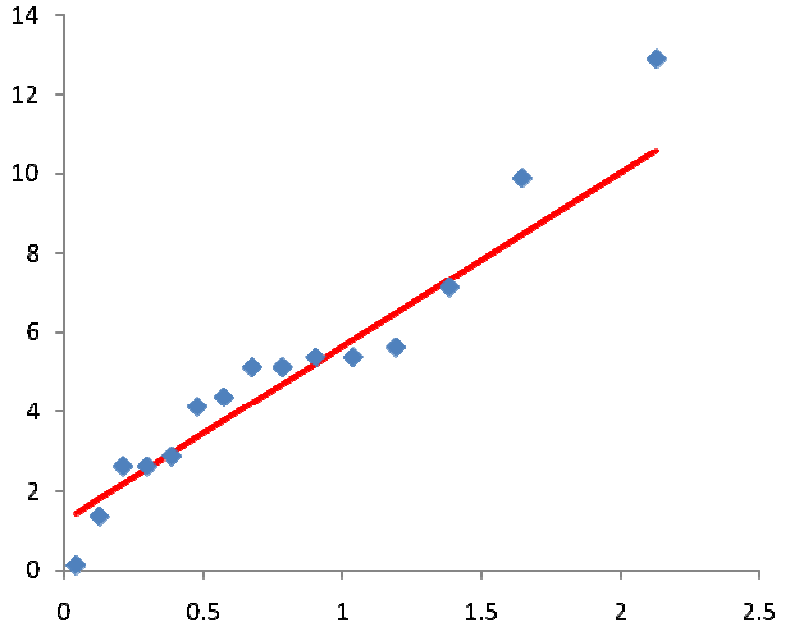

Maximum peak frequency

D(-)	Sharp die	D(+)	Worn die
P(-)	Sharp punch	P(+)	Worn punch
C(-)	3% clear	C(+)	9% clear
M(-)	*A2*	M(+)	*A4*

Run	D	P	C	M	Max peak freq
1	-	-	-	-	478
2	+	-	-	-	415
3	-	+	-	-	178
4	+	+	-	-	305
5	-	-	+	-	205
6	+	-	+	-	305
7	-	+	+	-	102
8	+	+	+	-	639
9	-	-	-	+	512
10	+	-	-	+	548
11	-	+	-	+	585
12	+	+	-	+	590
13	-	-	+	+	468
14	+	-	+	+	498
15	-	+	+	+	448
16	+	+	+	+	375

D	P	DxP	C	DxC	PxC	M	DxM	PxM	CxM	DxPxC	DxCxM	PxCxM	DxPxM	DxPxCxM	Max peak freq
-1	-1	+1	-1	+1	+1	--1	+1	+1	+1	--1	-1	-1	--1	+1	478
+1	-1	-1	-1	-1	+1	--1	-1	+1	+1	+1	+1	-1	+1	-1	415
-1	+1	-1	-1	+1	-1	--1	+1	-1	+1	+1	-1	+1	+1	-1	178
+1	+1	+1	-1	-1	-1	--1	-1	-1	+1	--1	+1	+1	-1	+1	305
-1	-1	+1	+1	-1	-1	--1	+1	+1	-1	+1	+1	+1	-1	--1	205
+1	-1	-1	+1	+1	-1	--1	-1	+1	-1	-1	-1	+1	+1	+1	305
-1	+1	-1	+1	-1	+1	--1	+1	-1	-1	-1	+1	-1	+1	+1	102
+1	+1	+1	+1	+1	+1	--1	-1	-1	-1	+1	-1	-1	-1	-1	639
-1	-1	+1	-1	+1	+1	+1	-1	-1	-1	-1	+1	+1	+1	-1	512
+1	-1	-1	-1	-1	+1	+1	+1	-1	-1	+1	-1	+1	-1	+1	548
-1	+1	-1	-1	+1	-1	+1	-1	+1	-1	+1	+1	-1	-1	+1	585
+1	+1	+1	-1	-1	-1	+1	+1	+1	-1	-1	-1	-1	+1	-1	590
-1	-1	+1	+1	-1	-1	+1	-1	-1	+1	+1	-1	-1	+1	+1	468
+1	-1	-1	+1	+1	-1	+1	+1	-1	+1	-1	+1	-1	-1	-1	498
-1	+1	-1	+1	-1	+1	+1	-1	+1	+1	-1	-1	+1	-1	-1	448
+1	+1	+1	+1	+1	+1	+1	+1	+1	+1	+1	+1	+1	+1	+1	375

Divisor	8	8	8	8	8	8	8	8	8	8	8	8	8	8	8
Contrast value	87.4	25.9	61.63	-71	61.13	47.875	175	-87.9	18.9	-40.1	21.88	-82.13	-112.4	-95.13	-39.875

Half normal plot		a	b
		59.64	19.5
0.0418	18.9	0.042	22
0.1257	21.9	0.126	27
0.2104	25.9	0.21	32.1
0.2967	39.9	0.297	37.2
0.3853	40.1	0.385	42.5
0.477	47.9	0.477	48
0.573	61.1	0.573	53.7
0.6745	61.6	0.674	59.8
0.7835	71.4	0.784	66.3
0.9027	82.1	0.903	73.4
1.0364	87.4	1.036	81.3
1.1918	87.9	1.192	90.6
1.383	95.1	1.383	102
1.6449	112	1.645	118
2.128	175	2.128	146